Controlled/living Group Transfer Polymerization of Acrylamide using Organic Acid Leading to Linear, Cyclic, and Star-shaped Macromolecular Architectures

A Dissertation for the Degree of Doctor of philosophy

Seiya Kikuchi

Hokkaido University

Contents

Chapter 1

General introduction

1.1. Acrylamide polymers

Acrylamide polymers, especially, those without a substituent on the amide nitrogen (polyacrylamide), are important polymer materials for industrial applications, such as flocculants for water treatment, viscosifiers for oil recovery, retention and drainage aid for paper making, and subdermal fillers for aesthetic facial surgery.[1-3] Apart from non-substituted polyacrylamide, the mono- or di-substituted polyacrylamides are some of the important raw materials for the design and synthesis of functional materials based on the acrylamide polymer because the *N*-substituents in the polyacrylamide significantly define the functional properties, such as its water solubility. For example, poly(*N*-methylacrylamide) and poly(*N*,*N*-dimethylacrylamide) (PDMAAm) are soluble in water, while poly(*N*-tert-butylacrylamide), poly(*N*-phenylacrylamide), poly(*N*,*N*-di-*n*-propylacrylamide), and poly(*N*-*n*-butyl,*N*-methylacrylamide) are insoluble in water.[4] In contrast, some acrylamide polymers with moderately bulky *N*-substituents display a temperature-dependent reversible water solubility in their aqueous solution, which are categorized as thermoresponsive polymers.[5] The thermal phase transition temperatures during the heating and cooling process, which are denoted as the lower critical solution temperature (LCST) and cloud point (T_c), can be optimized by changing the *N*-substituents. For example, poly(*N*-ethyl,*N*-methylacrylamide) (PEMAAm), poly(acryloylpyrrolidine) (PAPY), poly(*N*-isopropylacrylamide) (PNIPAM) and poly(*N*,*N*-diethylacrylamide) (PDEAAm), and poly(*N*-*n*-propylacrylamide) (P*n*PAAm) show LCSTs at 70 °C, 50 °C, 32 °C, 32 °C and 25 °C, respectively (Figure 1-1).[4] Besides the polymer structure itself, the LCST is significantly affected by solution concentration, molecular weight, terminal structure, and polymer architecture, of which the terminal structure and polymer architecture have a potential of controlling the LCST over a wide range on the same polymer backbone.[6-14] These unique properties of the acrylamide polymers provide a significant potential for various applications in “smart materials”. To determine the desired properties, a

precise synthetic methodology of the acrylamide polymers is required.

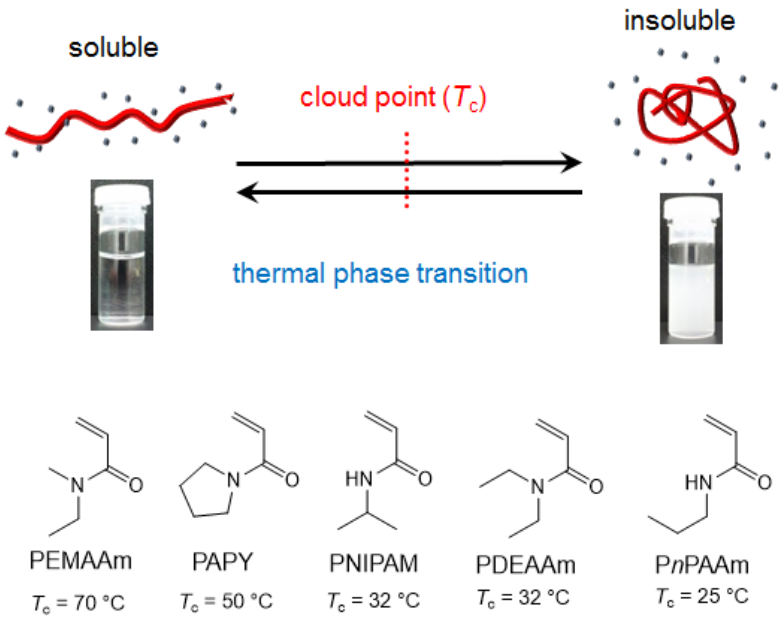

Figure 1-1. An illustration of thermal phase transition for thermoresponsive polymer and the representative thermoresponsive acrylamide polymers

1.2. Controlled/living polymerization method for acrylamide monomers

Since Szwarc et al. first reported the living anionic polymerization of styrene in 1956,[15,16] the controlled/living polymerization methods including radical, anionic, cationic, and coordination polymerizations, have been developed to synthesize well-controlled polymers in terms of their molecular weight and molecular weight distributions, applicable monomer, copolymer synthesis, and control of the primary structure.[17-22] The controlled/living polymerization of polar vinyl monomers, such as (meth)acrylates, has been established using radical, anionic, and coordination polymerization methods since the late 1980s to early 1990s.[17,20,22] On the other hand, the synthesis of a well-controlled acrylamide polymer using the controlled/living polymerization had not been achieved until the late 1990s due to the high reactivity of the acrylamide monomer.

1.2.1. Controlled/living radical polymerization (CRP)

Controlled/living radical polymerizations (CRPs) including the nitroxide-mediated free radical polymerization (NMP), atom transfer radical polymerization (ATRP), and reversible addition-fragmentation chain transfer (RAFT) polymerization, have been employed for preparing well-controlled acrylamide polymers, by which the initiating systems were efficiently improved. Hawker et al. reported the first successful synthesis of an acrylamide polymer using NMP in 1999, *i.e.*, PDMAAm with a molecular weight up to 48.0 kg mol^{-1} and polydispesity index (PDI) below 1.21 was afforded using the alkoxyamine derivatives as an initiator (Scheme 1-1a).[23] Thereafter, ATRP has been used to synthesize acrylamide polymers with the initiating system of 2-chloropropionate as the initiator and CuCl/tris[2-(dimethylamino)ethyl]amine (Me_6TREN) as the catalyst, affording PDMAAm with a low PDI (Scheme 1-1b).[24,25] In addition, the RAFT polymerization was successfully used to synthesize the well-controlled PNIPAM, in which azobisisobutyronitrile (AIBN) as the radical initiator and dithioester as the chain transfer agent (CTA) were used for the initiating system (Scheme 1-1c).[26,27] Since the development of CRP methods, various types of well-defined acrylamide polymers, including homo and copolymers, have been successfully prepared as building blocks for intelligent applications, such as drug delivery or a gene carrier, and filtering materials.[28-32]

Scheme 1-1. Representative controlled/living radical polymerization for acrylamide monomer

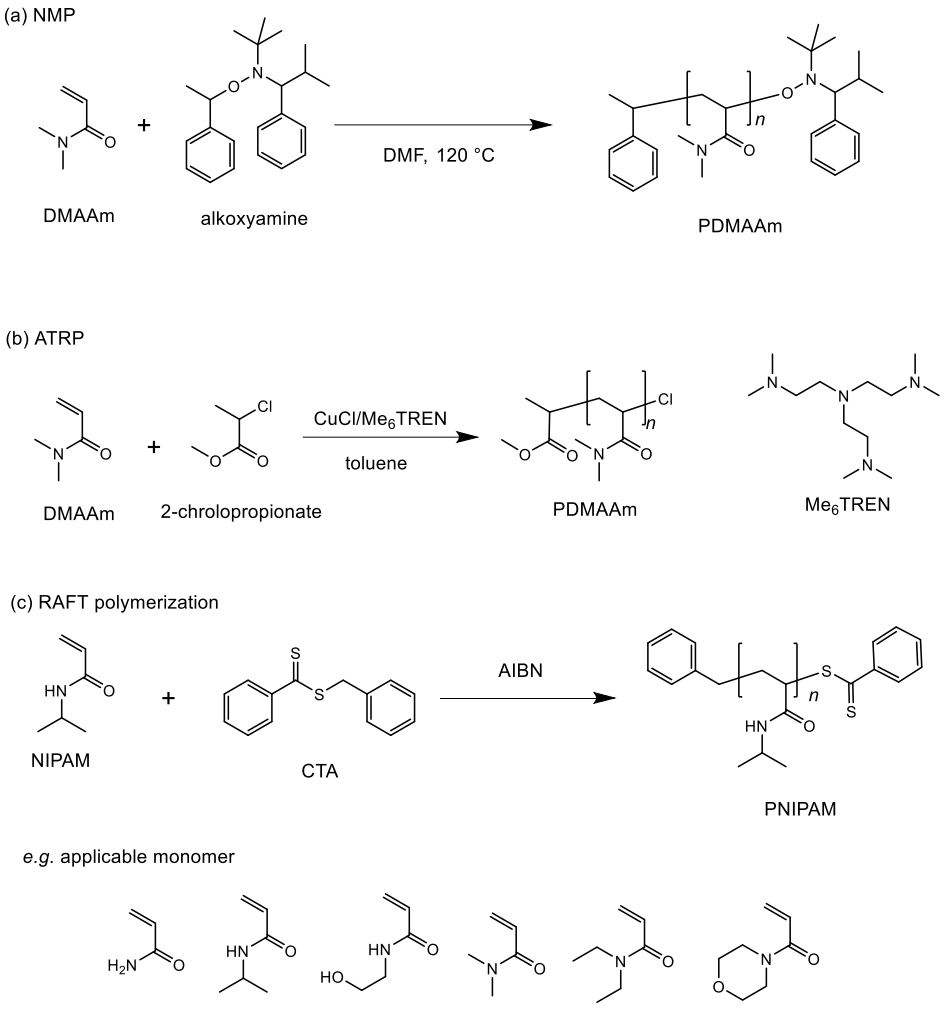

1.2.2. Controlled/living anionic polymerization

Although the CRP methods have been widely used for synthesizing various types of acrylamide polymers, anionic polymerization is still the most reliable method to synthesize such polymers with well-controlled molecular weights, low PDIs, and fidelity of the primary structure. For the synthesis of the acrylamide polymers using the anionic polymerization method, Hogen et al. first revealed that initiating systems, such as (triphenylmethyl)cesium or cesium naphthalenide, were suitable for the polymerization of *N*,*N*-dimethlacrylamide (DMAAm), which afforded the monodispersed PDMAAm with a low PDI.[33] Nakahama and Ishizone et al. have successfully

expanded the applicable acrylamide monomers to DMAAm,[34-36] *N*,*N*-diethylacrylamide (DEAAm),[35-38] *N*,*N*-di-*n*-propylacrylamide (D*n*PAAm),[36] *N*-ethylmethylacrylamide (EMAAm),[36] *N*-acryloylpyrrolidine (APY),[36] *N*-acryloylpiperidine (API),[36] *N*-acryloylmorpholine (NAM),[36] *N*-acryloyl-2-methylaziridine,[39] *N*-acryloylazetidine,[39] and *N*-methoxymethyl-*N*-isopropylacryl-amide,[40] using the combination of a strong nucleophile, such as diphenylmethyl potassium as the initiator, and weak Lewis acids of triethylborane (Et_3B) and triethylzinc (Et_3Zn) as additives (Scheme 1-2). However, broadening the application by anionic polymerization has still been a challenging task due to the difficulty of anionic polymerization involving severe polymerization conditions and limitation of the initiating system.

Scheme 1-2. Anionic polymerization of acrylamide monomers

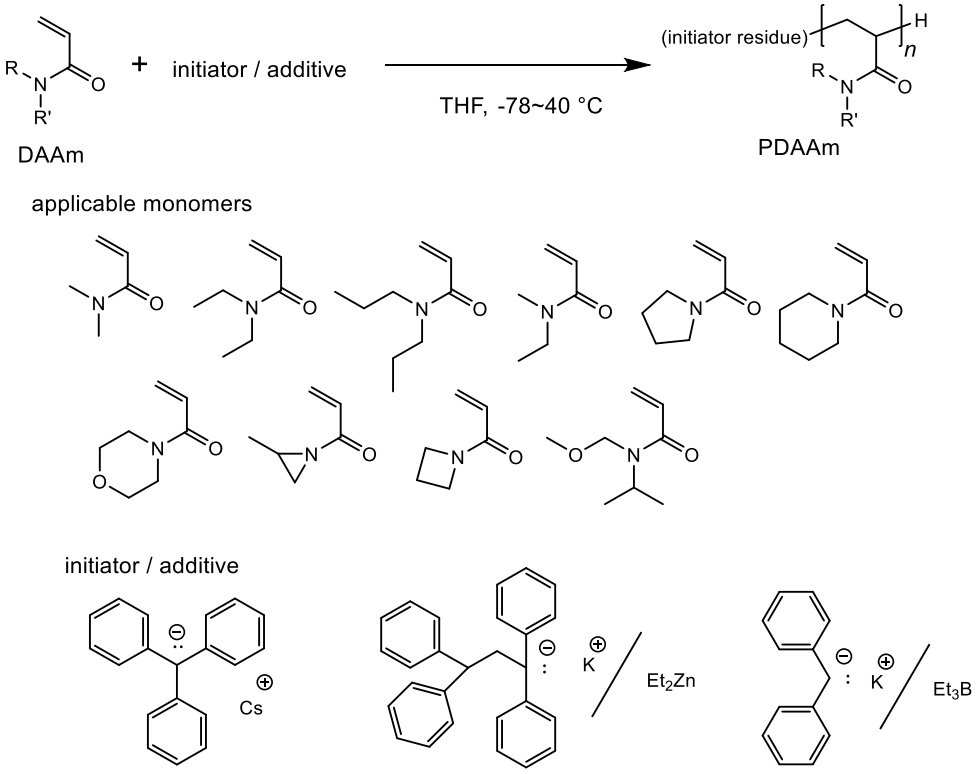

1.2.3. Synthesis of complex macromolecular architecture by controlled/living polymerizations

The progress in controlled/living polymerization techniques has been able to tailor the complex macromolecular architectures, such as the block copolymer, graft, star-shape, and cyclic polymers.[18,41-47] The living nature has been used to synthesize the block copolymers, which can be afforded by the addition of different monomers after completion of the first polymerization. However, the block copolymer synthesis using the sequential monomer addition has been limited to the block copolymer with a similar polymer backbone due to the difference in the monomer reactivity. Apart from utilizing the living nature to design the macromolecular architecture, functionalization of the polymer chain ends is one of the key techniques for preparing complex macromolecular architectures, which enables easy access to various macromolecular architectures by the following coupling reaction or transformation of the functional groups. The synthesis of end-functionalized polymers has been established through the design of initiators and terminators depending on the polymerization characteristics.[48] Especially, the ATRP and RAFT polymerizations have been widely used to synthesize the end-functionalized polymer due to the easy design of the initiator and transformation of the ω-chain ends.

For the synthesis of an acrylamide polymer with a complex macromolecular architecture, star-shaped and cyclic acrylamide polymers have been synthesized by the ATRP and RAFT polymerization methods. For example, Whittaker et al. reported the thermoresponsive behavior of the four-arm star-shaped PNIPAM synthesized using the core-first synthesis RAFT polymerization (Scheme 1-3a).[49] Liu et al. synthesized seven- and twenty-one-armed PNIPAMs by ATRP using cyclodextrin-based initiators and cyclic-PNIPAM by the combination of ATRP and the azide-alkyne cycloaddition reaction (click reaction) of the telechelic PNIPAM with an alkyne group at the α-chain end and an azide group at the ω-chain end (Scheme 1-3b).[50-51] Winnik

et al. synthesized cyclic-PNIPAM by combination of the RAFT polymerization and click reaction of the telechelic PNIPAM with an azide group at the α-chain end and an alkyne group at the ω-chain end (Scheme 1-3c).[53,54] The thermoresponsive properties of these synthesized PNIPAMs were investigated and compared to the corresponding linear counterparts. However, no comprehensive evaluation of the topological effect on the thermoresponsive behavior has been systematically investigated.

Scheme 1-3. Synthesis of star-shaped and cyclic acrylamide polymers by CRP methods

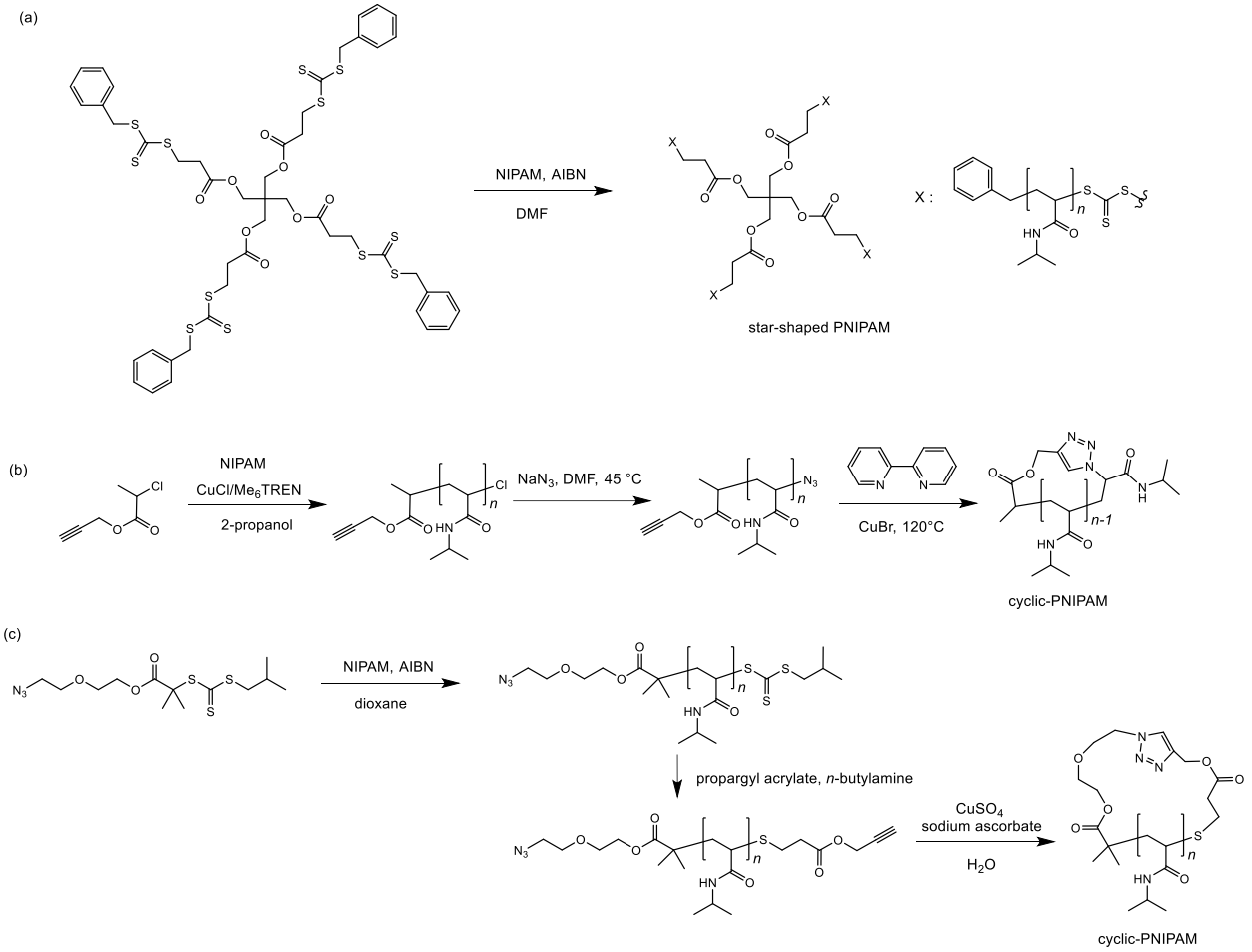

1.3. Group transfer polymerization

1.3.1. Conventional group transfer polymerization

Group transfer polymerization (GTP), a class of anionic polymerization methods, proceeds through numerous iterations of the Mukaiyama-Michael reaction between the monomer and active polymer chain end of the silyl enolate moiety (scheme 1-4).[55-57] Since Webster and coworkers established the concept of GTP in 1983, many efforts have been made to precisely control the polymerizations of (meth)acrylates, leading to well-defined polymers. 1-Methoxy-1-trimethylsiloxy-2-methyl-1-propene (SKA^{Me}), one of the most traditionally used silyl ketene acetals, was generally used as an initiator, and Lewis bases, such as the tris(dimethylamino)sulfonium (TAS) or tetra-*n*-butylammonium (TBA) salts of the hydrogen bifluoride anion (HF_2^-), cyanide anion (CN^-), azide anion (N_3^-), and carboxylate anion (AcO^-), and Lewis acids, such as zinc halides and alkyl aluminum, have been used as the catalyst for the conventinal GTP (Scheme 1-4).[55-59] Because the active center at the polymer chain ends capped by a tri-alkyl silyl group is less reactive and more stable than the enolate anion during the typical anionic polymerization, the GTP system can be implemented under ambient temperature conditions without any undesirable side reactions, which is of great advantage compared to the typical anionic polymerization. However, the conventional GTP had not been extensively developed due to the limitation of the applicable monomer and molecular weight controllability.

Scheme 1-4. A general illustration of group transfer polymerization

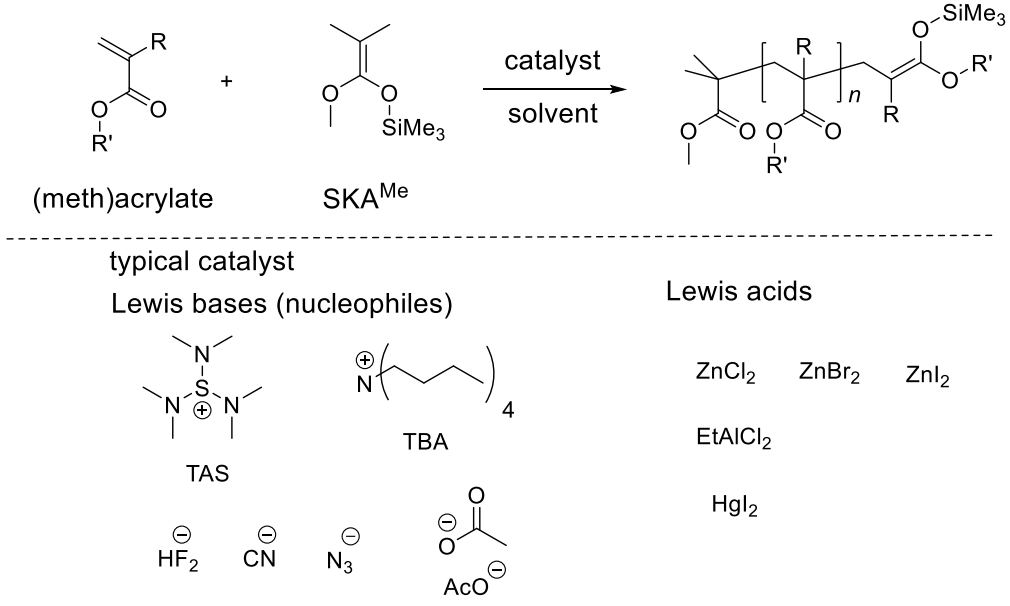

1.3.2. Advanced group transfer polymerization using an organocatalyst

A breakthrough in the GTP technique has been achieved using an organocatalyst in 2008.[60] Taton et al. and Waymouth et al. independently reported the GTP of methyl methacrylate (MMA) and alkyl acrylate using *N*-heterocyclic carbene (NHC) as an organocatalyst.[61-64] In addition, Taton et al. found that a phosphine Lewis base was efficient for the GTP of (meth)acrylates.[65] Chen et al. first achieved the GTP of MMA and alkyl acrylate using organic acids, such as the Lewis acid of the triphenylmethyl salts and the Brønsted acid of List's sulfonamide.[66-68] Kakuchi et al. also made contributions to the GTP using organic bases and organic acids (Scheme 1-5). For example, the phosphazene base, 1-*tert*-butyl-4,4,4-tris(dimethylamino)-2,2-bis-[tris(dimethylamino)-phosphoranylidenamino]-2Λ^5,4Λ^5catenadi (phosphazene) (*t*-Bu-P_4), as a very strong organic base was an extremely efficient catalyst for the synthesis of the poly(methyl methacrylate)s (PMMAs).[69] In addition, super strong Brønsted acids, such as trifluoromethanesulfonimide ($HNTf_2$) and pentafluorophenylbis(triflyl)methane ($C_6F_5CHTf_2$),[70,71] and the Lewis acid, such as *N*-(trimethylsilyl)triflylimide (Me_3SiNTf_2),[72,73] could promote the GTP of methacrylates and

acrylates using SKA^{Me} for the methacrylate and 1-methoxy-1-(triisopropyl siloxy)-2-methyl-1-propene (SKA^{iPr}) for the acrylate, affording well-controlled polymethacrylates and polyacrylates without any obvious side reactions.

The organocatalyzed GTP system can be used to control the primary structures of polymers and synthesize complex macromolecular architectures. For example, Kakuchi et al. reported the syntheses of α,ω-end-functionalized PMMA and poly(*n*-butylacrylate) using designed initiators and 2-phenyl acrylate derivatives, which were structurally defect-free end-functionalized polymers.[74-76] In architectural design, the core-first synthesis of the star-shaped PMMA was successfully achieved using a multi-functional initiator.[72,77]

Scheme 1-5. Organocatalyzed-GTP for methacrylates and acrylates

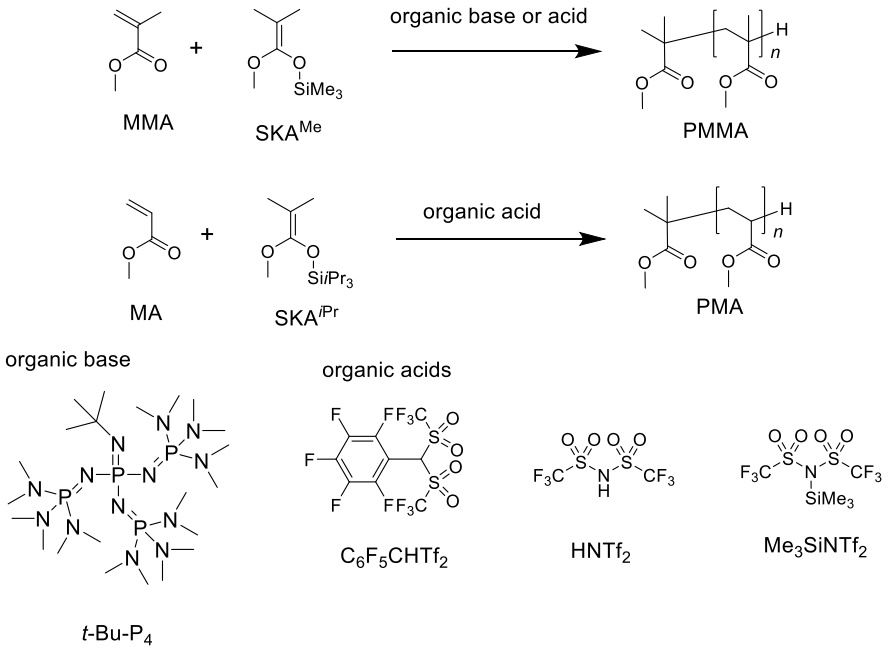

1.3.3. Group transfer polymerization for acrylamide monomers

Although the conventional GTP of acrylamide has been attempted using typical GTP catalysts, such as TAS-HF_2 and TBA-AcO, it was very hard to synthesize a well-defined acrylamide

polymer.[78-80] For example, Sogah et al. synthesized PDMAAm with the M.W. of 2.0 kg mol^{-1} and PDI of 1.62, using SKA^{Me} as the initiator and TAS-HF_2 as the catalyst. Fraitag et al. obtained PDEAAm with the M.W. of < 3.0 kg mol^{-1} and PDI below 1.20 using SKA^{Me} as the initiator and TAS-AcO as the catalyst.

The organocatalyzed-GTP system has significantly contributed to the synthesis of well-defined acrylamide polymers. Taton et al. first achieved the syntheses of the PDMAAm and acrylamide-methacrylate block copolymer using the initiating system of NHC and SKA^{Me} (Scheme 1-6a).[63,64] In addition, Kakuchi et al. found that the combination of the organic acid of $HNTf_2$ and $C_6F_5CHTf_2$, and the silyl ketene aminal (SKAm) of (*Z*)-1-dimethylamino-1-trimethylsiloxy-1-propene was a suitable initiating system for the GTP of DMAAm leading to the well-defined PDMAAms (Scheme 1-6b).[81,82] However, the synthesis of acrylamide polymers by the organocatalyzed-GTP has been limited to a few papers, which reported only the synthesis of PDMAAm, in spite of great potential for producing well-defined acrylamide polymers.

Scheme 1-6. Organocatalyzed-GTP for DMAAm

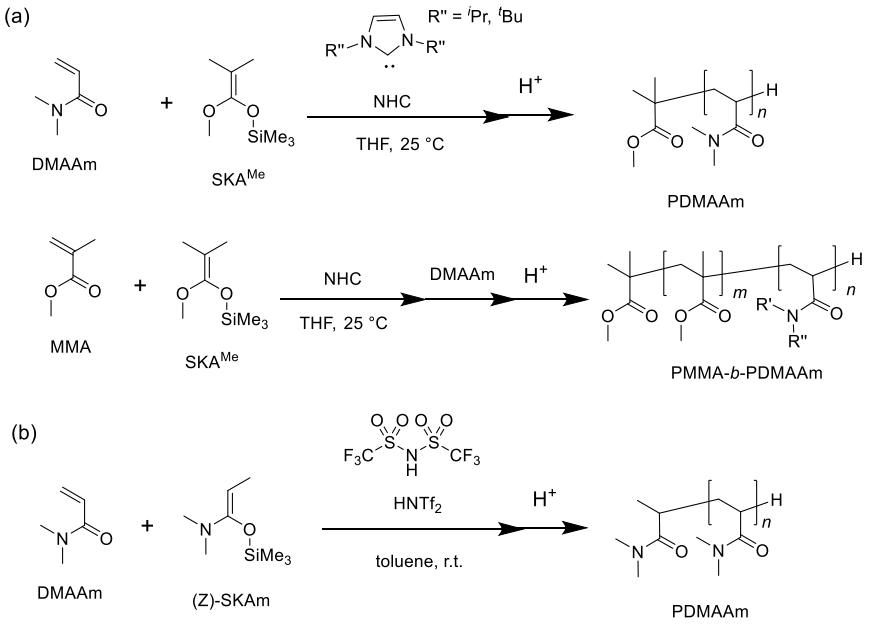

1.4. Objectives and outline of this thesis

As already described, the acrylamide polymer is a sort of functional material leading to various applications due to the variable properties related to its *N*-substituents. Among the acrylamide polymers, those with moderately bulky *N*-substituents show a temperature-dependent reversible solubility in aqueous media, that is, one of the thermoresponsive polymers. For accurate evaluation of the inherent thermoresponsive properties of the polymers and control for the desired property, controlled/living polymerization techniques for the preparation of well-defined acrylamide polymers with controlled molecular weights, narrow polydispersities, and no structural defects, have been highly required, though they have been extensively used for other polar vinyl monomers, such as methacrylates and acrylates.

The recent progress in the GTP using an organocatalyst, a class of controlled/living polymerizations, has enabled reseachers to synthesize PDMAAm. Although this organocatalyzed-GTP has been expected to have a great potential for preparing various acrylamide polymers, the synthesis of the acrylamide polymer using GTP has been limited to a few papers. Thus, this thesis will focus on the development of a powerful GTP method, aiming to establish the initiating system of GTP for the acrylamide monomer, expand the applicable monomer, and control the primary structure.

The following is an outline of this thesis.

Chapter 2 describes the GTP of DAAm using various combinations of organic acids and silyl ketene acetals (SKAs) for establishing an efficient initiating system to synthesize acrylamide polymers (Scheme 1-7). Among the candidates for the catalyst and the initiator, the combination of tris(pentafluorophenyl)borane ($B(C_6F_5)_3$) and 1-methoxy-1-(triethylsiloxy)-2-methyl-1-propene (SKA^{Et}) afforded a relatively better control over the molecular weight distribution. The

polymerization behavior of DEAAm using $B(C_6F_5)_3$ and SKA^{Et} was then intensively investigated in terms of the polymerization kinetics, chain extension experiments, and MALDI-TOF MS analyses, by which the polymerization was proven to proceed in a living fashion. The $B(C_6F_5)_3$-catalyzed GTP was further extended to various DAAms. Finally, the livingness of the polymerization was used to synthesize the acrylamide-acrylamide block copolymers and methacrylate-acrylamide hetero block copolymers.

Scheme 1-7

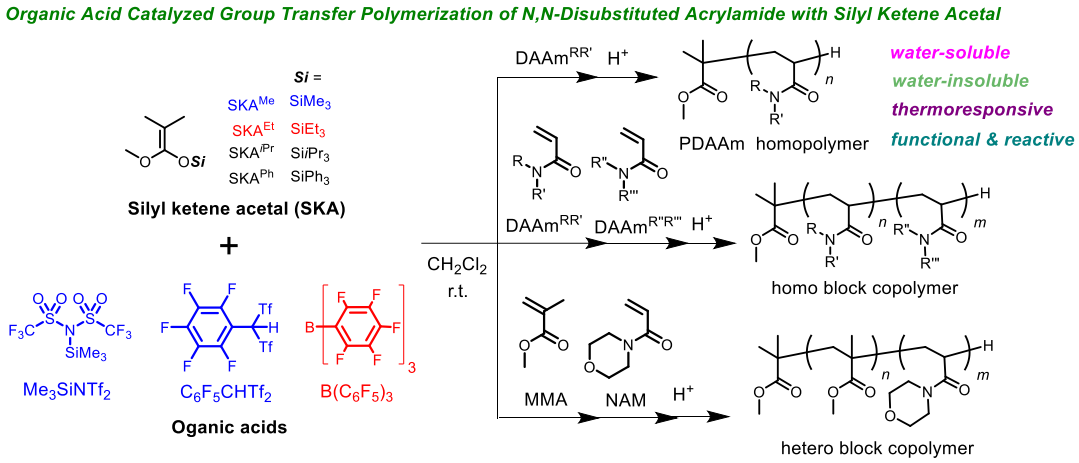

Chapter 3 describes the synthesis of the linear, cyclic, and star-shaped PDEAAms in order to clarify the topologycal effect on their thermoresponsive properties (Scheme 1-8). For the GTP of DEAAm using $B(C_6F_5)_3$ as the organocatalyst, the α-, ω-, and α,ω-end-functionalizations of the PDEAAms with well-controlled molecular weights and narrow polydispersities were quantitatively produced using the SKAms with hydroxyl, ethynyl, and vinyl groups as the functional initiators and 2-phenyl acrylate derivatives with hydroxyl, ethynyl, and bromo groups as the functional terminators. The ω-end-functionalized PDEAAm with the azido group and the α,ω-end-functionalized PDEAAm with the ethynyl and azido groups were used as the starting materials for the inter- and intramolecular copper(I)-catalyzed click reactions leading to the 3-armed star-shaped and cyclic PDEAAms (s_3-PDEAAm and *c*-PDEAAm, respectively). In order to eliminate the unit effect of the triazole (*taz*) group on the thermoresponsive behavior, the linear

PDEAAm with the *taz* group at the center of the polymer chain (*l*-*taz*-PDEAAm) was prepared by the click reaction between the end-functionalized PDEAAm with the ethynyl group and that with the azido group. The thermoresponsive property of these PDEAAms was evaluated by the cloud point (T_c) determined by the turbidity measurements and the enthalpy changes (ΔH) of water molecules per molar monomer unit by highly sensitive differential scanning calorimetry (micro-DSC) measurements. In addition, a molecular dynamics (MD) simulation of the PDEAAms corresponding to the synthesized polymer structures was carried out in order to evaluate the topological effect on a molecular scale.

Scheme 1-8

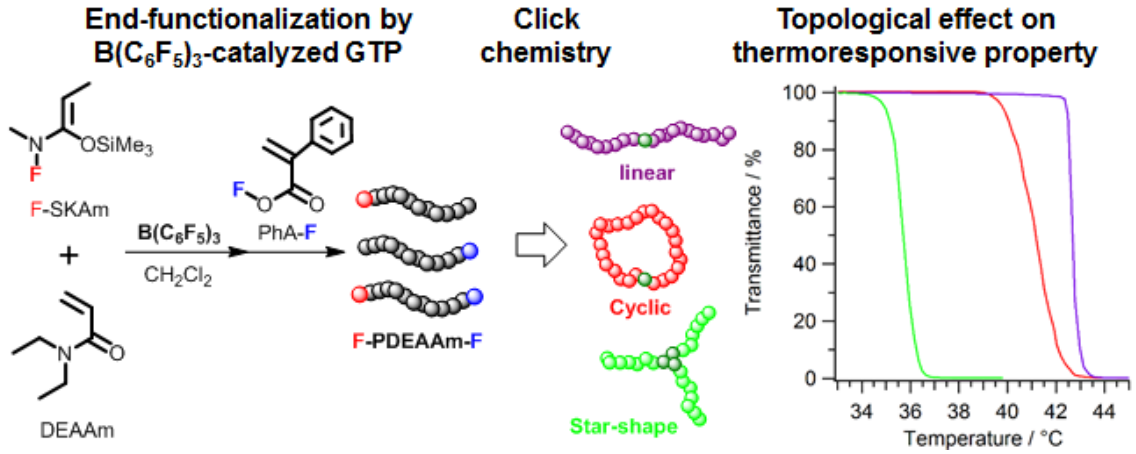

Chepter 4 describes the $B(C_6F_5)_3$-catalyzed GTP of DAAm using a moisture-tolerant hydrosilane (H*Si*) as part of the initiator, which the $B(C_6F_5)_3$ promoted the *in situ* synthesis of the true-initiator by the 1,4-hydrosilation of DAAm with *H*Si (Scheme 1-9). The screening experiment using various H*Si*s suggested that dimethylethylsilane (Me_2EtSiH) with the lowest steric bulkiness was the most appropriate reagent for the polymerization control. The chemical structure of the DAAms significantly affected the livingness of the polymerization. For instance, the polymerization of DEAAm using Me_2EtSiH only showed better control over the molecular

weight distribution, while that of NAM with a more obstructive side group using the same H*Si* afforded precise control of the molecular weight as well as its distribution. Given that the entire polymerization was composed of the monomer activation, the *in situ* formation of a silyl ketene aminal as the true initiator by the 1,4-hydrosilylation of DAAm, and the GTP process, the polymerization mechanism was discussed in detail. Finally, the convenient α-end-functionalization of PDAAm was achieved by the *in situ* preparation of functional silyl ketene aminals through the 1,4-hydrosilylation of functional methacrylamides, which has no polymerization reactivity in the Lewis acid-catalyzed GTP, followed by the Me_3SiNTf_2-catalyzed GTP of DAAms.

Scheme 1-9

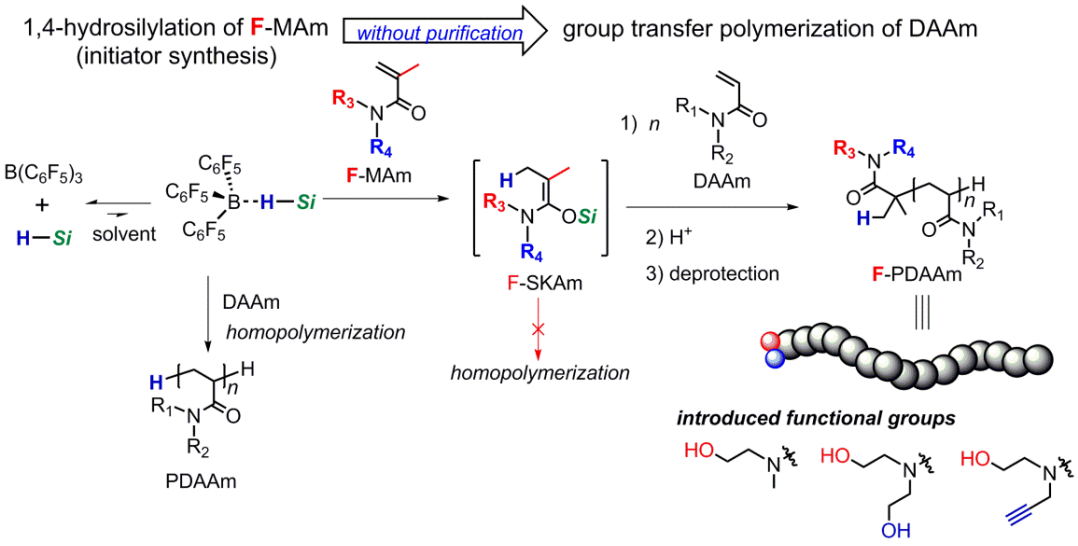

1.5. References and Notes

(1) Qian, J. W.; Xiang, X. J.; Yang, W. Y.; Wang, M.; Zheng, B. Q. *Eur. Polym. J.* **2004**, *40*, 1699-1704.

(2) Christensen, L. H. *Dermatologic Surgery* **2009**, *35*, 1612-1619.

(3) Wong, S. S.; Teng, T. T.; Ahmad, A. L.; Zuhairi, A.; Najafpour, G. *J. Hazardous Mater.* **2006**, *135*, 378-388.

(4) Cao, Y.; Zhu, X. X.; Luo, J.; Liu, H. *Macromolecules* **2007**, *40*, 6481-6488.

(5) Schild, H. G. *Prog. Polym. Sci.* **1992**, *17*, 163-249.

(6) Liu, H. Y.; Zhu, X. X. *Polymer* **1999**, *40*, 6985-6990.

(7) Qiu, X. P.; Koga, T.; Tanaka, F.; Winnik, F. M. *Sci. China Chem.* **2013**, *56*, 56-64.

(8) Narumi, A.; Fuchise, K.; Kakuchi, R.; Toda, A.; Satoh, T.; Kawaguchi, S.; Sugiyama, K.; Hirao, A.; Kakuchi, T. *Macromol. Rapid Commun.* **2008**, *29*, 1126-1133.

(9) Xia, Y.; Burke, A. D.; Stover, H. D. H. *Macromolecules* **2006**, *39*, 2275-2283.

(10) Plummer, R.; Hill, D. J. T.; Whittaker, A. W. *Macromolecules*, **2006**, *39*, 8379-8388.

(11) Yusa, S.; Endo, T.; Ito, M. *J. Polym. Sci., Part A* **2009**, *47*, 6827-6838.

(12) Xu, J.; Liu, S. *J. Polym. Sci., Part A* **2009**, *47*, 404-419.

(13) Xu, J.; Ye, J.; Liu, S. *Macromolecules* **2007**, *40*, 9103-9110.

(14) Qiu, X.-P.; Tnaka, F.; Winnik, F. M. *Macromolecules* **2007**, *40*, 7069-7071.

(15) Szwarc, M.; Levy, M.; Milkovich, R. *J. Am. Chem. Soc.* **1956**, *78*, 2656-2657.

(16) Szwarc, M. *Science* **1970**, *170*, 23-32.

(17) Baskaran, D. *Prog. Polym. Sci.* **2003**, *28*, 521-281.

(18) Hadjichristidis, N.; Iatrou, H.; Pitsikalis, M.; Mays, J. *Prog. Polym. Sci*. **2006**, *31*, 1068-1132.

(19) Hawker, C. J.; Bosman, A. W.; Harth, E. *Chem. Rev.* **2001**, *101*, 3661-3688.

(20) Kamigaito, M.; Ando, T.; Sawamoto, M. *Chem. Rev.* **2001**, *101*, 3689-3746.

(21) Tsarevski, N. V.; Matyjaszewski, K. *Chem. Rev.* **2007**, *107* 2270-2299.

(22) Lowe, A. B.; McCormick, C. L. *Prog. Polym. Sci.* **2006**, *31*, 1068-1132.

(22) Aoshima, S.; Kanaoka, S. *Chem. Rev.* **2007**, *107* 2270-2299.

(23) Benoit, D.; Chaplinski, V.; Braslau, R.; Hawker, C. J. *J. Am. Chem. Soc.* **1999**, *121*, 3904-3920.

(24) Huang, X.; Wirth, M. J. *Macromolecules* **1999**, *32*, 1694-1696.

(25) Teodorescu, M.; Matyjaszewski, K. *Macromol. Rapid Commun.* **2000**, *21*, 190-194.

(26) Ganachaud, F.; Monteiro, M. J.; Gilbert, R. G.; Dourges, M. A.; Thang, S. H.; Rizzardo, E. *Macromolecules* **2000**, *33*, 6738-6745.

(27) Thomas, D. B.; Sumerlin, B. S.; Lowe, A. B.; McCormick, C. L. *Macromolecules* **2003**, *36*, 1436-1439.

(28) Neugebauer, D.; Matyjaszewski, K. *Macromolecules* **2003**, *36*, 2598-2603.

(29) Li, C.; Ma, Y.; Niu, H.; Zhang, H. *ACS Appl. Mater. Interfaces* **2015**, *7*, 27340-27350.

(30) Wan, L. S.; Yang, Y. F.; Tian, J.; Hu, M. X.; Xu, Z. K. *J. Membrane Sci.* **2009**, *327*, 174-181.

(31) Convertine, A. J.; Lokitz, B. S.; Lowe, A. B.; Scales, C. W.; Myrick, L. J.; McCormick, C. L. *Macromol. Rapid Commun.* **2005**, *26*, 791-795.

(32) Ahmed, M.; Bhuchar, N.; Ishihara, K.; Narain, R. *Bioconjugate Chem.* **2011**, *22*, 1228-1238.

(33) Xie, X.; Hogen-Esch, T. E. *Macromolecules* **1996**, *29*, 1746-1752.

(34) Kobayashi, M.; Ishizone, T.; Nakahama, S. *Macromolecules* **2000**, *33*, 4411-4416.

(35) Kobayashi, M.; Okuyama, S.; Ishizone, T.; Nakahama, S. *Macromolecules* **1999**, *32*, 6466-6477.

(36) Kobayashi, M.; Ishizone, T.; Nakahama, S. *J. Polym. Sci., Part A: Polym. Chem.* **2000**, *38*, 4677-4685.

(37) Ishizone, T.; Yashiki, D.; Kobayashi, M.; Suzuki, T. Ito, M. Nakahama, S. *J. Polym. Sci., Part A: Polym. Chem.* **2007**, *45*, 1260-1271.

(38) Suzuki, T.; Kusakabe, J.; Ishizone, T. *Macromolecules* **2008**, *41*, 1929-1936.

(39) Suzuki, T.; Kusakabe, J.; Kitazawa, K.; Nakagawa, T.; Kawauchi, S.; Ishizone, T. *Macromolecules* **2010**, *43*, 107-116.

(40) Ito, M.; Ishizone, T. *J. Polym. Sci., Part A: Polym. Chem.* **2006**, *44*, 4832-4845.

(41) Gao, H.; Matyjaszewski, K. *Macromolecules* **2006**, *39*, 3154-3160.

(42) Mayadunne, R. T. A.; Jeffery, J.; Moad, G.; Rizzardo, E. *Macromolecules* **2003**, *36*, 1505-

1513.

(43) Schappacher, M.; Deffieux, A. *Macromolecules* **2001**, *34*, 5827-5832.

(44) Laurent, B. A.; Grayson, S. M. *J. Am. Chem. Soc.* **2006**, *128*, 4238-4239.

(45) Lonsdale, D. E.; Bell, C. A.; Monteiro, M. J. *Macromolecules* **2010**, *43*, 3331-3339.

(46) Hoskins, J. N.; Grayson, S. M. *Macromolecules* **2009**, *42*, 6406-6413.

(47) Ito, S.; Goseki, R.; Ishizone, T.; Hirao, A. *Polym. Chem.* **2014**, *5*, 5523-5534.

(48) Tasdelen, M. A.; Kahveci, M. U.; Yagci, Y. *Prog. Polym. Sci.* **2011**, *36*, 455-567.

(49) Plummer, R.; Hill, D. J. T.; Whittaker, A. W. *Macromolecules*, **2006**, *39*, 8379-8388.

(50) Xu, J.; Liu, S. *J. Polym. Sci., Part A: Polym. Chem.* **2009**, *47*, 404-419.

(51) Xu, J.; Ye, J.; Liu, S. *Macromolecules* **2007**, *40*, 9103-9110.

(52) Ye, J.; Xu, J.; Hu, J.; Wang, X.; Zhang, G.; Liu, S.; Wu, C. *Macromolecules* **2008**, *41*, 4416-4422.

(53) Qiu, X.-P.; Tnaka, F.; Winnik, F. M. *Macromolecules* **2007**, *40*, 7069-7071.

(54) Satokawa, Y.; Shikata, T.; Tnaka, F.; Qiu, X.-P.; Winnik, F. M. *Macromolecules* **2009**, *42*, 1400-1403.

(55) Webster, O. W.; Hertler, W. R.; Sogah, D. Y.; Farnham W. B.; RajanBabu, T. V. *J. Am. Chem. Soc.* **1983**, *105*, 5706-5708.

(56) Sogah, D. Y.; Hertler, W. R.; Webster, O. W.; Cohen, G. M. *Macromolecules* **1987**, *20*, 1473-1488.

(57) Hertler, W. R.; Sogah, D. Y.; Webster, O. W.; Trost, B. M. *Macromolecules* **1984**, *17*, 1415-1419.

(58) Zhuang, R.; Müller, A. H. E. *Macromolecules* **1995**, *28*, 8035-8042.

(59) Zhuang, R.; Müller, A. H. E. *Macromolecules* **1995**, *28*, 8043-8050.

(60) Fuchise, K.; Chen, Y.; Satoh, T.; Kakuchi, T. *Polym. Chem.* **2013**, *4*, 4278-4291.

(61) Raynaud, J.; Ciolino, A.; Beceiredo, A.; Destarac, M.; Bonnette, F.; Kato, T.; Gnanou, Y.; Taton, D. *Angew. Chem. Int. Ed.* **2008**, *47*, 5390-5393.

(62) Scholten, M. D.; Hedrick, J. L.; Waymouth, R. M. *Macromolecules* **2008**, *41*, 7399-7404.

(63) Raynaud, J.; Liu, N.; Gnanou, Y.; Taton, D. *Macromolecules* **2009**, *42*, 5996-6005.

(64) Raynaud, J.; Liu, N.; Fèvre, M.; Gnanou, Y.; Taton, D. *Polym. Chem.* **2011**, *2*, 1706-1712.

(65) Fèvre, M.; Vignolle, J.; Heroguez, V.; Taton, D. *Macromolecules* **2012**, *45*, 7711-7718.

(66) Zhang, Y.; Chen, E. Y.-X. *Macromolecules* **2008**, *41*, 36-42.

(67) Zhang, Y.; Chen, E. Y.-X. *Macromolecules* **2008**, *41*, 6353-6360.

(68) Zhang, Y.; Lay, F.; García, P. G.; List, B.; Chen, E. Y.-X. *Chem. Eur. J.* **2010**, *16*, 10462-10473.

(69) Kakuchi, T.; Chen, Y.; Kitakado, J.; Mori, K.; Fuchise, K.; Satoh, T. *Macromolecules*, **2011**, *44*, 4641-4647.

(70) Kakuchi, R.; Chiba, K.; Fuchise K.; Sakai, R.; Satoh, T.; Kakuchi, T. *Macromolecules* **2009**, *42*, 8747-8750.

(71) Takada, K.; Fuchise, K.; Chen, Y.; Satoh, T.; Kakuchi, T. *J. Polym. Sci. Part A: Polym. Chem.* **2012,** *50*, 3560-3566.

(72) Chen, Y.; Takada, K.; Fuchise, K.; Satoh, T.; Kakuchi, T. *J. Polym. Sci. Part A: Polym. Chem.* **2012**, *50*, 3277-3285.

(73) Takada, K.; Ito, T.; Kitano, K.; Tsuchida, S.; Takagi, Y.; Chen, Y.; Satoh, T.; Kakuchi, T. *Macromolecules* **2015**, *48*, 511-519.

(74) Takada, K.; Fuchise, K.; Kubota, N.; Ito, T.; Chen, Y.; Satoh, T.; Kakuchi, T. *Macromolecules* **2014**, *47*, 5514-5525.

(75) Chen, Y.; Takada, K.; Kubota, N.; Eric, O.-T., Ito, T.; Isono, T.; Satoh, T.; Kakuchi, T.

Polym.Chem. **2015**, *6*, 1830-1837.

(76) Eric, O.-T.; Chen, Y.; Takada, K.; Sato, S.; Satoh, T.; Kakuchi, T. *Polym.Chem.* **2015**, *6*, 7841-7850.

(77) Chen, Y.; Fuchise, K.; Narumi, A.; Kawaguchi, S.; Satoh, T.; Kakuchi, T. *Macromolecules*, **2011**, *44*, 9091-9098.

(78) Eggert, M.; Freitag, R. *J. Polym. Sci., Part A: Polym. Chem.* **1994**, *32*, 803-813.

(79) Freitag, R.; Baltes, T.; Eggert, M. *J. Polym. Sci., Part A: Polym. Chem.* **1994**, *32*, 3019-3030.

(80) Baltes, T.; Garret-Flaudy, F.; Freitag, R. *J. Polym. Sci., Part A: Polym. Chem.* **1999**, *37*, 2977-2989.

(81) Fuchise, K.; Sakai, R.; Satoh, T.; Sato, S.; Narumi, A.; Kawaguchi, S.; Kakuchi, T. *Macromolecules* **2010**, *43*, 5589-5594.

(82) Fuchise, K.; Chen, Y.; Takada, K.; Satoh, T.; Kakuchi, T. *Macromol. Chem. Phys.* **2012**, *213*, 1604-1611.

Chapter 2

Organic Acids as Efficient Catalyst for Group Transfer Polymerization of *N*,*N*-Disubstituted Acrylamide with Silyl Ketene Acetal; Polymerization Mechanism and Synthesis of Diblock Copolymers

2.1. Introduction

Polyacrylamides are a one of important polymer materials for industrial applications, such as flocculants,[1] viscosifiers for oil recovery, and subdermal fillers for aesthetic facial surgery. [2] Although most of the industrial polyacrylamide products have been undoubtedly prepared by conventional radical polymerizations, the precise, efficient, and green synthesis of such polyacrylamides is still an interesting subject from the viewpoint of polymer synthesis. The living polymerization of various acrylamides has been achieved by the living/controlled radical polymerizations (CRPs), such as atom transfer radical polymerization,[3,4] nitroxide-mediated radical polymerization, [5] and reversible addition-fragmentation chain transfer (RAFT) polymerization, [6-8] or anionic polymerization. These CRPs are applicable to acrylamide, *N*-monosubstituted acrylamide, and *N*,*N*-disubstituted acrylamide (DAAm) except for those bearing radical-sensitive groups, such as *N*-allyl acrylamide and *N*-2-thioethyl acrylamide. On the other hand, anionic polymerization is only suitable for DAAs without any anion-sensitive groups though applicable DAAms are limited to *N*,*N*-dimethylacrylamide (DMAAm),[9-11] *N*,*N*-diethylacrylamide (DEAAm),[10-13] *N*,*N*-di-*n*-propylacrylamide (D*n*PAAm),[11] *N*-ethylmethylacrylamide (EMAAm),[11] *N*-acryloylpyrrolidine (APY),[11] *N*-acryloylpiperidine (API),[11] *N*-acryloylmorpholine (NAM),[11] *N*-acryloyl-2-methylaziridine,[14] *N*-acryloylazetidine,[15] *N*-methoxymethyl-*N*-isopropylacryl-amide,[16] *N*-propyl-*N*-(3-triisopropoxysilylpropyl)acryl-amide,[17] and *N*-propyl-*N*-(3-triethoxysilylpropyl)-acrylamide.[17] Nevertheless, the anionic polymerization of DAAm is still the most reliable method for the precise synthesis of the structurally defect-free acrylamide polymers because the CRPs inevitably cause side reactions due to radical transfers. Hence, the author turned our attention to the GTP, one of the anionic polymerization methods, which is principally suitable for acrylic monomers.[18-21] The living

polymer chain-ends capped by silyl groups in the GTP process are much less reactive than the living anions during the anionic polymerization processes, which is one of the reasons why the GTP proceeds at a moderate temperature and is tolerant to functional moieties, such as vinyl and epoxy groups.[22, 23] In particular, the use of organocatalysts for the GTP of methacrylate and acrylate monomers has significantly improved the livingness of the polymerizations leading to well defined polymers with high molecular weights. [24-34] In addition, organocatalysts significantly improved the controlled/living characteristics for the GTP of acrylamides compared to previous methods those using conventional catalysts; [18,19,35-37] for example, Kakuchi and coworker reported that organic Brønsted acids, such as bis(trifluoromethanesulfonyl)imide ($HNTf_2$) and 1-(2,3,4,5,6-pentafluorophenyl)-1,1-bis(trifluoromethanesulfonyl)methane ($C_6F_5CHTf_2$), were used for the controlled GTP of DMAAm with a silyl ketene aminal of (*Z*)-1-dimethylamino-1-trimethylsiloxy-1-propene ((*Z*)-SKAm) as the initiator to produce poly(*N*,*N*-dimethylacrylamide)s (PDMAAms) with molecular weights up to 53.9 kg mol^{-1} and polydispersities of less than 1.06, which was the first report to achieve the living polymerization of DAAm in the GTP chemistry.[38,39] Furthermore, Taton and Gnanou reported that *N*-heterocyclic carbene was used as an efficient organocatalyst for the GTP of DMAAm and the block GTP of DMAAm and methyl methacrylate to produce tailored PDMAAms and diblock copolymers.[40,41] Thus, of great importance is to elucidate the scope and limit for the GTP of DAAm in terms of applicable monomers, available organocatalysts, and initiator design. For example, it is interesting to expand the applicable monomers, such as the DAAs with nucleophilic hetero atoms of oxygen, nitrogen, and sulfur, because these atoms would deactivate the true catalytic species of a silylium cation. In addition, the $HNTf_2$-catalyzed GTP of DMAAm required the use of the silyl ketene aminal though its synthesis turned out to be more difficult than a silyl ketene acetal (SKA), and the GTP with the silyl ketene aminal as the initiator could not be used to synthesize hetero block copolymers because the silyl ketene aminal group of

the growing polymer chain-end could not initiate the GTP of the methacrylate and acrylate monomers. Thus, the comprehensive study for the GTP of DAAm coupled with available organocatalysts and initiator design is still one of the challenging and remaining tasks in GTP chemistry.

In this chapter, the author describes the new efficient combinations of organic acids and SKAs for the GTPs of various DAAms, as shown in Scheme 2-1. This study describes: (1) the evaluation of the combinations of organic acids and SKAs for the GTP of DEAAm, (2) the investigation of the livingness and mechanism of the $B(C_6F_5)_3$-catalyzed GTP of DAAms, (3) the monomer expansion, and (4) the synthesis of polyacrylamide-*b*-polyacrylamide homo and polymethacrylate-*b*-polyacrylamide hetero block copolymers.

Scheme 2-1. Syntheses of homo acrylamide polymers, homo acrylamide block copolymers, and hetero block copolymers by organic acid-catalyzed group transfer polymerization method.

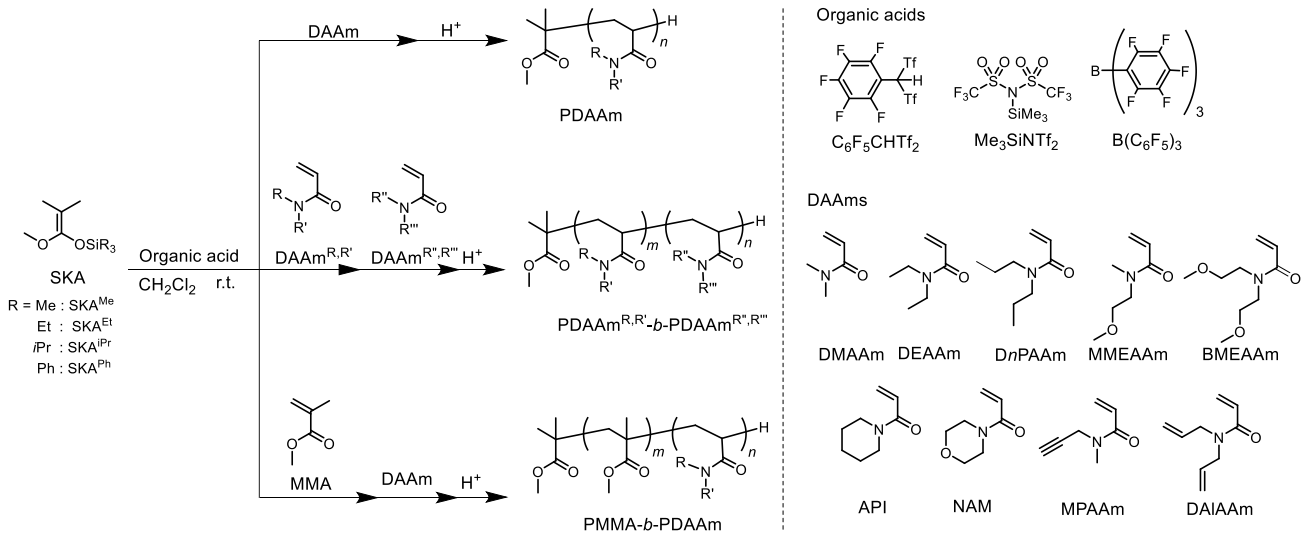

2.2. Experimental Section

Materials. Dichloromethane (CH_2Cl_2, >99.5%; water content, <0.001%), methanol (MeOH), and deuterated chloroform ($CDCl_3$, > 99.8%) were purchased from Kanto Chemicals Co., Inc. DEAAm, 1-methoxy-1-trimethyl-siloxy-2-methyl-1-propene (SKA^{Me}), *N*-(trimethylsilyl)bis-(trifluoromethanesulfonyl)imide (Me_3SiNTf_2), 1-(2,3,4,5,6-pentafluorophenyl)-1,1-bis(trifluoromethane-sulfonyl)methane ($C_6F_5CHTf_2$), *trans*-3-indoleacrylic acid, DMAAm, NAM, and methyl methacrylate (MMA) were purchased from Tokyo Kasei Kogyo Co., Ltd. 1-*tert*-Butyl-4,4,4-tris(dimethylamino)-2,2-bis[tris(dimethylamino)-phosphoranylidenamino]-2Λ^5,4Λ^5-catenadi(phosphazene) (*t*-Bu-P_4, 1.0 mol L^{-1} in *n*-hexane) and sodium trifluoroacetate were purchased from the Sigma-Aldrich Chemicals Co. Tris(pentafluorophenyl)borane ($B(C_6F_5)_3$) was purchased from Wako Pure Chemical Industries, Ltd., and was used after recrystallization from *n*-hexane at –30 °C. DEAAm, DMAAm, NAM, MMA, and CH_2Cl_2 were distilled from CaH_2, degassed by three freeze-pump-thaw cycles, and stored under an Ar atmosphere prior to use. 1-Methoxy-1-(triethylsiloxy)-2-methyl-1-propene (SKA^{Et}),[42] 1-methoxy-1-(triisopropyl siloxy)-2-methyl-1-propene (SKA^{iPr}), and 1-methoxy-1-(triphenylsiloxy)-2-methyl-1-propene (SKA^{Ph}) were synthesized according to previous reports.[43] The Spectra/Por® 6 Membrane (MWCO: 1000) was used for the dialysis. All other chemicals were purchased from available suppliers and used without purification.

Measurements. The ^1H (400 MHz) and ^{13}C NMR (100 MHz) spectra were recorded using a JEOL ECS400. The preparation of the polymerization solution was carried out in an MBRAUN stainless steel glove box equipped with a gas purification system (molecular sieves and copper catalyst) and a dry argon atmosphere (H_2O, O_2 <1 ppm). The moisture and oxygen contents in the glove

box were monitored by an MB-MO-SE 1 and MB-OX-SE 1, respectively. Size exclusion chromatography (SEC) in DMF containing lithium chloride (0.01 mol L^{-1}) was performed at 40 °C using a Jasco high performance liquid chromatography (HPLC) system (PU-980 Intelligent HPLC pump, CO-965 column oven, RI-930 Intelligent RI detector, and Shodex DEGAS KT-16) equipped with a Shodex Asahipak GF-310 HQ column (linear, 7.6 mm × 300 mm; pore size, 20 nm; bead size, 5 μm; exclusion limit, 4×10^4) and a Shodex Asahipak GF-7M HQ column (linear, 7.6 mm × 300 mm; pore size, 20 nm; bead size, 9 μm; exclusion limit, 4×10^7) at the flow rate of 0.6 mL min^{-1}. The $M_{n,SEC}$ and M_w/M_n of the obtained polymers were determined by the RI based on poly(methyl methacrylate) (PMMA) with the M_w (M_w/M_n)s of 1.25×10^6 g mol^{-1} (1.07), 6.59×10^5 g mol^{-1} (1.02), 3.003×10^5 g mol^{-1} (1.02), 1.385×10^5 g mol^{-1} (1.05), 6.015×10^4 g mol^{-1} (1.03), 3.053×10^4 g mol^{-1} (1.02), and 1.155×10^4 g mol^{-1} (1.04), 4.90×10^3 g mol^{-1} (1.10), 2.87×10^3 g mol^{-1} (1.06), and 1.43×10^3 g mol^{-1} (1.15), respectively. The matrix-assisted laser desorption/ionization time-of-flight mass spectrometry (MALDI-TOF MS) measurements were performed using an Applied Biosystems Voyager-DE STR-H mass spectrometer with a 25 kV acceleration voltage. The positive ions were detected in the reflector mode (25 kV). A nitrogen laser (337 nm, 3 ns pulse width, 106–107 W cm^{-2}) operating at 3 Hz was used to produce the laser desorption, and the 200 shots were summed. The spectra were externally calibrated using a sample prepared from narrow-dispersed polystyrene (Chemco Scientific Co., Ltd., M_n = 3.6 kg mol^{-1}, M_w/M_n = 1.08, 30 μL, 10 mg mL^{-1} in THF), the matrix (1,8-dihydroxy-9-(10*H*)-anthracenone, 30 mg mL^{-1}, 100 μL), and the cationizing agent (silver trifluoroacetate, 10 mg mL^{-1}, 15 μL) with a linear calibration. Samples for the MALDI-TOF MS were prepared by mixing the polymer (1.5 mg mL^{-1}, 10 μL), the matrix (*trans*-3-indoleacrylic acid, 10 mg mL^{-1}, 90 μL), and the cationizing agent (sodium trifluoroacetate, 10 mg mL^{-1}, 10 μL) in THF.

Synthesis of *N,N*-di-*n*-propylacrylamide (D*n*PAAm). To a suspension of di-*n*-propylamine

(25.0 mL, 182 mmol), 1-methylimidazole (1.37 mL, 17.3 mmol), *N*,*N*,*N'*,*N'*-tetramethyl-ethylenediamine (TMEDA, 2.58 mL, 17.3 mmol), and K_2CO_3 (25.2 g, 182 mmol) in acetonitrile (300 mL), acryloyl chloride (14.0 mL, 173 mmol) was added dropwise at 0 °C. After stirring for 6 h, the reaction mixture was filtered, and then condensed under reduced pressure. The crude product was purified by column chromatography (hexane:ethyl acetate = 2:1, R_f = 0.35) followed by distillation over CaH_2 under reduced pressure (50 °C/ 0.17 mmHg), affording *N*,*N*-di-*n*-propylacrylamide as a transparent liquid. Yield, 11.1 g (41.2 %). ^{1}H NMR (400 MHz, $CDCl_3$): δ (ppm) 0.78-0.88 (m, 6H, -C*H*$_3$), 1.45-1.58 (m, 4H, -C*H*$_2$CH$_3$), 3.15-3.29 (m, 4H, -NC*H*$_2$-), 5.52-5.59 (m, 1H, CH$_2$=C*H*-), 6.20-6.28 (m, 1H, *trans* C*H*$_2$=CH-), 6.42-6.52 (m, 1H, *cis* C*H*$_2$=CH-). ^{13}C NMR (100 MHz, $CDCl_3$): δ (ppm) 11.2, 11.5, 21.0, 22.9, 48.3, 49.8, 127.4, 127.9.

Synthesis of *N*-acryloylpiperidine (API). To a solution of piperidine (25.0 mL, 253 mmol), trimethylamine (42.0 mL, 303 mmol), and CH_2Cl_2 (300 mL), acryloyl chloride was added dropwise at 0 °C. After stirring for 16 h at r.t., the reaction mixture was extracted by 0.5N HCl, NaCl aq., and distilled water. Organic layer was dried over $MgSO_4$, and then condensed under reduced pressure. The crude product was purified by distillation using CaH_2 under reduced pressure (97 °C/ 6.0 mmHg), affording *N*-acryloylpiperidine as a transparent liquid. Yield, 9.79 g (29.3 %). ^{1}H NMR (400 MHz, $CDCl_3$): δ (ppm) 1.49-1.59 (m, 4H, -C*H*$_2$CH$_2$C*H*$_2$-), 1.59-1.67 (m, 2H, -CH$_2$C*H*$_2$CH$_2$-), 3.40-3.64 (m, 4H, -NC*H*$_2$-), 5.58-5.65 (m, 1H, CH$_2$=C*H*-), 6.17-6.25 (m, 1H, *trans* C*H*$_2$=CH-), 6.50-6.59 (m, 1H, *cis* C*H*$_2$=CH-). ^{13}C NMR (100 MHz, $CDCl_3$): δ (ppm) 24.6, 25.5, 26.6, 43.0, 47.0, 127.0, 128.1, 165.2.

Synthesis of *N*-methoxyethyl-*N*-methyl-acrylamide (MMEAAm). To a suspension of KOH (22.4 g, 400 mmol) in DMSO (200 mL), *N*-2-hydroxyethyl-*N*-methylacrylamide (11.5 g, 100 mmol) was added, and then iodomethane (24.9 mL, 400 mmol) was added at room temperature. After stirring for 30 min with exothermic reaction, reaction mixture was quenched by excess

amount of water followed by the extraction with ethyl acetate. The organic phase dried over anhydrous $MgSO_4$, and concentrated under reduced pressure. The crude product was purified by column chromatography (ethyl acetate, R_f = 0.31) and distillation from CaH_2 under reduced pressure (55-56 °C/ 0.10 mmHg), affording *N*-methoxyethyl-*N*-methyl-acrylamide as pale yellow solid. Yield, 3.46 g (24.2 %). ^{1}H NMR (400 MHz, $CDCl_3$): δ (ppm) 2.92, 3.04 (s, 3H, NC*H*$_3$), 3.23 (s, 3H, OC*H*$_3$), 3.37-3.53 (m, 4H, -C*H*$_2$C*H*$_2$-), 5.51-5.60 (m, 1H, CH_2=C*H*-), 6.15-6.24 (m, 1H, *trans* C*H*$_2$=CH-), 6.46-6.57 (m, 1H, *cis* C*H*$_2$=CH-). ^{13}C NMR (100 MHz, $CDCl_3$): δ (ppm) 34.5, 37.1, 48.0, 49.7, 58.8, 59.2, 70.6, 71.0, 127.4, 127.7, 127.8, 128.0, 166.3, 166.9. Anal. Calcd for $C_7H_{13}NO_2$ (143.18): C, 58.72; H, 9.15; N, 9.78. Found: C, 58.72; H, 9.23; N, 9.81.

Synthesis of *N,N*-bis(methoxyethyl)acrylamide (BMEAAm). The procedure of synthesis of D*n*PAA was applied to bis(methoxyethyl)amine (15.0 mL, 102 mmol), 1-methylimidazole (0.87 mL, 11.0 mmol), TMEDA (1.64 mL, 11.0 mmol), K_2CO_3 (34.5 g, 250 mmol), acetonitrile (200 mL), and acryloyl chloride (8.89 mL, 110 mmol). *N*,*N*-bis(methoxyethyl)acrylamide was obtained as transparent liquid purified by distillation using CaH_2 under reduced pressure (77 °C/ 0.03 mmHg). Yield, 6.08 g (32.5 %). ^{1}H NMR (400 MHz, $CDCl_3$): δ (ppm) 3.20 (s, 6H, OC*H*$_3$), 3.35-3.54 (m, 8H, -C*H*$_2$C*H*$_2$-), 5.50-5.57 (m, 1H, CH_2=C*H*-), 6.15-6.23 (m, 1H, *trans* C*H*$_2$=CH-), 6.50-6.59 (m, 1H, *cis* C*H*$_2$=CH-). ^{13}C NMR (100 MHz, CDCl3): δ (ppm) 47.0, 48.9, 58.7, 59.0, 71.0, 71.1, 127.6, 128.1, 166.6. Anal. Calcd for $C_9H_{17}NO_3$ (187.23): C, 57.73; H, 9.15; N, 7.48. Found: C, 57.42; H, 9.18; N, 7.48.

Synthesis of *N,N*-diallylacrylamide (DAlAAm). The procedure for the synthesis of API was applied to diallylamine (25.0 mL, 203 mmol), trimethylamine (36.6 mL, 264 mmol), CH_2Cl_2 (300 mL), and acryloyl chloride (14.8 mL, 183 mmol). *N*,*N*-diallylacrylamide was obtained as a transparent liquid purified after distillation over CaH_2 under reduced pressure (61 °C/ 0.07 mmHg). Yield, 14.7 g (53.2 %). ^{1}H NMR (400 MHz, $CDCl_3$): δ (ppm) 3.85-4.10 (m, 4H, -NC*H*$_2$-),

5.05-5.25 (m, 4H, -$CH_2CH=CH_2$), 5.60-5.70 (m, 1H, $CH_2=CH$-), 5.70-5.85 (m, 2H, -$CH_2CH=CH_2$), 6.30-6.40 (m, 1H, *trans* CH_2=CH-), 6.40-6.50 (m, 1H, *cis* CH_2=CH-). ^{13}C NMR (100 MHz, $CDCl_3$): δ (ppm) 48.5, 49.2, 116.9, 117.6, 127.7, 128.4, 132.9, 133.1, 166.5. Anal. Calcd for $C_9H_{13}NO$ (151.21): C, 71.49; H, 8.67; N, 9.25. Found: C, 71.08; H, 8.77; N, 9.18.

Synthesis of *N*-propargylacrylamide. To a solution of propargylamide (13.0 mL, 204 mmol), *N*,*N*-dimethylaminopyridine (2.44 g, 20.0 mmol), and CH_2Cl_2 (150 mL), acryloyl chloride was added dropwise at 0 °C. After stirring for 8 h at r.t., the reaction mixture was filtered, and then condensed under reduced pressure. The crude product was purified by column chromatography (hexane:ethyl acetate = 1:1, R_f = 0.29), affording *N*-propargylacrylamide as transparent liquid. Yield, 6.20 g (29.9 %). ^{1}H NMR (400 MHz, $CDCl_3$): δ (ppm) 2.22-2.26 (t, 1H, -C≡C*H*), 4.10-414 (m, 2H, -NCH_2-), 5.64-5.70 (m, 1H, $CH_2=CH$-), 5.90-6.10 (br, 1H, N*H*), 6.06-6.15 (m, 1H, *trans* CH_2=CH-), 6.27-6.34 (m, 1H, *cis* CH_2=CH-).

***N*-methyl-*N*-propargyl acrylamide (MPAAm).** To a suspension of NaH (3.72 g, 60 wt%, 85.2 mmol) in dry-THF (200 mL), *N*-propargylacrylamide (6.20 g, 56.8 mmol) was added at 0 °C under nitrogen atmosphere. After stirring for 1 h, iodomethane (10.6 mL, 170 mmol) was added at 0 °C under nitrogen atmosphere. The reaction mixture was stirred at r.t. for 24 h, and then, quenched with a portion of water followed by extraction with ethyl acetate. The organic phase was dried over anhydrous $MgSO_4$, and concentrated under reduced pressure. The crude product was purified by distillation over CaH_2 under reduced pressure (85 °C/ 6.0 mmHg), affording *N*-propargyl-*N*-methylacrylamide as a pale yellow solid. Yield, 2.34 g (33.5 %). ^{1}H NMR (400 MHz, $CDCl_3$): δ (ppm) 2.19-2.23, 2.29-2.33 (t, 1H, -C≡C*H*), 3.03-3.07, 3.12-3.16 (s, 3H, NCH_3), 4.08-412, 4.26-4.29 (m, 2H, -NCH_2-), 5.68-5.75 (m, 1H, $CH_2=CH$-), 6.26-6.39 (m, 1H, *trans* CH_2=CH-), 6.50-6.62 (m, 1H, *cis* CH_2=CH-). ^{13}C NMR (100 MHz, $CDCl_3$): δ (ppm) 33.6, 34.5, 36.5, 39.7, 72.2, 73.1, 78.0, 78.5, 127.3, 127.6, 128.2, 128.8, 166.1, 166.6.

Polymerization of acrylamide monomers. A typical procedure for the polymerization is as follows. A stock solution (40.0 μL, 2.00 μmol) of $B(C_6F_5)_3$ in CH_2Cl_2 (0.05 mol L^{-1}) was added to a solution of DEAAm (127 mg, 1.00 mmol) and ^{Et}SKA (8.65 mg, 40.0 μmol) in CH_2Cl_2 (1.81 mL) at room temperature (25 °C). After 70 min of the polymerization, MeOH was added to the solution to quench the polymerization. The crude product was purified by dialysis against MeOH followed by lyophilization of the resulting polymers from their aqueous solutions. Yield: 80.0 mg (63%); SEC (RI): $M_{n,SEC}$ = 3.36 kg mol^{-1}, M_w/M_n = 1.14. In the post polymerization experiments and block copolymerizations, the additional monomer was added to the reaction mixture just after a small portion of the reaction mixture was taken for the determination of the monomer conversion and the $M_{n,SEC}$ and M_w/M_n of the product in the first polymerization.

2.3. Results and discussion

2.3.1. GTP of *N,N*-diethylacrylamide using various organic acids and silyl ketene acetals. The GTP of DEAAm was carried out using various organocatalysts and silyl ketene acetals (SKAs), such as SKA^{Me}, SKA^{Et}, SKA^{iPr}, and SKA^{Ph}, in CH_2Cl_2 at room temperature (~25 °C) to find a suitable combination of a catalyst and an initiator for the controlled/living GTP of DEAAm. We employed three types of organocatalysts, such as the Lewis acid of $B(C_6F_5)_3$ and Me_3SiNTf_2, the Brønsted acid of $C_6F_5CHTf_2$, and the Lewis base of *t*-Bu-P_4, which have been previously reported as efficient catalysts for the GTP of (meth)acrylates.[24] The polymerizations of DEAAm were carried out under the conditions of $[DEAAm]_0$ = 0.5 mol L^{-1} and $[DEAAm]_0/[Initiator]_0$ = 50, and the polymerization results are summarized in Table 2-1. The acidic organic catalysts were obviously more effective than the basic catalyst of *t*-Bu-P_4, since the molecular weights obtained from the

acid-catalyzed GTP were better controlled. Given that the *t*-Bu-P_4-catalyzed GTP proceeding through the dissociative mechanism, in which the active species was an enolate anion conjugating with a carbanion, was rather similar to the conventional anionic polymerization, the propagating ends of the enolate anions were so reactive that they readily caused side reactions or termination reactions which led to broad molecular weight distributions (MWDs) or no polymerization. Kakuchi and coworkers reported that the GTPs of acrylates, such as methyl acrylate and *n*-butyl acrylate, using the acidic catalysts smoothly proceeded in a quantitative monomer conversion by optimizing the bulkiness of the silyl group of the employed SKA, in which SKA^{iPr} was found to be the most effective initiator for preparing the corresponding well-defined polymers.[34] In this study, all the acid-catalyzed GTPs of DEAAm were completed with quantitative monomer consumption within the set polymerization times except for the $B(C_6F_5)_3$-catalyzed polymerization using SKA^{iPr}. The acid-catalyzed polymerizations using SKA^{Me} and SKA^{Ph} (runs 2-5, 2-8, 2-9, 2-12, 2-13 and 2-16) afforded broad MWDs as M_w/M_ns >1.22 and those using SKA^{iPr} (runs 2-7 and 2-11) produced PDEAAms with MWDs of 1.19. In contrast, the polymerizations using SKA^{Et} with a moderately bulky silyl group produced the most narrowly-distributed PDEAAms, among which the $B(C_6F_5)_3$-catalyzed polymerization afforded the narrowest MWD. The number-averaged molecular weights ($M_{n,SEC}$s) of these resulting PDEAAms were estimated using size exclusion chromatography based on PMMA standards due to the lack of appropriate PDEAAm standards, meaning that the $M_{n,SEC}$ values should be slightly deviated from the exact values. In this study, we mainly used the MWD as the evaluating criterion and thus selected $B(C_6F_5)_3$ as the catalyst for the following polymerizations due to its operating convenience, unless otherwise instructed.

Table 2-1. Organocatalyzed GTPs of DEAAm using various SKAs at room temperature (~ 25 °C) [a]

run	Catalyst (Cat.)	Initiator (I)	$[DEAAm]_0/[I]_0/[Cat.]_0$	Time (h)	Conv. (%) [b]	$M_{n,SEC}$ [c] ($M_{n,calcd.}$ [d]) (kg mol^{-1})	M_w/M_n [c]
2-1	*t*-Bu-P_4 [e]	SKA^{Me}	50/1/0.05	24	55.5	3.74 (3.53)	2.4 [f]
2-2		SKA^{Et}		24	32.2	5.96 (2.15)	12.4 [f]
2-3		SKA^{iPr}		24	<1	n.d. [g]	n.d. [g]
2-4		SKA^{Ph}		24	<1	n.d. [g]	n.d. [g]
2-5	Me_3SiNTf_2	SKA^{Me}	50/1/0.02	2	>99	6.95 (6.45)	1.24
2-6		SKA^{Et}		2	>99	5.60 (6.45)	1.22
2-7		SKA^{iPr}		24	>99	4.09 (6.45)	1.19
2-8		SKA^{Ph}		2	>99	7.04 (6.45)	1.28
2-9	$C_6F_5CHTf_2$	SKA^{Me}	50/1/0.02	2	>99	6.40 (6.45)	1.22
2-10		SKA^{Et}		2	>99	5.90 (6.45)	1.18
2-11		SKA^{iPr}		23	>99	3.82 (6.45)	1.19
2-12		SKA^{Ph}		2	>99	5.84 (6.45)	1.27
2-13	$B(C_6F_5)_3$	SKA^{Me}	50/1/0.05	2.5	>99	6.68 (6.45)	1.23
2-14		SKA^{Et}		3.0	>99	5.18 (6.45)	1.16
2-15		SKA^{iPr}		20	<1	n.d. [g]	n.d. [g]
2-16		SKA^{Ph}		20	>99	6.73 (6.45)	1.26

[a] Ar atmosphere; $[DEAAm]_0$ = 0.5 mol L^{-1}; solvent, CH_2Cl_2. [b] Determined by ^{1}H NMR in $CDCl_3$. [c] Determined by SEC in DMF containing 0.01 mol L^{-1} LiCl calibrated with PMMA. [d] Calculated from $[DEAAm]_0/[I]_0$ × (MW of DEAAm = 127.18) × conv. + (MW of initiator residue = 102.13). [e] Solvent, toluene. [f] Shape of SEC trace was bimodal. [g] Not determined.

2.3.2. Living nature of the $B(C_6F_5)_3$-catalyzed GTP of DEAAm. The living nature of the $B(C_6F_5)_3$-catalyzed GTP of DEAAm was assessed by the kinetic studies, the MALDI-TOF MS measurements, and the post-polymerization experiments. The polymerization using SKA^{Et} for the kinetic study was implemented in CH_2Cl_2 at 25 °C, $[DEAAm]_0/[SKA^{Et}]_0/[B(C_6F_5)_3]_0$ = 25/1/0.05, and $[DEAAm]_0$ = 0.5 mol L^{-1}. Figure 2-1 shows the zero- and first-order kinetic plots and the $M_{n,SEC}$ and M_w/M_n dependence on the monomer conversion (Conv.). Surprisingly, the kinetic plots displayed a distinct induction period of ca. 25 min. The further discussion in this regard is described in greater detail in the following section about polymerization mechanism. After the induction period, the polymerization normally proceeded as a propagation reaction till the complete consumption of the monomer in 20 min, during which no retardation of the polymerization was observed, indicating that no termination reaction occurred during the entire propagation process. The polymerization turned out to be zero-order, rather than a first-order reaction. The $M_{n,SEC}$ and M_w/M_n dependence on the Conv. shown in Figure 2-1(b) indicated that the $M_{n,SEC}$ of the obtained PDEAAm linearly increased from 1.65 to 4.00 kg mol^{-1} with the increasing monomer conversion, while their M_w/M_ns were as narrow as <1.17, which indicated the homogeneous growth of the PDEAAm chain in the propagation stage. Excluding the induction period, the above polymerization possessed true living characteristics.

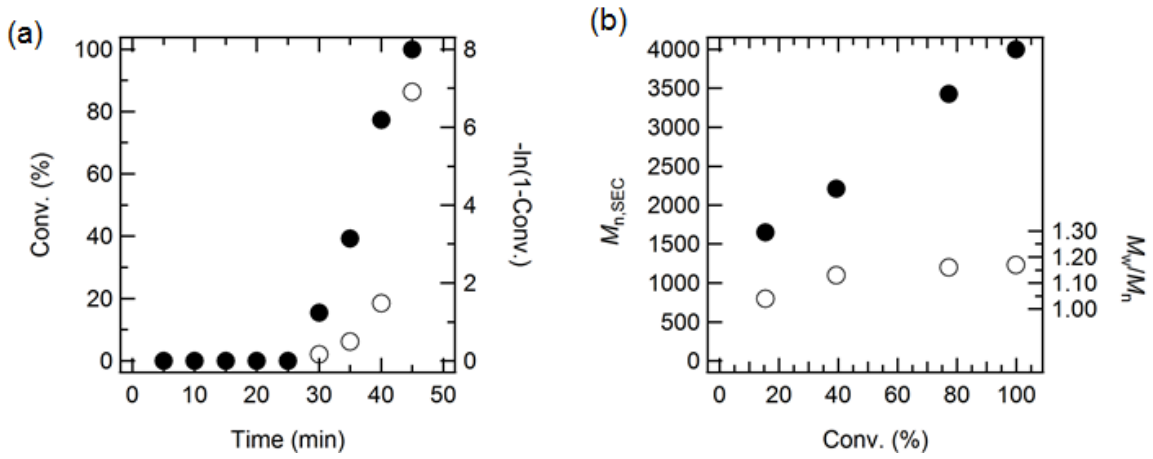

Figure 2-1. (a) Zero- (●) and first- (○) order kinetic plots of the $B(C_6F_5)_3$-catalyzed GTP of DEAAm at 25 °C under the conditions of $[DEAAm]_0/[SKA^{Et}]_0/[B(C_6F_5)_3]_0$ = 25/1/0.05 and $[DEAAm]_0$ = 0.50 mol L^{-1} and (b) Dependence of $M_{n,SEC}$ (●) and M_w/M_n (○) of the obtained PDEAAm on Conv..

A MALDI-TOF MS spectrum of the obtained PDEAAm in Figure 2-2 provided a more detailed insight into the chemical structure of the resulting polymer and further into the polymerization reaction. The spectrum showed only one population of molecular ion peaks and the distance between any two neighboring molecular ion peaks was ca. 126.9 Da, which well corresponded to the exact molecular weight of DEAAm as the repeating unit. In addition, the *m*/*z* value of each molecular ion peak definitely suggested the sodium-cationized polymer composition of $[MeO_2CMe_2C\text{-}DEAAm_n\text{-}H + Na^+]$ (molecular formula: $C_{7n+5}H_{13n+10}N_nO_{n+2}Na$), *e.g.*, the *m*/*z* value of 3302.33 Da for a specified peak corresponded to a sodium-cationized 25-mer polymer structure of $[MeO_2CMe_2C\text{-}DEAAm_{25}\text{-}H + Na^+]$ with the theoretical monoisotopic value of 3302.55 (molecular formula: $C_{180}H_{335}O_{27}N_{25}Na$). This result strongly supported the fact that the polymerization proceeded without any side-reactions. However, the molecular ion peaks had a broad distribution ranging from 1500 to 9000 Da, which is considered to be caused by the lower initiation rate than that of the propagation. The initiating end was also confirmed by the ^1H NMR

measurements, *i.e.*, the methoxy protons of the SKA^{Et} residue at the α-terminal of PDEAAm was clearly observed at 3.64 ppm (peak b) along with those due to the main-chain protons of PDEAAm at 0.82-1.98 (peaks c and f), 2.20-2.86 (peak d), and 2.90-3.62 (peak e) ppm (Figure 2-5(a)).

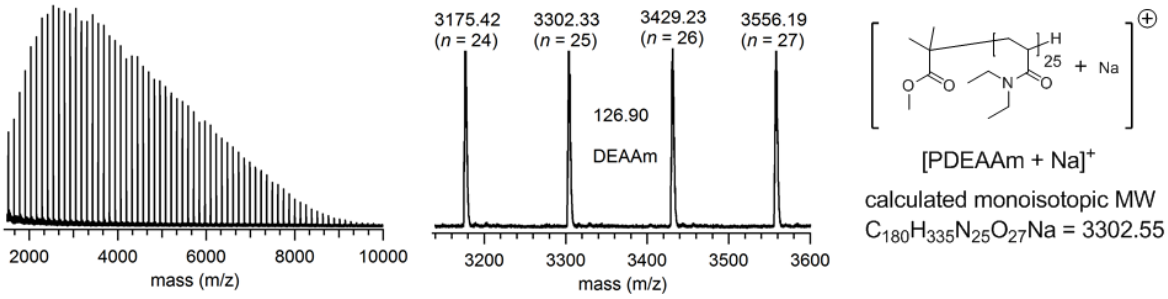

Figure 2-2. MALDI-TOF MS spectrum of a low molecular weight PDEAAm ($M_{n,SEC}$ = 3.36 kg mol^{-1}, M_w/M_n = 1.14) obtained from the GTP of DEAAm using SKA^{Et}.

The chain extension experiment was further carried out to prove the living nature of the propagating end of PDEAAm. Under the conditions of $[DEAAm]_0/[SKA^{Et}]_0/[B(C_6F_5)_3]_0$ = 25/1/0.05 in CH_2Cl_2 at room temperature (~25°C), 25 equivalents of DEAAm were initially polymerized for 80 min to afford a quantitative monomer conversion and an intermediate PDEAAm product with $M_{n,SEC}$ of 3.20 kg mol^{-1} and M_w/M_n of 1.18. After the polymerization mixture was placed in the argon atmosphere for a short time, another fresh 50 equivalents of DEAAm were further added to the polymerization system to observe the chain extension behavior. The second-stage polymerization was completed within 80 min with a quantitative monomer conversion to afford the final PDEAAm product with the $M_{n,SEC}$ of 7.33 kg mol^{-1} and the M_w/M_n of 1.22. The SEC traces of the first- and second-stage PDEAAms are shown in Figure 2-3(a), in which the SEC trace obtained from the second-stage polymerization exhibited a rather clear shift toward the high molecular weight region when referred to the one obtained from the first-stage polymerization. This result definitely indicated that the propagating end of the growing PDEAAm

possessed a truly living propagation end, which brought about the chain extension after the sequential addition of the monomer. In summary, the living nature of the $B(C_6F_5)_3$-catalyzed GTP of DEAAm using SKA^{Et} was proved by all of the above results.

The living characteristics of this polymerization system were used to prepare various PDEAAms with different molecular weights by varying the $[DEAAm]_0/[SKA^{Et}]_0$ ratios from 25 to 200 under a fixed $[B(C_6F_5)_3]_0/[SKA^{Et}]_0$ ratio of 0.05. All the polymerizations underwent a quantitative monomer consumption and the SEC traces of the obtained polymers in Figure 2-3(b) showed mono-distributions, from which the $M_{n,SEC}$ (kg mol^{-1}) (M_w/M_n)s were estimated to be 3.36 (1.14), 5.18 (1.16), 10.3 (1.21), and 21.5 (1.24), corresponding to the related $[DEAAm]_0/[SKA^{Et}]_0$ ratios of 25, 50, 100, and 200, respectively.

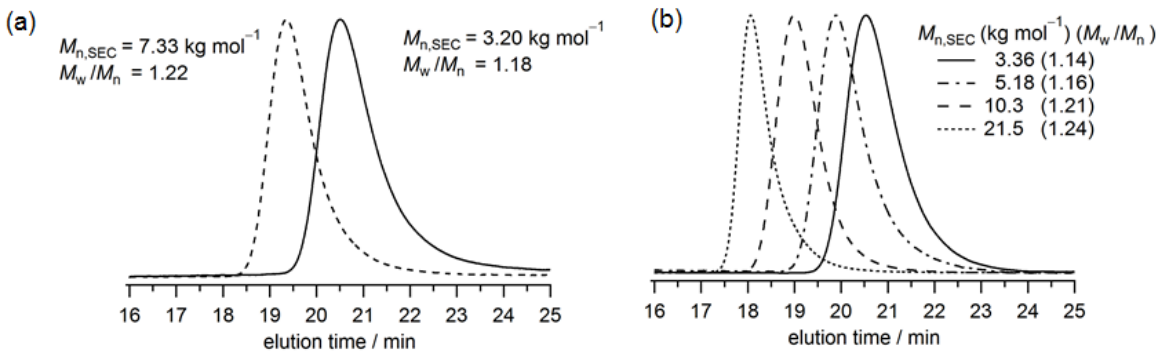

Figure 2-3. SEC traces of the PDEAAm products obtained from (a) the first-stage PDEAAm (solid line) and the second-stage PDEAAm (dashed line) in the chain extension experiment and (b) various $[DEAAm]_0/[SKA^{Et}]_0$ ratios of 25, 50, 100, and 200.

2.3.3. Mechanism of the $B(C_6F_5)_3$-catalyzed GTP of DEAAm. Given the unique polymerization behavior of the $B(C_6F_5)_3$-catalyzed GTP of DEAAm using SKA^{Et}, we proposed a plausible mechanism, as shown in Scheme 2-2. The $B(C_6F_5)_3$-catalyzed GTP of DEAAm has three

elementary reactions, including (1) monomer activation by $B(C_6F_5)_3$, (2) initiation reaction, and (3) propagation reaction. For (1), it was reported that an aromatic amide showed an extremely high coordination affinity toward the highly electrophilic $B(C_6F_5)_3$ and the equilibria lay far toward the formation of coordination adducts (a high equilibrium constant).[44] This trend is also adaptable to the α-unsaturated amide of DEAAm in our case. As shown in Figure 2-4(a), the proton signals of the equimolar mixture of DEAAm and $B(C_6F_5)_3$ for $[DEAAm]_0 = [B(C_6F_5)_3]_0 = 0.167$ mol L^{-1} showed very clear chemical shifts, which suggests the formation of the coordinating products of DEAAm*. In addition, each peak showed an almost complete shift, indicating the equilibrium constant (K_{eq}) for (1) is rather high though we did not calculate the exact K_{eq} value. The high K_{eq} implies that $B(C_6F_5)_3$ in the solution mixture almost exists in the DEAAm*. It should be noted that the signals due to the vinyl protons of DEAAm showed an upfield shift after coordinating with $B(C_6F_5)_3$, while those due to the ethyl group showed a downfield shift. This result might indicate that $B(C_6F_5)_3$ is located in an *anti* fashion toward the diethylamino group of DEAAm because the upfield shift is considered to be caused by the ring current effect of the pentafluorophenyl ring of $B(C_6F_5)_3$. The monomer activation was also verified by ^{13}C NMR measurements, as shown in Figure 2-4(b). For (2), the initiation reaction occurs between the SKA^{Et} and DEAAm* and produces a silyl ketene aminal from the silyl ketene acetal of SKA^{Et}. The initiation reaction turns out to slowly proceed and shows a distinct induction period. This phenomenon can be firmly attributed to the mismatch of the chemical structures between SKA^{Et} and DEAAm because the $B(C_6F_5)_3$-catalyzed GTP of DEAAm using a silyl ketene aminal does not have such an induction period, as determined in our unpublished study. When comparing the structures of SKA^{Et} and the generated silyl ketene aminal, the SKA^{Et} has an additional methyl group bonded to the ene group, which hinders the initiation reaction; on the other hand, the acetal group in SKA^{Et} has a lower electron-donating ability than that of the aminal group in the silyl

ketene aminal, which indicates that the ene group of SKA^{Et} is less nucleophilic toward DEAAm* in comparison to that of the silyl ketene aminal. Therefore, these two structural factors of SKA^{Et} result in the induction period and relatively slow initiation reaction. This fact, in turn, suggests that it is of great significance to design the initiator possessing a similar structure with the monomer. For (3), the propagation reaction shows the living characteristics commonly appearing in a living polymerization. It should be emphasized that the propagation reaction of this polymerization system is strongly suggested to be a zero-order reaction, as shown in Figure 1(a). This can be well explained by the following description. As a premise, the propagation rate (k_p) in each addition reaction is assumed to be a constant. The total monomer consumption rate can then be expressed as

$$-\frac{\mathbf{d[DEAAm]}}{\mathbf{dt}} = \boldsymbol{k_p}[\mathbf{SKA}][\mathbf{DEAAm}^*] \quad \text{(i)}$$

It is assumed that no side reactions take place during the polymerization process. Thus,

$$[\mathbf{SKA}] = [\mathbf{SKA^{Et}}]_\mathbf{0} \quad \text{(ii)}$$

Considering that the real-time [DEAAm] is much higher than $[B(C_6F_5)_3]$ and K_{eq} is significantly high, it is thus rational to assume that the [DEAAm*] remains constant, the same as $[B(C_6F_5)_3]_0$, except for the very late time of the entire propagation period. Thus,

$$[\mathbf{DEAAm}^*] = [\mathbf{B(C_6F_5)_3}]_\mathbf{0} \quad \text{(iii)}$$

Equation (iv) is derived from equations (i), (ii), and (iii) as

$$[\mathbf{DEAAm}]_\mathbf{0} - [\mathbf{DEAAm}] = \boldsymbol{k_p}[\mathbf{SKA^{Et}}]_\mathbf{0}[\mathbf{B(C_6F_5)_3}]_\mathbf{0}\boldsymbol{t} \quad \text{(iv)}$$

Namely,

$$\mathbf{Conv.}\,(\%) = \frac{\boldsymbol{k_p}[\mathbf{SKA^{Et}}]_\mathbf{0}[\mathbf{B(C_6F_5)_3}]_\mathbf{0}\boldsymbol{t}}{[\mathbf{DEAAm}]_\mathbf{0}} \times \mathbf{100}\% \quad \text{(v)}$$

in which k_p, $[SKA^{Et}]_0$, $[DEAAm]_0$, and $[B(C_6F_5)_3]_0$ are constants and t is the given polymerization time. We define the observed rate constant as $\boldsymbol{k_{p.obs.}} = \frac{k_p[\mathbf{SKA^{Et}}]_0[\mathbf{B(C_6F_5)_3}]_0}{[\mathbf{DEAAm}]_0}$s. Thus, equation (v) can be changed to

$$\mathbf{Conv.}(\%) = \boldsymbol{k_{p.obs.}t} \times \mathbf{100}\% \qquad \text{(vi)}$$

When the induction time (t_i) is taken into consideration, the corrected equations, (vii) and (viii), can be obtained as

$$\mathbf{Conv.}(\%) = \mathbf{0} \qquad (\boldsymbol{t \leq t_i}) \qquad \text{(vii)}$$

$$\mathbf{Conv.}(\%) = \boldsymbol{k_{p.obs.}}(\boldsymbol{t - t_i}) \times \mathbf{100}\% \qquad (\boldsymbol{t > t_i}) \qquad \text{(viii)}$$

Obviously, the propagation is a zero-order reaction. During the propagation period, the monomer consumption is linearly dependent on the polymerization time once the initial conditions are fixed, except for that in the late stage of the propagation period due to the changing [DEAAm*] after consumption of most of the monomer, and independent of the monomer concentration, which has also been fully reflected in the following zero-order kinetic plots of the $B(C_6F_5)_3$-catalyzed GTPs of other acrylamide monomers (Figure 2-8).

Scheme 2-2. A plausible mechanism for the $B(C_6F_5)_3$-catalyzed GTP

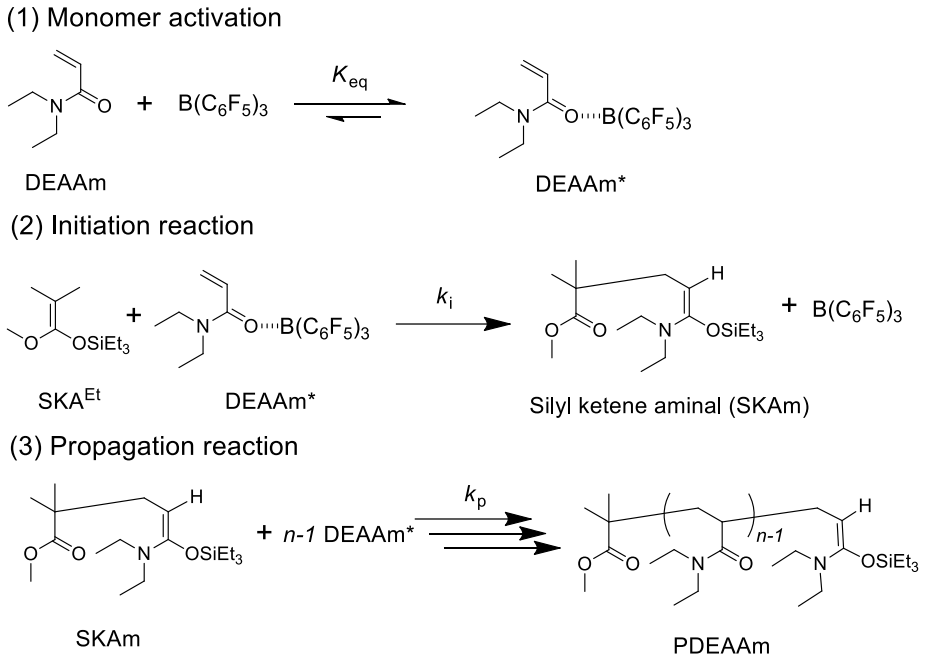

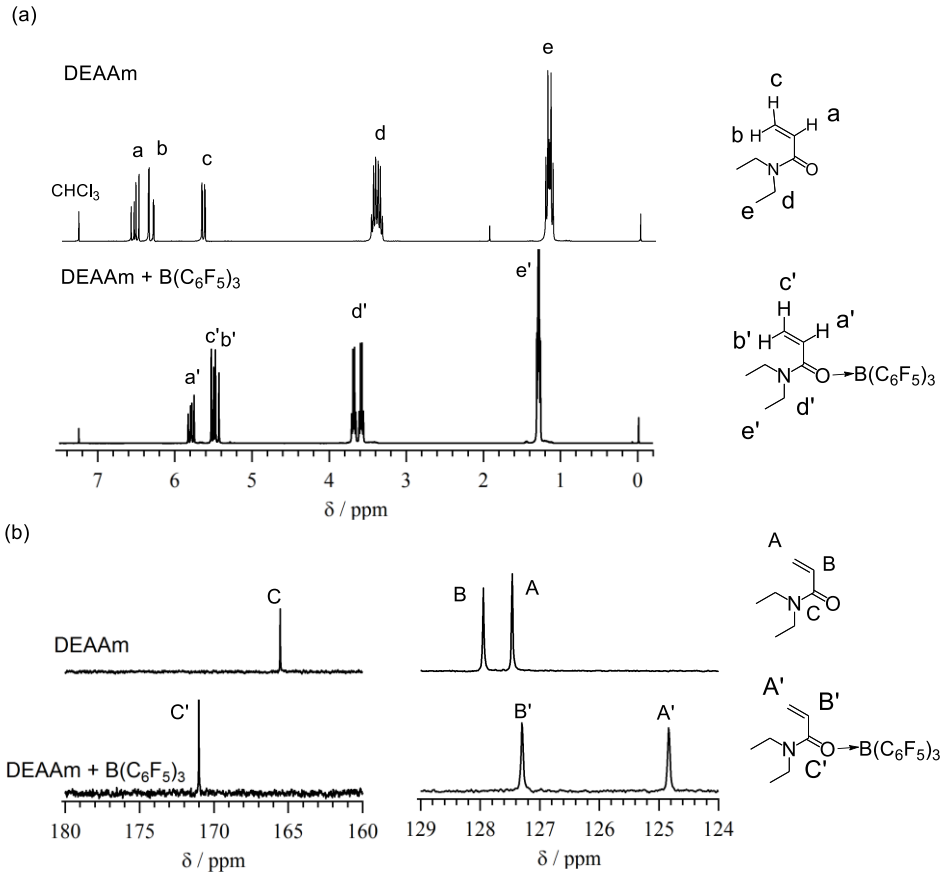

Figure 2-4. (a) ^{1}H and (b) ^{13}C NMR spectra of DEAAm and an equimolar mixture of DEAAm and $B(C_6F_5)_3$ ($[DEAAm]_0 = [B(C_6F_5)_3]_0 = 0.167$ mol L^{-1}) in $CDCl_3$.

2.3.4. $B(C_6F_5)_3$-catalyzed GTPs of various *N*,*N*-disubstituted acrylamides. To explore the suitability of this polymerization, we further applied this method to various *N*,*N*-disubstituted acrylamide monomers (DAAm) (Scheme 2-1), such as *N*,*N*-dimethylacrylamide (DMAAm), *N*,*N*-di-*n*-propylacrylamide (D*n*PAAm), *N*-acryloylpiperidine (API), *N*-acryloylmorpholine (NAM), *N*-(2-methoxyethyl)-*N*-methylacrylamide (MMEAAm), *N*,*N*-bis(2-methoxyethyl)acrylamide (BMEAAm), *N*,*N*-diallylacrylamide (DAlAAm), and *N*-methyl-*N*-propargylacrylamide (MPAAm), to synthesize their corresponding acrylamide polymers, among which poly(*N*,*N*-dimethylacrylamide) (PDMAAm) and poly(*N*-acryloylmolpholine) (PNAM) are water-soluble; poly(*N*,*N*-di-*n*-propylacrylamide) (PD*n*PAAm) and poly(*N*-acryloylpiperidine) (PAPI) are water-insoluble; poly(*N*-acryloylmolpholine) (PNAM), poly(*N*-(2-methoxyethyl)-*N*-methylacrylamide) (PMMEAAm), and poly(*N*,*N*-bis(2-methoxyethyl)acrylamide) (PBMEAAm) are thermoresponsive; poly(*N*,*N*-diallylacrylamide) (PDAlAAm) and poly(*N*-methyl-*N*-propargylacrylamide) (PMPAAm) are functionalized and reactive. The polymerizations were done in CH_2Cl_2 at room temperature by optimizing the parameters in terms of the $[monomer]_0/[SKA^{Et}]_0$ ratio, monomer concentration, the polymerization time, and the catalyst amount, depending on the monomer used; their polymerization results are summarized in Table 2-2. All the polymerizations homogeneously proceeded and gave quantitative monomer conversions within the set polymerization time. The $M_{n,SEC}$s estimated by the SEC measurements (Figure 2-5) of the obtained PDMAAm, PD*n*PAAm, PAPI, PNAM, PMMEAAm, PBMEAAm, PDAlAAm, and PMPAAm were 6.35, 14.7, 8.65, 13.5, 8.40, 16.2, 13.5, 8.44 kg mol^{-1} when their corresponding $[DAAm]_0/[SKA^{Et}]_0$ ratios were 100, 100, 100, 100, 50, 100, 100, 50, respectively. It should be emphasized that it is meaningless to do the

comparison between the $M_{n,SEC}$s and the theoretical molecular weights ($M_{n,calcd.}$s) because of the inconsistency between the obtained polymers and the PMMA standards. Interestingly, the resulting PDMAAm, PD*n*PAAm, and PMMEAAm had broad MWDs of 1.22, 1.23, and 1.28, respectively, while PAPI, PNAM, PBMEAAm, PDAlAAm, and PMPAAm had narrow ones of 1.11, 1.15, 1.14, 1.09, and 1.10, respectively. The M_w/M_n value significantly depended on the used monomer. This dependence should be significantly assigned to the k_i/k_p difference in the polymerizations of the above monomers, *i.e.*, the polymerizations of API, NAM, BMEAAm, DAlAAm, and MPAAm seem to have good balance between k_i and k_p, while those of DMAAm, D*n*PAAm, and MMEAAm have a poorer balance. It is rather understandable that both k_i and k_p vary when the used monomer is changed, which results in the k_i/k_p variation. Since it is seemingly impossible to accurately measure the k_is due to the induction period, we did not obtain the detailed k_i/k_p values and do not undertake a further discussion in this regard. The chemical structures of the obtained polymers were also confirmed by ^{1}H NMR and MALDI-TOF MS measurements like that for PDEAAm, as shown in Figures 2-6 and 2-7.

Apart from DEAAm, the polymerization kinetics of DMAAm, API, MMEAAm, BMEAAm, and DAlAAm were also carried out in CH_2Cl_2 at room temperature and an argon atmosphere for the same $[M]_0/[SKA^{Et}]_0/[B(C_6F_5)_3]_0$ ratio of 25/1/0.05 and $[M]_0$ = 0.50 mol L^{-1}. The zero-order kinetic plots are shown in Figure 2-8 and all the t_is and $k_{p.obs.}$s are summarized in Table 2-3. It is significant clear that all the propagation reactions of the polymerizations of DMAAm, DEAAm, API, MMEAAm, BMEAAm, and DAlAAm are zero-order reactions, except for the late propagation period. Under the same $[M]_0/[SKA^{Et}]_0$ ratio of 25, the t_is were estimated to be 16.9, 26.2, 65.9, 20.4, 27.3, and 25.4 min, and the

$k_{p.obs.}$s were 0.0256, 0.0523, 0.0040, 0.0086, 0.0069, and 0.0099 min^{-1} for DMAAm, DEAAm, API, MMEAAm, BMEAAm, and DAlAAm, respectively. According to $k_{p.obs.} = \frac{k_p[\mathrm{SKA^{Et}}]_0[\mathrm{B(C_6F_5)_3}]_0}{[\mathrm{DAAm}]_0}$, the k_ps for DMAAm, DEAAm, API, MMEAAm, BMEAAm, and DAlAAm were calculated to be 640, 1308, 100, 215, 173, 248 L mol^{-1} min^{-1}, respectively. API had the longest induction period, DEAAm, MMEAAm, BMEAAm, and DAlAAm in the middle, and DMAAm the shortest, which well corresponded to the bulkiness order of their substituents at the nitrogen atom. On the other hand, the propagation rates were in the monomer order of DEAAm > DMAAm > DAlAAm > MMEAAm > BMEAAm > API, indicating that the hindrance of the functional and bulky substituents of the *N*-allyl, *N*-2-methoxyethyl, and *N*-piperidyl groups significantly decreased the propagation rate.

Table 2-2. $B(C_6F_5)_3$-catalyzed GTP of DAAm using SKA^{Et} in CH_2Cl_2 at room temperature [a]

run	Monomer (M)	$[M]_0/[SKA^{Et}]_0$ /$[B(C_6F_5)_3]_0$	$[M]_0$ (mol L^{-1})	Time (h)	$M_{n,SEC}$ [c] ($M_{n,calcd.}$ [d]) (kg mol^{-1})	M_w/M_n [c]
2-17	DMAAm	100/1/0.05	0.5	22	6.35 (10.0)	1.22
2-18	D*n*PAAm	100/1/0.1	0.5	25	14.7 (15.6)	1.23
2-19	API	100/1/0.1	1.0	20	8.65 (14.0)	1.11
2-20	NAM	100/1/0.5	2.0	30	13.5 (14.2)	1.15
2-21	MMEAAm	50/1/0.1	1.0	5	8.40 (7.26)	1.28
2-22	BMEAAm	100/1/0.3	1.0	71	16.2 (18.8)	1.14
2-23	DAlAAm	100/1/0.1	0.5	19	13.5 (15.2)	1.09
2-24	MPAAm	50/1/0.05	0.5	20	8.44 (6.26)	1.10

[a] Ar atmosphere; Conv. (determined by ^1H NMR in $CDCl_3$), >99 %. [b] Determined by SEC in DMF containing 0.01 mol L^{-1} of LiCl calibrated with PMMA. [c] Calculated from $[M]_0/[SKA^{Et}]_0$ × (MW of monomer: DMAAm = 99.17, D*n*PAAm = 155.24, API = 139.20, NAM = 141.17, MMEAAm = 143.18, BMEAAm = 187.24, DAlAAm = 151.21, and MPAAm = 123.15) × Conv. + (MW of initiator residue: ^{Et}SKA = 102.13).

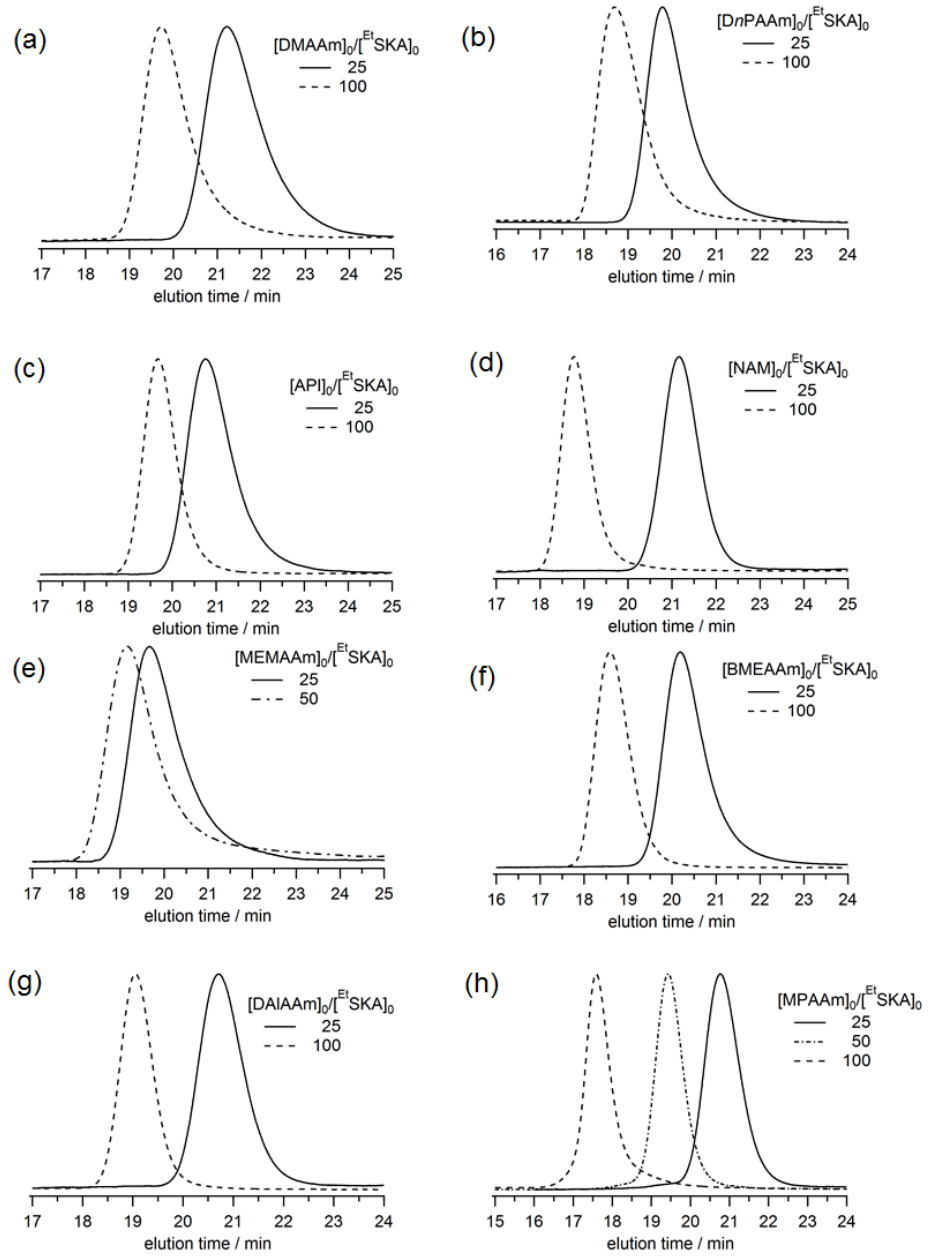

Figure 2-5. SEC traces of the PDAAms obtained from the $B(C_6F_5)_3$-catalyzed GTPs of (a) DMAAm, (b) D*n*PAAm, (c) API, (d) NAM, (e) MMEAAm, (f) BMEAAm, (g) DAlAAm, and (h) MPAAm at various $[monomer]_0$ to $[^{Et}SKA]_0$ ratios (eluent, DMF containing 0.01 mol L^{-1} LiCl; flow rate, 0.6 mL min^{-1}).

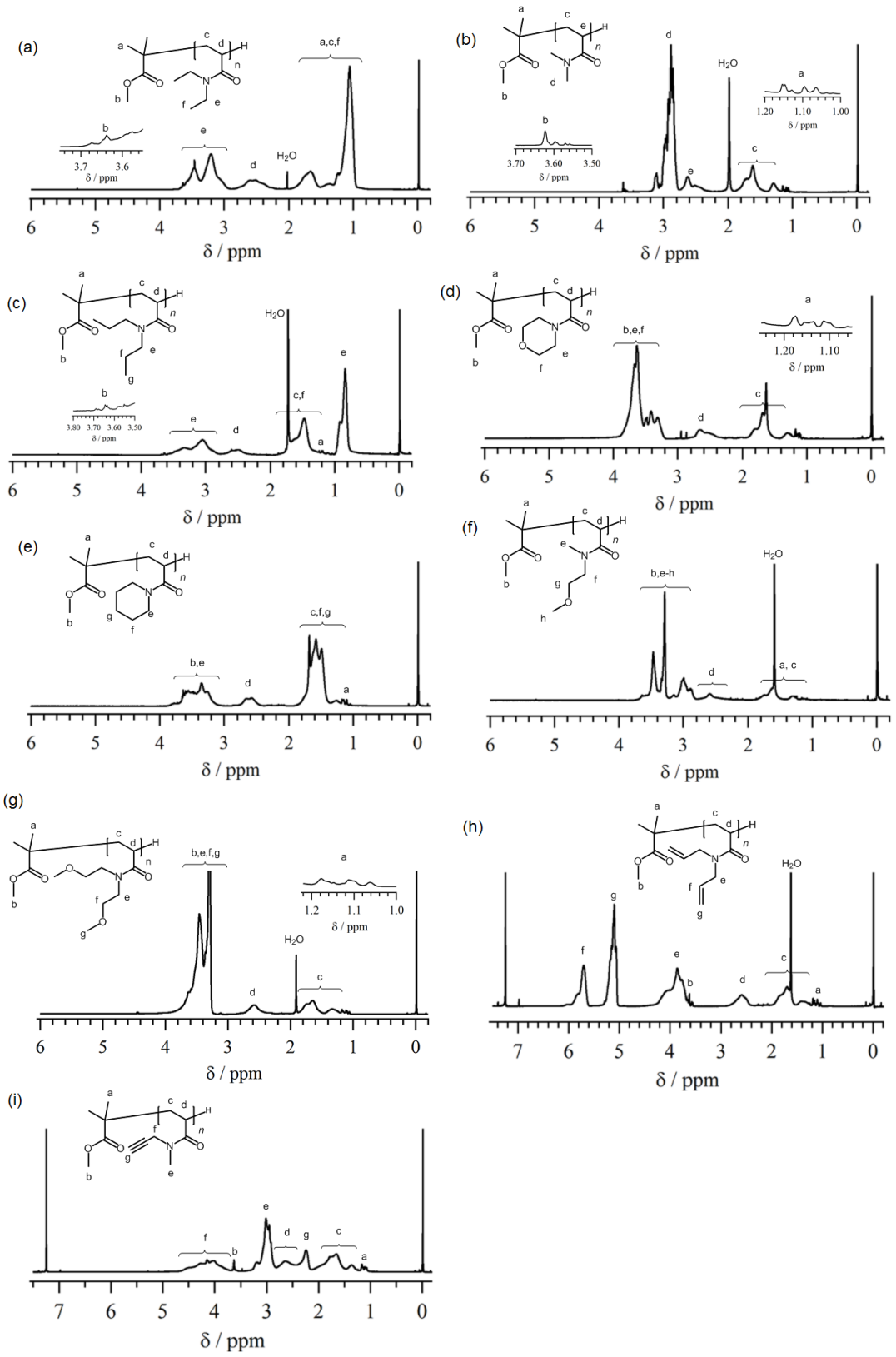

Figure 2-6. ^{1}H NMR spectra of (a) PDEAAm, (b) PDMAAm, (c) PD*n*PAAm, (d) PAPI, (e) PNAM, (f) PMMEAAm, (g) PBMEAAm, (h) PDAlAAm, and (i) PMPAAm in $CDCl_3$. (Theoretical DP, 25)

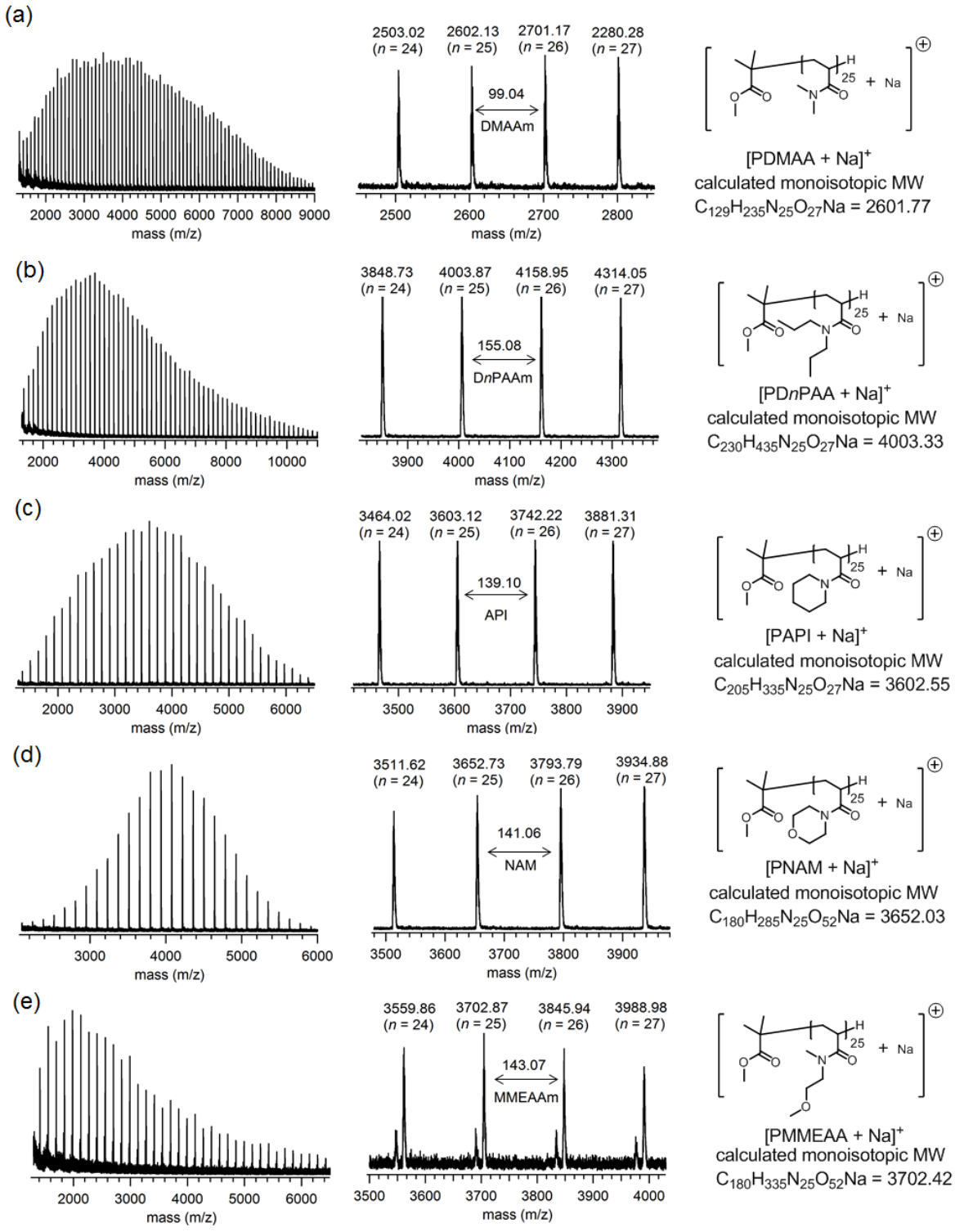
(a)
2503.02 (n = 24)
2602.13 (n = 25)
2701.17 (n = 26)
2280.28 (n = 27)
99.04
DMAAm
mass (m/z)
[PDMAA + Na]+
calculated monoisotopic MW
C129H235N25O27Na = 2601.77
(b)
3848.73 (n = 24)
4003.87 (n = 25)
4158.95 (n = 26)
4314.05 (n = 27)
155.08
DnPAAm
mass (m/z)
[PDnPAA + Na]+
calculated monoisotopic MW
C230H435N25O27Na = 4003.33
(c)
3464.02 (n = 24)
3603.12 (n = 25)
3742.22 (n = 26)
3881.31 (n = 27)
139.10
API
mass (m/z)
[PAPI + Na]+
calculated monoisotopic MW
C205H335N25O27Na = 3602.55
(d)
3511.62 (n = 24)
3652.73 (n = 25)
3793.79 (n = 26)
3934.88 (n = 27)
141.06
NAM
mass (m/z)
[PNAM + Na]+
calculated monoisotopic MW
C180H285N25O52Na = 3652.03
(e)
3559.86 (n = 24)
3702.87 (n = 25)
3845.94 (n = 26)
3988.98 (n = 27)
143.07
MMEAAm
mass (m/z)
[PMMEAA + Na]+
calculated monoisotopic MW
C180H335N25O52Na = 3702.42

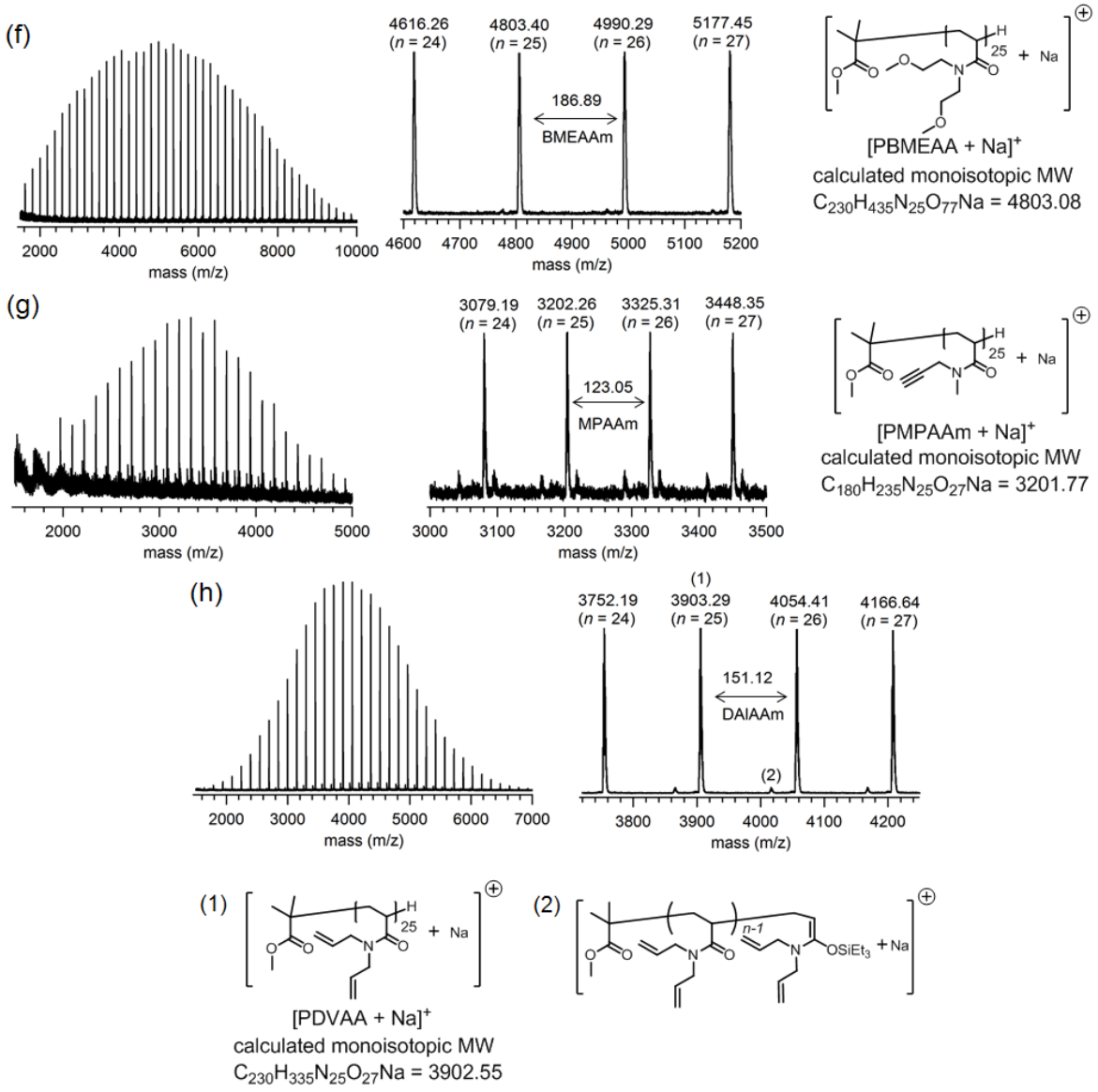

Figure 2-7. MALDI-TOF MS spectra of (a) PDMAAm, (b) PD*n*PAAm, (c) PAPI, (d) PNAM, (e) PMMEAAm, (f) PBMEAAm, (g) PDAlAAm, and (h) PMPAAm. (Theoretical DP for each polymer, 25)

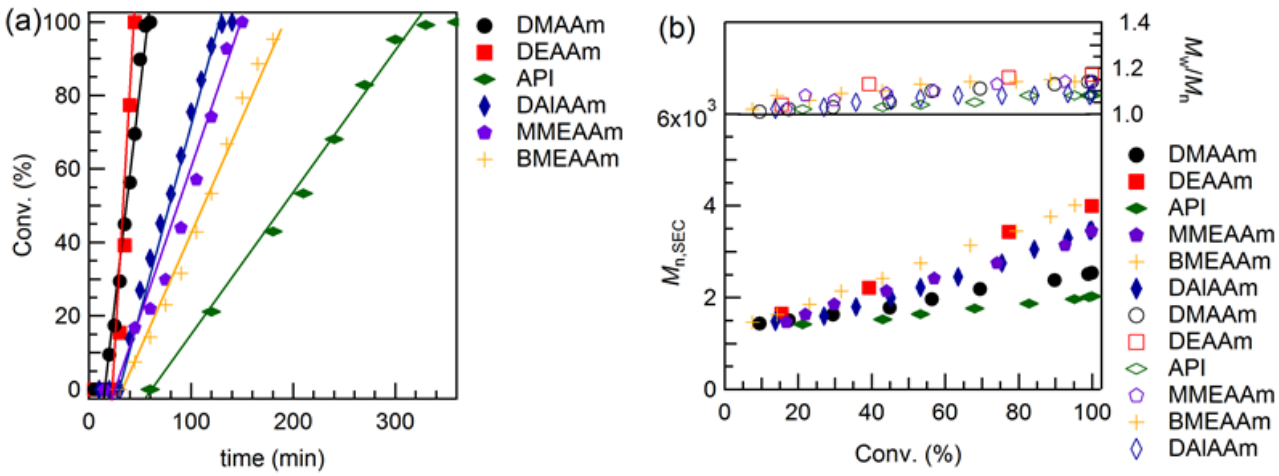

Figure 2-8. (a) Zero-order kinetic plots of the $B(C_6F_5)_3$-catalyzed GTPs of DMAAm, DEAAm, API, MMEAAm, BMEAAm, and DAlAAm at 25 °C and (b) $M_{n,SEC}$ and M_w/M_n dependence of the obtained PDAAm on monomer conversion (Conv.). $([M]_0/[SKA^{Et}]_0/[B(C_6F_5)_3]_0 = 25/1/0.05$

Table 2-3. A summary of the induction time (t_i), $k_{p.obs.}$s, and k_ps of the $B(C_6F_5)_3$-catalyzed GTPs of DMAAm, DEAAm, API, MMEAAm, BMEAAm, and DAlAAm [a]

Monomer (M)	$[M]_0/[SKA^{Et}]_0$	t_i (min)	$k_{p.obs.}$ (min^{-1})	k_p (L mol^{-1} min^{-1})
DMAAm	25	16.9	0.0256	640
DEAAm	25	26.2	0.0523	1308
API	25	65.9	0.0040	100
MMEAAm	25	20.4	0.0086	215
BMEAAm	25	27.3	0.0069	173
DAlAAm	25	25.4	0.0099	248

[a] $[M]_0$, 0.50 mol L^{-1}; $[M]_0/[B(C_6F_5)_3]_0/[^{Et}SKA]_0$, 25/1/0.05; Ar atmosphere; room temperature (~ 25 °C); solvent, CH_2Cl_2.

2.3.5. Synthesis of acrylamide homo diblock copolymer by the $B(C_6F_5)_3$-catalyzed GTP. The living nature of the $B(C_6F_5)_3$-catalyzed GTP of DAAm was also used to prepare acrylamide diblock copolymers. DMAAm and DAlAAm were used for the block copolymerization with DEAAm by a sequential monomer addition method. Table 2-4 summarizes the polymerization results, and Figure 2-9 shows the SEC traces of resulting products. Twenty-five equivalents of the first monomer were quantitatively polymerized to produce the first-stage polymer product, after which 50 equivalents of the second monomer were added to continue the polymerization, leading to producing the acrylamide diblock copolymers. For all the polymerizations, the monomers were fully consumed in the fixed time no matter during which polymerization stage. The polymerizations of DEAAm with DMAAm and DAlAAm produced the corresponding diblock copolymers of PDEAAm-*b*-PDMAAm and PDEAAm-*b*-PDAlAAm, respectively. In addition, the same diblock copolymers could also be obtained by changing the addition order of the acrylamide monomers. The resulting PDEAAm-*b*-PDMAAms had relatively broad MWDs, while the PDEAAm-*b*-PDAlAAm s had MWDs narrower than 1.17. As already mentioned, PDEAAm, PDMAAm, and PDAlAAm are thermoresponsive, water-soluble, and reactive acrylamide polymers. Therefore, these diblock copolymers are expected to have unique properties.

Table 2-4. Synthesis of acrylamide block copolymers by sequential $B(C_6F_5)_3$-catalyzed GTP using SKA^{Et} [a]

run	Monomer (M)		$[M]_0/[^{Et}SKA]_0$	Time (h)	$M_{n,SEC}$ [b] ($M_{n,calcd.}$ [c]) (kg mol^{-1})	M_w/M_n [b]
2-25	1st	DEAAm	25	1.25	3.83 (3.28)	1.18
	2nd	DMAAm	50	1	5.69 (8.24)	1.28
2-26	1st	DMAAm	25	1	2.33 (2.58)	1.13
	2nd	DEAAm	50	2	6.64 (8.94)	1.26
2-27	1st	DEAAm	25	1.25	3.59 (3.28)	1.16
	2nd	DAlAAm	50	6	8.69 (11.04)	1.17
2-28	1st	DAlAAm	25	3	3.24 (3.98)	1.08
	2nd	DEAAm	50	2	7.67 (8.24)	1.15

[a] Ar atmosphere; $[M]_0$, 0.5 mol L^{-1}; $[B(C_6F_5)_3]_0/[SKA^{Et}]_0$, 0.05; temp., r.t.; Conv. (determined by ^{1}H NMR in $CDCl_3$), >99%. [b] Determined by SEC in DMF containing 0.01 mol L^{-1} of LiCl calibrated with PMMA. [c] Calculated from $[M]_0/[SKA^{Et}]_0$ × (MW of monomer: DMAAm = 99.17, DEAAm = 127.18, DAlAAm = 151.21) × Conv. + (MW of initiator or propagation residue).

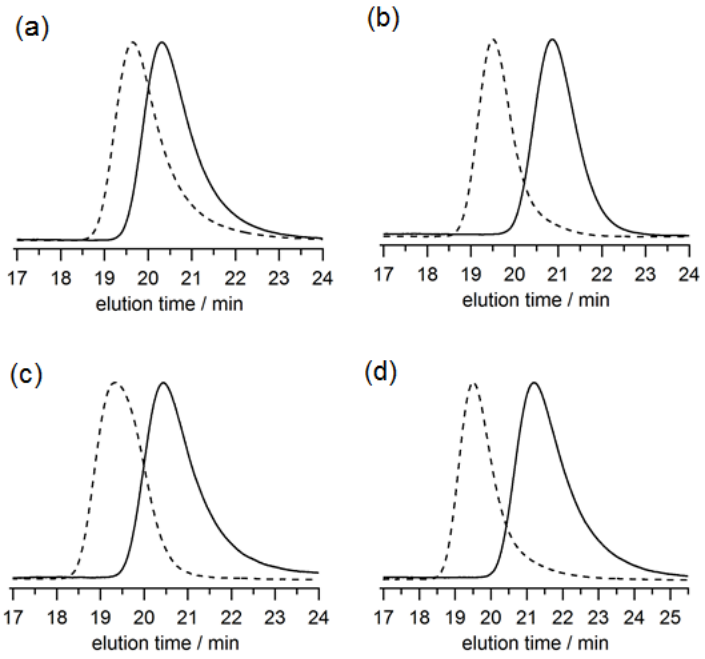

Figure 2-9. SEC traces of the obtained block copolymers, (a) run 2-25, (b) run 2-26, (c) run 2-27, (d) run 2-28 (eluent, DMF containing 0.01 mol L^{-1} LiCl; flow rate, 0.6 mL min^{-1}).

2.3.6. Synthesis of hetero diblock copolymer by the Lewis acid-catalyzed GTP. Given the fact that a SKA initiator has been applicable for the Lewis acid-catalyzed GTPs of both methacrylate and acrylamide monomers, we then attempted the synthesis of hetero-block copolymers composed of methacrylate and acrylamide blocks by the sequential GTP method. Twenty-five equivalents of MMA were first completely polymerized; afterwards, 50 equivalents of a DAAm monomer (DEAAm, DAlAAm, or NAM) were added to continue the second-stage polymerization. The block copolymerization under the reverse addition of MMA and a DAAm monomer did not work because the first polymerization of an acrylamide monomer produces a PDAAm bearing a silyl ketene aminal (SKAm) as the living end, which has been known not to initiate the polymerization of a methacrylate monomer. The block copolymerization of MMA and DEAAm (run 2-29, Table 2-5) was first undergone using $B(C_6F_5)_3$ as the catalyst. However, the second-stage polymerization of DEAAm did not proceed at all though the first-stage polymerization of MMA was fairly successful, probably because the large amount of $B(C_6F_5)_3$ required by GTP of MMA stopped the polymerization of DEAAm. To solve this problem, $C_6F_5CHTf_2$ and Me_3SiNTf_2 with a much higher acidity than $B(C_6F_5)_3$ were then used. The block copolymerizations (runs 2-30~35, Table 2-5) afforded quantitative monomer conversions for both the MMA and DAAm monomers and perfect molecular weight control of the PMMAs were obtained in the first-stage polymerizations. The initiation efficiencies of the first-stage polymerizations of MMA estimated from the $M_{n,calcd.}/M_{n.SEC}$s were extremely close to 100%. However, the sequential polymerization of a DAAm monomer afforded mixed polymer products as confirmed by the SEC measurements in Figure 2-10, of which one trace points to the hetero-block copolymer of PMMA-*b*-PDAAm and the other to the unreacted PMMAm. For example, the $C_6F_5CHTf_2$-catalyzed block copolymerization of

MMA and DEAAm using SKA^{Et} (run 2-30) afforded the mixed polymer products of PMMA-*b*-PDEAAm and PMMA. The $M_{n.SEC}$ of PMMA-*b*-PDEAAm was 47.2 kg mol^{-1}, which was significantly higher than the $M_{n.calcd.}$ of 8.96 kg mol^{-1} calculated based on the premise that all the SKA ends of PMMA obtained in the first-stage polymerization initiated the second-stage polymerization of DEAAm. The mixed polymer products were isolated to obtain the pure PMMA-*b*-PDEAAm and PMMA by preparative SEC in order to estimate the initiation efficiency in the second-stage polymerization and confirm the chemical structure of the unreacted PMMA. Because of the perfect polymerization control in the first-stage and the nearly 100% initiation efficiency of the polymerization of MMA, it is rational to assume that the average degree of polymerization (DP) of the PMMA block is the same with the $[MMA]_0/[SKA^{Et}]_0$ ratio of 25. Based on this assumption, the ^1H NMR measurements of PMMA-*b*-PDEAAm indicated that the PDEAAm block had an average DP of 161. Thus, the initiation efficiency of the second-stage polymerization was estimated by $([DEAAm]_0/[SKA^{Et}]_0)/DP$ as 31%. On the other hand, the analysis of the chemical structure of the unreacted PMMA by MALDI-TOF MS in Figure 2-11 indicated that this unreacted PMMA product was due to the desilylated PMMA obtained after quenching with MeOH. This result strongly suggested that no side reactions occurred during the entire polymerization course of MMA, and supported the fact that a part of the living SKA ends of PMMA did not initiate the second-stage polymerization of DEAAm, leading to the eventual low initiation efficiency. This phenomenon can be well explained by the fact that the polymerization rate of DEAAm from a SKAm end is significantly greater than the initiation rate, *i.e.*, the reaction rate of the Mukaiyama-Micheal reaction of the SKA end of PMMA with DEAAm*.[38] This leads to the fact that the polymerization of DEAAm was completed upon the initial SKAm formation from the Mukaiyama-Micheal reaction of only

a part of the SKA ends of PMMA with DEAAm*, and that the unreacted living PMMAs were left in the polymer products, as depicted in Scheme 2-3. The slower initiation rate than the polymerization rate is also the reason why the resulting block copolymers showed relatively broad polydispersities. In contrast, the $C_6F_5CHTf_2$-catalyzed block copolymerization of MMA and DEAAm using the more reactive SKA^{Me} (run 2-31) showed an improved initiation efficiency of the second-stage polymerization of DEAA (36%) and produced a PMMA-*b*-PDEAAm with a $M_{n.SEC}$ (44.8 kg mol^{-1}) lower than that of PMMA-*b*-PDEAAm obtained in run 2-30 due to the enhanced initiation rate between SKA^{Me} and DEAAm*. These polymerization behaviors were also observed for the Me_3SiNTf_2-catalyzed block copolymerizations of MMA and DEAAm using ^{Et}SKA and ^{Me}SKA (runs 2-32 and 2-33).

It is rather clear that in order to obtain a higher initiation efficiency and better polymerization control of the second-stage polymerization is to have the appropriate balance between the initiation (from SKA end of PMMA) and polymerization rates. Considering this, the block copolymerizations using the more reactive SKA^{Me} and less reactive DAAm monomers of DAlAAm or NAM were further investigated by the Me_3SiNTf_2-catalyzed GTP, as shown in runs 2-34~35. SKA^{Me} was used to enhance the initiation rate, while DAlAAm and NAM were used to reduce the polymerization rate. Obviously, the polymerization control over the molecular weight and polydispersity of the final block copolymers was remarkably improved in these two block copolymerizations as the $M_{n.SEC}$s of 17.0 (PMMA-*b*-PDAlAAm, run 2-34) and 11.4 (PMMA-*b*-PNAM, run 2-35) kg mol^{-1} were much closer to their corresponding $M_{n.calcd.}$s of 10.2 and 9.66 kg mol^{-1}, respectively. Especially when NAM was used as the second monomer, the block copolymerization turned out to be almost perfect (Figure 2-10(f)). In short summary, these

results strongly suggest that the perfect block copolymerization of different acrylic monomers can be achieved by carefully selecting the reactivity-matched comonomers. This has been the first finding in this regard in the GTP field.

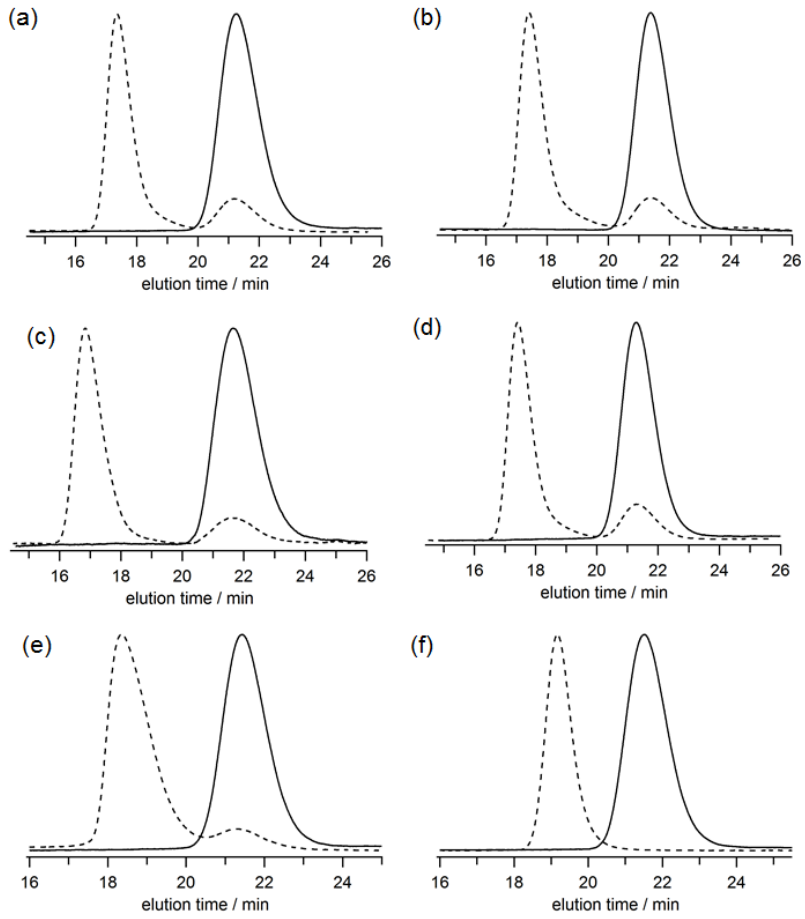

Figure 2-10. SEC traces of the obtained block copolymers, (a) run 2-30, (b) run 2-31, (c) run 2-32, (d) run 2-33, (e) run 2-34, (f) run 2-35 (eluent, DMF containing 0.01 mol L^{-1} LiCl; flow rate, 0.6 mL min^{-1}).

Table 2-5. Synthesis of hetero-block copolymers by sequential acid-catalyzed GTP of MMA and DAAm [a]

run	Monomer (M)		Initiator	Catalyst	$[M]_0/[SKA]_0$	$[B(C_6F_5)_3]_0/[^{Et}SKA]_0$	time (h)	$M_{n,SEC}$ [b] ($M_{n,calcd.}$ [c]) (kg mol^{-1})	M_w/M_n [b]
2-29	1st	MMA	SKA^{Et}	$B(C_6F_5)_3$	25	0.30	2	2.49 (2.50)	1.09
	2nd	DEAAm			50		45	n.d. [d]	n.d. [d]
2-30	1st	MMA	SKA^{Et}	$C_6F_5CHTf_2$	25	0.02	2	2.57 (2.50)	1.10
	2nd	DEAAm			50		12	47.2 (8.96)	1.27 [e]
2-31	1st	MMA	SKA^{Me}	$C_6F_5CHTf_2$	25	0.02	2	2.59 (2.50)	1.07
	2nd	DEAAm			50		5	44.8 (8.96)	1.26 [e]
2-32	1st	MMA	SKA^{Et}	Me_3SiNTf_2	25	0.02	1.5	2.16 (2.50)	1.07
	2nd	DEAAm			50		7.5	78.4 (8.96)	1.30 [e]
2-33	1st	MMA	SKA^{Me}	Me_3SiNTf_2	25	0.02	1.5	2.51 (2.50)	1.06
	2nd	DEAAm			50		3	43.5 (8.96)	1.30 [e]
2-34	1st	MMA	SKA^{Me}	Me_3SiNTf_2	25	0.02	1.25	2.43 (2.50)	1.07
	2nd	DAlAAm			50		13	17.0 (10.2)	1.26 [e]
2-35	1st	MMA	SKA^{Me}	Me_3SiNTf_2	25	0.02	1	2.34 (2.50)	1.06
	2nd	NAM			50		21	11.4 (9.66)	1.11

[a] Ar atmosphere; temp., r.t.; $[monomer]_0$ = 1.0 mol L^{-1}; conv., >99% as determined by ^{1}H NMR in $CDCl_3$. [b] Determined by SEC in DMF containing 0.01 mol L^{-1} of LiCl calibrated with PMMA. [c] Calculated from $[monomer]_0/[initiator]_0$ × (MW of monomer: MMA = 100.12, DEAAm = 127.18, DAlAAm = 151.21, NAM = 141.17) × conv. + (MW of initiator or propagation residue). [d] Not determined due to no second-stage polymerization. [e] The shape of SEC was bimodal.

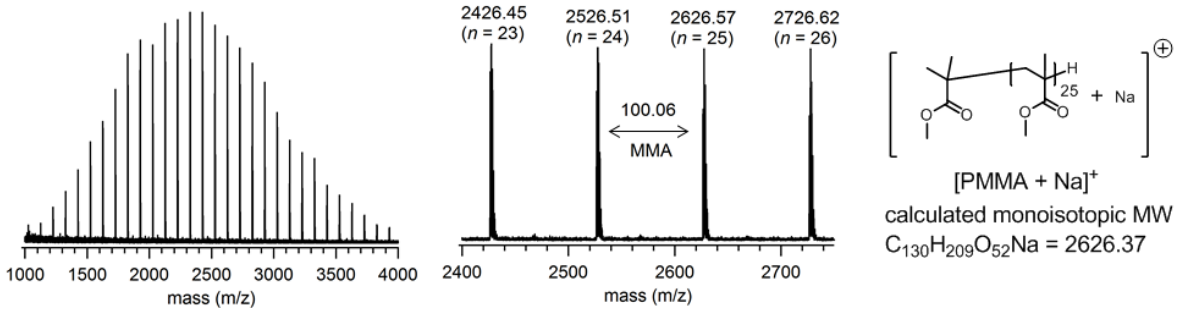

Figure 2-11. MALDI-TOF MS spectrum of the PMMA residue obtained from the low molecular weight part of run 2-31 shown in Figure 2-10(b) (dashed line) after purification by preparative SEC.

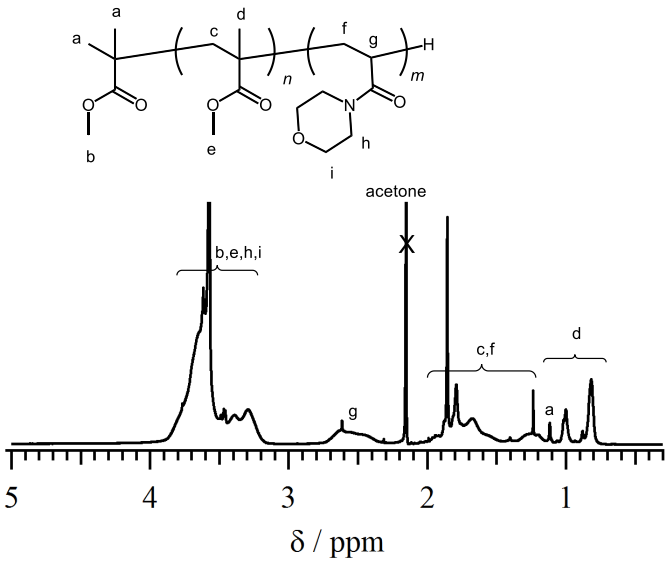

Figure 2-12. ^{1}H NMR spectrum of the obtained block copolymer from run 2-35 in $CDCl_3$ (400 MHz).

Scheme 2-3. A schematic diagram for the diblock GTP of MMA and DAAm.

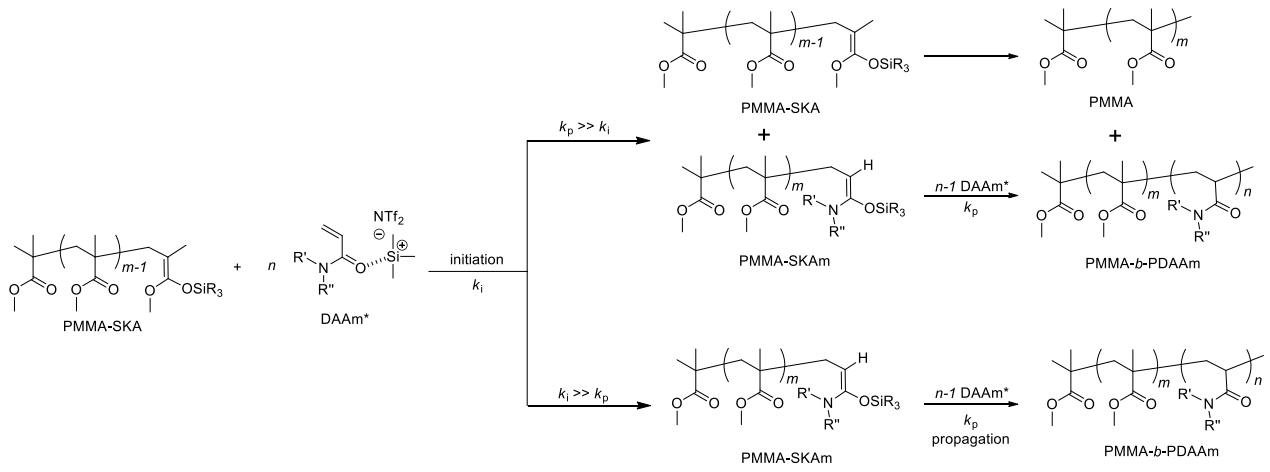

2.4. Conclusions

Various combinations of acidic organocatalysts (Me_3SiNTf_2, $C_6F_5CHTf_2$, and $B(C_6F_5)_3$) and SKAs (SKA^{Me}, SKA^{Et}, SKA^{iPr}, and SKA^{Ph}) were proven to be significantly efficient for the GTPs of DEAAm to produce well-defined PDEAAms, among which the polymerization using $B(C_6F_5)_3$ and SKA^{Et} showed a relatively better control over the molecular weight distribution. The $B(C_6F_5)_3$-catalyzed GTP using SKA^{Et} was applicable to various DAAms including the water-soluble, thermoresponsive, and reactive ones. All the $B(C_6F_5)_3$-catalyzed polymerizations showed an obvious induction period of tens of minutes, after which it proceeded as a zero-order reaction in a living fashion. The occurrence of the induction period was clearly attributed to the structural mismatch between the SKA and DAAm. In addition, the initiation and propagation rates of a DAAm were significantly dependent on its *N*-disubstituents and the balance between them was the key factor for well controlling the polymerization, *i.e.*, the GTPs of API, NAM, BMEAAm, and DAlAAm with relatively bulky substituents were well-controlled due to the good balance of the initiation and propagation rates, while those of DMAAm, DEAAm,

D*n*PAAm, and MMEAAm with less bulky substituents had worse polymerization control. Acrylamide polymers with an average DP of no more than 200 could be synthesized by the $B(C_6F_5)_3$-catalyzed GTP method. The livingness of the polymerization system was suitable for synthesizing homo block copolymers composed of different acrylamide blocks and hetero block copolymers of PMMA-*b*-PDAAm by the sequential GTP method. Importantly, it has been shown for the first time that a perfect hetero-block copolymer of PMMA-*b*-PNAM could be synthesized by selecting the reactivity-matched comonomers of MMA and NAM using the combination of the much stronger Lewis acid catalyst, Me_3SiNTf_2, and SKA^{Me}. This information is crucially helpful for designing the well-defined hetero-block copolymers, which are currently under investigation. As an expectation, these resulting homo acrylamide polymers, homo block acrylamide copolymers, and hetero block copolymers in this study are applicable for various purposes such as polymer electrolytes, smart polymer materials, and flocculating agents. This study has provided significant progress in the organocatalyzed GTP of DAAms and is expected to help polymer chemists in designing new acrylamide polymers.

2.5. References and Notes

(1) Qian, J. W.; Xiang, X. J.; Yang, W. Y.; Wang, M.; Zheng, B. Q. *Eur. Polym. J.* **2004**, *40*, 1699-1704.

(2) Christensen, L. H. *Dermatologic Surgery* **2009**, *35*, 1612-1619.

(3) Huang, X.; Wirth, M. J. *Macromolecules* **1999**, *32*, 1694-1696.

(4) Teodorescu, M.; Matyjaszewski, K. *Macromol. Rapid Commun.* **2000**, *21*, 190-194.

(5) Benoit, D.; Chaplinski, V.; Braslau, R.; Hawker, C. J. *J. Am. Chem. Soc.* **1999**, *121*, 3904-3920.

(6) Convertine, A. J.; Lokitz, B. S.; Lowe, A. B.; Scales, C. W.; Myrick, L. J.; McCormick, C. L. *Macromol. Rapid Commun.* **2005**, *26*, 791-795.

(7) Cao, Y.; Zhu, X. X.; Luo, J.; Liu, H. *Macromolecules* **2007**, *40*, 6481-6488.

(8) Thomas, D. B.; Sumerlin, B. S.; Lowe, A. B.; McCormick, C. L. *Macromolecules* **2003**, *36*, 1436-1439.

(9) Xie, X.; Hogen-Esch, T. E. *Macromolecules* **1996**, *29*, 1746-1752.

(10) Kobayashi, M.; Ishizone, T.; Nakahama, S. *Macromolecules* **2000**, *33*, 4411-4416.

(11) Kobayashi, M.; Okuyama, S.; Ishizone, T.; Nakahama, S. *Macromolecules* **1999**, *32*, 6466-6477.

(12) Kobayashi, M.; Ishizone, T.; Nakahama, S. *J. Polym. Sci., Part A: Polym. Chem.* **2000**, *38*, 4677-4685.

(13) Ishizone, T.; Yashiki, D.; Kobayashi, M.; Suzuki, T. Ito, M. Nakahama, S. *J. Polym. Sci., Part A: Polym. Chem.* **2007**, *45*, 1260-1271.

(14) Suzuki, T.; Kusakabe, J.; Ishizone, T. *Macromolecules* **2008**, *41*, 1929-1936.

(15) Suzuki, T.; Kusakabe, J.; Kitazawa, K.; Nakagawa, T.; Kawauchi, S.; Ishizone, T. *Macromolecules* **2010**, *43*, 107-116.

(16) Ito, M.; Ishizone, T. *J. Polym. Sci., Part A: Polym. Chem.* **2006**, *44*, 4832-4845.

(17) Kobayashi, M. Chiba, T.; Tsuda, K.; Takeishi, M. *J. Polym. Sci., Part A: Polym. Chem.* **2005**, *43*, 2754-2764.

(18) Webster, O. W.; Hertler, W. R.; Sogah, D. Y.; Farnham W. B.; RajanBabu, T. V. *J. Am. Chem. Soc.* **1983**, *105*, 5706-5708.

(19) Sogah, D. Y.; Hertler, W. R.; Webster, O. W.; Cohen, G. M. *Macromolecules* **1987**, *20*, 1473-1488.

(20) Webster, O. W. *J. Polym. Sci., Part A: Polym. Chem.* **2000**, *38*, 2855-2860.

(21) Webster, O. W. *Adv. Polym. Sci.* **2004**, *167*, 1-34.

(22) Zhuang, R.; Müller, A. H. E. *Macromolecules* **1995**, *28*, 8035-8042.

(23) Zhuang, R.; Müller, A. H. E. *Macromolecules* **1995**, *28*, 8043-8050.

(24) Fuchise, K.; Chen, Y.; Satoh, T.; Kakuchi, T. *Polym. Chem.* **2013**, *4*, 4278-4291.

(25) Ute, K.; Ohnuma, H.; Kitayama, T. *Polym. J.* **2000**, *32*, 1060-1062.

(26) Raynaud, J.; Ciolino, A.; Beceiredo, A.; Destarac, M.; Bonnette, F.; Kato, T.; Gnanou, Y.; Taton, D. *Angew. Chem. Int. Ed.* **2008**, *47*, 5390-5393.

(27) Scholten, M. D.; Hedrick, J. L.; Waymouth, R. M. *Macromolecules* **2008**, *41*, 7399-7404.

(28) Raynaud, J.; Liu, N.; Gnanou, Y.; Taton, D. *Macromolecules* **2009**, *42*, 5996-6005.

(29) Zhang, Y.; Chen, E. Y.-X. *Macromolecules* **2008**, *41*, 36-42.

(30) Zhang, Y.; Chen, E. Y.-X. *Macromolecules* **2008**, *41*, 6353-6360.

(31) Fevre, M.; Vignolle, J.; Heroguez, V.; Taton, D. *Macromolecules* **2012**, *45*, 7711-7718.

(32) Kakuchi, R.; Chiba, K.; Fuchise K.; Sakai, R.; Satoh, T.; Kakuchi, T. *Macromolecules* **2009**, *42*, 8747-8750.

(33) Kakuchi, T.; Chen, Y.; Kitakado, J.; Mori, K.; Fuchise, K.; Satoh, T. *Macromolecules* **2011**, *44*, 4641-4647.

(34) Takada, K.; Fuchise, K.; Chen, Y.; Satoh, T.; Kakuchi, T. *J. Polym. Sci. Part A: Polym. Chem.* **2012**, *50*, 3560-3566.

(35) Eggert, M.; Freitag, R. *J. Polym. Sci., Part A: Polym. Chem.* **1994**, *32*, 803-813.

(36) Freitag, R.; Baltes, T.; Eggert, M. *J. Polym. Sci., Part A: Polym. Chem.* **1994**, *32*, 3019-3030.

(37) Baltes, T.; Garret-Flaudy, F.; Freitag, R. *J. Polym. Sci., Part A: Polym. Chem.* **1999**, *37*, 2977-2989.

(38) Fuchise, K.; Sakai, R.; Satoh, T.; Sato, S.; Narumi, A.; Kawaguchi, S.; Kakuchi, T. *Macromolecules* **2010**, *43*, 5589-5594.

(39) Fuchise, K.; Chen, Y.; Takada, K.; Satoh, T.; Kakuchi, T. *Macromol. Chem. Phys.* **2012**, *213*, 1604-1611.

(40) Raynaud, J.; Liu, N.; Gnanou, Y.; Taton, D. *Macromolecules* **2010**, *43*, 8853-8861.

(41) Raynaud, J.; Liu, N.; Fèvre, M.; Gnanou, Y.; Taton, D. *Polym. Chem.* **2011**, *2*, 1706-1712.

(42) Hasegawa, A.; Naganawa, Y.; Fushimi, M.; Ishihara, K.; Yamamoto, H. *Org. Lett.* **2006**, *8*, 3175-3178.

(43) Liu, S.-Y.; Hills, I. D.; Fu, G. *J. Am. Chem. Soc.* **2005**, *127*, 15352-15353.

(44) Parks, D. J.; Piers, W. E.; Parvez, M.; Atencio, R.; Zaworotko, M. J. *Organometallics* **1998**, *17*, 1369-1377.

Chapter 3

Synthesis and Thermoresponsive Property of Linear, Cyclic, and Star-shaped Poly(*N*,*N*-diethylacrylamide)s Using $B(C_6F_5)_3$-catalyzed Group Transfer Polymerization as Facile End-functionalization Method

3.1. Introduction

The topological effects of macromolecules on their bulk and solution properties, such as the glass transition temperature,[1,2] viscosity,[1,2] thermoresponsivity,[3,4] micellarization,[5,6] and microphase separation,[7,8] have been intensively studied in terms of experimental and theoretical aspects.[9] For instance, a cyclic macromolecular architecture, one of the most representative and well-known topologies, has been paid much attention to its unique property due to the absence of chain ends versus a comparative linear counterpart.[10] For the synthetic methodology of the cyclic polymer, the intramolecular cyclization of the telechelic α,ω-end functionalized polymers has been used as one of the reliable methods.[11] Therefore, the development of controlled/living polymerization methods involving reliable end-functionalizations has been of significant importance from the viewpoint of α,ω-end functionalized polymer syntheses.[12-15] Recently, organocatalyzed polymerization has been rapidly developed as one of the controlled/living techniques, such as the ring-opening polymerization (ROP) of epoxides, lactones, lactide, and cyclic carbonates, which proceeded in a relatively controlled/living way to produce their corresponding well-defined polymers.[16] In particular, the ROPs using functional initiators easily produced various α-end-functionalized polymers, and a further chemical transformation for the ω-end of these α-end-functionalized polymers afforded α,ω-end functionalized polymers as the starting materials for the intramolecular cyclization.[17]

Apart from the organocatalyzed ROP, the GTP using an organocatalyst has been developed as an important organocatalytic polymerization method in past years.[18] Both the basic and acidic organocatalysts can be used for the GTP. For example, Waymouth et al. and Taton et al. independently reported that *N*-heterocyclic carbene performed as an efficient basic organocatalyst for the GTP of acrylate, methacrylate, and acrylamide monomers using silyl ketene acetal (SKA) as the initiator.[19-22] Kakuchi et al. also reported that organic Brønsted acids of

trifluoromethanesulfonimide ($HNTf_2$) and pentafluorophenylbis(triflyl)methane ($C_6F_5CHTf_2$), organic Lewis acids of *N*-(trimethylsilyl)triflylimide (Me_3SiNTf_2) and tris(pentafluorophenyl)borane ($B(C_6F_5)_3$), and the organic Lewis bases of proazaphosphatrane and phosphazene effectively catalyzed the controlled/living GTP of acrylic monomers by suitably tuning the combination of the organocatalyst and initiator.[23-26] In greater detail, $HNTf_2$, Me_3SiNTf_2, and the phosphazene base were used with a commercially available SKA of 1-methoxy-1-trimethylsilyloxy-2-methyl-propene (SKA^{Me}) for methacrylate monomers, $HNTf_2$ and Me_3SiNTf_2 with 1-methoxy-1-triisopropylsilyloxy-2-methyl-propene (SKA^{iPr}) for acrylate monomers, and $HNTf_2$ and $C_6F_5CHTf_2$ with a silyl ketene aminal (SKAm) of (*Z*)-1-(*N*,*N*-dimethylamino)-1-trimethylsiloxy-1-propene ((*Z*)-SKAm) and $B(C_6F_5)_3$ with 1-methoxy-1-(triethylsiloxy)-2-methyl-1-propene (SKA^{Et}) for acrylamide monomers.

The GTP is recognized as the repetitive Mukaiyama-Michael reaction between SKA or SKAm and acrylic monomers, which has been essentially potential to modify the chain end groups by initiation and termination approaches. The SKA group at the propagating polymer chain-end is able to react with various substrates, such as aldehydes, ketones, imines, and ketoesters. For example, Sogah et al. reported that α-end-functionalized poly(methyl methacrylate)s (PMMAs) with hydroxyl and carboxylic acid groups were synthesized by the conventional GTP using functional SKAs.[27] Sivaram et al. reported the synthesis of ω-end-functionalized PMMAs with hydroxyl, primary amine, and lactone groups by the conventional GTP using benzaldehyde, *N*-(trimethylsilyl)benzaldimine, and 5,6-dihydro-2H-pyran-2-one, respectively, as terminators though their functionalization degrees were insufficient.[28] Our group have already developed the end-functionalization at both chain ends by the organocatalyzed GTP, leading to structurally defect-free polymers with well-controlled molecular weights and molecular weight distributions.[29-31] For the *α*-end-functionalization of poly(*n*-butyl acrylate)s (P*n*BAs) and PMMAs,

Kakuchi et al. designed and used functional SKA^{iPr} and SKA^{Me} with hydroxyl, vinyl, ethynyl, and norbornenyl groups.[29,30] The ω-end-functionalized PMMAs were synthesized using functional benzaldehydes and functional 2-phenylacrylates (PhA-Fs) and the ω-end functionalized P*n*BA using PhA-Fs.[29,30] Furthermore, these initiation and termination approaches realized the α,ω-end-functionalization of P*n*BAs using functional SKA^{iPr}s and PhA-Fs. The synthesis of the end-functionalized poly(*N*,*N*-disubstituted acrylamide) (PDAAm) was exceedingly limited such as the functionalization of the α- or ω-ends using the RAFT polymerization technique,[32,33] and there is no report about the synthesis of the α,ω-end-functionalized PDAAm. Therefore, the facile and comprehensive synthesis of α-, ω-, and α,ω-end-functionalized PDAAms is required and still a challenging issue.

In this chapter, the author focuses on the end-functionalization of the thermoresponsive (PDEAAm), which is applicable as a polymeric precursor for preparing various macromolecular architectures, such as well-defined PDEAAms with cyclic and star-shaped structures. The study for the thermoresponsive property of PDEAAm is insufficient in comparison with poly(*N*-isopropylacrylamide).[34,35] In particular, there is no report about the topological effect of PDEAAm on its thermoresponsive property, which is, therefore, interesting to elucidate the synthetic method for cyclic and star-shaped PDEAAms and characterize their thermal phase transition properties in terms of the thermoresponsive feature of polyacrylamides. In this study, the α-, ω-, and α-,ω-end-functionalized PDEAAms were synthesized by the B(C_6F_5)$_3$-GTP of *N*,*N*-diethylacrylamide (DEAAm) using functional initiators and terminators, respectively, and the synthetic procedures of the cyclic and star-shaped PDEAAms are shown in Scheme 1. This study describes (1) the α-end functionalized PDEAAm (F-PDEAAm) prepared using the functional initiator of F-SKAm (Scheme 3-1a), (2) the ω-end functionalized PDEAAm (PDEAAm-F) prepared using the functional terminator of PhA-F and the synthesis of star-shaped PDEAAm (*s*-PDEAAm) by the

azide-alkyne cycloaddition between the ω-azide functionalized PDEAAm and a core linking agent with three ethynyl groups (Scheme 3-1b), (3) the synthesis of the α-ethylnyl,ω-azide end-functionalized PDEAAm (F-PDEAAm-F) and its intramolecular azido-alkyne cycloaddition leading to a macrocyclic PDEAAm (*c*-PDEAAm) (Scheme 3-1c), and (4) the topological effect of the linear, cyclic, and star-shaped PDEAAms on their thermoresponsive properties in aqueous solution.

Scheme 3-1. Synthesis of Well-defined Linear, Cyclic, and Star-shaped PDEAAms Using α-, ω-, and α,ω-End-functionalized Poly(*N*,*N*-diethylacrylamide)s by $B(C_6F_5)_3$-catalyzed Group Transfer Polymerization

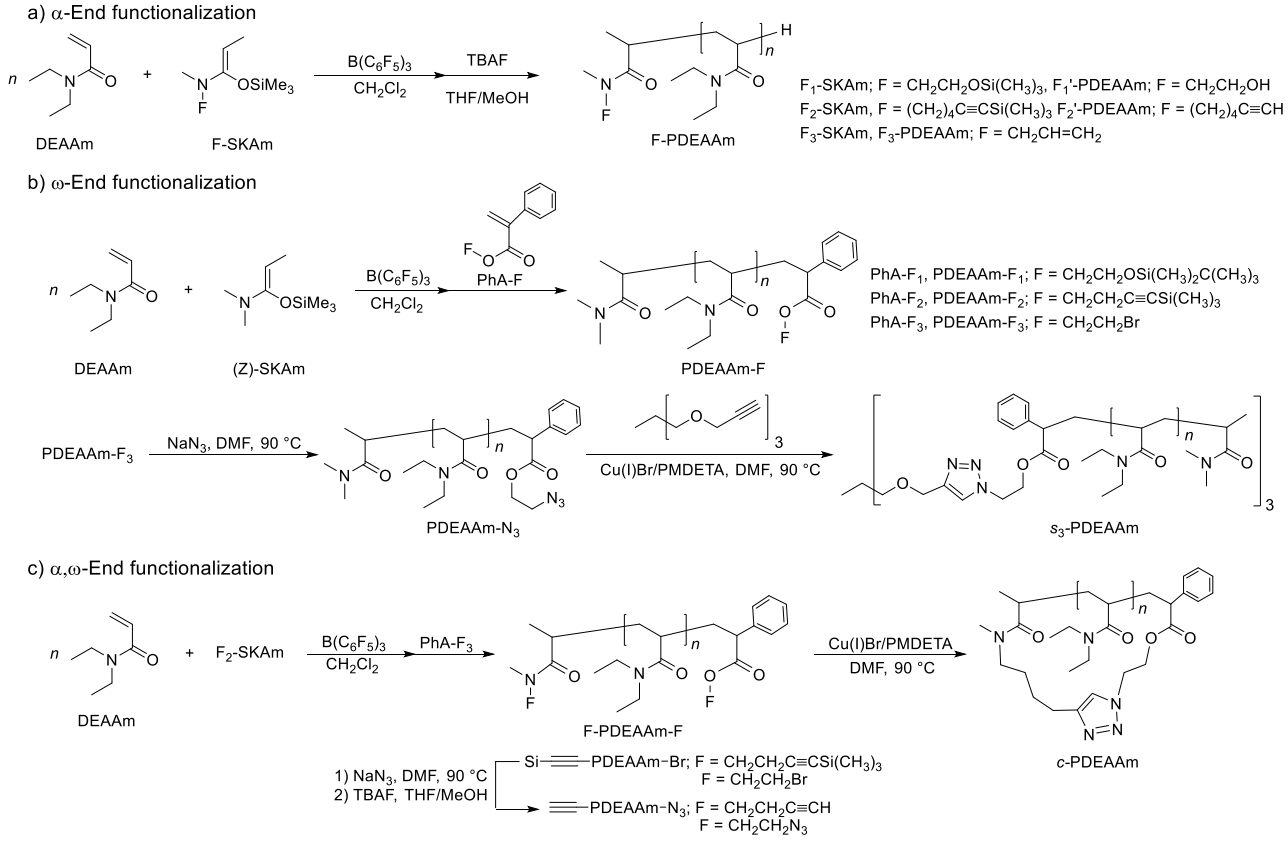

3.2. Experimental section

Materials. Dichloromethane (CH_2Cl_2, >99.5%; water content, <0.001%), methanol (MeOH), *N*,*N*-dimethylformamide (DMF), deuterated chloroform ($CDCl_3$, >99.8%), acetone-d_6, and *n*-butyl lithium (1.60 mol L^{-1} in *n*-hexane) were purchased from Kanto Chemicals Co., Inc. *N*,*N*-Diethylacrylamide (DEAAm) and *trans*-3-indoleacrylic acid were purchased from Tokyo Kasei Kogyo Co., Ltd. Sodium trifluoroacetate was purchased from the Sigma-Aldrich Chemicals Co. Tris(pentafluorophenyl)borane ($B(C_6F_5)_3$) was purchased from Wako Pure Chemical Industries, Ltd. and was used after recrystallization from *n*-hexane at 30 °C. DEAAm and CH_2Cl_2 were distilled from CaH_2 and degassed by three freeze-pump-thaw cycles prior to use. (*Z*)-1-Dimethylamino-1-trimethylsiloxy-1-propene ((*Z*)-SKAm) and the 2-phenylacrylate derivatives (PhA-F_1, PhA-F_2, and PhA-F_3) were synthesized according to previous reports.[23,29] A Spectra/Por® 6 Membrane (MWCO: 1000) was used for the dialysis. All other chemicals were purchased from available suppliers and used without purification.

Measurements. The polymerization solution was prepared in an MBRAUN stainless steel glovebox equipped with a gas purification system (molecular sieves and copper catalyst) having a dry argon atmosphere (H_2O, O_2 < 1 ppm). The moisture and oxygen contents in the glovebox were monitored by an MB-MO-SE 1 and an MB-OX-SE 1, respectively. The ^1H (400 MHz) and ^{13}C NMR (100 MHz) spectra were recorded using a JEOL ECS400. Size exclusion chromatography (SEC) in DMF containing lithium chloride (0.01 mol L^{-1}) was performed at 40 °C using a Jasco high performance liquid chromatography (HPLC) system (PU-980 Intelligent HPLC pump, CO-965 column oven, RI-930 Intelligent RI detector, and Shodex DEGAS KT-16) equipped with a Shodex Asahipak GF-310 HQ column (linear, 7.6 mm × 300 mm; pore size, 20 nm; bead size, 5 μm; exclusion limit, 4×10^4) and a Shodex Asahipak GF-7M HQ column (linear, 7.6 mm × 300 mm; pore size, 20 nm; bead size, 9 μm; exclusion limit, 4×10^7) at the flow rate of

0.4 mL min^{-1}. The M_n and M_w/M_n of the obtained polymers were determined by the RI based on poly(methyl methacrylate) (PMMA) with the M_w (M_w/M_n)s of 1.25×10^6 g mol^{-1} (1.07), 6.59×10^5 g mol^{-1} (1.02), 3.003×10^5 g mol^{-1} (1.02), 1.385×10^5 g mol^{-1} (1.05), 6.015×10^4 g mol^{-1} (1.03), 3.053×10^4 g mol^{-1} (1.02), 1.155×10^4 g mol^{-1} (1.04), 4.90×10^3 g mol^{-1} (1.10), 2.87×10^3 g mol^{-1} (1.06), and 1.43×10^3 g mol^{-1} (1.15). The preparative SEC was performed in $CHCl_3$ (4.0 mL min^{-1}) at room temperature using a JAI LC-9201 equipped with a JAI JAIGEL-2.5H column (20 mm × 600 mm; exclusion limit, 2×10^4), and a JAI RI-50s refractive index detector. The intrinsic viscosity ([η]) was estimated by size exclusion chromatography (SEC) in DMF containing of 0.01 mol L^{-1} LiCl (1.0 mL min^{-1}) at 40 °C using an Agilent 1100 series instrument equipped with a Shodex KD-806 column (linear, 8.0 mm × 300 mm; exclusion limit, 2×10^7; bead size, 10 μm), a DAWN 8 multi-angle laser light scattering (MALS) detector (Wyatt Technology, Santa Barbara, CA), a Viscostar viscosity detector (Wyatt Technology), and an Optilab rEX refractive index detector (Wyatt Technology). The IR spectra were recorded using a Perkin-Elmer Paragon 1000 FT-IR instrument. The matrix-assisted laser desorption/ionization time-of-flight mass spectrometry (MALDI-TOF MS) measurements were performed using an Applied Biosystems Voyager-DE STR-H mass spectrometer with a 25 kV acceleration voltage. The positive ions were detected in the reflector mode (25 kV). A nitrogen laser (337 nm, 3 ns pulse width, 106–107 W cm^{-2}) operating at 3 Hz was used to produce the laser desorption, and 100-300 shots were summed. The spectra were externally calibrated using a sample prepared from narrow-dispersed polystyrene (Chemco Scientific Co., Ltd., M_n = 3.8 kg mol^{-1}, M_w/M_n = 1.08, 25 μL, 10 mg mL^{-1} in THF), the matrix (1,8-dihydroxy-9-(10*H*)-anthracenone, 50 mg mL^{-1}, 20 μL), and the cationizing agent (silver trifluoroacetate, 10 mg mL^{-1}, 10 μL) with a linear calibration. Samples for the MALDI-TOF MS were prepared by mixing the polymer (1.5 mg mL^{-1}, 10 μL), the matrix (*trans*-3-indoleacrylic acid, 10 mg mL^{-1}, 90 μL), and the cationizing agent (sodium

trifluoroacetate, 10 mg mL^{-1}, 10 μL) in THF. The cloud point measurements were performed on the ultraviolet-visible (UV-vis) spectra by passing through a 10-mm path-length quartz cell using a Jasco V-550 spectrophotometer equipped with an EYELA NCB-1200 temperature controller. The highly sensitive differential scanning calorimetry (micro-DSC) measurements were performed using a Micro-DSCVII from SETRAM. The thermogram was measured at 1.0 °C min^{-1} during the heating and cooling cycles, and the enthalpy changes per monomer repeating units (ΔH) were estimated from the thermogram of the second heating cycle.

Synthesis of functional initiators

Scheme 3-2. Synthetic pathway of the functional silyl ketene aminal

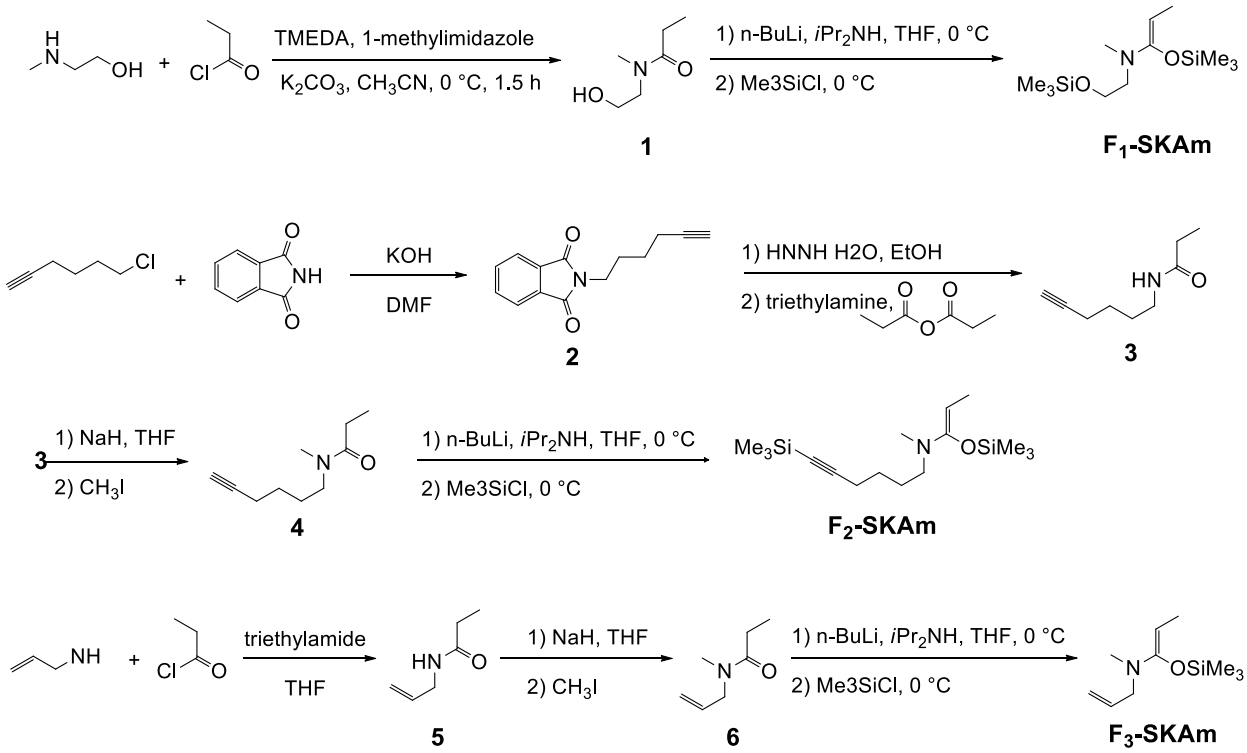

6-Phthalimide-1-hexyne (2)[36] and *N*-2-propenylpropionamide (5)[37] were synthesized according to the literature.

***N*-(2-Hydroxyethyl)-*N*-methylpropionamide (1).** To a suspension of 2-(methylamino)ethanol (15.0 mL, 188 mmol), 1-methylimidazole (1.24 mL, 15.7 mmol), TMEDA (2.33 mL, 15.7 mmol), and K_2CO_3 (26.3 g, 190 mmol) in acetonitrile (200 mL), propionyl chloride (13.7 mL, 157 mmol) was dropwise added at 0 °C. After stiring for one hour, the reaction mixture was filtered, then condensed under reduced pressure. The crude product was purified by distillation from CaH_2 under reduced pressure (120 °C/ 0.08 mmHg), affording 1 as a transparent liquid. Yield, 14.85 g (72.3 %). ^{1}H NMR (400 MHz, $CDCl_3$): δ (ppm) 1.00-1.08 (t, 3H, C*H*$_3$CH$_2$-), 2.23-2.38 (m, 2H, CH$_3$C*H*$_2$-), 2.86, 2.98 (s, 3H, NC*H*$_3$), 3.34-3.39, 3.42-3.47 (t, *J* = 6.0 Hz, 2H, -NC*H*$_2$CH$_2$OH), 3.63-3.68 (t, *J* = 5.6 Hz, 2H, -NCH$_2$C*H*$_2$OH).

(*Z*)-1-(*N*-Methyl-*N*-2-trimetylsiloxyethyl)amino)-1-trimethylsiloxy-1-propene (F$_1$-SKAm). To a solution of diisopropylamine (12.8 mL, 90.8 mmol) in dry-THF (ca.70 mL) in a 200-mL three-necked flask, *n*-butyllithium (50.9 mL, 82.5 mmol; 1.60 mol L^{-1} in *n*-hexane) was dropwise added at 0 °C under an argon atmosphere. After stirring for 30 min, 1 (5.41 g, 41.2 mmol) was slowly added. The reaction mixture was stirred at 0 °C for 1 h, then chlorotrimethylsilane (15.7 mL, 124 mmol) was added. After stirring for an 1 h at 0 °C, the solvent was removed under reduced pressure, and directly distilled under reduced pressure (97-101 °C, 7.50 mmHg). The purity of the product was estimated to be 60 % by ^{1}H NMR measurements. The further trimethylsilylation of the product was thus carried out once more by the same procedures as described above with diisopropylamine (3.76 mL, 26.7 mmol), *n*-butyllithium (15.0 mL, 24.3 mmol; 1.60 mol L^{-1} in *n*-hexane), and chlorotrimethylsilane (3.836 mL, 30.4 mmol) in dry-THF (ca. 30 mL), affording F$_1$-SKAm as a transparent liquid. Yield, 1.84 g (16.2 %). ^{1}H NMR (400 MHz, $CDCl_3$): δ (ppm) 0.18 (s, 9H, -Si(C*H*$_3$)$_3$), 1.49-1.53 (d, *J* = 6.4 Hz, 3H, C*H*$_3$CH=C-), 2.52 (s, 3H, NC*H*$_3$), 2.93-3.00 (t, *J* = 6.4 Hz, 2H, -NC*H*$_2$CH$_2$O-), 3.61-3.66 (m, 3H, -NCH$_2$C*H*$_2$O-, CH$_3$C*H*=C-). ^{13}C NMR (100 MHz, $CDCl_3$): δ (ppm) -0.45, 0.20, 10.9, 38.3, 53.2, 59.9, 80.9, 153.2.

***N*-(Hex-5-yn-1-yl)propionamide (3).** To a solution of 2 (39.1 g, 172 mmol) in ethanol (400 mL), hydrazine monohydrate (29.3 mL, 602 mmol) was added. After stirring for 2 h at 70 °C, the crude product was obtained by filtration, and directly used for the next reaction. Under a nitrogen atmosphere, to the solution of the crude product, propionic acid anhydride (9.79 mL, 76.4 mmol) was dropwise added. After stirring 13 h at r.t., the reaction mixture was concentrated under reduce pressure, then the crude product was purified by column chromatography (ethyl acetate:acetone = 3:1(v/v), R_f = 0.57), affording 3 as a brown liquid. Yield, 6.30 g (54.0 %). ^{1}H NMR (400 MHz, $CDCl_3$): δ (ppm) 1.16 (t, *J* = 7.6 Hz, 3H, -CH_2CH_3), 1.51-1.68 (m, 4H, -$NHCH_2CH_2CH_2$-), 1.96 (t, *J* = 2.7 Hz, 1H, -C≡C*H*), 2.21 (q, *J* = 7.2 Hz, 2H, -CH_2CH_3), 2.23 (t, *J* = 6.2 Hz, 2H, -CH_2C≡CH), 3.29 (q, *J* = 6.6 Hz, 2H, -CH_2NH-), 5.55 (br s, 1H, -N*H*-).

***N*-(Hex-5-yn-1-yl)-*N*-methylpropionamide (4).** To a suspension of NaH (3.30 g, 60 wt%, 82.4 mmol) in dry-THF (150 mL) was added 3 (6.30 g, 41.2 mmol) at 0 °C under a nitrogen atmosphere. After stirring for 1 h, iodomethane (5.13 mL, 82.4 mmol) was added at 0 °C under a nitrogen atmosphere. The reaction mixture was stirred at r.t. for 12 h, then quenched with a portion of water following extraction with ethyl acetate. The organic phase dried over anhydrous $MgSO_4$ and concentrated under reduced pressure. The crude product was purified by column chromatography (ethyl acetate, R_f = 0.37) and distillation under reduced pressure (60-62 °C, 0.7 mmHg), affording 4 as a transparent liquid. Yield, 3.35 g (48.8 %). ^{1}H NMR (400 MHz, $CDCl_3$): δ (ppm) 1.14-1.15 (t, *J* = 6.9 Hz, 3H, -CH_2CH_3), 1.45-1.79 (m, 4H, -$NCH_2CH_2CH_2$-), 1.95, 1.98 (t, *J* = 2.6 Hz, 1H, -CC*H*), 2.20-2.27 (m, 2H, -CH_2CCH), 2.32, 2.34 (q, *J* = 7.4 Hz, 2H, -CH_2CH_3), 2.93, 2.97 (s, 3H, -NCH_3), 3.29, 3.40 (t, *J* = 7.4 Hz, 2H, -CH_2N-)

(*Z*)-1-[*N*-(6-Trimethylsilylhex-5-ine-1-yl)-*N*-methyamino]-1-trimethylsiloxy-1-propene (F_2-SKAm). The procedure of F_1-SKAm was applied to dry-THF (ca. 40 mL), diisopropylamine (6.80 mL, 48.4 mmol), *n*-butyllithium (27.0 mL, 27.0 mmol; 1.60 mol L^{-1} in *n*-hexane), *N*-(hex-5-yn-

1-yl)-*N*-methylpropionamide (3.35 g, 20.1 mmol), and chlorotrimethylsilane (6.60 mL, 52.2 mmol) to afford F_2-SKAm as a transparent liquid (b.p. 79-81 °C/0.1 mmHg). Yield, 1.65 g (26.3 %). ^{1}H NMR (400 MHz, $CDCl_3$): δ (ppm) 0.07, 0.14 (s, 9H, -CSi(C*H*$_3$)$_3$), 0.12, 0.19 (s, 9H, -OSi(C*H*$_3$)$_3$), 1.52 (d, *J* = 6.3 Hz, 3H, -CCHC*H*$_3$), 1.45-1.59 (m, 4H, -NCH$_2$C*H*$_2$C*H*$_2$-), 2.23 (t, *J* = 6.9 Hz, 2H, -C*H*$_2$N-), 2.46 (s, 3H, -NC*H*$_3$), 2.79 (t, *J* = 7.3 Hz, 2H, -C*H*$_2$CC-), 3.65 (q, *J* = 6.6 Hz, 1H, -CC*H*CH$_3$).

***N*-2-Propenyl-*N*-methylpropionamide (6).** To a suspension of NaH (9.33 g, 60 wt%, 214 mmol) in dry-THF (300 mL) was added 5 (12.1 g, 107 mmol) at 0 °C under a nitrogen atmosphere. After stirring for 1 h, iodomethane (20.0 mL, 321 mmol) was added at 0 °C under a nitrogen atmosphere. The reaction mixture was stirred at r.t. for 24 h, then quenched with a portion of water following extraction with ethyl acetate. The organic phase dried over anhydrous $MgSO_4$ and concentrated under reduced pressure. The crude product was purified by distillation from CaH_2 under reduced pressure (69-71 °C, 3.00 mmHg), affording 6 as a transparent liquid. Yield, 8.49 g (62.4 %). ^{1}H NMR (400 MHz, $CDCl_3$): δ (ppm) 1.06-1.13 (m, 3H, C*H*$_3$CH$_2$-), 2.23-2.35 (m, 2H, CH$_3$C*H*$_2$-), 2.86-2.90 (s, 3H, NC*H*$_3$), 3.82-3.86, 3.92-3.97 (m, 2H, CH$_2$=CHC*H*$_2$-), 5.04-5.18 (m, 2H, C*H*$_2$=CHCH$_2$-), 5.63-5.77 (m, 1H, CH$_2$=C*H*CH$_2$-).

(*Z*)-1-[*N*-(2-Propenyl)-*N*-methylamino]-1-trimethylsiloxy-1-propene (F$_3$-SKAm). The procedure of F_1-SKAm was applied to dry-THF (ca. 30 mL), diisopropylamine (5.01 mL, 35.6 mmol), *n*-butyl lithium (20.0 mL, 32.4 mmol; 1.60 mol L^{-1} in *n*-hexane), 6 (3.75 g, 29.5 mmol), and chlorotrimethylsilane (5.59 mL, 44.3 mmol) to afford F_3-SKAm as a transparent liquid (b.p. 51-55 °C/4.5 mmHg). Yield, 0.52 g (8.8 %). ^{1}H NMR (400 MHz, $CDCl_3$): δ (ppm) 0.18-0.21 (s, 9H, -Si(C*H*$_3$)$_3$), 1.50-1.55 (d, *J* = 6.8 Hz, 3H, C*H*$_3$CH$_2$-), 2.38-2.42 (s, 3H, NC*H*$_3$), 3.39-3.42 (m, 2H, CH$_2$=CHC*H*$_2$-), 3.64-3.70 (m, 1H, CH$_3$C*H*-), 5.07-5.17 (m, 2H, C*H*$_2$=CHCH$_2$-), 5.70-5.82 (m, 1H, CH$_2$=C*H*CH$_2$-). ^{13}C NMR (100 MHz, $CDCl_3$): δ (ppm) 0.20, 10.9, 37.0, 54.6, 81.5, 117.0,

135.2, 153.5.

Synthesis of End-functionalized PDEAAms

α-End-functionalized Poly(*N*,*N*-diethylacrylamide) (F-PDEAAm). A typical procedure for the polymerization of DEAAm using a functional initiator is as follows: To a stock solution (80.0 μL, 2.00 μmol) of $B(C_6F_5)_3$ in CH_2Cl_2 (0.05 mol L^{-1}) was added a solution of DEAAm (127 mg, 1.00 mmol) and F_1-SKAm (12.4 μL, 40.0 μmol) in CH_2Cl_2 (1.82 mL) at 25 °C under an Ar atmosphere. After 1h, methanol was added to the polymerization solution to quench the polymerization. After the solvent was removed, the residue was dissolved in a mixture of THF and methanol, then a TBAF solution (249 μL, 249 μmol; 1.00 mol L^{-1} in THF) was added to remove the trimethylsilyl group. After stirring for 5 h, the crude product was purified by dialysis against methanol. Yield: 0.12 g (92%); SEC (RI): M_n = 2.39 kg mol^{-1}, M_w/M_n = 1.05.

ω-End-functionalized Poly(*N*,*N*-diethylacrylamide) (PDEAAm-F). The procedure for the synthesis of F-PDEAAm was applied to the polymerization of DEAAm (1.27 g, 10.0 mmol) with (Z)-SKAm (69.3 mg, 400 μmol) and $B(C_6F_5)_3$ (800 μL, 40.0 μmol; 0.05 mol L^{-1} in CH_2Cl_2) in CH_2Cl_2 (17.7 mL). After the complete monomer conversion was confirmed by analyzing an aliquot of the polymerization mixture, PhA-F_3 (1.02 g, 4.00 mmol) was added to the polymerization solution, then the entire mixture was stirred for a further 24 h. The crude product was purified by the dialysis against methanol to give PDEAAm-F_3 as a colorless solid. Yield: 0.92 g (88.1%); SEC (RI): M_n = 2.95 kg mol^{-1}, M_w/M_n = 1.07.

End-functionalized Poly(*N*,*N*-diethylacrylamide) with α-Trimethylsilylethynyl and ω-Bromo Groups (Si-≡-PDEAAm-Br). The procedure for the synthesis of PDEAAm-F was applied to the polymerization of DEAAm (1.91 g, 15.0 mmol) with F_2-SKAm (98.5 mg, 300 mmol), $B(C_6F_5)_3$ (800 μL, 30.0 μmol; 0.05 mol L^{-1} in CH_2Cl_2), and PhA-F_3 (0.765 g, 3.00 mmol) in CH_2Cl_2 (12.2 mL) to afford Si-≡-PDEAAm-Br as a colorless solid. Yield: 1.60 g (88.1%); SEC

(RI): M_n = 6.06 kg mol^{-1}, M_w/M_n = 1.07.

End-functionalized Poly(*N,N*-diethylacrylamide) with α-Ethynyl and ω-Bromo Groups (≡-PDEAAm-N$_3$). Sodium azide (0.321 g, 494 mmol) was added to a solution of Si-≡-PDEAAm-Br (1.50 g, 247 μmol) in DMF (20.0 mL) at room temperature. After stirring at 90 °C for 48 h, the solvent was removed under reduced pressure. The residue was diluted with acetone and filtered, then the filtrate was dialyzed against methanol following the evaporation of acetone. After the residue from the dialysis was dissolved in methanol (250 μL), a THF solution of TBAF (1.38 mL, 1.38 mmol; 1.0 mol L^{-1} in THF) was added to remove the trimethylsilyl group. After stirring for 24 h, the crude product was purified by dialysis against methanol. Yield, 0.95 g (62.6%).

Synthesis of Cyclic and Star-shaped PDEAAms

Cyclic Poly(*N,N*-diethylacrylamide) (*c*-PDEAAm). To a deoxygenized solution of PMDETA (4.22 mL, 20.2 mmol) and Cu(I)Br (1.45 g, 10.1 mmol) in DMF (250 mL) was added a deoxygenated DMF solution of ≡-PDEAAm-N$_3$ (373 mg, 101 μmol) at the dropwise rate of 0.3 mL h^{-1}. After entire the whole polymer solution, polystyrene resin bearing ethynyl groups were added to the reaction mixture to remove any unreacted polymer. After removing the solvents, the residue was diluted with THF and passed through a silica gel pad, followed by filtration and evaporation of the solvent. The product was purified using preparative SEC. Yield, 73.0 mg (19.6%).

3-Arm Star-shaped Poly(*N,N*-diethylacrylamide) (*s*$_3$-PDEAAm). A degassed mixture of ω-azido-functionalized PDEAAm (400 mg, 114 μmol), the core molecule with three ethynyl groups (7.42 mg, 31.7 μmol), and PMDETA (132 μL, 634 μmol) in DMF (10 mL) was added to a Schlenk flask containing Cu(I)Br (45.5 mg, 317 μmol) under an Ar atmosphere. After stirring at 80 °C for 24 h, the DMF was evaporated, then the residue was diluted with THF and passed through a short silica gel column to remove the copper catalyst. The crude product was purified by preparative

SEC. Yield, 64.1 mg, (19.2%)

Synthesis of Poly(*N,N*-diethylacrylamide) with the triazole group (*l-taz*-PDEAAm)

Scheme 3-3. Synthesis of *l-taz*-PDEAAm

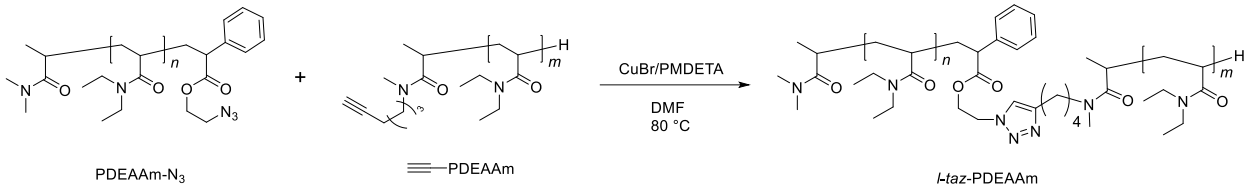

A degassed mixture of ω-azido-functionalized PDEAAm (176 mg, 83.8 μmol), α-ethynyl-functionalized PDEAAm (144 mg, 69.8 μmol), and PMDETA (165 μL, 790 μmol) in DMF (10 mL) was added to a Schlenk flask containing Cu(I)Br (56.7 mg, 395 μmol) under an Ar atmosphere. After stirring at 80 °C for 24 h, the DMF was evaporated, then the residue was diluted with THF and passed through a short silica gel column to remove the copper catalyst. The crude product was purified using preparative SEC. Yield, 50.8 mg, (17.5%)

Computational details. Full atomistic models of the linear, cyclic, and 3-armed star-PDEAAm chains consisting of 25-mer were built with the monomer DEAAm or the core parts using XLEAP, a modeling tool for generating input files of Amber14. Geometry optimization and restrained electrostatic potential (RESP) fitting of each part of the structures needed for construction of the polymer architecture was calculated at the B3LYP/6-31G(d,p) level with Gaussian 09. Using the strategy of parameterizing GAFF, [38] the partial atomic charges of each part were derived from the B3LYP/6-31G(d,p) electrostatic potentials generated by the Gaussian 09.

MD simulations and analyzing processes were performed with an AMBER14 program package. Full atomistic simulations were performed in an octahedral water box using the TIP3P model at 298 K, 313 K, and 328 K. [39] The solvated structures were then subjected to 1000 steps of the

steepest descent minimization of the potential energy, followed by 2500 steps of conjugate gradient minimization. During this minimization, the PDEAAm molecules remained fixed in their starting conformation using harmonic constraint with a force constant of 500 kcal/mol/Å. This allowed the water molecules to eliminate bad contact with the PDEAAm molecules. This was followed by another 2500 steps of conjugate gradient minimization while decreasing the force constant of the harmonic restraints from 10 kcal/mol/Å to zero.

The minimized structures were initially heated from 0 to 298 K, 313K, and 328 K for a 40 ps MD simulation using weak harmonic constraints (10 kcal/mol/Å^2) on the solute to its starting structure. Subsequently, the heated systems were equilibrated for 20 ps using no restraint on the solute. Finally, for each PDEAAm-water system, constant pressure-constant temperature (*NPT* ensemble) dynamics were carried out for 20 ns with a time step of 2 fs at 298 K, 313 K, and 328 K at 1 atm pressure. The temperature and pressure were maintained using the Langevin thermostat and barostat with time constants of 1 ps and 2 ps, respectively.[40] The electrostatic interactions were evaluated using the particle mesh Ewald (PME) method with periodic boundary conditions and a cut off of 9 Å.[41] In addition, SHAKE constraints were imposed on all the covalent bonds involving the hydrogen atoms.[42] The atomic trajectories were accumulated and stored every 1 ps. Trajectory files obtained from these simulations were used for analyzing the various structural and dynamic properties.

3.3. Results and Discussion

3.3.1. α-End-functionalization of Poly(*N*,*N*-diethylacrylamide) (F-PDEAAm). The silyl ketene aminal of (*Z*)-1-dimethylamino-1-trimethylsiloxy-1-propene ((*Z*)-SKAm) was a suitable initiator for the controlled/living GTP of DAAms.[23] For the α-end-functionalization of PDEAAm, we designed functional silyl ketene aminals (F-SKAms), such as (*Z*)-1-(*N*-Methyl-*N*-2-

trimetylsiloxyethyl)amino)-1-trimethylsiloxy-1-propene (F_1-SKAm), (*Z*)-1-[*N*-(6-trimethylsilylhex-5-ine-1-yl)-*N*-methyamino]-1-trimethylsiloxy-1-propene (F_2-SKAm), and (*Z*)-1-[*N*-(2-propenyl)-*N*-methylamino]-1-trimethylsiloxy-1-propene (F_3-SKAm), as initiators, in which the hydroxyl group in F_1-SKAm and the ethynyl group in F_2-SKAm were protected using the trimethylsilyl group in order to avoid any undesired side reactions due to the acidic protons of the hydroxyl and ethynyl groups during the GTP process. These F-SKAms were synthesized by the trimethylsilylation of respective propionamide derivatives using LDA/Me_3SiCl, as shown in Scheme 3-2. All the F-SKAms were obtained with high purities after distillation, and their chemical structures were confirmed by its ^{1}H NMR spectra and the *Z* conformation of F-SKAm by the 1D-NOE measurements, as shown in Figure 3-1.

The polymerization of DEAAm was carried out in CH_2Cl_2 at the DEAAm concentration of 0.50 mol L^{-1} with a 10 mol% amount of $B(C_6F_5)_3$ relative to each F-SKAm except that the polymerizations at high DEAAm-to-F-SKAm feed ratios required a high $B(C_6F_5)_3$ amount of 30 mol%. Tables 3-1 summarizes the polymerization results. All the polymerizations showed complete consumption of DEAAm within their set polymerization times. Since the hydroxyl and ethynyl groups in the PDEAAms obtained using F_1-SKAm and F_2-SKAm were still protected by the trimethylsilyl group, its removal was followed by treating the polymerization solutions with *tetra-n*-butylammonium fluoride (TBAF). To prove the living character of the polymerization using every F-SKAm, the polymerizations with different monomer-to-F-SKAm ratios of 25, 50, 100, and 200 were examined; runs 3-1~4 for F_1-SKAm, runs 3-5~8 for F_2-SKAm, and runs 3-9~12 for F_3-SKAm. The molecular weights of the obtained PDEAAms versus the DEAAm-to-F-SKAm ratios are plotted in Figure 3-2. Obviously, a linear correlation between $M_{n,SEC}$ and the $[DEAAm]_0/[F\text{-}SKAm]_0$ ratio was obtained for each polymerization using F-SKAm though the $M_{n,SEC}$ showed a slight deviation from the $M_{n,calcd.}$, due to the mismatch between the obtained

polymer and employed standard PMMA as the calibration polymer. The polydispersities of all the resulting polymers of M_w/M_ns ≤1.19 were rather low, which strongly suggested that the GTP process of the DEAAm using the F-SKAms was indeed a living system. The determination of the exact molecular weights of the obtained polymers was further attempted by ^{1}H NMR measurements in $CDCl_3$. The molecular weights estimated from the ^{1}H NMR spectroscopy ($M_{n,NMR}$) of F_3-PDEAAm (runs 3-9~12) were in the range of 3.65-26.3 kg mol^{-1}, each of which was quite consistent with its related $M_{n,calcd.}$. On the contrary, the attempts for F_1-PDEAAm and F_2-PDEAAm failed due to the overlap of the proton signals of the F-SKAm residue with those of the PDEAAm chains.

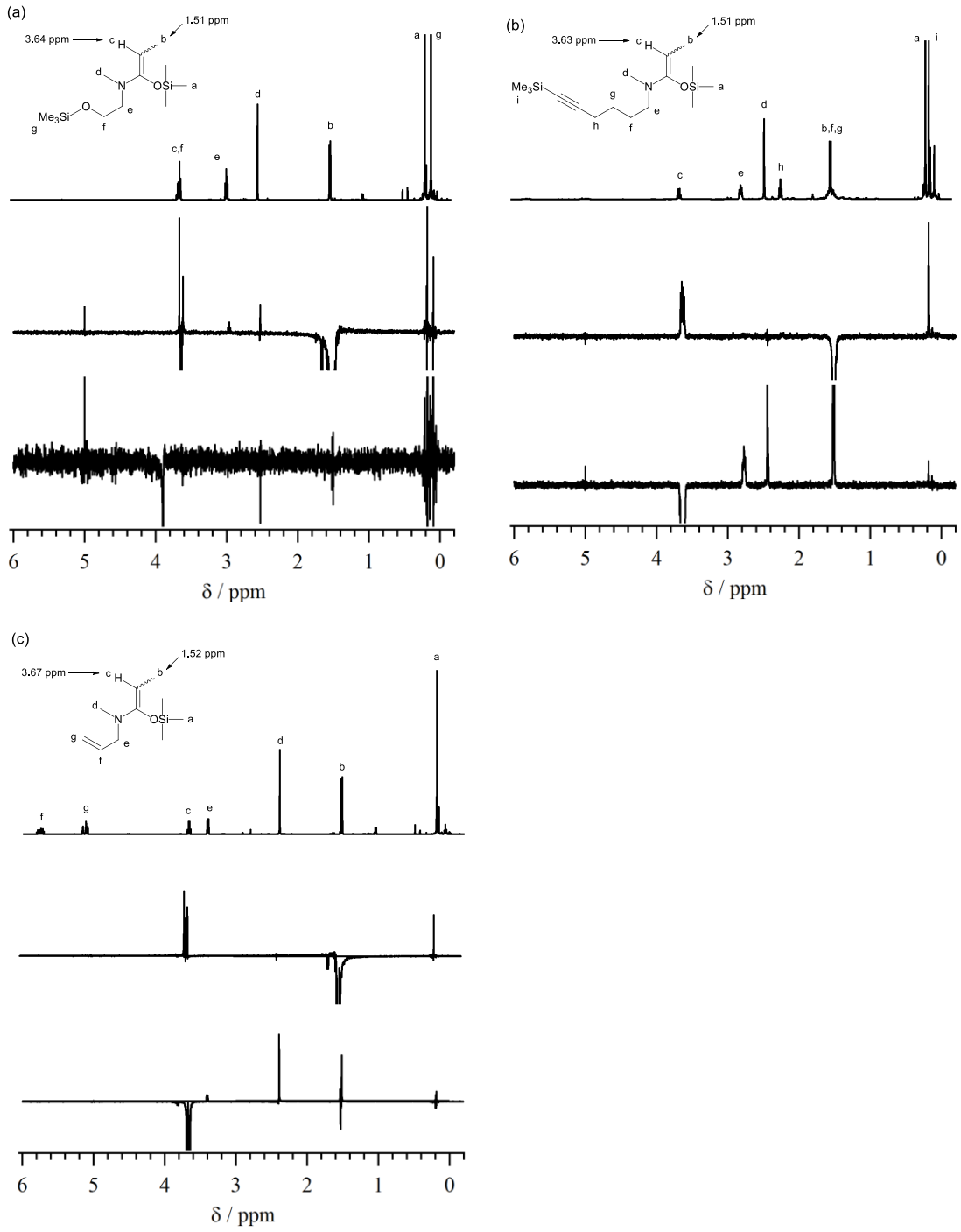

Figure 3-1. ^{1}H NMR spectra of functional silyl ketene aminal, (a) F_1-SKAm, (b) F_2-SKAm, and (c) F_3-SKAm (upper) and their NOE difference spectra; irradiation of CH_3-CH=C- (b, 1.51-1.52 ppm) (middle) and irradiation of CH_3-C*H*=C- (c, 3.63-3.37 ppm) (lower) ($CDCl_3$, 400 MHz).

Table 3-1. Synthesis of α-end functionalized PDEAAm by $B(C_6F_5)_3$-catalyzed GTP using F-SKAm.

Run	F-SKAm	$[DEAAm]_0/[F\text{-}SKAm]_0/[B(C_6F_5)_3]_0$	Time (h)	$M_{n,calcd.}$ (kg mol^{-1}) [b]	$M_{n,SEC}$ (kg mol^{-1}) [c]	M_w/M_n [c]
3-1	F_1-SKAm	25/1/0.10	3	3.30	2.39	1.05
3-2	F_1-SKAm	50/1/0.10	5	6.49	4.71	1.06
3-3	F_1-SKAm	100/1/0.10	21	12.8	9.47	1.09
3-4	F_1-SKAm	200/1/0.30	45	25.6	24.1	1.17
3-5	F_2-SKAm	25/1/0.10	1	3.35	3.01	1.06
3-6	F_2-SKAm	50/1/0.10	3.5	6.52	4.03	1.06
3-7 [e]	F_2-SKAm	100/1/0.10	7	12.9	8.20	1.08
3-8 [e]	F_2-SKAm	200/1/0.10	22	25.6	17.8	1.16
3-9	F_3-SKAm	50/1/0.10	2.5	3.31	2.52 (3.69) [d]	1.06
3-10	F_3-SKAm	50/1/0.10	4	6.49	4.44 (6.87) [d]	1.07
3-11 [e]	F_3-SKAm	100/1/0.10	18	12.8	10.5 (14.5) [d]	1.09
3-12 [e]	F_3-SKAm	200/1/0.30	18	25.6	21.3 (26.3) [d]	1.19

[a] Ar atmosphere; $[DEAAm]_0$ = 0.5 mol L^{-1}, Conv. determined by ^{1}H NMR in $CDCl_3$, >99%. [b] Calculated from $[DEAAm]_0/[F\text{-}SKAm]_0$ × (MW of monomer: DEAAm = 127.18) × conv. + (MW of initiator residue: F_1-SKAm = 131.18, F_2-SKAm = 167.25, F_3-SKAm = 127.18). [c] Determined by SEC in DMF containing 0.01 mol L^{-1} LiCl calibrated with PMMA. [d] Number average molecular weight ($M_{n,NMR}$, kg mol^{-1}) determined by ^{1}H NMR in $CDCl_3$. [e] $[DEAAm]_0$ = 1.0 mol L-$^{-1}$.

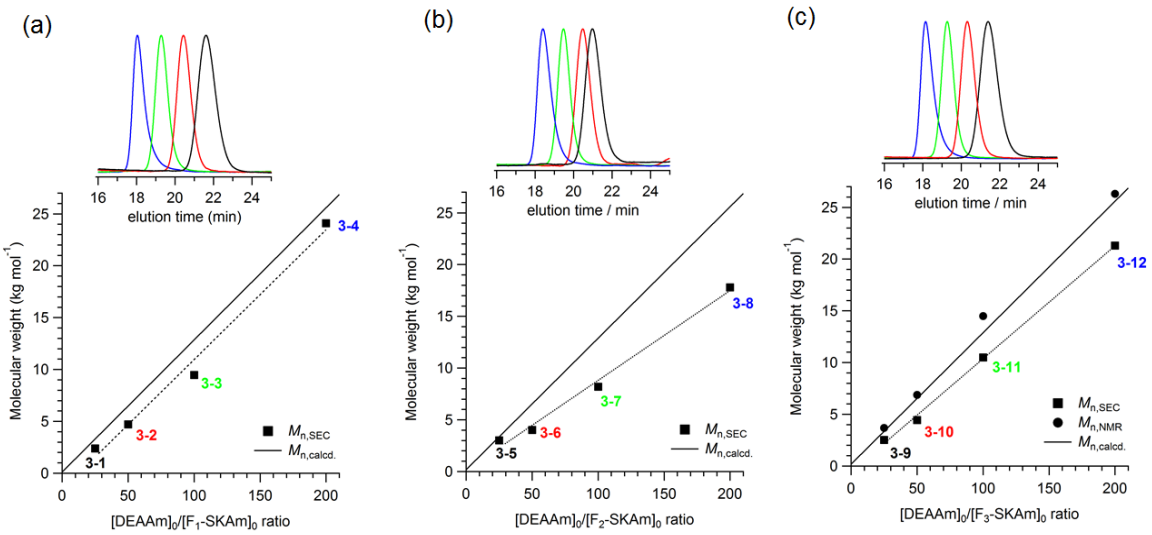

Figure 3-2. Molecular weight plots of the obtained PDEAAms prepared using F-SKAm versus the $[DEAAm]_0/[F\text{-}SKAm]_0$ ratio, and SEC traces of (a) runs 3-1~4, (b) runs 3-5~8, and (c) runs 3-9~12.

The chemical structure of the obtained polymer was confirmed by ^1H NMR and MALDI-TOF MS measurements, as shown in Figures 3-3 and 3-4, respectively. All the ^1H NMR spectra showed proton signals due to the polymer main chains at 0.9 - 1.3, 1.3 - 2.0, 2.2 - 2.8, and 2.9 - 3.7 ppm, and the proton signals due to the vinyl group of F_3-SKAm were observed at 5.0 - 5.2 and 5.6 - 5.8 ppm though those for F_1-SKAm and F_2-SKAm were overlapped with the polymer main-chain. Thus, the MALDI-TOF MS was used to determine the isotopically resolved molecular weights of the polymer products. For every F-PDEAAm, only one series of ion peaks was observed and the interval between two adjacent ion peaks exactly corresponded to the molecular weight of the DEAAm unit, strongly indicating that no undesired reaction occurred during the entire GTP process. In addition, the observed molecular weight of every ion peak agreed with the related theoretical isotopic molecular weight, *i.e.*, every ion peak corresponded to a targeted sodium-cationized polymeric formula of $[C_{7n+6}H_{13n+12}N_{n+1}O_{n+2}Na]^+$ for the PDEAAm using F_1-SKAm, $[C_{7n+10}H_{13n+17}N_{n+1}O_{n+1}Na]^+$ using F_2-SKAm, and $[C_{7n+7}H_{13n+12}N_{n+1}O_{n+1}Na]^+$ using F_3-SKAm; the

peak observed at the *m*/*z* of 3331.95 Da corresponded to the theoretical isotopic 25-mer of PDEAAm bearing a F_1-SKAm residue at the α-end (molecular formula: $C_{180}H_{337}N_{26}O_{27}Na$), as shown in Figure 2a, and the ion peaks for the PDEAAms using F_2-SKAm and F_3-SKAm also agreed with their theoretical isotopic polymers, as shown in Figures 3-4b and 3-4c, respectively. These results apparently indicated that the desired functional groups were introduced into the α-end of the polymer chain, *i.e.*, the obtained polymer structures were the α-end-functionalized PDEAAms with the hydroxyl, ethynyl, and vinyl groups, F_1-PDEAAm, F_2-PDEAAm, and F_3-PDEAAm, respectively.

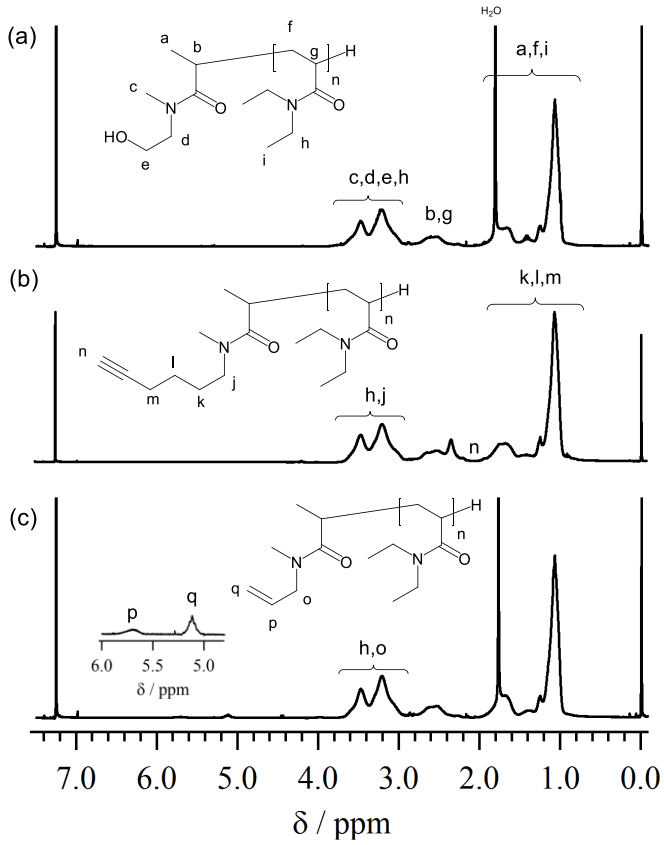

Figure 3-3. ^{1}H NMR spectra of (a) F_1-SKAm (run 3-1), (b) F_2-SKAm (run 3-5), and (c) F_3-SKAm (run 3-9) obtained by the $B(C_6F_5)_3$-catalyzed GTP of DEAAm using functional initiators ($CDCl_3$, 400 MHz).

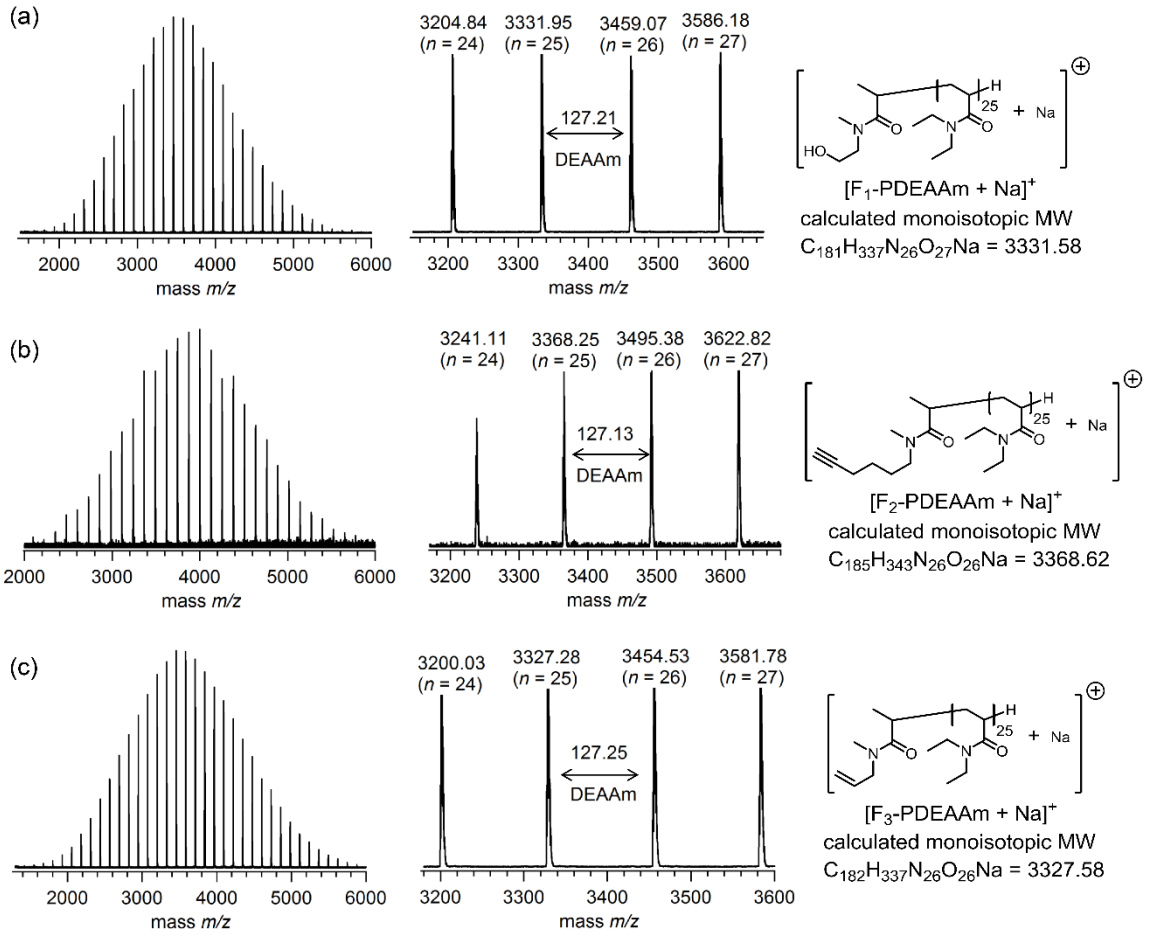

Figure 3-4. MALDI-TOF MS spectra of the PDEAAm synthesized using (a) F_1-SKAm (run 3-1), (b) F_2-SKAm (run 3-5), and (c) F_3-SKAm (run 3-9).

3.3.2. ω-End-functionalization of Poly(*N*,*N*-diethylacrylamide) (PDEAAm-F). For the ω-end-functionalization of acrylamide polymer, we first examined the termination reaction for the $B(C_6F_5)_3$-catalyzed GTP of DEAAm using several terminator candidates, such as dimethyl itaconate (DMI), benzaldehyde (BA), *N*-benzylidenemethylamine (*N*-BMA), and methyl 2-phenyl acrylate (MPhA). After the polymerization with the [DEAAm]/[(Z)-SKAm] ratio of 25 for 1 h, the trimethylsilyl ketene aminal group at the ω-end of PDEAAm was terminated by adding a 10-fold terminating agent to the polymerization system and the termination reaction was further continued for 24 h. The *ω*-end-functionalization efficiency (F_n) was estimated from the intensity

of the MALDI-TOF MS spectra. Table 3-2 summarizes the results of the termination experiments. The F_n using MPhA gave the highest F_n of 76.7%. The further modification of the reaction conditions led to the supernumerary addition of 10 mol% $B(C_6F_5)_3$ (relative to active ω-ends) after polymerization that could finally give a quantitative ω-end-functionalization, which was confirmed by the simultaneous appearance of phenyl (around 7.0 ppm due to MPhA) and main-chain signals in the ^{1}H NMR spectrum (Figure 3-5), together with the perfect MALDI-TOF MS spectrum of the resulting MPhA-terminated PDEAAm (Figure 3-7a), indicating that one polymer chain definitely contained an end group of the MPhA residue. The results of the ^{1}H NMR and MALDI-TOF MS analyses for the ω-end-functionalized PDEAAms were significantly similar to those for the α-end-functionalized PDEAAms.

Based on the screening experiment, we determined the 2-phenyl acrylate derivative as the suitable terminator for the synthesis of the ω-end-functionalized PDEAAms and used functional 2-phenylacrylate terminators bearing hydroxyl, ethynyl, and bromo groups (PhA-F_1, PhA-F_2, and PhA-F_3, respectively). The polymerization at $[DEAAm]_0/[(Z)\text{-}SKAm]_0/[B(C_6F_5)_3]_0$ = 25/1/0.05 was carried out for investigating the ω-end-functionalization of PDEAAm. The polymerization and F_n results are summarized in Table 3-3. As expected, all the ω-end-functionalized PDEAAms (PDEAAm-Fs) with F_ns >99% (*i.e.*, quantitative end-functionalization) were obtained, as confirmed by the ^{1}H NMR (Figure 3-6) and MALDI-TOF MS (Figure 3-7) measurements.

These results lead to the conclusion that the 2-phenyl acrylate derivative is a versatile terminator for producing ω-end-functionalized polymers using the organocatalyzed GTP of (meth)acrylate and acrylamide monomers.

Table 3-2. $B(C_6F_5)_3$-catalyzed GTP of DEAAm using terminator candidates [a]

Run	Terminator	$[DEAAm]_0/[(Z)\text{-}SKAm]_0$ /$[B(C_6F_5)_3]_0$/$[terminator]_0$	$M_{n,SEC.}$ [b] (kg mol^{-1})	M_w/M_n [b]	F_n (%) [c]
3-13	DMI	25/1/0.05/10	2.67	1.05	4.9
3-14	BA	25/1/0.05/10	2.38	1.05	21.7
3-15	*N*-BMA	25/1/0.05/10	2.78	1.05	65.5
3-16	MPhA	25/1/0.05/10	2.46	1.05	76.7
3-17	MPhA	25/1/0.05/20	2.14	1.05	89.5
3-18	MPhA	25/1/0.05 + 0.05/10[d]	2.50	1.05	95.6
3-19	MPhA	25/1/0.05 + 0.10/10 [d]	2.50	1.07	>99.9

[a] Ar atmosphere; $[DEAAm]_0$ = 0.5 mol L^{-1} in CH_2Cl_2; temperature, r.t.; monomer conversions determined by ^{1}H NMR in $CDCl_3$, >99.9 %. [b] Determined by SEC in DMF containing 0.01 mol L^{-1} of LiCl using PMMA standards. [c] Estimated by the intensity of MALDI-TOF MS spectrum. [d] Additional $B(C_6F_5)_3$ of 0.05 or 0.10 eq. molar against (*Z*)-SKAm was added for the termination reaction.

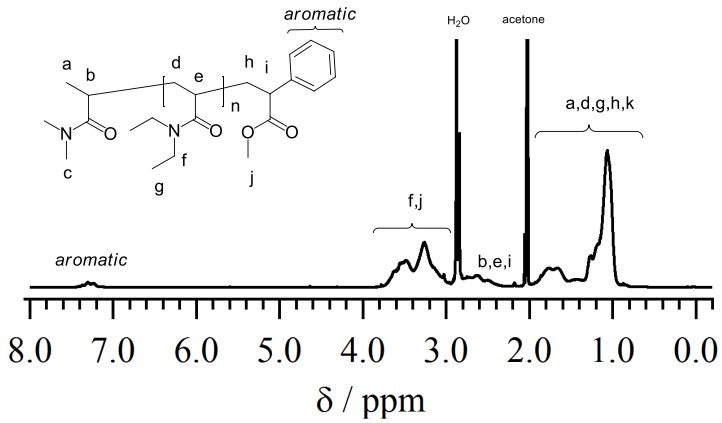

Figure 3-5. ^{1}H NMR spectrum of the PDEAAm terminated with MPhA (Table 3-2, run 3-19) (Acetone-d_6, 400 MHz).

Table 3-3. $B(C_6F_5)_3$-catalyzed GTP of DEAAm using functional 2-phenyl acrylates (PhA-Fs) as terminators [a]

run	Terminator	$M_{n,calcd.}$ [b] (kg mol^{-1})	$M_{n,SEC}$ [c] (kg mol^{-1})	$M_{n,NMR}$ [d] (kg mol^{-1})	M_w/M_n [c]	F_n (%) [e]
3-20	PhA-F_1	3.59	2.32	3.01	1.05	>99
3-21	PhA-F_2	3.55	2.49	2.84	1.05	>99
3-22	PhA-F_3	3.54	1.97	2.48	1.04	>99

[a]Ar atmosphere; initiator, (*Z*)-SKAm; $[DEAAm]_0$ = 0.5 mol L^{-1} in CH_2Cl_2; $[DEAAm]_0/[(Z)\text{-SKAm}]_0/[B(C_6F_5)_3]_0/[PhA\text{-}F]_0$ = 25/1/0.05 + 0.1/10; temperature, r.t.; Conv. >99% by ^{1}H NMR in $CDCl_3$. [b] Calculated from $([DEAAm]_0/[PhA\text{-}F]_0)$ × (Conv.) × (M.W. of DEAAm) + (M.W. of desilylated initiator) + (M.W. of PhA-F). [c] Determined by SEC in DMF containing 0.01 mol L^{-1} of LiCl using PMMA standards. [d] Determined by ^{1}H NMR in $CDCl_3$ [e] Estimated by the MALDI-TOF MS and ^{1}H NMR spectra.

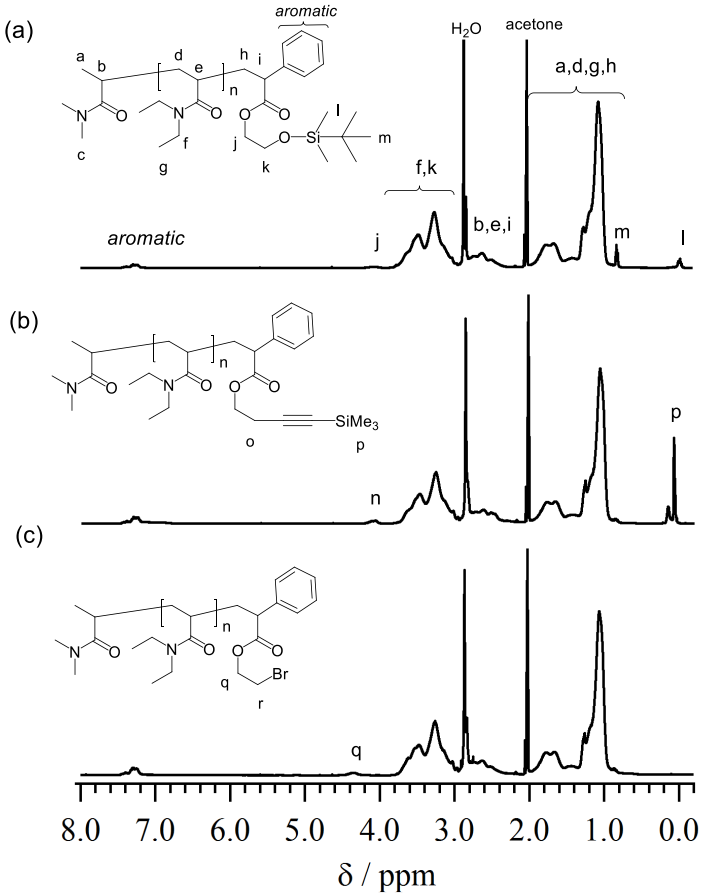

Figure 3-6. ^{1}H NMR spectra of (a) PhA-F_1 (run 2-20), (b) PhA-F_2 (run 2-21), and (c) PhA-F_3 (run 2-22) obtained by the $B(C_6F_5)_3$-catalyzed GTP of DEAAm using functional terminators (acetone-d_6, 400 MHz).

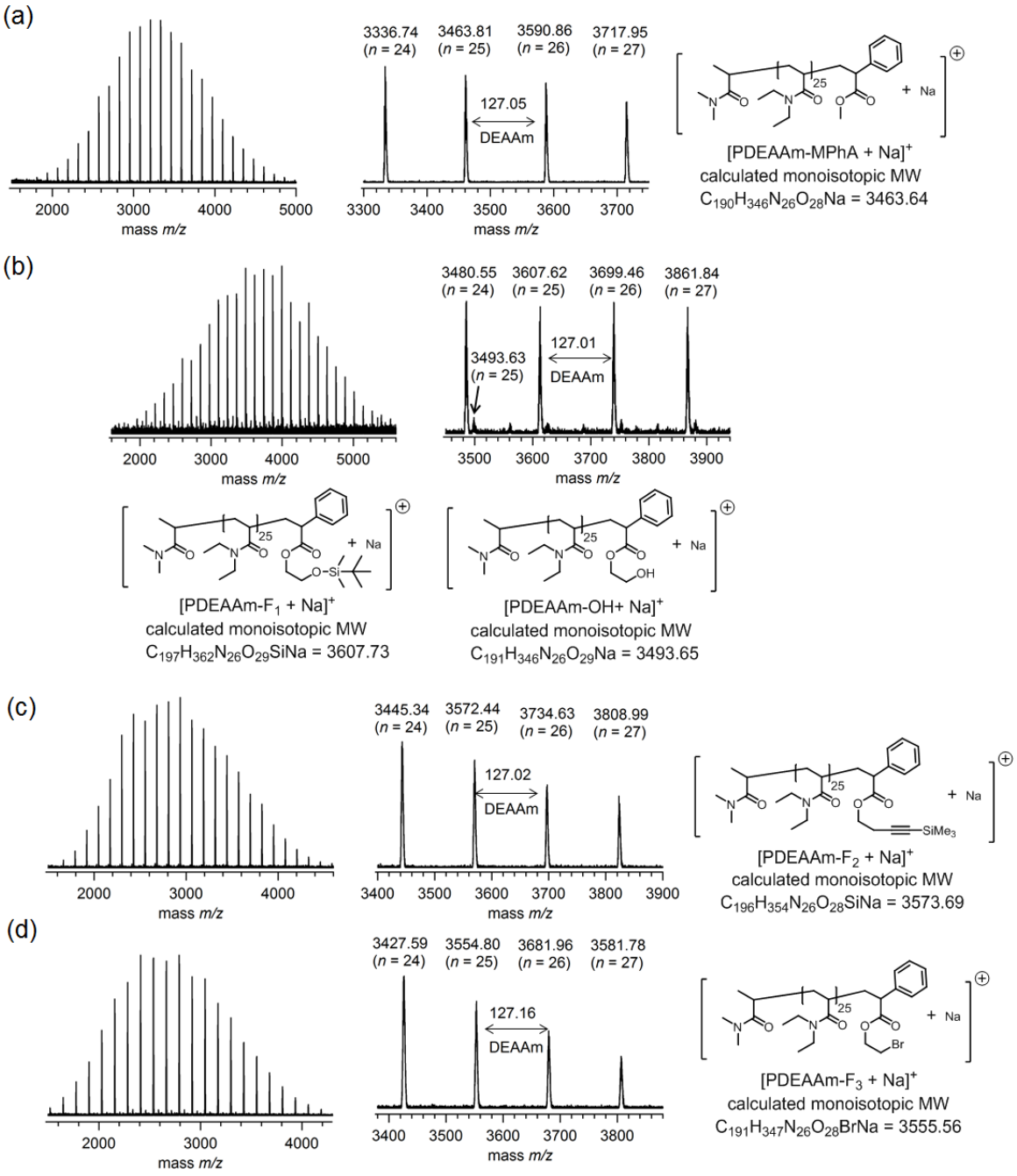

Figure 3-7. MALDI-TOF MS spectra of (a) the PDEAAm terminated with MPhA (run 3-19), and the ω-end functionalized PDEAAm terminated with (b) PhA-F_1 (run 3-20), (c) PhA-F_2 (run 3-21), and (d) PhA-F_3 (run 3-22).

3.3.3. α,ω-End-functionalization of Poly(*N*,*N*-diethylacrylamide) (F-PDEAAm-F). For the preparation of the macrocyclic PDEAAm (*c*-PDEAAm), we used the Cu(I)-catalyzed azide-alkyne cycloaddition approach, such as the intramolecular cyclization of the end-functionalized PDEAAm with the α-ethynyl and ω-azido groups (≡-PDEAAm-N_3), as shown in Scheme 1c. Thus, the end-functionalized PDEAAm with the α-ethynyl and ω-bromo groups (Si-≡-PDEAAm-Br) was initially synthesized using F_2-SKAm and PhA-F_3 as the functional initiator and terminator, respectively. The $B(C_6F_5)_3$-catalyzed GTP of DEAAm was carried out at the $[DEAAm]_0/[F_2\text{-}SKAm]_0$ ratios of 25, 50 and 75 with a 10-20 mol% amount of $B(C_6F_5)_3$ (relative to F_2-SKAm). The polymerization results are summarized in Table 3-4. The $M_{n,NMR}$s of the obtained Si-≡-PDEAAm-Brs were almost the same as the targeted ones ($M_{n,calcd.}$s), *i.e.*, the $M_{n,NMR}$s of 3.80, 6.89, and 10.5 kg mol^{-1} were extremely close to the $M_{n,calcd.}$s of 3.67, 6.89, and 10.0 kg mol^{-1} for Si-≡-$PDEAAm_{26}$-Br, Si-≡-$PDEAAm_{50}$-Br, and Si-≡-$PDEAAm_{79}$-Br, respectively. In addition, all the resulting polymers had low polydispersities of M_w/M_ns ≤1.10. The quantitative introduction of the trimethylsilylethynyl group due to F_2-SKAm at the α-end and the bromoethyl group due to PhA-F_3 at the ω-end was confirmed by the ^{1}H NMR spectrum (Figure 3-8a) of the resulting polymer product because the characteristic signals of the $Si(CH_3)_3$ at 0.2 ppm (signal *a*) due to the α-end and $BrCH_2CH_2OCO$- at 4.3 ppm (signal *b*) due to the ω-end were clearly observed and their integration ratio agreed with the calculated value of 9:2.

Table 3-4. $B(C_6F_5)_3$-catalyzed GTP of DEAAm using F_2-SKAm and PhA-F_3 as the functional initiator and terminator, respectively [a]

run	$[DEAAm]_0/[F_2\text{-}SKAm]_0/[B(C_6F_5)_3]_0$	Termination condition $[B(C_6F_5)_3]_0/[PhA\text{-}F_3]_0$ [b]	$M_{n,calcd.}$ [c] (kg mol^{-1})	$M_{n,SEC}$ [d] (kg mol^{-1})	$M_{n,NMR}$ [e] (kg mol^{-1})	M_w/M_n [d]	F_n [f] (%)
3-23	25/1/0.05	0.1/10	3.67	2.92	3.80	1.06	>99
3-24	50/1/0.05	0.1/10	6.89	6.03	6.89	1.07	>99
3-25	75/1/0.1	0.2/10	10.0	8.69	10.5	1.10	>99

[a] Ar atmosphere; $[DEAAm]_0$ = 0.5 mol L^{-1} in CH_2Cl_2; temperature, r.t.; Conv. >99% by ^{1}H NMR in $CDCl_3$. [b] this ratios based on $[F_2\text{-}SKAm]_0$ [c] Calculated from ($[DEAAm]_0/[F_2\text{-}SKAm]_0$) × (Conv.) × (M.W. of DEAAm) + (M.W. of desilylated F_2-SKAm) + (M.W. of PhA-F_3). [d] Determined by SEC in DMF containing 0.01 mol L^{-1} of LiCl using PMMA standards. [e] Determined by ^{1}H NMR in $CDCl_3$ [f] Estimated by ^{1}H NMR spectrum.

3.3.4. Synthesis of Cyclic and Star-shaped Poly(*N*,*N*-diethylacrylamide). For the synthesis of a cyclic PDEAAm, Si-≡-PDEAAm-Br was used as the starting polymer, as shown in Scheme 3-1c. The chemical conversion from the *ω*-bromo group to the azido group and the deprotection of the trimethylsilyl group at the ethynyl group were implemented; Si-≡-PDEAAm-Br was treated with sodium azide in DMF at 90 °C for 16 h, followed by deprotection of the trimethylsilyl group using TBAF in a mixed solvent of THF and MeOH. The obtained polymer structure of ≡-PDEAAm-N_3 was verified by the disappearance of the proton signals of Si(C*H*$_3$)$_3$ and the compete signal shift from BrCH$_2$C*H*$_2$OCO- at 4.3 ppm (signal *b*) to N_3CH$_2$C*H*$_2$OCO- at 4.1 ppm (signal *b'*) after the azidation in the ^{1}H NMR spectra, as shown in Figure 3-8b. Additionally, the azidation was supported by the appearance of the stretching peak due to the azido group at 2098 cm^{-1} in the FT-IR spectrum, as shown in Figure 3-9.

The intramolecular click reaction of ≡-PDEAAm-N_3 was carried out in DMF at 90 °C under the conditions of the [CuBr]$_0$/[PMDETA]$_0$/[≡-PDEAAm-N_3]$_0$ of 150/300/1 and the [≡-PDEAAm-N_3]$_0$ of 3.0 mmol L^{-1} using a slow addition technique (0.3 mL h^{-1}). The results are summarized in Table 3-5. The progress of the click reaction was monitored by FT-IR spectra. After the click reaction of ≡-PDEAAm$_{50}$-N_3, the crude product showed no absorption signal due to the azido group at 2098 cm^{-1} in the FT-IR spectrum, but showed new proton signals at 4.4 ppm (signal *b'''*) due to the triazole (*taz*)-CH$_2$C*H*$_2$OCO- group and at 4.2 - 4.6 ppm due to the *taz*-C*H*$_2$CH$_2$OCO- group (peak *c*) and the *taz*-C*H*$_2$(CH$_2$)$_3$- group (peak *d*). Although these results indicated the complete click reaction, the SEC trace of the crude product displayed a bimodal distribution, as shown in Figure 3-10, suggesting that the intra- and intermolecular click reactions should simultaneously proceed. The crude product was thus subjected to preparative SEC to separate the two click products. After cutting off the high molecular weight product, the purified polymer showed a monomodal distribution and obviously shifted to a slightly lower molecular weight

region in the SEC trace compared to the starting polymer of ≡-PDEAAm$_{50}$-N$_3$. The molecular weights of 2.67, 5.19, and 7.14 kg mol^{-1} for the purified polymers were clearly lower than those of 2.95, 5.63, and 8.42 kg mol^{-1} for the ≡-PDEAAm-N$_3$s, respectively. The shrinking factors (<*G*> = $M_{p,SEC}$(purified polymer)/$M_{p,SEC}$(starting polymer)) were 0.86 - 0.93, whose decrease in the hydrodynamic volume undoubtedly suggested the change from a linear to cyclic topology.[43,44] Apart from the shifting observed in the SEC trace, the intrinsic viscosities of the purified polymers, which were measured by the SEC equipped with a viscometer, had the lower values of 4.1, and 5.9 mL g^{-1} (runs 3-27 and 3-28) than those of the linear precursors of 5.6, and 6.8 mL g^{-1}, which supported the production of cyclic polymers. Furthermore, the MALDI-TOF MS measurement of the purified polymer provided a deep insight into the chemical structure forming a cyclic architecture. Although the molecular formula of the precursor, ≡-PDEAAm-N$_3$, was the same as that of *c*-PDEAAm, the MALDI-TOF MS spectrum of ≡-PDEAAm$_{26}$-N$_3$ showed the main series of ion peaks corresponding to the N$_2$ eliminated polymer peaks as ≡-PDEAAm$_{26}$-NH$_2$ due to the laser irradiation (Figure 3-11a). On the other hand, the MALDI-TOF MS spectrum of *c*-PDEAAm$_{26}$ exhibits only one series of ion peaks, as shown in Figure 3-11b, and the observed molecular weight of every ion peak corresponded to the targeted sodium-cationized polymeric formula of $[C_{7n+21}H_{13n+28}N_{n+4}O_{n+3}Na]^+$; the peak observed at the *m*/*z* of 3584.89 Da corresponded to the theoretical isotopic 25-mer of PDEAAm with a *taz* group (molecular formula: $C_{196}H_{353}N_{29}O_{28}Na$). Based on all the results, the production of *c*-PDEAAm was proven.

For the synthesis of the 3-armed star-shaped PDEAAm (*s*$_3$-PDEAAms) using the arm-first method, the intermolecular click reaction of PDEAAm-N$_3$ and a core molecule possessing three ethynyl groups was carried out under the conditions of the $[CuBr]_0/[PMDETA]_0/[PDEAAm\text{-}N_3]_0/[\text{ethynyl core}]_0$ of 10/20/3.6/1 in DMF at 90 °C. The synthetic results are summarized in Table 3-6. After the click reaction, the crude product was purified by preparative SEC to remove

any residual unreacted PDEAAm-N_3. The SEC trace of the separated product obviously shifted to a higher molecular weight range compared to PDEAAm-N_3, while keeping a narrow and monomodal shape, as shown in Figures 3-12. The azido group completely disappeared at 2098 cm^{-1} in the FT-IR spectrum and the methylene proton peaks of the adjacent *taz* group appeared at 4.3 - 4.7 ppm in the ^1H NMR spectrum, as shown in Figures 3-13 and 3-14, respectively. In addition, the $M_{n,SEC}$ increased by changing the macromolecular architecture from the linear to star-shaped PDEAAms, such as from 1.46 to 3.19 kg mol^{-1} (runs 3-29 and 3-30), from 2.10 to 5.22 kg mol^{-1} (runs 3-31 and 3-32), and from 2.66 to 7.58 kg mol^{-1} (runs 3-33 and 3-34). These results firmly proved the production of s_3-PDEAAm$_{27}$, s_3-PDEAAm$_{51}$, and s_3-PDEAAm$_{78}$.

Table 3-5. Synthesis of *c*-PDEAAm by intramolecular azide-alkyne cycloaddition using ≡-PDEAAm-N_3 [a]

run	polymer	$M_{n,calcd.}$ [b] (kg mol^{-1})	$M_{n,SEC}$ [c] (kg mol^{-1})	M_w/M_n [c]	<*G*> [d]	[η] [e] (mL g^{-1})
3-26	*c*-PDEAAm$_{26}$	3.56	2.67	1.07	0.86	n.d. [f]
3-27	*c*-PDEAAm$_{50}$	6.74	5.19	1.08	0.93	4.1
3-28	*c*-PDEAAm$_{79}$	9.92	7.14	1.11	0.93	5.9

[a]Ar atmosphere; $[DEAAm]_0$ = 0.5 mol L^{-1} in CH_2Cl_2; $[DEAAm]_0/[F_2\text{-SKAm}]_0/[B(C_6F_5)_3]_0/[PhA\text{-}F_3]_0$ = 25/1/0.05 + 0.1/10 (run 4-1), 50/1/0.05 + 0.1/10 (run 4-2), and 75/1/0.1 + 0.2/10 (run 4-3); temperature, r.t.; Conv. was determined by ^1H NMR in $CDCl_3$, >99%. [b] Calculated from $([DEAAm]_0/[(Z)\text{-SKAm}]_0) \times$ (Conv.) × (M.W. of DEAAm) + (M.W. of desilylated F_2-SKAm) + (M.W. of PhA-F_3). [c] Determined by SEC in DMF containing 0.01 mol L^{-1} of LiCl using PMMA standards. [d] <*G*> was the ratio of molecular weight from peak tops of SEC traces between *c*-PDEAAm before purification and linear counterparts. [e] Intrinsic viscosity ([η]) was determined by the SEC equipped with viscometry. [f] Not determined.

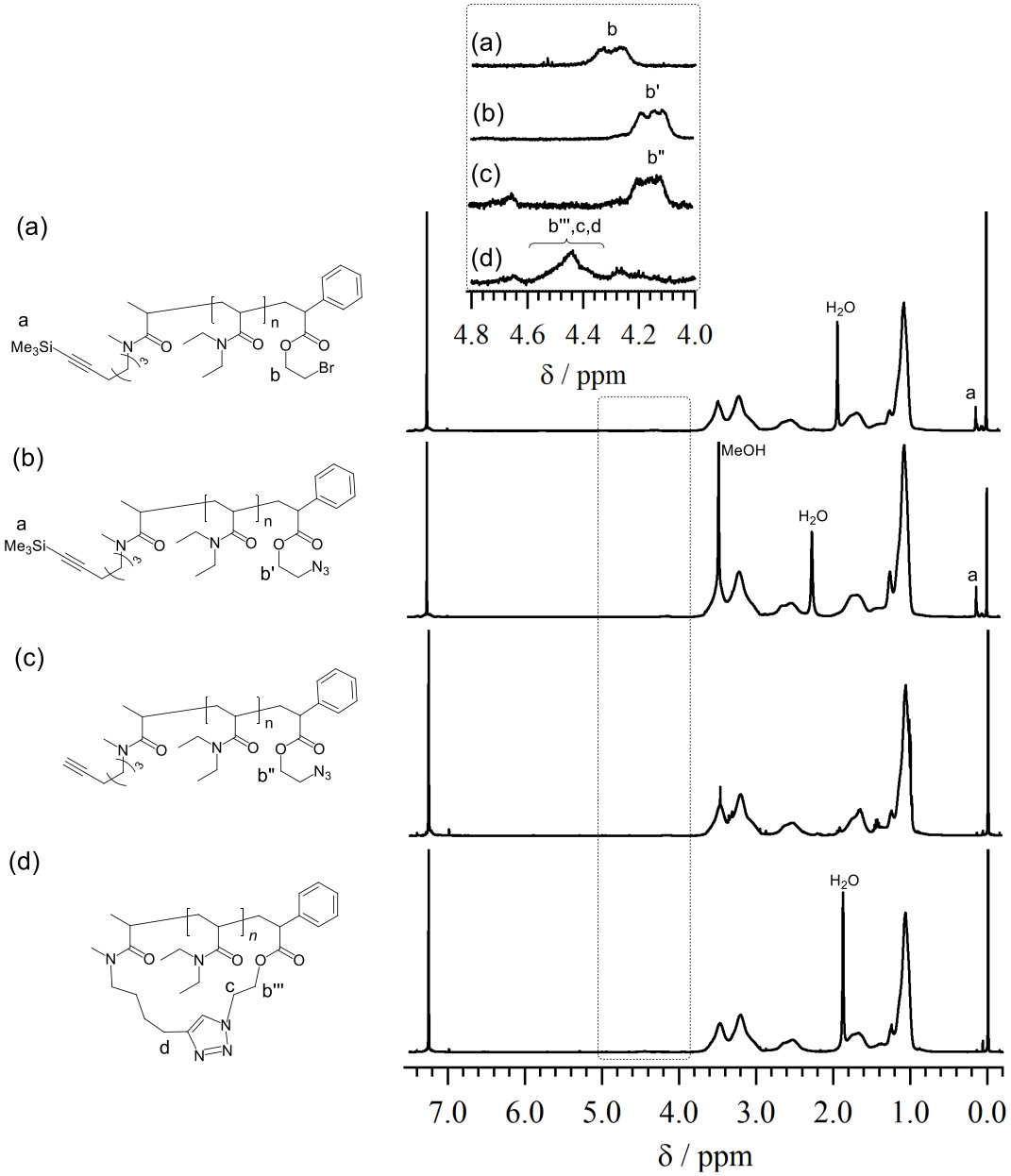

Figure 3-8. ^{1}H NMR spectra of (a) Si-≡-PDEAAm$_{50}$-Br, (b) Si-≡-PDEAAm$_{50}$-N$_3$, (c) ≡-PDEAAm$_{50}$-N$_3$, and (d) *c*-PDEAAm$_{50}$ in CDCl$_3$ (400 MHz).

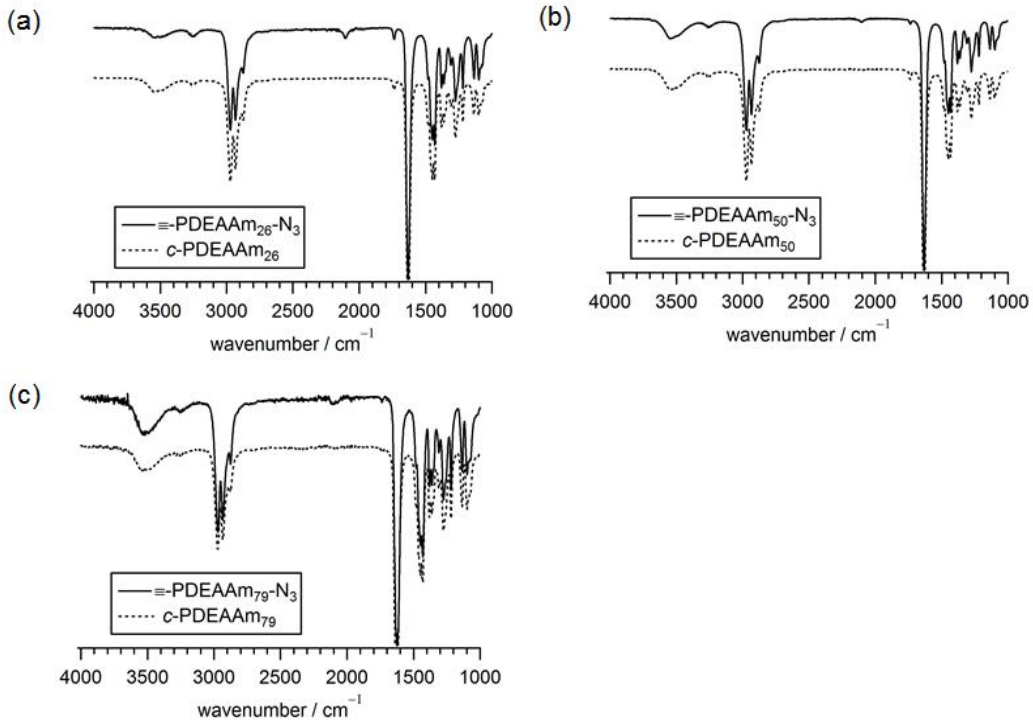

Figure 3-9. FT-IR spectra of ≡-PDEAAm-N_3 and *c*-PDEAAm.

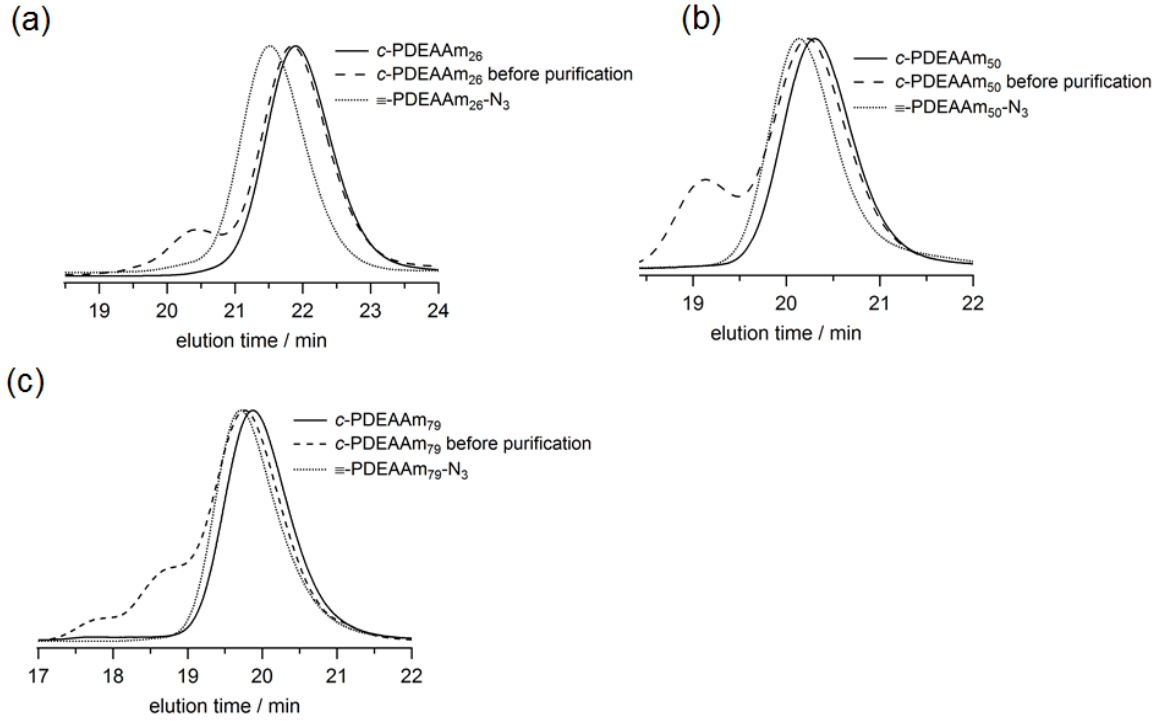

Figure 3-10. SEC traces of ≡-PDEAAm-N_3, its click reaction product, and *c*-PDEAAm (eluent, DMF containing 0.01 mol L^{-1} LiCl; flow rate, 0.6 mL min^{-1}).

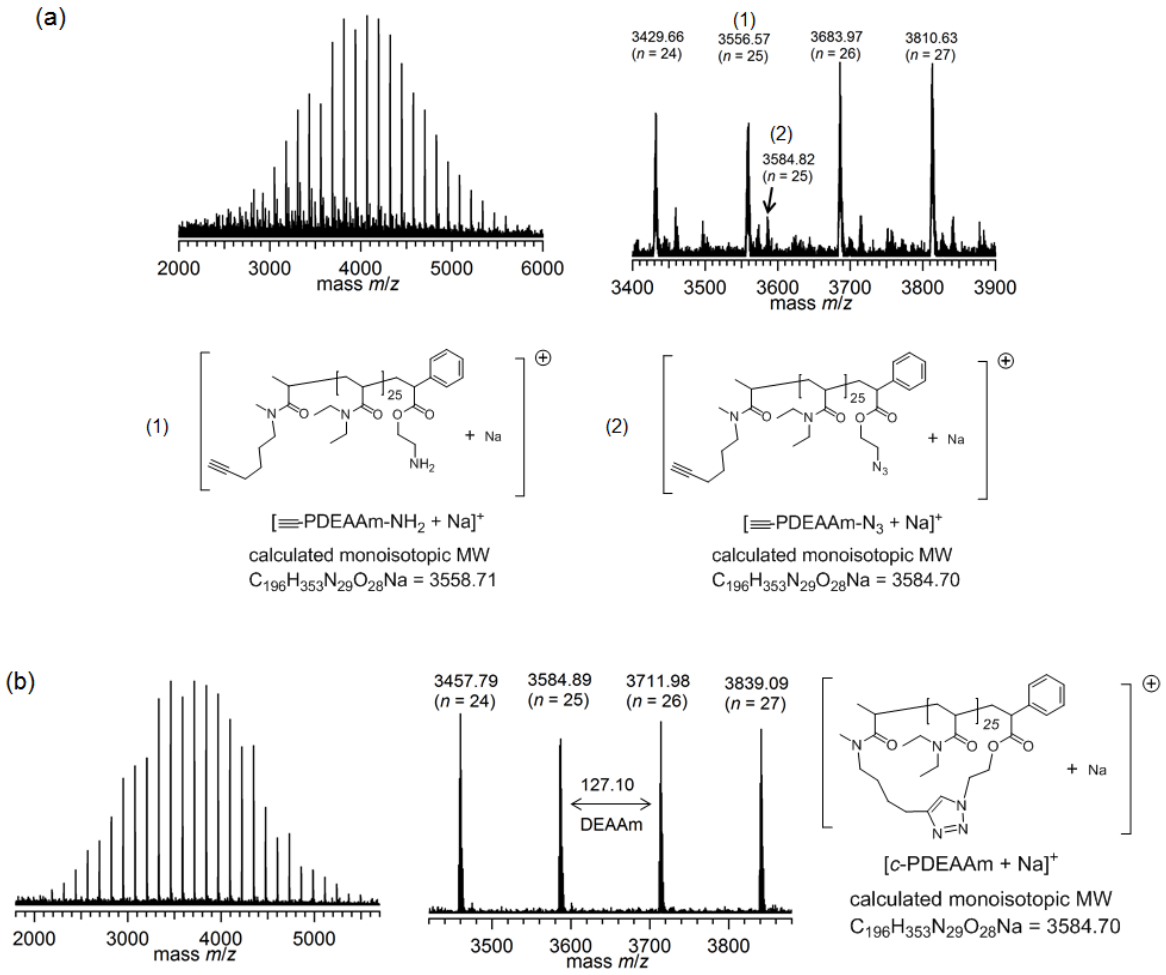

Figure 3-11. MALDI-TOF MS spectra of (a) ≡-PDEAAm$_{26}$-N$_3$ and (b) *c*-PDEAAm$_{26}$.

Table 3-6. Synthesis of *s*$_3$-PDEAAm and *l-taz*-PDEAAm [a]

Run	polymer	$M_{n,calcd.}$ [b] (kg mol^{-1})	$M_{n,SEC}$ [c] (kg mol^{-1})	$M_{n,NMR}$ (DP) [d] (kg mol^{-1})	M_w/M_n [c]
3-29	PDEAAm$_9$-N$_3$	1.40	1.46	1.46 (9)	1.02
3-30	*s*$_3$-PDEAAm$_{27}$	4.43	3.19	4.62 (27)	1.07
3-31	PDEAAm$_{17}$-N$_3$	2.44	2.10	2.48 (17)	1.07
3-32	*s*$_3$-PDEAAm$_{51}$	7.56	5.22	7.65 (51)	1.13
3-33	PDEAAm$_{26}$-N$_3$	3.50	2.66	3.63 (26)	1.07
3-34	*s*$_3$-PDEAAm$_{78}$	10.7	7.58	11.5 (78)	1.14
3-35	≡-PDEAAm$_{15}$	1.76	1.73	2.08 (15)	1.04
3-36	PDEAAm$_{14}$-N$_3$	1.91	1.63	2.10 (14)	1.03
3-37	*l-taz*-PDEAAm$_{14+15}$	3.67	3.04	4.17 (29)	1.07
3-38	≡-PDEAAm$_{26}$	3.35	3.01	3.47 (26)	1.06
3-39	PDEAAm$_{26}$-N$_3$	3.50	2.66	3.63 (26)	1.07
3-40	*l-taz*-PDEAAm$_{26+26}$	6.85	6.27	7.10 (52)	1.09
3-41	≡-PDEAAm$_{42}$	5.25	3.71	5.51 (42)	1.11
3-42	PDEAAm$_{38}$-N$_3$	4.77	3.38	5.15 (38)	1.08
3-43	*l-taz*-PDEAAm$_{38+42}$	10.0	7.59	10.7 (80)	1.09

[a] Azide-alkyne cycloaddition was carried out using Cu(I)Br/PMDETA catalytic system in DMF at 80 °C. [b] Calculated from ([DEAAm]$_0$/[I]$_0$) × (Conv.) × (M.W. of DEAAm) + (M.W. of desilylated initiator) + (M.W. of Terminator). [c] Determined by SEC in DMF containing 0.01 mol L^{-1} of LiCl using PMMA standards. [d] Determined from ^{1}H NMR spectrum.

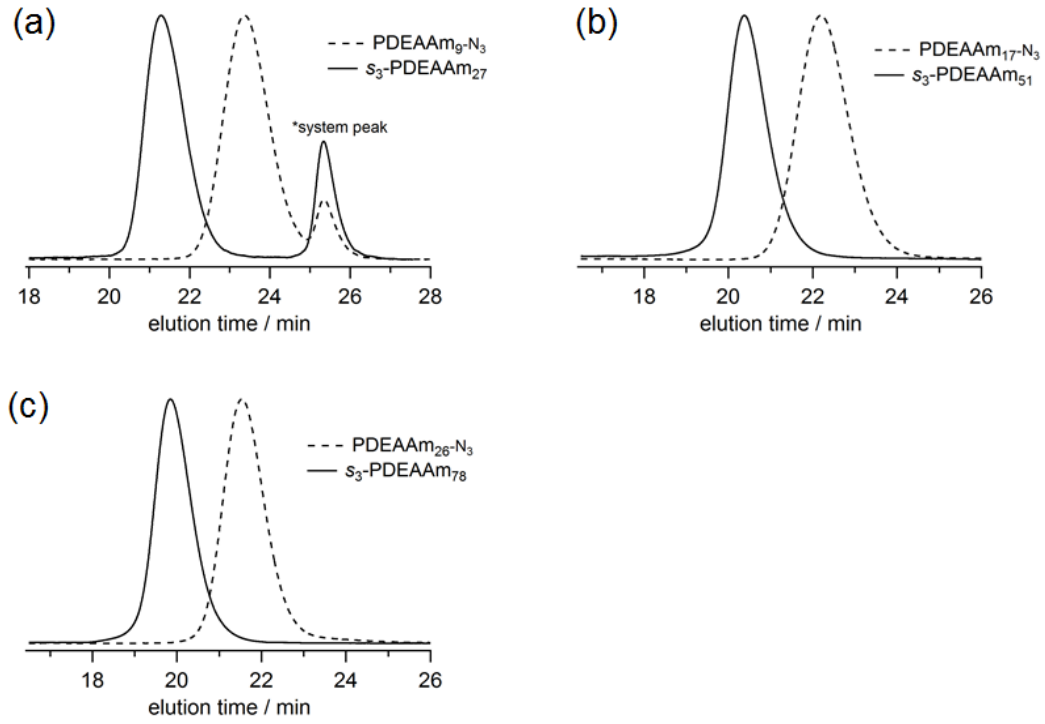

Figure 3-12. SEC traces of the s_3-PDEAAm and PDEAAm-N_3 (eluent, DMF containing 0.01 mol L^{-1} LiCl; flow rate, 0.6 mL min^{-1}).

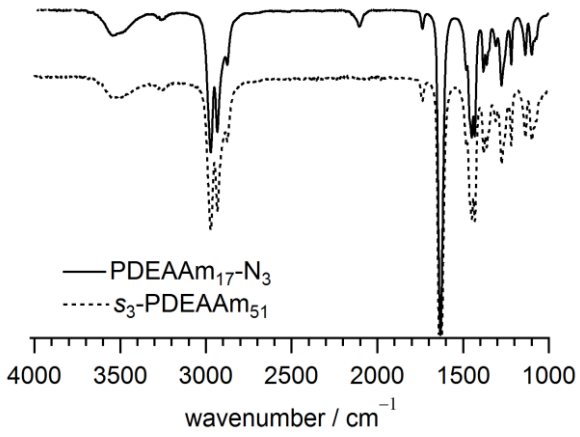

Figure 3-13. FT-IR spectra of $PDEAAm_{17}$-N_3 and s_3-$PDEAAm_{51}$.

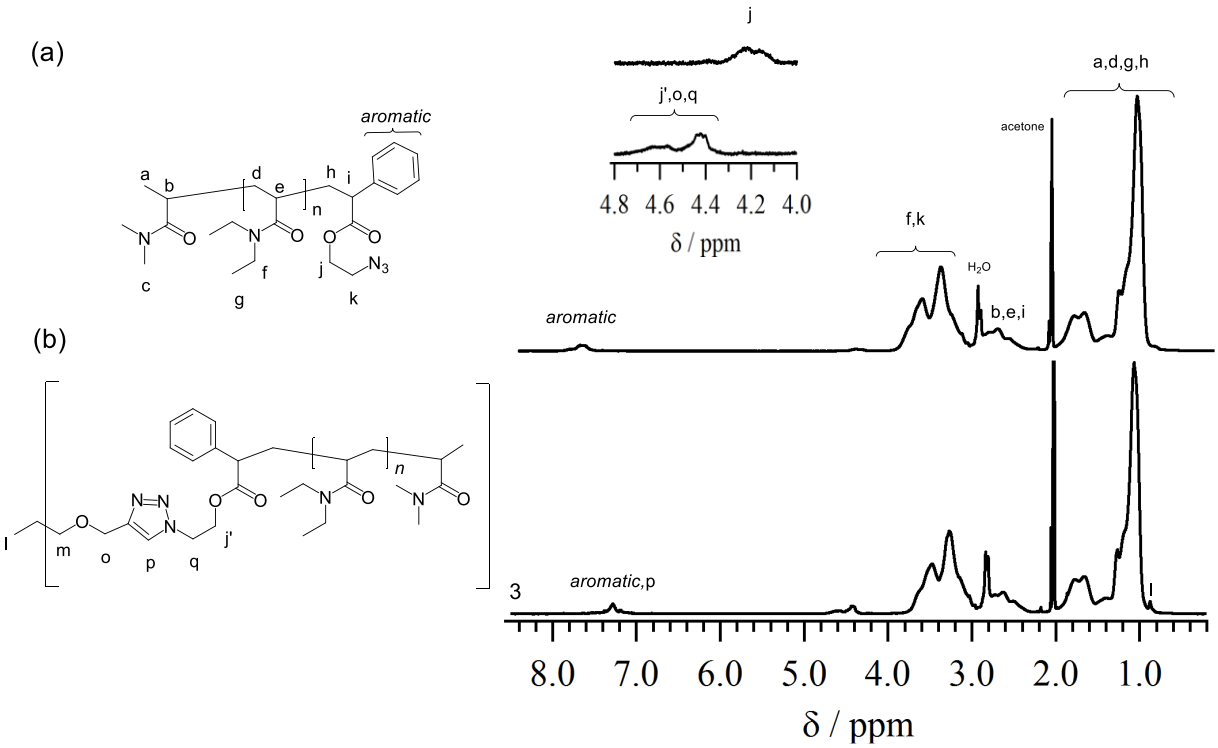

Figure 3-14. ^{1}H NMR spectra of (a) PDEAAm$_{17}$-N$_3$ and (b) *s*$_3$-PDEAAm$_{51}$ (acetone-*d*$_6$, 400 MHz).

3.3.5. Topological Effect of Linear, Cyclic, and Star-shaped PDEAAms on Thermoresponsive Property. *c*-PDEAAm and *s*$_3$-PDEAAm with comparable molecular weights were used to elucidate the topological effect on the thermoresponsive property. These polymers possessed the *taz* group in the polymer chains, which was suggested to significantly affect the thermal phase transition temperature.[45] In order to eliminate the effect of the *taz* group on the thermoresponsive property, the author prepared the linear PDEAAm with the *taz* group at the center of the polymer chain, *l*-*taz*-PDEAAm, by the click reaction between ≡-PDEAAm and PDEAAm-N$_3$, as shown in Scheme 3-3, which corresponds to the ring-opened structure of *c*-PDEAAm. For evaluating the thermoresponsive property of the PDEAAm in aqueous solution, the cloud point (*T*$_c$), which is defined as the temperature at the solution transmittance of 50%, was

determined by a turbidity measurement using a UV-visible spectrophotometer, and the enthalpy change (ΔH) of the water molecules per molar monomer unit during the thermal phase transition was monitored by a highly sensitive differential scanning calorimetry (micro-DSC) measurement. Figure 3-15 shows the transmittance curves at the fixed weight concentration of 2.0 g L^{-1}, and Table 3-7 summarizes the results of the T_c, the onset temperature ($T_{c,onset}$) of phase transition observed in a micro-DSC thermogram, and the ΔH. Initially, *l-taz*-PDEAAm and *c*-PDEAAm were compared in order to clarify the effect of the presence and absence of the polymer chain-end. All aqueous solutions of the polymer samples showed clear phase transitions during the heating cycle. The slopes of the transmittance curves for *c*-PDEAAm were gentle in comparison to those for *l-taz*-PDEAAm. Tanaka et al. reported that the slope value was related to the cooperative hydration state of the surrounding water molecules, which suggested that a stronger cooperativity led to a steeper slope.[46] Considering that the cyclic polymer was restricted in a ring and less stretched in dimensions than the linear polymer due to the absence of chain ends,[47] the gentle decrease in the optical transmittance of *c*-PDEAAm solution with increasing temperature was thus, on one hand, assumed to be attributed to the fact that the water molecules hydrated within the *c*-PDEAAm ring were easier and earlier to release during the phase transition because the cooperative interaction of such water molecules was much weaker than that formed by the water molecules outside the polymer ring, which led to the conculsion that the cooperatively hydrated water molecules inside and outside the *c*-PDEAAm were not simultaneously dehydrated, causing the dehydration in a broader temperature range, *i.e.*, low responsivity. On the other hand, the cyclic polymer should be more repulsive than the linear polymer due to the reduced entanglement between the polymer chains during the coil-to-globule aggregation of the dehydrated polymers, which also contributed to the slower phase transition, *i.e.*, low responsivity. These two facts could be considered to be the reason why *c*-PDEAAm showed a slower decreasing trend on the solution

transmittance plot.

The T_cs of 41.1 - 35.2 °C for *c*-PDEAAm were lower than those of 42.7 - 36.5 °C for *l-taz*-PDEAAm over the entire molecular weight range. The difference in the T_c values could be due to the varying hydration states of the two polymers, as that of *c*-PDEAAm as was already discussed to some extent. In more detail, the hydrogen-bonding network formed by *c*-PDEAAm was much weaker than that formed by *l-taz*-PDEAAm due to the existence of the spatially constrained cyclic inner region. The micro-DSC measurements suggested that the hydration number for *c*-PDEAAm was lower than that for *l-taz*-PDEAAm, as shown in Figure 3-16. The thermograms of each polymer showed endothermic peaks, and the $T_{c,onset}$s of 40.9 - 35.6 °C for *c*-PDEAAm were lower than those of 42.1 - 36.7 °C for *l-taz*-PDEAAm, which well agreed with the tendency of T_c from the transmittance curve. The ΔHs of 3.33 - 3.70 kJ mol^{-1} for *c*-PDEAAm were lower than those of 4.23 - 4.81 kJ mol^{-1} for *l-taz*-PDEAAm, indicating that the number of water molecules dehydrated during the phase transition of *c*-PDEAAm was lower than that of *l-taz*-PDEAAm. Hence, it is clear that the topological change from linear to cyclic architectures led to lowering the T_c and also affected the responsivity during the thermal phase transition.

In order to further elucidate the topological effect, we then compared the thermoresponsive property among *l-taz*-PDEAAm, *c*-PDEAAms, and s_3-PDEAAm. The T_c values decreased in the order of *l-taz*-PDEAAm > *c*-PDEAAm > s_3-PDEAAm. The T_c of the star-shaped polymer lower than that of the linear polymer well agreed with other literature reports.[3] The difference in T_c between s_3-PDEAAm and *c*-PDEAAm was similar to that between s_3-PDEAAm and *l-taz*-PDEAAm. However, the ΔHs of 3.45 - 3.98 kJ mol^{-1} for s_3-PDEAAm were almost same as those of 3.33 - 3.70 kJ mol^{-1} for *c*-PDEAAm. This result indicated that the number of water molecules dehydrated from s_3-PDEAAm and *c*-PDEAAm were extremely similar in spite of the different topological structures. The phase transition behavior of s_3-PDEAAm on the transmittance curve

was similar to that of *l-taz*-PDEAA, rather than *c*-PDEAAm. It is rational that s_3-PDEAAm showed a lower ΔH and faster response because the hydrogen-bonding network around the star core was weaker due to the limited space to accommodate sufficient cooperative water molecules.[3] The T_c change of 35.7 - 34.6 °C over the entire DP range for s_3-PDEAAm was significantly low, which was rather different from those of *l-taz*-PDEAAm (42.7 - 36.5 °C) and *c*-PDEAAm (41.1 - 35.2 °C). This should be caused by the significantly strong effect of the linker core in s_3-PDEAAm, which made the effect of arm length in the range of 9 - 26-mers on the T_c negligible. However, the number of cooperative water molecules of the two nonlinear PDEAAms with comparable molecular weights were significantly similar, though their phase transitions showed a significant difference in molecular weight dependence as well as responsivity.

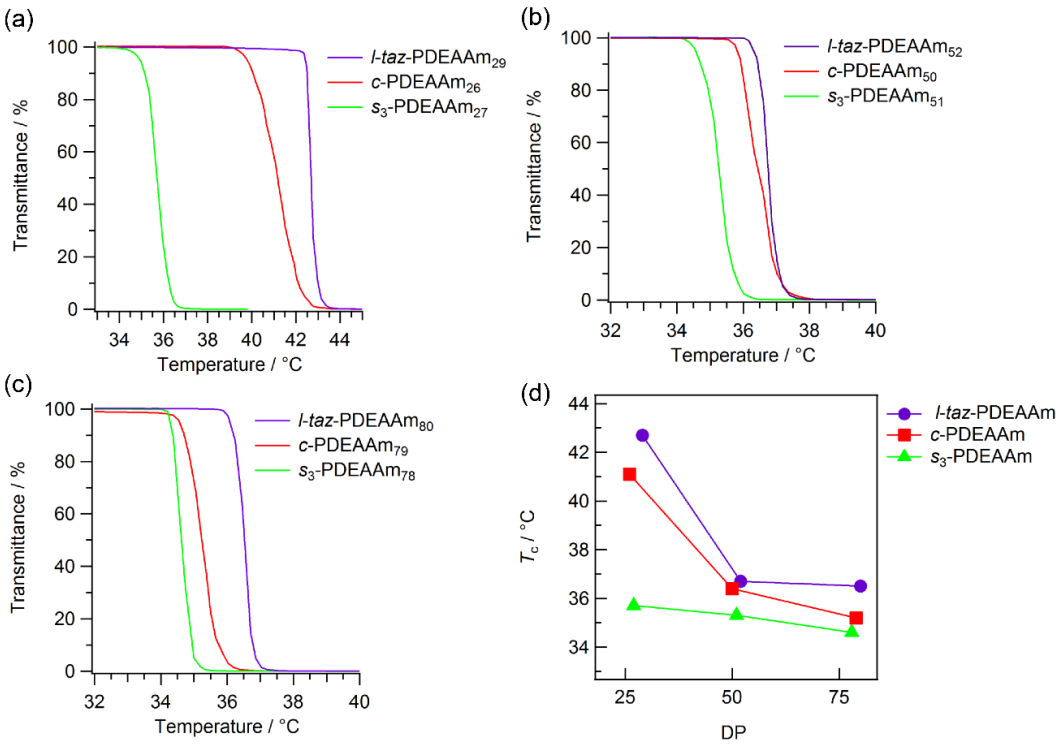

Figure 3-15. Molecular weight dependence on thermal phase transition of *l-taz*-, *c*-, and s_3-PDEAAms at the fixed mass concentration of 2.0 g L^{-1}; (a) $PDEAAm_{26\text{-}29}$, (b) $PDEAAm_{50\text{-}52}$, and (c) $PDEAAm_{78\text{-}80}$, and (d) the plots of T_c versus DP.

Table 3-7. Thermoresponsive property of linear, cyclic, and star-shaped PDEAAms in aqueous solution

Polymer	$M_{n,NMR}$ (kg mol^{-1})	T_c (°C) [a]	$T_{c,onset.}$(°C)	ΔH (kJ mol^{-1}) [b]
l-taz-PDEAAm$_{29}$	4.17	42.7	42.1	4.81
c-PDEAAm$_{26}$	3.65	41.1	40.9	3.33
s$_3$-PDEAAm$_{27}$	4.62	35.7	35.2	3.98
l-taz-PDEAAm$_{52}$	6.99	36.7	36.7	4.23
c-PDEAAm$_{50}$	6.78	36.4	35.8	3.39
s$_3$-PDEAAm$_{51}$	7.65	35.3	34.4	3.45
l-taz-PDEAAm$_{80}$	10.7	36.5	36.7	4.23
c-PDEAAm$_{79}$	10.4	35.2	35.6	3.70
s$_3$-PDEAAm$_{78}$	11.5	34.6	34.1	3.67

[a] T_c was defined as the temperature where transmittance reached at 50% during heating cycle, determined by turbidity measurement using UV-vis spectrophotometer. [b] Determined by micro-DSC using an aqueous polymer solution of 2.0 g L^{-1} at the heating rate of 1.0 °C min^{-1}.

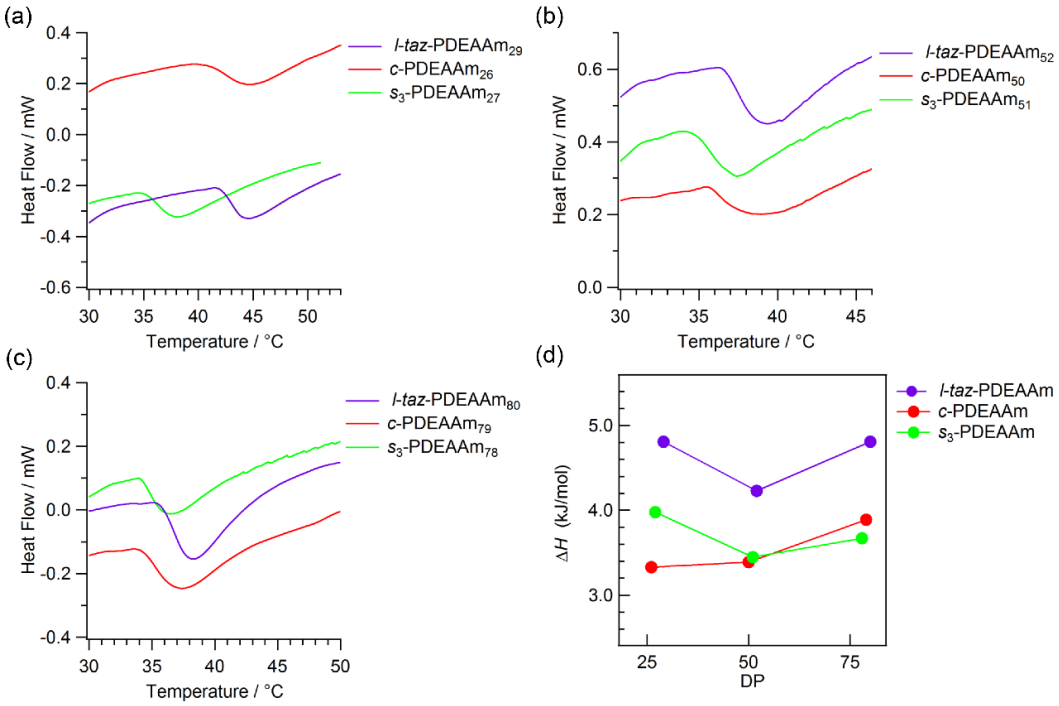

Figure 3-16. Micro-DSC thermograms for aqueous solutions of *l-taz*-, *c*-, and s_3-PDEAAms at the fixed weight concentration of 2.0 g L^{-1}, approximate DPs of (a) $PDEAAm_{26\text{-}29}$, (b) $PDEAAm_{50\text{-}52}$, and (c) $PDEAAm_{78\text{-}80}$, and (d) the plots of ΔH versus DP.

3.3.6. Molecular dynamics (MD) simulation of linear-, cyclic-, and 3-armed star-shaped PDEAAm in aqueous solution. In order to evaluate the topological effect on the thermoresponsive property of the PDEAAm in detail, MD simulations of the unimolecular PDEAAms with the architecture, linear, cyclic, and 3-armed star-shapes were carried out. The modeling polymers of 25 mer were used for this simulation, which well-corresponded to the synthesized polymers. The MD simulation of each polymer architecture was carried out for 20 ns at 298 K, 313 K, and 328 K, respectively, where the temperatures were before, after the cloud point, and its intermediate temperature. Other simulation details are described in the experimental section.

Figure 3-17 and Figure 3-19 show the time-dependence of the radius of gyration (R_g) at each temperature and their histograms, and Table 3-8 summaries the values of the averaged R_g ($R_{g,ave}$).

The $R_{g,ave}$ of *l-taz*-PDEAAm decreased from 12.31 ± 0.37 to 10.19 ± 0.25 Å by increasing the temperature from 298 K to 328K, and the conformational changes in *l-taz*-PDEAAm from a coil to globule was clearly observed as shown in Figure 3-18a. On the other hand, the $R_{g,ave}$ of s_3-PDEAAm slightly decreased by the increasing temperature, and that of *c*-PDEAAm underwent almost no change. In Figures 3-17b and c, the time-dependent traces of *c*-PDEAAm and s_3-PDEAAm at 328 K converged after 20 ns though the fluctuation was greater in the early time region due to the thermal energy. The conformational changes in s_3-PDEAAm suggested that each arm seemed to be aggregated one by one, as shown in Figure 3-18c. However, no conformational changes in *c*-PDEAAm were observed though the conformation with the higher R_g seemed to be an extended structure compared to that with the lower R_g (Figure 3-18b). Based on the results of the R_g analysis, it was revealed that the R_gs of *c*-PDEAAm, and s_3-PDEAAm could not undergo drastic changes during the phase transition due to the structural restriction for the cyclic and star-shapes.

Figure 3-20 shows the radial distribution function (RDF) for the whole PDEAAm carbonyl oxygen on the side chain with hydrogen of the water, which the RDF provides direct information about the change in the hydration state during the phase transition. Table 3-9 summaries the hydration number between the carbonyl oxygen for the PDEAAm monomer unit and hydrogen of the water within 3.0 Å from the carbonyl oxygen. All the RDF profiles showed the first and second peaks located at around 2.0 Å and 3.2 Å, where the first peak shows direct hydrogen bonding between the carbonyl oxygen and hydrogen of water and the second peak shows the long distance correlation for forming a second hydration shell. In Figure 3-18a, *l-taz*-PDEAAm showed clear changes in the hydration state at around 2.0 Å with the increasing temperature, *i.e.*, the hydration number decreased from 33.00 ± 2.6 (298 K) to 28.63 ± 2.8 (328 K), meaning the collapse of the hydrogen bonding between the carbonyl oxygen for the PDEAAm monomer unit and hydrogen

of water. Similar to the *l-taz*-PDEAAm, the first peaks of *c*-PDEAAm and s_3-PDEAAm on the RDF were decreased through the cloud point though the decreasing degrees of the peaks were less than that of *l-taz*-PDEAAm. However, the hydration number between the carbonyl oxygen for the *c*-PDEAAm monomer unit and water hydrogen increased from 24.20 ± 2.0 to 25.43 ± 2.3 with the increasing temperature from 298K to 328K. This discrepancy is explained in the next section.

In order to further evaluate the difference in the topological effect, the RDF for each differently located carbonyl oxygen on the side chain of PDEAAm with the hydrogen of water was analyzed, *e.g.*, the carbonyl oxygen located at the neighbor connected parts by the click reaction, chain end, and middle of the monomer repeating units, for *l-taz*-PDEAAm (Figure 3-21), that of the neighbor core unit, outer side, and middle part, for s_3-PDEAAm (Figure 3-22), and, that of the neighbor connected parts by the click reaction, and inward or outward on the cyclic architecture, for *c*-PDEAAm (Figure 3-23). The RDFs for each carbonyl oxygen on the *l-taz*-PDEAAm with the hydrogen of water showed quite similar behaviors though that of the neighbor phenyl group drastically changed because of its hydrophobic effect by the phenyl group. On the other hand, the RDF for each carbonyl oxygen on s_3-PDEAAm with the hydrogen of water showed a significantly different behavior. Especially, the first and second peaks of the inner part disappeared at 313 K then reforming the hydration shell at 328K. This phenomenon is rationally explained by the fact that the hydration state neighbor core unit should be less-structured due to the high atomic density near the branching core. In addition, the RDF for each carbonyl oxygen on *c*-PDEAAm with the hydrogen of water showed a unique behavior. The RDF of the neighbor connected parts by the click reaction and outward carbonyl oxygen with the hydrogen of water showed the same tendency as that of *l-taz*-PDEAAm. The RDF of the inward carbonyl oxygen on the cyclic architecture showed an inverse behavior compared to the other RDFs, in which the first peak height was very low at 298 K, then the peak intensity increased with the increasing temperature. The reason for

this phenomenon was considered to be caused by two factors as follows: (1) the inward carbonyl oxygen was difficult to form a stable hydration shell due to the small cavity of the cyclic inside, and (2) the direction of the carbonyl oxygen might be changed during the thermal phase transition, leading to more hydrophilic surroundings for the carbonyl oxygen. These unexpected results of the RDFs for each carbonyl oxygen on *c*-PDEAAm supported why the hydration number of *c*-PDEAAm increased with the increasing temperature, because the hydration number was estimated using the whole carbonyl oxygen on the monomer units.

As the results of the MD simulation, it was revealed that the difference in topology among the three architectures, linear, cyclic, and 3-arm star, was significantly affected by the coil-to-globule transition of the PDEAAm.

Table 3-8. A summary of R_g values at each temperature

	$R_{g.ave}$ (Å)[a]		
	298K	313K	328K
l-taz-PDEAAm	12.31 ± 0.37	10.41 ± 0.15	10.19 ± 0.25
c-PDEAAm	10.20± 0.43	10.25 ± 0.19	10.28 ± 0.20
s_3-PDEAAm	10.59 ± 0.24	10.18 ± 0.19	9.94 ± 0.29

[a] $R_{g,ave}$s were estimated using last 5 ns.

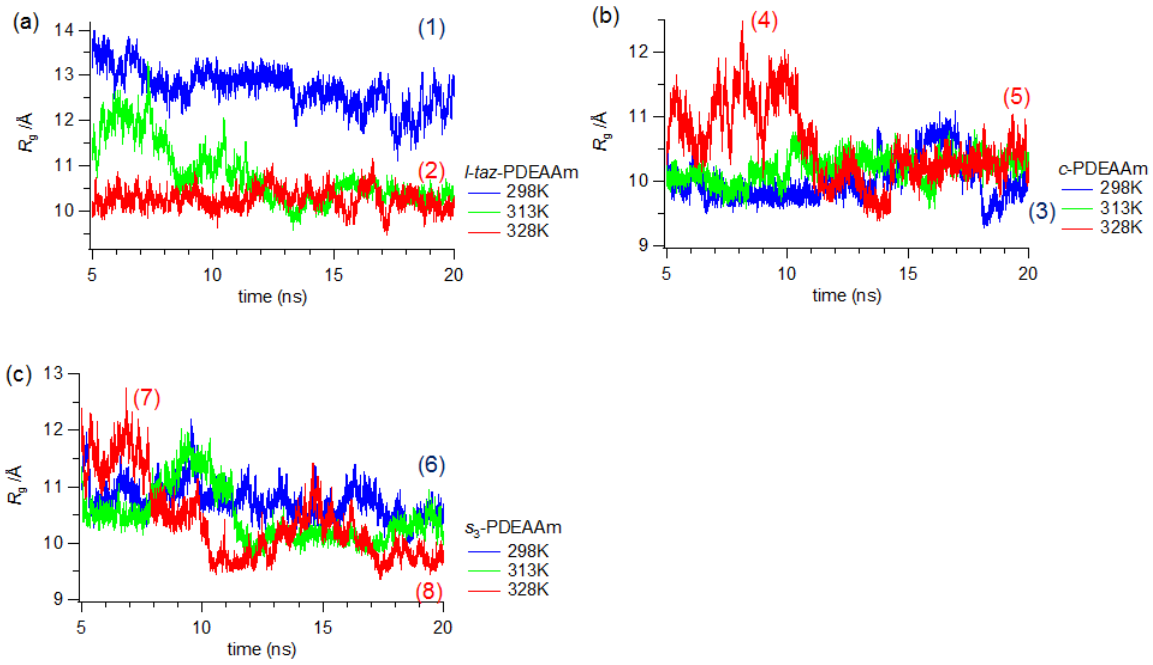

Figure 3-17. Time-dependence of R_g changes for (a) *l-taz*-PDEAAm, (b) *c*-PDEAAm, and (c) s_3-PDEAAm.

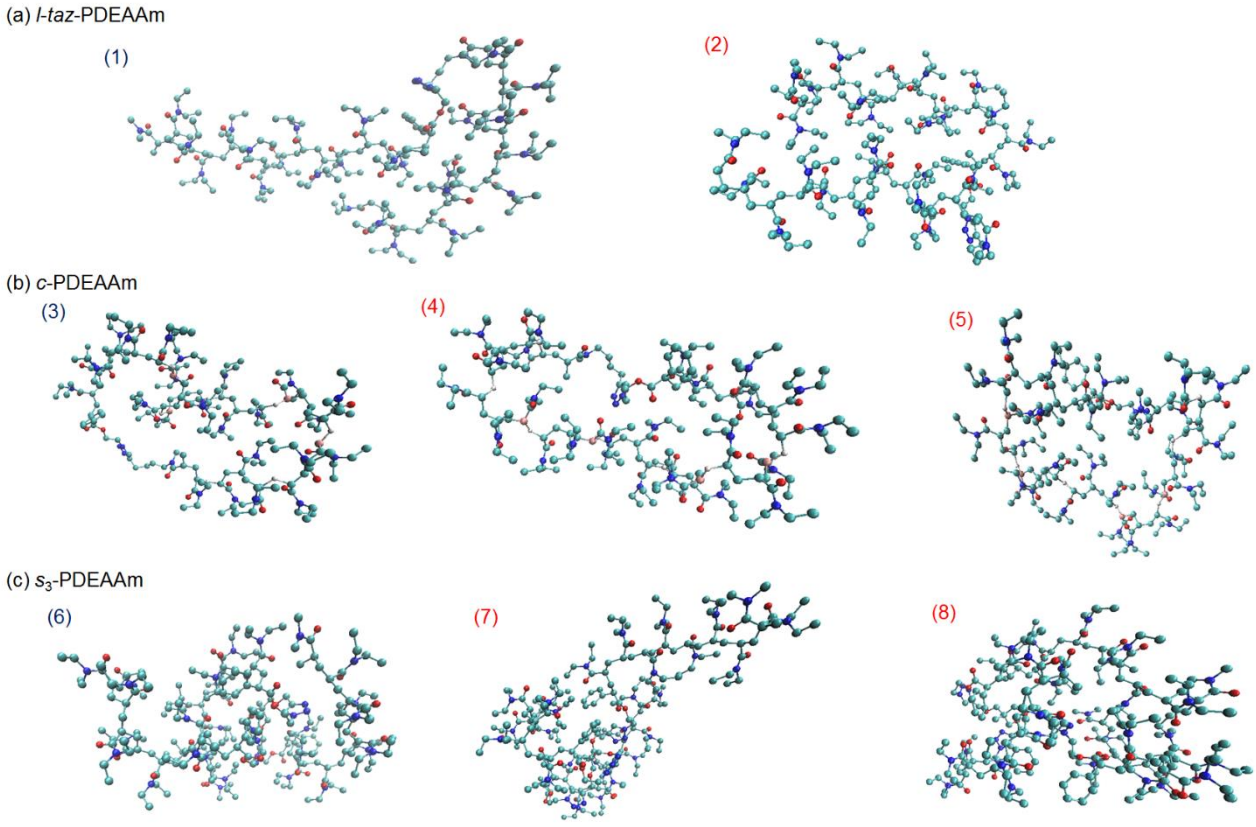

Figure 3-18. Snapshots of (a) *l-taz*-PDEAAm, (b) *c*-PDEAAm, and (c) s_3-PDEAAm, where carbon, oxgen, and nitrogen are denoted in green, red, and blue, respectively (each number with snapshot corresponds to the number shown in Figure 3-17)

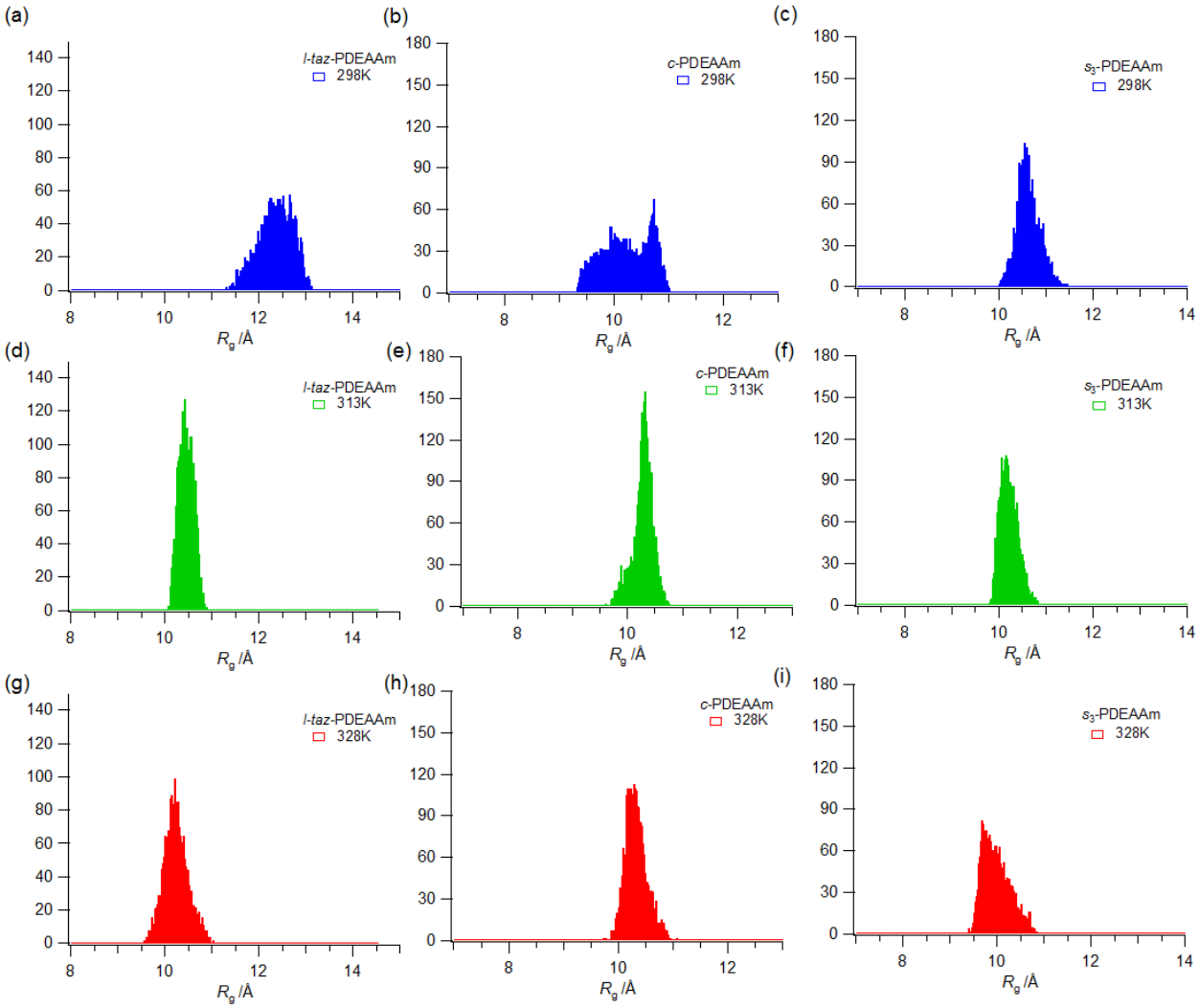

Figure 3-19. Histograms of R_g for *l-taz*-PDEAAm, *c*-PDEAAm, and s_3-PDEAAm at 298 K (blue), 313 K (green), and 328 K (red) (last 5 ns data were used for the histogram).

Table 3-9. The hydration number between water molecules and carbonyl groups of PDEAAm

	hydration number (>=O···H-O-H)		
	298K	313K	328K
l-taz-PDEAAm	33.00 ± 2.6	30.22 ± 2.6	28.63 ± 2.8
c-PDEAAm	24.20 ± 2.0	24.39 ± 2.1	25.43 ± 2.3
s_3-PDEAAm	33.44 ± 2.6	31.85 ± 3.1	30.73 ± 2.9

[a] Data were averaged over last 5 ns.

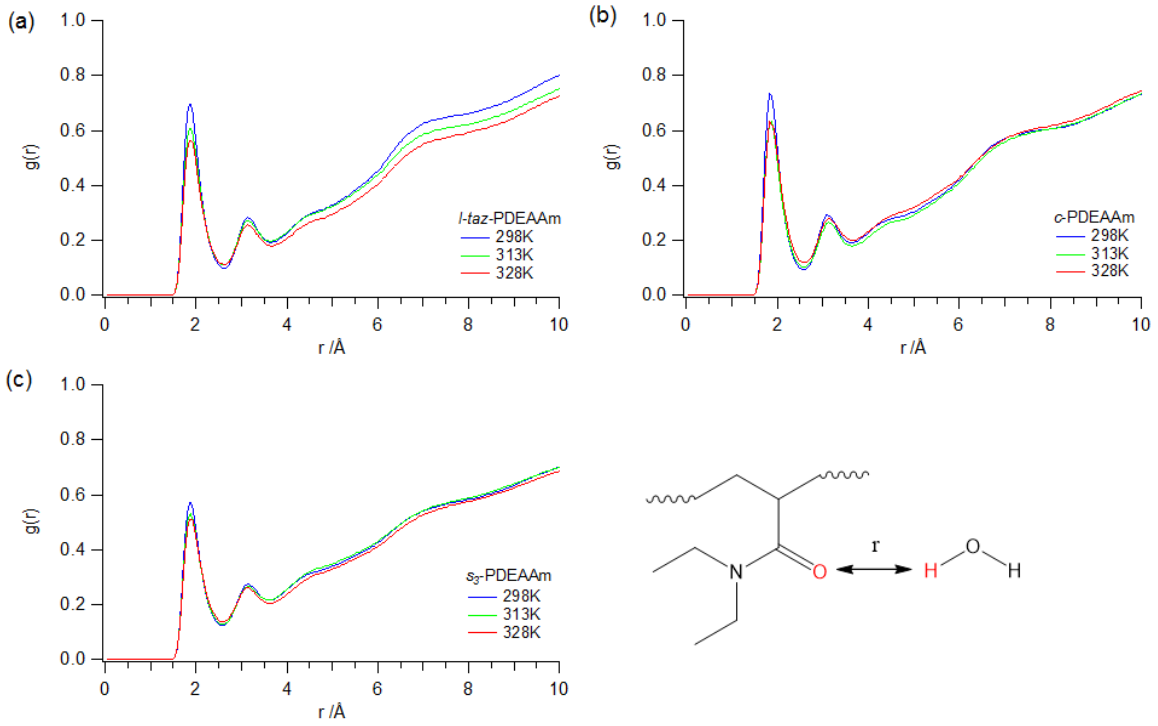

Figure 3-20. RDF for hydrogen of water with carbonyl oxygen of monomer unit on (a) *l-taz*-PDEAAm, (b) *c*-PDEAAm, and (c) s_3-PDEAAm at 298 K (blue line), 313 K (green line), and 328 K (red line).

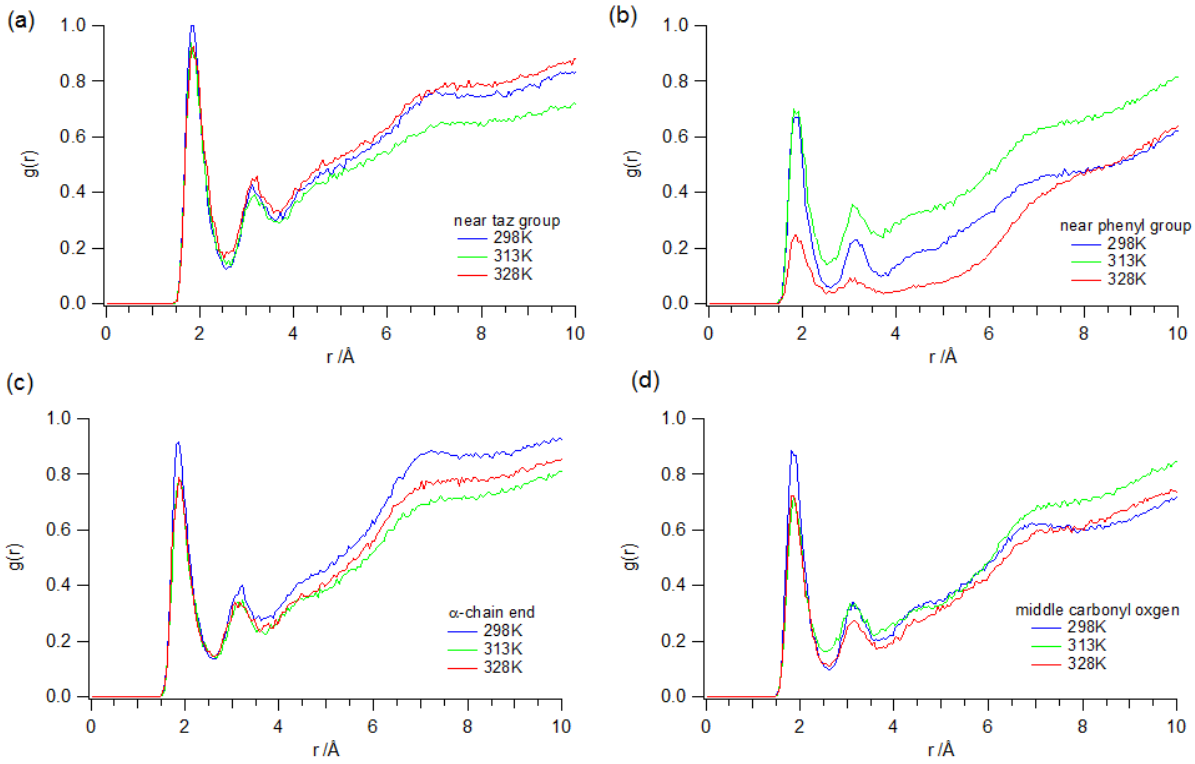

Figure 3-21. RDFs for hydrogen of water with carbonyl oxygen of monomer unit on *l-taz*-PDEAAm located at (a) α-chain end, (b) in the middle, (c) neighbor *taz* group, and (c) neighbor phenyl group at 298 K (blue line), 313 K (green line), and 328 K (red line).

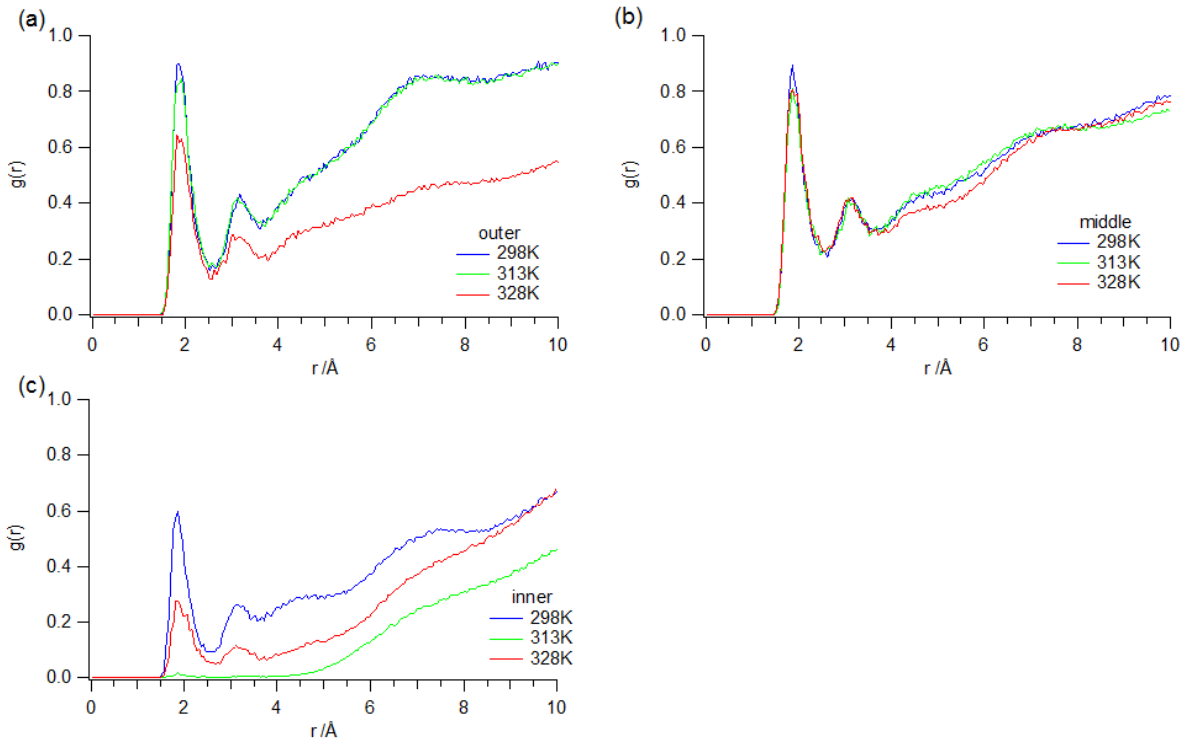

Figure 3-22. RDFs for hydrogen of water with carbonyl oxygen of monomer unit on s_3-PDEAAm located at (a) outer, (b) middle, and (c) inner part at 298 K (blue line), 313 K (green line), and 328 K (red line).

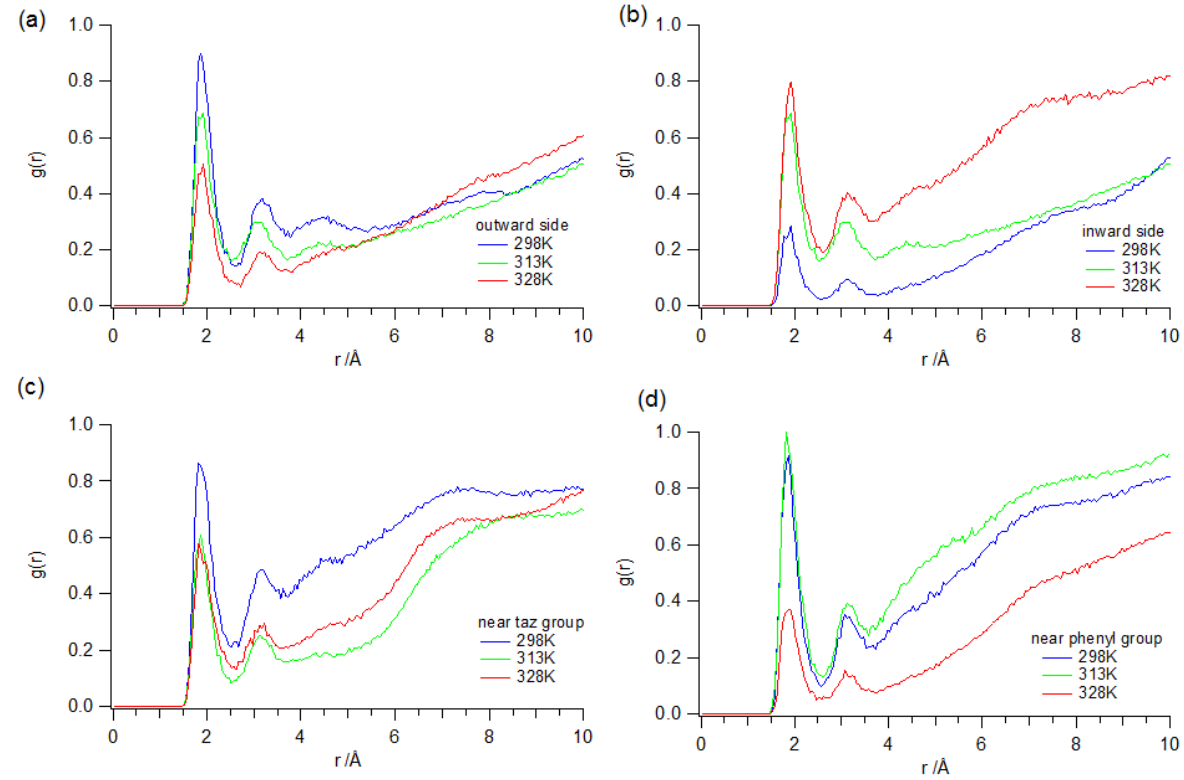

Figure 3-23. RDFs for hydrogen of water with carbonyl oxygen of monomer unit on *c*-PDEAAm located at (a) outward side, (b)inward side, (c) neighboring *taz* group, and (c) neighboring phenyl group at 298 K (blue line), 313 K (green line), and 328 K (red line).

The results of the MD simulation were in strong agreement with the experimental results. For example, the MD simulation results of the higher R_g and hydration number changes of *l-taz*-PDEAAm than that of *c*-PDEAAm supported the fact that the enthalpy changes during the phase transition of *l-taz*-PDEAAm was higher than that of *c*-PDEAAm, in other words, the cyclic architectures prevent the intermolecular entanglement, leading to a lower responsivity of *c*-PDEAAm during the phase transition. In addition, the MD simulation results of the RDFs for each carbonyl oxygen on the PDEAAms with the hydrogen of water proved that the cyclic and branching architectures restrict forming the hydration shell at the cyclic inside and neighboring star core, respectively, compared to the linear counterpart, leading to a lower phase transition temperature than *l-taz*-PDEAAm. Thus, the author achieved the evaluation of the topological effect on the thermoresponsive properties of PDEAAm varying from a macroscopic to atomic scale.

3.4. Conclusions

The author demonstrated a facile end-functionalization method of PDEAAm at both the α- and ω-chain ends through the $B(C_6F_5)_3$-catalyzed GTP of DEAAm using functional silyl ketene aminals (SKAms) as the initiator and functional 2-phenyl acrylates (PhA-Fs) as the terminator. The SKAm designed with hydroxyl, ethynyl, and vinyl groups were quantitatively introduced at the α-chain end of PDEAAm with well-controlled molecular weights, narrow polydispersities, and structural fidelity. As well as the initiation approaches, PhAs functionalized with hydroxyl, ethynyl, and bromo groups were quantitatively introduced at the ω-chain end of PDEAAm, whose structural fidelity was definitely confirmed by ^{1}H NMR and MALDI-TOF MS measurements. In addition, the intra- or inter-molecular azide-alkyne cycloaddition of the end-functionalization of PDEAAm successfully produced the PDEAAms with nonlinear topological architectures, *i.e.*,

macrocyclic and star-shaped. Both of the cyclic-PDEAAm and 3-armed star-shaped PDEAAm were successfully prepared with three different DPs of 26 - 29, 50 - 52, and 78 - 80. The topology of the polymer architectures, such as linear, cyclic, and star-shaped PDEAAms, significantly reflected to their thermoresponsive property in terms of molecular weight dependence and responsivity for the phase transition, among which the cyclic and star architectures led to a lower phase transition temperature compared to its linear counterpart. Additionally, molecular dynamics simulations of unimolecular PDEAAm architectures gave deep insight for the effect of topology on thermoresponsive properties in atomic scale, which well-supported the experimental results. To the best of knowledge, this is the first report of the comprehensive study of the topological effect among linear, cyclic, and star-shaped PDEAAms on their thermoresponsive properties, of which the chemical structures of comparative PDEAAms were carefully considered. These results make a significant contribution to polymer chemistry regarding the design of well-defined acrylamide polymers and polymer architecture along with the control of the phase transition temperature.

3.5. References and Notes

(1) Kricheldorf, H.R. *J. Polym. Sci., Part A: Polym. Chem.* 2010, *48*, 251-284.

(2) Hogen-Esch, T. E. *J. Polym. Sci., Part A: Polym. Chem.* 2006, *44*, 2139-2155.

(3) Xu, J.; Liu, S. *J. Polym. Sci., Part A: Polym. Chem.* 2009, *47*, 404-419.

(4) Xu, J.; Ye, J.; Liu, S. *Macromolecules* 2007, *40*, 9103-9110.

(5) Honda, S.; Yamamoto, T.; Tezuka, Y. *J. Am. Chem. Soc.* 2010, *132*, 10251-10253.

(6) Khanna, K.; Varshney, S.; Kakkar, A. *Polym. Chem.* 2010, *1*, 1171-1185.

(7) Poelma, J. E.; Ono, K.; Miyajima, D.; Aida, T.; Satoh, K.; Hawker, C. J. *ACS Nano* 2012, *6*, 10845-10854.

(8) Zhao, L.; Lin, Z. *Soft Matter* 2011, *7*, 10520-10535.

(9) Maury-Evertsz, J. R.; López, G. E. *J. Chem. Phys.* 2005, *123*, 054903.

(10) Yamamoto, T.; Tezuka, Y. *Polym. Chem.* 2011, *2*, 1930-1941.

(11) Tu, X.-Y.; Liu, M.-Z.; Wei, H. *J.Polym.Sci., Part A: Polym. Chem.* 2016, *54*, 1447-1458.

(12) Schappacher, M.; Deffieux, A. *Macromolecules* 2001, *34*, 5827-5832.

(13) Laurent, B. A.; Grayson, S. M. *J. Am. Chem. Soc.* 2006, *128*, 4238-4239.

(14) Lonsdale, D. E.; Bell, C. A.; Monteiro, M. J. *Macromolecules* 2010, *43*, 3331-3339.

(15) Hoskins, J. N.; Grayson, S. M. *Macromolecules* 2009, *42*, 6406-6413.

(16) Kamber, N. E.; Jeong, W.; Waymouth, R. M.; Pratt, R. C.; Lohmeijer, B. G. G.; Hedrick, J. L. *Chem. Rev.* 2007, *107*, 5813-5840.

(17) Makiguchi, K.; Ogasawara, Y.; Kikuchi, S.; Satoh, T.; Kakuchi, T. *Macromolecules* 2013, *46*, 1772-1782.

(18) Fuchise, K.; Chen, Y.; Satoh, T.; Kakuchi, T. *Polym. Chem.* 2013, *4*, 4278-4291.

(19) Scholten, M. D.; Hedrick, J. L.; Waymouth, R. M. *Macromolecules* 2008, *41*, 7399-7404.

(20) Raynaud, J.; Ciolino, A.; Beceiredo, A.; Destarac, M.; Bonnette, F.; Kato, T.; Gnanou, Y.; Taton, D. *Angew. Chem. Int. Ed.* 2008, *47*, 5390-5393.

(21) Raynaud, J.; Liu, N.; Gnanou, Y.; Taton, D. *Macromolecules* 2009, *42*, 5996-6005.

(22) Raynaud, J.; Liu, N.; Fèvre, M.; Gnanou, Y.; Taton, D. *Polym. Chem.* 2011, *2*, 1706-1712.

(23) Fuchise, K.; Sakai, R.; Satoh, T.; Sato, S.; Narumi, A.; Kawaguchi, S.; Kakuchi, T. *Macromolecules* 2010, *43*, 5589-5594.

(24) Takada, K.; Fuchise, K.; Chen, Y.; Satoh, T.; Kakuchi, T. *J. Polym. Sci. Part A: Polym. Chem.* 2012, *50*, 3560-3566.

(25) Kikuchi, S.; Chen, Y.; Kitano, K.; Takada, K.; Satoh, T.; Kakuchi, T. *Polym. Chem.* 2015, *6*, 6845-6856.

(26) Kakuchi, T.; Chen, Y.; Kitakado, J.; Mori, K.; Fuchise, K.; Satoh, T. *Macromolecules*, 2011, *44*, 4641-4647.

(27) Sogah, D. Y.; Hertler, W. R.; Webster, O. W.; Cohen, G. M. *Macromolecules* 1987, *20*, 1473-1488.

(28) Gnaneshwar, R.; Sivaram, S. *J. Polym. Sci. Part A: Polym. Chem.* 2007, *45*, 2514-2531.

(29) Takada, K.; Fuchise, K.; Kubota, N.; Ito, T.; Chen, Y.; Satoh, T.; Kakuchi, T. *Macromolecules* 2014, *47*, 5514-5525.

(30) Chen, Y.; Takada, K.; Kubota, N.; Eric, O.-T., Ito, T.; Isono, T.; Satoh, T.; Kakuchi, T. *Polym.Chem.* 2015, *6*, 1830-1837.

(31) Eric, O.-T.; Chen, Y.; Takada, K.; Sato, S.; Satoh, T.; Kakuchi, T. *Polym.Chem.* 2015, *6*, 7841-7850.

(32) Li. H.; Yu, B.; Matsushima, H.; Hoyle, C. E.; Lowe, A. B. *Macromolecules* 2009, *42*, 6537-6542.

(33) Reinelt, S.; Steinke, D.; Ritter, H. *Beilstein J. Org. Chem.* 2014, *10*, 680-691.

(34) Schild, H. G. *Prog. Polym. Sci.* 1992, *17*, 163-249.

(35) Halperin, A.; Kröger, M.; Winnik, F. K. *Angew. Chem. Int. Ed.* 2015, *54*, 15342-15367.

(36) Rozkiewicz, D. I.; Janczewski, D.; Verboom, W.; Ravoo, B. J.; Reinhoudt, D. N. *Angew. Chem. Int. Ed.*, 2006, *45*, 5292-5296.

(37) Maruyama, K.; Osuka, A.; Nakagawa, K. *Bull. Chem. Soc. Jpn.* 1987, *60*, 1021-1026.

(38) Wang, J.; Wolf, R. M.; Caldwell, J. W.; Kollman, P. A.; Case, D. A. *J. Comput. Chem.* 2004, *25*, 1157-1159

(39) Jorgensen, W. L.; Chandrasekhar, J.; Madura, J. D.; Impey, R. W.; Klein, M. L. *J. Chem. Phys.* 1983, *79*, 926-929.

(40) Berendsen, H. J. C.; Postma, J. P. M.; van Gunsteren, W. F.; DiNola, A.; Haak, J. R. *J. Chem.*

Phys. 1984, *81*, 3684-3688.

(41) Berendsen, H. J. C.; Darden, T. A.; York, D. M.; Pedersen, L. *J. Chem. Phys.* 1993, *98*, 10089-10092.

(42) Ryckaert, J. P.; Ciccotti, G.; Berendsen, H. J. C. *J. Comput. Phys.* 1977, *23*, 327-330.

(43) Lurbet, L. R.; Schappacher, M.; Deffieux, A. *Macromolecules* 1994, *27*, 6318-6324.

(44) Qiu, X.-P.; Tnaka, F.; Winnik, F. M. *Macromolecules* 2007, *40*, 7069-7071.

(45) Narumi, A.; Fuchise, K.; Kakuchi, R.; Toda, A.; Satoh, T.; Kawaguchi, S.; Sugiyama, K.; Hirao, A.; Kakuchi, T. *Macromol. Rapid Commun.* 2008, *29*, 1126-1133.

(46) Okada, Y.; Tanaka, F. *Macromolecules* 2005, *38*, 4465-4471.

(47) Iwata, K. *Macromolecules* 1989, *22*, 3702-3706.

Chapter 4

$B(C_6F_5)_3$-catalyzed Group Transfer Polymerization of *N*,*N*-Disubstituted Acrylamide Using Hydrosilane: Effect of Hydrosilane and Monomer Structures, Polymerization Mechanism, and Synthesis of α-End-functionalized Polyacrylamides

4.1. Introduction

Organocatalyzed polymerization has attracted increasing attention in the past decade because its metal-free nature provides a promising avenue for the synthesis of green polymers. Since Hedrick et al. first reported the ring-opening polymerization (ROP) of L-lactide using *N*,*N*-dimethylaminopyridine,[1] significant efforts have been made to develop new basic and acidic organocatalysts available for ROPs of epoxides,[2,3] cyclic esters,[4,5] cyclic amides,[6] cyclic carbonates,[7,8] etc.[9] Due to the advances made by polymer chemists, the organocatalyzed ROP has been well established in terms of monomer scope, elucidation of polymerization mechanisms, [10,11] theoretical simulation aspects,[12] and practical applications for the synthesis of complex macromolecular architectures,[13,14] and has been quite often utilized to prepare biocompatible polyepoxides, polyesters, polyamides, and polycarbonates for bio-related and medical applications.[15]

In addition, the recent significant progress of the organocatalyzed polymerization has been reflected in another polymerization type, that is, the organocatalyzed group transfer polymerization (GTP).[16] Compared to the conventional GTP method using the Lewis base of nucleophilic anions, such as $SiMe_3F_2^-$,[16] HF_2^-,[16] and CN^-[17] and the Lewis acid of transition metal compounds, such as zinc halide,[18] mercury iodide,[19,20] and organoaluminum,[18] the organocatalyzed GTP has made substantial improvement in the living characteristics because the base organocatalyst could suppress side reactions to a maximum degree due to its low nucleophilicity, while the acid organocatalyst significantly enhanced the monomer activation ability due to its strong Lewis acidity.[21] Several groups have made significant contributions to the GTP using organocatalysts; for example, Waymouth et al. and Taton et al. independently reported the GTPs of (meth)acrylates, (meth)acrylamides, and (meth)acrylonitriles using the Lewis bases of *N*-heterocyclic carbenes, [22-25] and Taton et al. also reported the GTP of (meth)acrylates using

phosphines.[26] Chen et al. mainly revealed the GTPs using the Lewis acid of triphenylmethyl salts and the Brønsted acid of List's sulfonimide.[27,28,29] Apart from these reports, our group has achieved the controlled/living GTPs of (meth)acrylate and acrylamide monomers using the base organocatalyst, such as the phosphazene base of *t*-Bu-P_4 and the proazaphosphatrane base of TiBP ($P(i\text{BuNCH}_2\text{CH}_2)_3\text{N}$),[30,31] the Brønsted acid, such as trifluoromethanesulfonimide ($HNTf_2$) and pentafluorophenylbis(triflyl)methane ($Tf_2CHC_6F_5$),[32-35] and the Lewis acid, such as *N*-(trimethylsilyl)triflylimide (Me_3SiNTf_2) and tris(pentafluorophenyl)borane ($B(C_6F_5)_3$). [36-39]

Recently, our group has realized a new polymerization method in the GTP chemistry, that is, the $B(C_6F_5)_3$-catalyzed 1,4-hydrosilylation of (meth)acrylate monomers with a moisture-stable hydrosilane (H*Si*) *in situ* produced moisture-sensitive silyl ketene acetals (SKAs), which were directly subjected to the forthcoming GTPs of the residual (meth)acrylate monomers.[40,41] Apart from $B(C_6F_5)_3$, Chen et al. reported that a silylium cation was also applicable for the GTP of methyl methacrylate (MMA) using dimethylphenylsilane (Me_2PhSiH), leading to a high molecular weight poly(methyl methacrylate) (PMMA) (42.0 kg mol^{-1}).[42] This new method makes the GTP process more convenient due to freedom from the preparation, preservation, and handling of such moisture-susceptible SKAs. The polymerizations of MMA and *n*-butyl acrylate (*n*BA) based on the new GTP method were found to be very different from each other. In greater detail, the $B(C_6F_5)_3$-catalyzed polymerization of MMA using Me_2PhSiH proceeded through the $B(C_6F_5)_3$-catalyzed 1,4-hydrosilylation of MMA that almost occurred prior to polymerization to first produce an SKA and the $B(C_6F_5)_3$-catalyzed polymerization of MMA consequently followed in the presence of the *in situ* produced SKA. On the contrary, the $B(C_6F_5)_3$-catalyzed 1,4-hydrosilylation and polymerization of *n*BA occurred synchronously due to its high monomer reactivity.

The monomer reactivities of the acrylate, methacrylate, and acrylamide are extremely

different from each other, which results in significantly diverse polymerization behaviors of these monomers. Thus, of great interest is the study of the scope of the new GTP method in terms of applicable monomers in the GTP chemistry. Since our group reported the $B(C_6F_5)_3$-catalyzed GTPs of *n*BA and MMA using Me_2PhSiH, it is important to clarify the difference in the polymerization characteristics of the new GTP method among the acrylate, methacrylate, and acrylamide. In this chapter, the author describes the $B(C_6F_5)_3$-catalyzed GTP of *N*,*N*-disubstituted acrylamide (DAAm) using H*Si*. This study describes 1) the screening of the polymerization using various H*Si*s, 2) the effect of the monomer structure on the livingness of the polymerization, 3) a discussion of the polymerization mechanisms, and 4) the synthesis of α-end-functionalized poly(*N*,*N*-diethylacrylamide)s (Fn-PDEAAms) using functional methacrylamides (Fn-MAms), as shown in Scheme 4-1.

Scheme 4-1. (a) The $B(C_6F_5)_3$-catalyzed GTP of *N*,*N*-disubstituted acrylamide (DAAm) using hydrosilane (H*Si*) and (b) the synthesis of α-end-functionalized poly(*N*,*N*-diethylacrylamide) (Fn-PDEAAm) using functional methacrylamides (Fn-MAms).

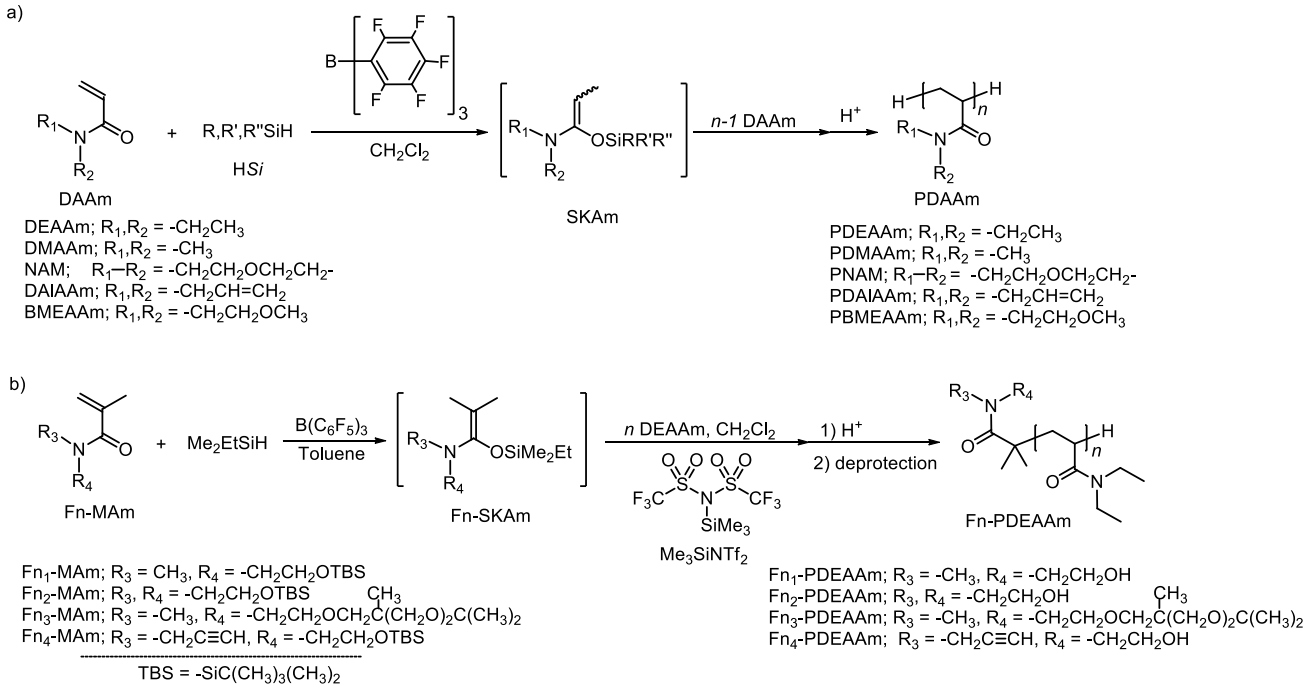

4.2. Experimental section

Materials. Dichloromethane (CH_2Cl_2, >99.5%; water content, <0.001%), toluene (>99.5%; water content, <0.001%), methanol (MeOH), calcium hydride (CaH_2), deuterated chloroform ($CDCl_3$, > 99.8%), and potassium carbonate (K_2CO_3) were purchased from Kanto Chemicals Co., Inc. *N*,*N*-Diethylacrylamide (DEAAm), *N*,*N*-dimethylacrylamide (DMAAm), *N*-acryloylmorpholine (NAM), *N*-(trimethylsilyl)bis(trifluoromethanesulfonyl)imide (**Me_3SiNTf_2**), dimethylphenylsilane (Me_2PhSiH), methyldiphenylsilane ($MePh_2SiH$), triisopropylsilane (iPr_3SiH), triphenylsilane (Ph_3SiH), *tert*-butyldimethylsilane ($tBuMe_2SiH$), tri-*n*-butylsilane (nBu_3SiH), triethylsilane (Et_3SiH), dimethylethylsilane (Me_2EtSiH), dimethylethylchlorosilane ($Me_2EtSiCl$), *tert*-butyldimethylchlorosilane (*tert*-$BuMe_2SiCl$), *N*,*N*-dimethylmethacrylamide (DMeMAm), imidazole, *N*,*N*,*N*,*N*-tetramethylethylenediamine (TMEDA), and *trans*-3-indoleacrylic acid were purchased from Tokyo Kasei Kogyo Co., Ltd. 1-Methylimidazole, sodium trifluoroacetate, silver trifluoroacetate, and 1,8-dihydroxy-9-(10*H*)-anthracenone were purchased from the Sigma-Aldrich Chemicals Co. Tris(pentafluorophenyl)borane ($B(C_6F_5)_3$) was purchased from Wako Pure Chemical Industries, Ltd., and used after recrystallization from *n*-hexane at –30 °C. DEAAm, DMAAm, MorAAm, DMeMAm, CH_2Cl_2, and H*Si*s, except for Ph_3SiH, were distilled from CaH_2, degassed by three freeze-pump-thaw cycles, and stored under an Ar atmosphere prior to use. Ph_3SiH was used after recrystallization from *n*-hexane. *N*,*N*-Diallyacrylamide (DAlAAm),[39] *N*,*N*-bis(2-methoxyethyl)acrylamide (BMEAAm),[39] 2,2,5-trimethyl-1,3-dioxan-5-ylmethanol -tosylate,[43] and *N*-(2-*tert*-butyldimethylsilyloxyethyl)-*N*-(prop-2-ynyl)amine,[44] were synthesized according to a previous report. The Spectra/Por® 6 Membrane (MWCO: 1000) was used for the dialysis. All other chemicals were purchased from available suppliers and used without purification.

Measurements. The ^1H (400 MHz) and ^{13}C NMR (100 MHz) spectra were recorded using a JEOL

ECS400. The preparation of the polymerization solution was carried out in an MBRAUN stainless steel glove box equipped with a gas purification system (molecular sieves and copper catalyst) and a dry argon atmosphere (H_2O, O_2 <1 ppm). The moisture and oxygen contents in the glove box were monitored by an MB-MO-SE 1 and MB-OX-SE 1, respectively. Size exclusion chromatography (SEC) in DMF containing lithium chloride (LiCl; 0.01 mol L^{-1}) was performed at 40 °C using a Jasco high performance liquid chromatography (HPLC) system (PU-980 Intelligent HPLC pump, CO-965 column oven, RI-930 Intelligent RI detector, and Shodex DEGAS KT-16) equipped with a Shodex Asahipak GF-310 HQ column (linear, 7.6 mm × 300 mm; pore size, 20 nm; bead size, 5 μm; exclusion limit, 4×10^4) and a Shodex Asahipak GF-7M HQ column (linear, 7.6 mm × 300 mm; pore size, 20 nm; bead size, 9 μm; exclusion limit, 4×10^7) at the flow rate of 0.6 mL min^{-1}. The $M_{n,SEC}$ and M_w/M_n of the acrylamide polymers were determined by the RI based on poly(methyl methacrylate) (PMMA) with the M_w (M_w/M_n)s of 1.25 × 10^6 g mol^{-1} (1.07), 6.59 × 10^5 g mol^{-1} (1.02), 3.003 × 10^5 g mol^{-1} (1.02), 1.385 × 10^5 g mol^{-1} (1.05), 6.015 × 10^4 g mol^{-1} (1.03), 3.053 × 10^4 g mol^{-1} (1.02), and 1.155 × 10^4 g mol^{-1} (1.04), 4.90 × 10^3 g mol^{-1} (1.10), 2.87 × 10^3 g mol^{-1} (1.06), and 1.43 × 10^3 g mol^{-1} (1.15), respectively. The matrix-assisted laser desorption/ionization time-of-flight mass spectrometry (MALDI-TOF MS) measurements were performed using an Applied Biosystems Voyager-DE STR-H mass spectrometer with a 25 kV acceleration voltage. The positive ions were detected in the reflector mode (25 kV). A nitrogen laser (337 nm, 3 ns pulse width, 106–107 W cm^{-2}) operating at 3 Hz was used to produce the laser desorption, and the 100-300 shots were summed. The spectra were externally calibrated using a sample prepared from narrow-dispersed polystyrene (Chemco Scientific Co., Ltd., M_n, 3.6 kg mol^{-1}; M_w/M_n, 1.08; 30 μL, 10 mg mL^{-1} in THF), the matrix (1,8-dihydroxy-9-(10*H*)-anthracenone, 30 mg mL^{-1}, 100 μL), and the cationizing agent (silver trifluoroacetate, 10 mg mL^{-1}, 15 μL) with a linear calibration. Samples for the MALDI-TOF MS

were prepared by mixing the polymer (1.5 mg mL^{-1}, 10 μL), the matrix (*trans*-3-indoleacrylic acid, 10 mg mL^{-1}, 90 μL), and the cationizing agent (sodium trifluoroacetate, 10 mg mL^{-1}, 10 μL) in THF.

Synthesis of 1-(4-morpholinyl)-1-dimethylethylsiloxy-1-propene (Mor-SKAm^{Me_2Et}). To a solution of diisopropylamine (3.37 mL, 24.0 mmol) in dry-THF (30 mL) in a 100-mL three-necked flask, *n*-butyllithium (13.6 mL, 22.0 mmol; 1.60 mol L^{-1} in *n*-hexane) was dropwise added at 0 °C under an argon atmosphere. After stirring for 30 min, 1-(4-morpholinyl)-1-propanone (2.68 mL, 20 mmol) was slowly added. The reaction mixture was stirred at 0 °C for 1 h. $Me_2EtSiCl$ (4.18 mL, 52.2 mmol) was then added. After stirring for 90 min at 0 °C, the solvent was removed under reduced pressure. The product was then directly distilled under reduced pressure (98-101 °C/4.50 mmHg) to afford Mor-SKAm^{Me_2Et} as a transparent liquid. Yield, 2.11 g (46.0%). ^{1}H NMR (400 MHz, $CDCl_3$): δ (ppm) 0.13 (s, 6H, -Si(CH_3)$_2$), 0.63 (q, *J* = 8.3 Hz, 2H, -Si$CH_2$$CH_3$), 0.94 (t, *J* = 8.4 Hz, 3H, -$SiCH_2CH_3$), 1.49 (d, *J* = 6.8 Hz, 3H, CH_3CH=C-), 2.72 (t, *J* = 5.6 Hz, 4H, N(CH_2CH_2)$_2$O), 3.64 (t, *J* = 5.4 Hz, 4H, N(CH_2CH_2)$_2$O), 3.69 (q, *J* = 6.8 Hz, 1H, CH_3C*H*=C-). ^{13}C NMR (100 MHz): δ (ppm) –2.0, 6.8, 8.5, 10.5, 49.2, 66.9, 82.2, 154.0.

Synthesis of functional methacrylamides (Fn-MAms)

Scheme 4-2. Synthetic route of functional methacrylamides (Fn-MAms).

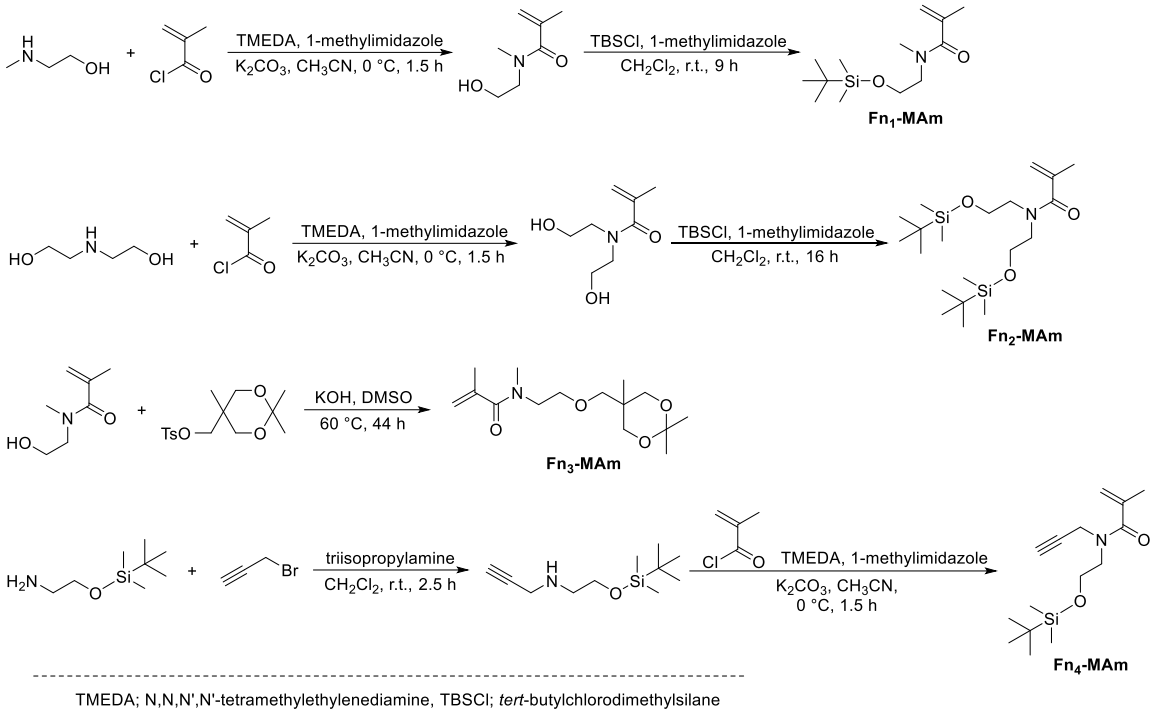

Synthesis of *N*-(2-hydroxyethyl)-*N*-methylmethacrylamide. Method SA: To a suspension of 2-(methylamino)ethanol (20.0 mL, 250 mmol), 1-methylimidazole (1.64 mL, 20.8 mmol), TMEDA (3.10 mL, 20.8 mmol), and K_2CO_3 (34.5 g, 250 mmol) in acetonitrile (200 mL), methacryloyl chloride (20.1 mL, 208 mmol) was added dropwise at 0 °C under a N_2 atmosphere. After stirring for 1 h, the reaction mixture was filtered and then condensed under reduced pressure. The crude product was purified by silica gel column chromatography (ethyl acetate → acetone), affording *N*-(2-hydroxyethyl)-*N*-methylmethacrylamide as transparent liquid. Yield, 22.1 g (74.2 %). ^{1}H NMR (400 MHz, $CDCl_3$): δ (ppm) 1.94 (s, 3H, CH_2=C(C*H*$_3$)-), 2.96, 3.07 (s, 3H, NC*H*$_3$), 3.40-3.60 (m, 3H, -NC*H*$_2$CH$_2$O*H*), 3.66-3.82 (m, 2H, -NCH$_2$C*H*$_2$OH), 5.00-5.24 (m, 2H, C*H*$_2$=C(CH$_3$)-). ^{13}C NMR (100 MHz):δ (ppm) 20.0, 20.6, 32.5, 37.9, 50.0, 52.8, 59.3, 60.2, 115.3, 115.9, 140.3, 140.7, 173.7.

Synthesis of *N*,*N*-bis(2-hydroxyethyl)methacrylamide. Method SA was used to react diethanolamine (21.0 g, 200 mmol), 1-methylimidazole (1.30 mL, 16.5 mmol), TMEDA (2.45

mL, 16.5 mmol), K_2CO_3 (34.5 g, 200 mmol), acetonitrile (150 mL), and methacryloyl chloride (16.0 mL, 165 mmol). *N*,*N*-Bis(2-hydroxyethyl)methacrylamide was obtained as a transparent liquid purified by silica gel column chromatography (ethyl acetate → acetone). Yield, 11.0 g (38.6 %). ^{1}H NMR (400 MHz, $CDCl_3$): δ (ppm) 1.91 (s, 3H, CH_2=C(C*H*$_3$)-), 2.96, 3.07 (s, 3H, NC*H*$_3$), 3.51 (m, 4H, -N(C*H*$_2$$CH_2OH)_2$), 3.62-3.85 (m, 4H, -N($CH_2$C*H*$_2$$OH)_2$), 4.2-4.7 (br, 2H, -N($CH_2CH_2$O*H*$)_2$), 5.05, 5.14 (m, 2H, C*H*$_2$=C(CH_3)-). ^{13}C NMR (100 MHz):δ (ppm) 20.7, 31.0, 49.3, 53.1, 60.6, 116.1, 140.6, 174.8.

Synthesis of *N*-(2-*tert*-butyldimethylsiloxyethyl)-*N*-methylmethacrylamide (Fn$_1$-MAm). Method SB: To a solution of *N*-(2-hydroxyethyl)-*N*-methylmethacrylamide (5.00 g, 34.9 mmol), imidazole (3.56 g, 52.4 mmol), and CH_2Cl_2 (100 mL), a solution of *tert*-butyldimethylchlorosilane (7.89 g, 52.4 mmol) in CH_2Cl_2 (10.0 mL) was added at room temperature under a N_2 atmosphere. After stirring for 9 h, the reaction mixture was filtered and washed with 0.5 N HCl aq. (100mL × 1), saturated $NaHCO_3$ aq. (100 mL × 2), and distilled water (100 mL × 1). The organic layer was concentrated under reduced pressure after drying with anhydrous $MgSO_4$. The residue was purified by distillation under reduced pressure (83 °C/0.03 mmHg) to afford Fn$_1$-MAm as a transparent liquid. Yield, 6.13 g (68.2 %). ^{1}H NMR (400 MHz, $CDCl_3$): δ (ppm) -0.02, (s, 6H, -Si(C*H*$_3$)$_2$C(CH_3)$_3$), 0.82 (s, 9H, -Si(CH_3)$_2$C(C*H*$_3$)$_3$) 1.88 (s, 3H, CH_2=C(C*H*$_3$)-), 2.90, 3.04 (s, 3H, NC*H*$_3$), 3.39-3.46 (m, 2H, -NC*H*$_2$$CH_2$O-), 3.61-3.77 (m, 2H, -NCH_2C*H*$_2$O-), 4.94, 5.30-5.11 (m, 2H, C*H*$_2$=C(CH_3)-). ^{13}C NMR (100 MHz): δ (ppm) -5.4, 18.2, 20.2, 21.0, 26.0, 32.6, 38.6, 49.7, 52.6, 60.9, 61.5, 115.0, 141.0, 172.0, 173.2. Anal. Calcd. for $C_{13}H_{27}NO_2Si$ (257.18): C, 60.65; H, 10.57; N, 5.44. Found: C, 60.31; H, 10.63; N, 5.42.

Synthesis of *N*,*N*-bis(2-*tert*-butyldimethylsiloxyethyl) methacrylamide (Fn$_2$-MAm). Method SB was used to react *N*,*N*-bis(2-hydroxyethyl)methacrylamide (6.00 g, 34.6 mmol), imidazole (5.89 g, 86.6 mmol), and CH_2Cl_2 (100 mL), and *tert*-butyldimethylchlorosilane (13.1 g, 86.6

mmol). Fn_2-MAm was obtained as a transparent liquid purified by distillation under reduced pressure (130-134 °C/0.03 mmHg). Yield, 6.99 g (50.3 %). ^{1}H NMR (400 MHz, $CDCl_3$): δ (ppm) -0.13, (s, 12H, (-Si(C*H*$_3$)$_2$C(CH$_3$)$_3$)$_2$), 0.71 (s, 18H, (-Si(CH$_3$)$_2$C(C*H*$_3$)$_3$)$_2$), 1.78 (s, 3H, CH$_2$=C(C*H*$_3$)-), 3.31-3.46 (m, 4H, -N(C*H*$_2$CH$_2$O-)$_2$), 3.46-3.67 (m, 4H, -N(CH$_2$C*H*$_2$O-)$_2$), 4.83, 4.95 (m, 2H, C*H*$_2$=C(CH$_3$)-). ^{13}C NMR (100 MHz): δ (ppm) -5.5, 20.8, , 25.8, 47.4, 51.8, 61.1, 114.6, 141.0, 172.8. Anal. Calcd. for $C_{20}H_{43}NO_3Si_2$ (401.73): C, 59.79; H, 10.79; N, 3.49. Found: C, 59.32; H, 10.90; N, 3.48.

Synthesis of *N*-(2,2,5-trimethyl-1,3-dioxan-5-ylmethoxyethyl)-*N*-methylmethacrylamide (Fn$_3$-MAm). To a suspension of *N*-(2-hydroxyethyl)-*N*-methylmethacrylamide (5.00 g, 34.9 mmol), KOH (3.91 g, 69.8 mmol), and DMSO (100 mL), 2,2,5-trimethyl-1,3-dioxan-5-ylmethanol-tosylate (13.2 g, 41.9 mmol) was added. After stirring for 45 h at 60 °C, distilled water (300 mL) was added after the reaction mixture was cooled to r.t., then the mixture was extracted with diethyl ether (200 mL × 4). The organic layer was concentrated under reduced pressure following by drying over anhydrous $MgSO_4$. The residue was purified by silica gel column chtomatography (ethyl acetate, R_f = 0.40) and distillation under reduced pressure (95 °C/0.03 mmHg) to afford Fn_3-MAm as a transparent liquid. Yield, 1.10 g (11.0 %). ^{1}H NMR (400 MHz, $CDCl_3$): δ (ppm) 0.78-0.86 (m, 3H, C*H*$_3$C(CH$_2$-)$_3$), 1.35, 1.39 (s, 6H, C(C*H*$_3$)$_2$), 1.92 (s, 3H, CH$_2$=C(C*H*$_3$)-), 2.95, 3.06 (s, 3H, NC*H*$_3$), 3.38-3.69 (m, 10H, NC*H*$_2$C*H*$_2$OC*H*$_2$C(CH$_3$)(C*H*$_2$O-)$_2$), 5.00, 5.10-5.18 (m, 2H, C*H*$_2$=C(CH$_3$)-). ^{13}C NMR (100 MHz, $CDCl_3$): δ (ppm) 18.2, 20.3, 20.8, 21.1, 26.5, 27.3, 32.9, 34.4, 38.3, 47.0, 50.4, 66.5, 69.5, 69.8, 74.0, 74.4, 97.9, 115.3, 141.0, 172.4. Anal. Calcd. for $C_{15}H_{27}NO_4$ (285.38): C, 63.13; H, 9.54; N, 4.91. Found: C, 62.68; H, 9.56; N, 4.88.

Synthesis of *N*-(2-*tert*-butyldimethylsilyloxyethyl)-*N*-(prop-2-ynyl)methacrylamide (Fn$_4$-MAm). Method SB was used to react *N*-(2-*tert*-butyldimethylsilyloxyethyl)-*N*-(prop-2-

ynyl)amine (13.3 g, 62.5 mmol), 1-methylimidazole (0.49 mL, 6.25 mmol), TMEDA (0.93 mL, 6.25 mmol), K_2CO_3 (10.4 g, 75.0 mmol), acetonitrile (100 mL), and methacryloyl chloride (5.46 mL, 62.5 mmol). Fn_4-MAm was obtained as a transparent liquid purified by silica gel column chromatography (CH_2Cl_2, R_f = 0.10) and distillation under reduced pressure (83 °C/0.03 mmHg). Yield, 0.69 g (3.92 %). ^{1}H NMR (400 MHz, $CDCl_3$): δ (ppm) -0.02, (s, 6H, -Si(C*H*$_3$)$_2$C(CH$_3$)$_3$), 0.81 (s, 9H, -Si(CH$_3$)$_2$C(C*H*$_3$)$_3$), 1.90 (s, 3H, CH$_2$=C(C*H*$_3$)-), 2.21 (s, 1H, -C≡C*H*), 3.51-3.59 (m, 2H, -NC*H*$_2$CH$_2$O-), 3.62-3.80 (m, 2H, -NCH$_2$C*H*$_2$O-), 4.22 (s, 2H, -C*H*$_2$C≡CH), 4.98-5.18 (m, 2H, C*H*$_2$=C(CH$_3$)-). ^{13}C NMR (100 MHz): δ (ppm) -5.4, 18.2, 20.6, 26.0, 33.7, 40.5, 46.9, 49.5, 61.0, 61.7, 72.0, 72.4, 79.0, 79.4, 115.9, 140.3, 172.2. Anal. Calcd. for $C_{15}H_{27}NO_2Si$ (281.47): C, 64.01; H, 9.67; N, 4.98. Found: C, 63.89; H, 9.76; N, 4.96.

Polymerization procedure

Polymerization of acrylamide monomers using hydrosilane and B(C$_6$F$_5$)$_3$. The typical polymerization procedure was as follows: Me_2EtSiH (5.28 μL, 40 μmol) was added to a solution of MorAAm (126 μL, 1.00 mmol) and $B(C_6F_5)_3$ (10.2 mg, 20.0 μmol) in CH_2Cl_2 (869 μL) at room temperature (~25 °C). After 13 h, MeOH was added to the solution to quench the polymerization. The crude product was purified by dialysis against MeOH. Yield, 60.4 mg (43%); $M_{n,NMR}$, 3.11 kg mol^{-1}, M_w/M_n, 1.04.

Synthesis of α-end functionalized poly(*N*,*N*-diethylacrylamide)s (Fn-PDEAAms) using hydrosilane and functional mthacrylamides. The typical procedure for the polymerization was as follows: Me_2EtSiH (14.5 μL, 110 μmol) was added to a solution of Fn_1-MAm (100 μL, 100 μmol; 1.00 mol L^{-1} in toluene) and $B(C_6F_5)_3$ (5.10 mg, 10.0 μmol) in toluene (96 μL) at room temperature (25 °C). After stirring for 6 h, a small portion of the reaction mixture was sampled to determine the efficiency of the 1,4-hydrosilylation. A mixture of DEAAm (343 μL, 2.5 mmol) and Me_3SiNTf_2 (20.0 μL, 2.00 μmol; 0.10 mol L^{-1} in CH_2Cl_2) in CH_2Cl_2 (1.93 mL) was then added to

the residual mixture to start the polymerization. After stirring for 15 min, a small amount of MeOH was added to the solution to quench the polymerization. The α-end functionalized PDEAAm with the dimethyl-*tert*-butylsiloxy group was deprotected using tetrabutylammoniumfluoride (TBAF; 500 μL, 500 μmol, 1.00 mol L^{-1} in THF) in MeOH. The crude product was purified by dialysis against MeOH. Yield, 260 mg (82%); $M_{n,NMR}$ = 3.89 kg mol^{-1}, M_w/M_n = 1.06.

4.3. Results and discussion

4.3.1. $B(C_6F_5)_3$-catalyzed group transfer polymerization of DEAAm using hydrosilane. To elucidate the effect of the hydrosilane (H*Si*) structure on the $B(C_6F_5)_3$-catalyzed polymerization of *N*,*N*-diethylacrylamide (DEAAm), a screening experiment using eight H*Si*s, such as Me_2PhSiH, $MePh_2SiH$, Ph_3SiH, *i*Pr_3SiH, *t*$BuMe_2SiH$, *n*Bu_3SiH, Et_3SiH, and Me_2EtSiH, was first carried out in CH_2Cl_2 at room temperature under the same starting conditions of $[DEAAm]_0/[HSi]_0/[B(C_6F_5)_3]_0$ = 25/1/0.5 and $[DEAAm]_0$ = 1.0 mol L^{-1}. The polymerization results are summarized in Table 1 and the SEC profiles of the obtained polymers are shown in Figure 4-1. The polymerization of DEAAm using Me_2PhSiH (run 4-1) was initially implemented because Me_2PhSiH was an efficient component, which was converted into the initiators for the group transfer polymerization (GTP) of methacrylate and the acrylate monomers.[40,41] However, the $B(C_6F_5)_3$-catalyzed polymerization of DEAAm using Me_2PhSiH was insufficiently controlled to produce two polymer products, *i.e.*, one polymer product with a $M_{n,SEC}$ (kg mol^{-1}) (M_w/M_n) of 2.70 (1.15) and the other with 87.3 (3.89), as shown in Figure 4-1a, though the monomer consumption was completed within 2 h. In addition, the polymerization characteristics using $MePh_2SiH$ (run 4-2) were similar to those using Me_2PhSiH, such as the bimodal SEC trace with $M_{n,SEC}$ (kg mol^{-1}) (M_w/M_n) of 29.7 (1.26) and 18.1×10^2 (1.90) (Figure 1b), and no polymerization proceeded using Ph_3SiH (run 4-3). For the aliphatic H*Si*s, no polymerization occurred using

iPr_3SiH (run 4-4) and *t*$BuMe_2$SiH (run 4-5), and the $M_{n,SEC}$s of 22.8 and 18.6 kg mol^{-1} for the obtained polymers using *n*Bu_3SiH (run 4-6) and Et_3SiH (run 4-7), respectively, were extremely higher than the calculated molecular weight ($M_{n,calcd.}$) of 3.18 kg mol^{-1}. Finally, we found a suitable H*Si* of Me_2EtSiH (run 4-8) such that the polymerization smoothly proceeded to quantitatively produce a poly(*N*,*N*-diethylacrylamide) (PDEAAm) with the $M_{n,SEC}$ of 3.14 kg mol^{-1}, which was almost the same as the targeted value of 3.18 kg mol^{-1}, and a moderate polydispersity of 1.22. These screening experiments suggested that the H*Si* with the smallest substituents was more preferred for the polymerization control. Since we previously reported that the silyl ketene aminal of (*Z*)-1-(*N*,*N*-dimethylamino)-1-trimethylsiloxy-1-propene ($SKAm^{Me_3}$) was a suitable initiator for the $HNTf_2$-catalyzed GTP of *N*,*N*-dimethylacrylamide (DMeAAm), it is rational that the true initiator of the 1-(*N*,*N*-diethylamino)-1-dimethylethylsiloxy-1-propene ($SKAm^{Me_2\,Et}$), which has the similar bulky silyl group of $SKAm^{Me_3}$, formed by the *in situ* $B(C_6F_5)_3$-catalyzed 1,4-hydrosilylation of DEAAm with Me_2EtSiH in the polymerization system, resulted in the good polymerization control.

Table 4-1. $B(C_6F_5)_3$-catalyzed GTP of DEAAm using various hydrosilanes (H*Si*s) [a]

run	Hydrosilane (H*Si*)	$[DEAAm]_0/[HSi]_0/[B(C_6F_5)_3]_0$	time (h)	Conv. [b] (%)	$M_{n,calcd.}$ [c] (kg mol^{-1})	$M_{n,SEC}$ [d] (kg mol^{-1})	M_w/M_n [d]
4-1	Me_2PhSiH	25/1/0.5	2	>99	3.18	2.70 87.3 [e]	1.15 3.89 [e]
4-2	$MePh_2SiH$	25/1/0.5	4	>99	3.18	29.7 18.1×10^2 [e]	1.26 1.90 [e]
4-3	Ph_3SiH	25/1/0.5	4	<1	n.d.[g]	n.d. [g]	n.d. [g]
4-4	*i*Pr_3SiH	25/1/0.5	4	<1	n.d. [g]	n.d. [g]	n.d. [g]
4-5	*t*$BuMe_2SiH$	25/1/0.5	8	<1	n.d. [g]	n.d. [g]	n.d. [g]
4-6	*n*Bu_3SiH	25/1/0.5	4	>99	3.18	22.8	1.32
4-7	Et_3SiH	25/1/0.5	4	>99	3.18	18.6	1.28
4-8	Me_2EtSiH	25/1/0.5	1	>99	3.18	3.14	1.22
4-9	Me_2EtSiH	100/1/1	5	>99	12.7	13.0	1.18
4-10[f]	Me_2EtSiH	150/1/1	6	>99	19.1	21.5	1.18
4-11[f]	Me_2EtSiH	200/1/1	20	>99	25.4	54.3	1.16

[a] Ar atmosphere; room temperature; $[DEAAm]_0$ = 1.0 mol L^{-1} in CH_2Cl_2. [b] Determined by ^1H NMR in $CDCl_3$. [c] $M_{n,calcd.} = [M]_0/[HSi]_0 \times$ (Conv.) $\times$ (M.W. of monomer: DEAAm = 127.19) + (M.W. of H) $\times$ 2. [d] Determined by SEC in DMF containing 0.01 mol L^{-1} of LiCl using PMMA standard. [e] SEC traces showed bimodal distribution. [f] $[DEAAm]_0$ = 2.0 mol L^{-1} in CH_2Cl_2. [g] Not determined.

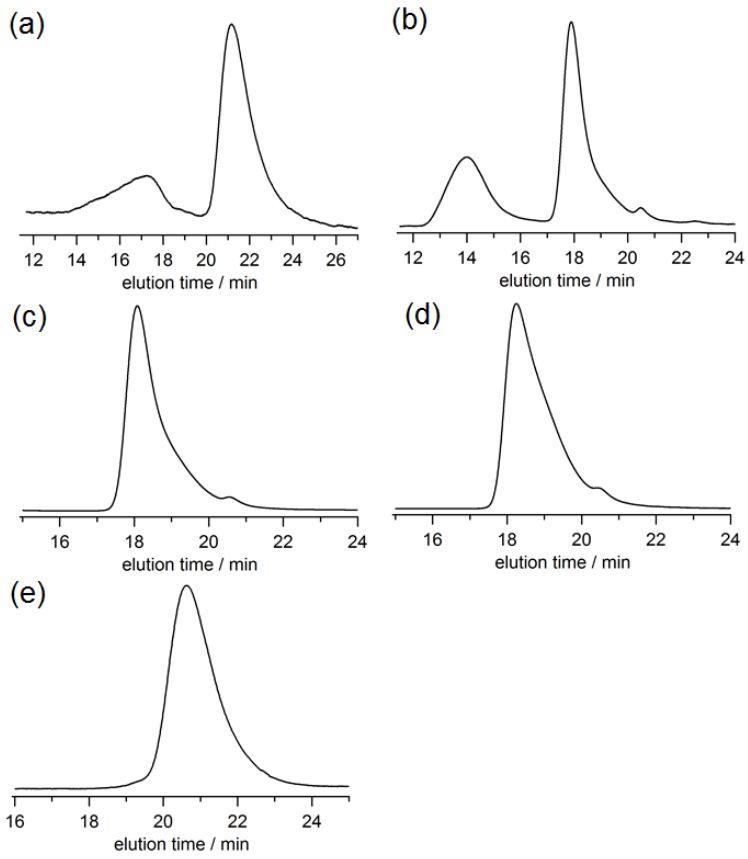

Figure 4-1. SEC traces of PDEAAms obtained from the GTP using (a) Me_2PhSiH (run 4-1), (b) $MePh_2SiH$ (run 4-2), (c) $(n\text{Bu})_3SiH$ (run 4-6), (d) Et_3SiH (run 4-7), and (e) Me_2EtSiH (run 4-8) (eluent, DMF containing of 0.01 mol L^{-1} LiCl; flow rate, 0.6 mL L^{-1}).

The kinetic investigation for the $B(C_6F_5)_3$-catalyzed GTP of DEAAm was carried out using Me_2EtSiH, Et_3SiH, $n\text{Bu}_3SiH$, and Me_2PhSiH. The zero-order kinetic plots in Figure 4-2a suggested that all the polymerizations displayed a distinct induction period (t_i), and the t_i and propagation rate ($k_{p,obs.}$) values are summarized in Table 4-2. The t_is of 7.04 and 8.24 min for Me_2EtSiH and Me_2PhSiH, respectively, were much lower than those of 76.9 and 87.2 min for $n\text{Bu}_3SiH$ and Et_3SiH, respectively, while the $k_{p,obs.}$s of 4.02×10^{-2} and 10.62×10^{-2} min^{-1} for Me_2PhSiH and Me_2EtSiH, respectively, were much higher than those of 1.45×10^{-2} and 1.87×10^{-2} min^{-1} for $n\text{Bu}_3SiH$ and Et_3SiH, respectively. The occurrence of the t_i should be attributed to the 1,4-hydrosilylation process because the Lewis acid-catalyzed GTP of DAAm using $SKAm^{Me_3}$

as the starting polymerization component smoothly proceeded without any induction period.[33,35] Piers et al. reported the detailed study of the 1,4-hydrosilylation of nucleophiles, such as ketones, imines, and esters, with the H*Si*, in which the coordination between $B(C_6F_5)_3$ and a nucleophile was rather more thermodynamically stable than that of H*Si*, leading to the conclusion that only a very small proportion of the uncoordinated $B(C_6F_5)_3$, a free $B(C_6F_5)_3$, is available to interact with the H*Si*. In addition, they pointed out that the availability of the free $B(C_6F_5)_3$ controlled to a large degree the overall rate of the 1,4-hydrosilylation because the hydride abstraction of the H*Si* was very likely to be the rate-determining step.[45,46] Furthermore, the direct observation of the formation of a B--H--Si complex using 1,2,3-tris(pentafluorophenyl)-4,5,6,7-tetrafluoro-1-boraindene, which is more Lewis acidic than $B(C_6F_5)_3$, suggested that the formation of the B--H--Si complex was thermodynamically unfavorable at room temperature because the containment of the complex species in solution is less than 5% relative to that of the borane species even in the absence of any nucleophilic substrate.[47] This investigation was supportive to suggest that the equilibrium constant for the formation of complex of $B(C_6F_5)_3$ and H*Si* ($K_{eq.HSi}$, Scheme 4-2) should be significantly small. By comprehensively considering these facts, the concentration of the free $B(C_6F_5)_3$ in the polymerization system containing the strong nucleophile of DEAAm should be extremely low due to the high equilibrium constant for the formation of complex of $B(C_6F_5)_3$ and DEAAm ($K_{eq.DEAAm}$) and low $K_{eq.HSi}$, which led to that only an extremely small amount of the complex of $B(C_6F_5)_3$ and H*Si* existed in the polymerization system. After the induction period, the monomer was consumed and the propagation reaction proceeded as a zero-order reaction, rather than a first-order one, without any retardation or termination until all the monomer was consumed. This propagation behavior was quite similar to that for the $B(C_6F_5)_3$-catalyzed GTP of DEAAm using a silyl ketene acetal of 1-methoxy-1-(triethylsiloxy)-2-methyl-1-propene because the propagation reactions in these two polymerization systems both happened

at the SKAm ends with DEAAm.[48] Considering the $k_{p.obs.}$ and t_i values, it is undoubtedly clear that both rates of the 1,4-hydrosilylation and propagation were enhanced by the decreasing bulkiness of the employed H*Si*.

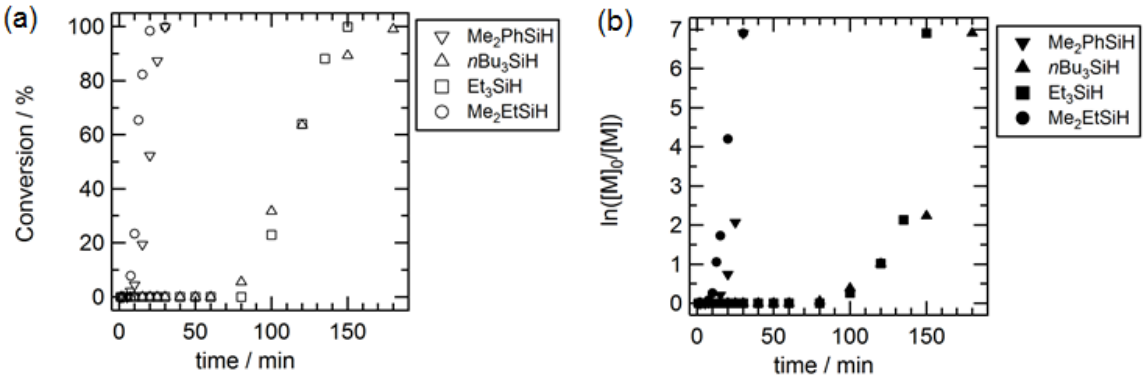

Figure 4-2. (a) Zero-order and (b) first-order kinetic plots for the $B(C_6F_5)_3$-catalyzed GTP of DEAAm using Me_2PhSiH, nBu_3SiH, Et_3SiH, and Me_2EtSiH ($[DEAAm]_0/[HSi]_0/[B(C_6F_5)_3]_0$ = 25/1/0.5).

Table 4-2. Effect of hydrosilane structures on observed propagation rates ($k_{p,obs.}$) and induction periods (t_i) for the $B(C_6F_5)_3$-catalyzed GTP of DEAAm [a]

Hydrosilane (H*Si*)	$k_{p,obs.} \times 10^2$ (min^{-1})	t_i (min)
nBu_3SiH	1.45	76.9
Et_3SiH	1.87	87.2
Me_2PhSiH	4.02	8.24
Me_2EtSiH	10.62	7.04

[a] Ar atmosphere; room temp.; solvent, CH_2Cl_2; $[DEAAm]_0$, 1.0 mol L^{-1}; $[DEAAm]_0/[HSi]_0/[B(C_6F_5)_3]_0$ = 25/1/0.5.

Scheme 4-2. Schematic representation for (a) coordination between DEAAm and $B(C_6F_5)_3$ and (b) abstraction of hydride from H*Si*

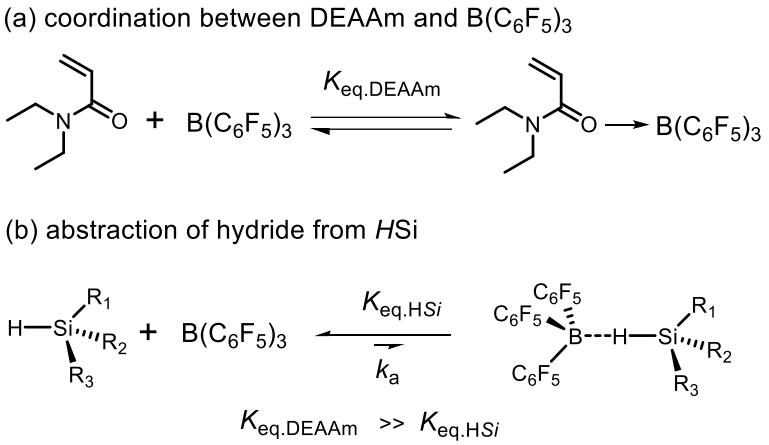

The MALDI-TOF MS spectrum of the PDEAAm obtained from the polymerization using Me_2EtSiH (run 8) provided the direct evidence for affording the well-defined PDEAAm, as shown in Figure 3. The MALDI-TOF MS spectrum exhibited a broad distribution of polymer ion peaks ranging from 1.0 to 10 kDa, though every ion peak had a satisfactory assignment as designated by [H-DEAAm$_n$-H + Na^+] (molecular formula: $C_{7n}H_{13n+2}N_nO_nNa$), *e.g.*, the observed *m*/*z* value of 3202.15 Da for a specific peak corresponding to the sodium-cationized 25-mer polymer structure of [H-DEAAm$_{25}$-H + Na^+] was extremely close to the theoretical monoisotopic value of 3202.50 (molecular formula: $C_{175}H_{327}O_{25}N_{25}Na$), indicating no side reactions during the entire polymerization process.

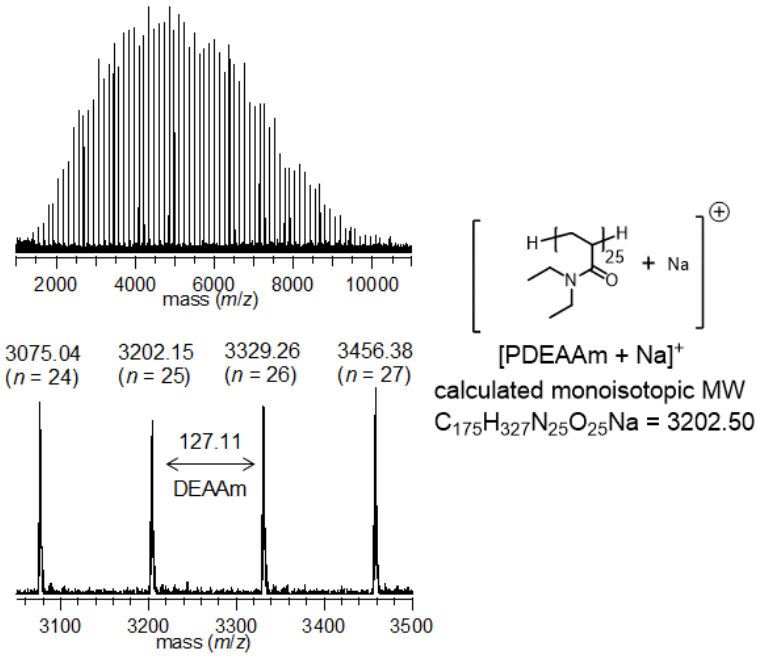

Figure 4-3. MALDI-TOF MS spectrum of PDEAAm (run 8) obtained by the $B(C_6F_5)_3$-catalyzed GTP of DEAAm using Me_2EtSiH.

4.3.2. $B(C_6F_5)_3$-catalyzed GTP of DAAm using Me_2EtSiH. In order to elucidate the effect of the monomer structure on polymerization characteristics, we investigated the polymerization of the DAAms, such as *N*,*N*-dimethylacrylamide (DMAAm), *N*,*N*-diallyacrylamide (DAlAAm), *N*,*N*-bis(2-methoxyethyl)acrylamide (BMEAAm), and *N*-acryloylmorpholine (NAM). The polymerization using Me_2EtSiH was carried out under the condition of $[DAAm]_0/[Me_2EtSiH]_0$ = 25 (Table 4-3). The polymerization of DMAAm, which showed a k_p similar to that of DEAAm, resulted in a behavior similar to that of DEAAm (Figures 4-4b and 4-5a). Furthermore, the polymerizations of DAlAAm, BMEAAm, and NAM, whose $B(C_6F_5)_3$-catalyzed GTPs have been known to proceed at a relatively low k_p, were carried out to confirm the polymerization control related to the balance between k_p and k_a. As anticipated, the polymerizations of each monomer quantitatively produced the corresponding poly(*N*,*N*-diallyacrylamide) (PDAlAAm), a poly(*N*,*N*-bis(2-methoxyethyl)acrylamide) (PBMEAAm), and a poly(*N*-acryloylmorpholine) (PNAM) with

well-controlled molecular weights and narrow molecular weight distributions, *i.e.*, $M_{n,NMR}$ (M_w/M_n) of 4.23 kg mol^{-1} (1.08) for PDAlAAm (run 4-14), 5.24 kg mol^{-1} (1.12) for PBMEAAm (run 4-16), and 3.11 kg mol^{-1} (1.04) for PNAM (run 4-18). Their chemical structures were confirmed by ^{1}H NMR (Figure 4-6) and MALDI-TOF MS (Figures 4-5) measurements. For example, in the ^{1}H NMR spectrum of PNAM (run 18, Figure 4-6c), the proton signals at 1.1-2.0 ppm (peak e) and 2.3-3.0 ppm (peaks b and f) due to the main-chain methylene and methine, 3.2-3.9 ppm (peaks c, d, g, and h) due to side-chain methylene, together with that at 0.9 ppm due to the α-end methyl group were clearly observed. The MALDI-TOF MS spectrum of PNAM (run 4-18, Figure 4-5d) showed a narrow gaussian distribution with the *m*/*z* value of every ion peak (*e.g.*, an observed 3552.30 Da for the sodium-cationized 25-mer polymer) assignable to the targeted sodium-cationized polymer structure of [H-NAM$_n$-H + Na$^+$] (the theoretical 25-mer monoisotopic value of 3551.98), strongly suggesting that no side reactions occurred during the entire polymerization, *i.e.*, the controlled/living polymerization. Once again, these results conclusively indicated that the balance of the complexation of $B(C_6F_5)_3$ toward DAAm and H*Si* was the key factor for achieving the livingness of the polymerization of acrylamide monomers, which will be discussed in detail in the following section.

In order to synthesize PDAAms with different targeted molecular weights by changing the initial DAAm-to-Me_2EtSiH ratios, the polymerizations of each monomer were carried out. For the polymerization of DEAAm, the moderately controlled PDEAAms were obtained with the molecular weights of 13.0-54.2 kg mol^{-1} by varying the $[DEAAm]_0/[Me_2EtSiH]_0$ ratios of 100, 150, and 200, as runs 4-9~4-11 shown in Table 4-1. As well as the DEAAm, the polymerizations of DMAAm, DAlAAm, and BMEAAm with the $[DAAm]_0/[Me_2EtSiH]_0$ of 100 quantitatively proceeded in a specific polymerization time to afford PDMAAm (run 4-13), PDAlAAm (run 4-15), and PBMEAAm (run 4-17) with predicted molecular weights and narrow polydispersities

below 1.14, as shown in Table 4-3. On the other hand, the monomer conversion for the polymerization of NAM (run 4-19) unexpectedly reached 85.4% even when varying polymerization conditions, such as a large amount of catalyst, higher monomer concentration, and a longer reaction time of more than 2 days. In addition, the SEC profile of the obtained polymer product showed a small peak due to the high molecular-weight contaminant (Figure 4-4e).

To alleviate this issue, we used *N*-(trimethylsilyl)bis(trifluoromethanesulfonyl)imide **(**Me_3SiNTf_2) as the additional organocatalyst for the GTP of NAM after the $B(C_6F_5)_3$-catalyzed 1,4-hydrosilylation of NAM with Me_2EtSiH was completed to afford Mor-SKAm^{Me_2Et}**,** because Me_3SiNTf_2 promoted a faster polymerization compared with $B(C_6F_5)_3$. Before using the double catalytic system of $B(C_6F_5)_3$ and Me_3SiNTf_2, the polymerization using Me_3SiNTf_2 alone was carried out as a control experiment. However, no polymerization proceeded at all because the activation of a hydrosilane and the 1,4-hydrosilylation of a monomer were prevented by the higher coordination strength of a silynium cation to the monomer. For the polymerizations with the $[NAM]_0/[Me_2EtSiH]_0$ ratios of 100 and 200, Me_3SiNTf_2 was added at the molar ratio of $[Me_2EtSiH]_0/[Me_3SiNTf_2]_0$ = 1/0.02 or 0.04 together with $B(C_6F_5)_3$. Both polymerizations were accelerated and finished after 20 and 40 h (runs 4-20 and 4-21, respectively). The SEC profiles in Figure 4f of the obtained polymers showed a monomodal distribution without any high molecular weight residue and the M_w/M_ns were 1.08 (run 4-20) and 1.13 (run 4-21). In addition, the $M_{n,NMR}$s of 11.9 and 27.5 kg mol^{-1} well agreed with the $M_{n,calcd.}$s of 14.3 and 28.6 kg mol^{-1}, respectively**.** These results lead to the conclusion that the dual catalytic system of $B(C_6F_5)_3$ and Me_3SiNTf_2 was efficient for the GTP of NAM using Me_2EtSiH to afford well-defined PNAMs.

Table 4-3. $B(C_6F_5)_3$-catalyzed GTPs of DMAAm, DAlAAm, BMEAAm, and NAM using Me_2EtSiH, and $B(C_6F_5)_3/Me_3SiNTf_2$-catalyzed GTP of MorAAm using Me_2EtSiH [a]

run	DAAm	$[DAAm]_0/[Me_2EtSiH]_0/[B(C_6F_5)_3]_0$	time (h)	Conv. [b] (%)	$M_{n,calcd.}$ [c] (kg mol^{-1})	$M_{n,NMR}$ [b] (kg mol^{-1})	M_w/M_n [d]
4-12	DMAAm	25/1/0.5	0.5	>99	2.48	3.57	1.09
4-13	DMAAm	100/1/0.5	21	>99	9.91	14.6	1.14
4-14	DAlAAm	25/1/0.5	3	>99	3.78	4.23	1.08
4-15	DAlAAm	100/1/0.5	18	>99	15.1	18.0	1.13
4-16	BMEAAm	25/1/0.5	3	>99	4.68	5.24	1.12
4-17	BMEAAm	100/1/1	26	96.8	18.7	n.d.[h]	1.11
4-18	NAM	25/1/0.5	13	>99	3.58	3.11	1.04
4-19	NAM	100/1/1	50	85.4	12.2	6.35	1.08[e]
4-20 [f]	NAM	100/1/0.5	20	>99	14.3	11.9	1.08
4-21 [f]	NAM [g]	200/1/0.8	40	>99	28.6	27.5	1.13

[a] Ar atmosphere; solvent, CH_2Cl_2; room temp.; $[DAAm]_0$, 1.0 mol L^{-1}. [b] Determined by ^{1}H NMR in $CDCl_3$. [c] $M_{n,calcd.} = [DAAm]_0/[Me_2EtSiH]_0 \times (Conv.) \times (M.W.\ of\ DAAm) + (M.W.\ of\ H) \times 2$. [d] Determined by SEC in DMF containing 0.01 mol L^{-1} of LiCl using PMMA standard. [e] SEC trace showed bimodal distribution. [f] $[NAM]_0/[Me_3SiNTf_2]_0$, 100/0.02. [g] $[NAM]_0$, 1.5 mol L^{-1}. [h] Not determined.

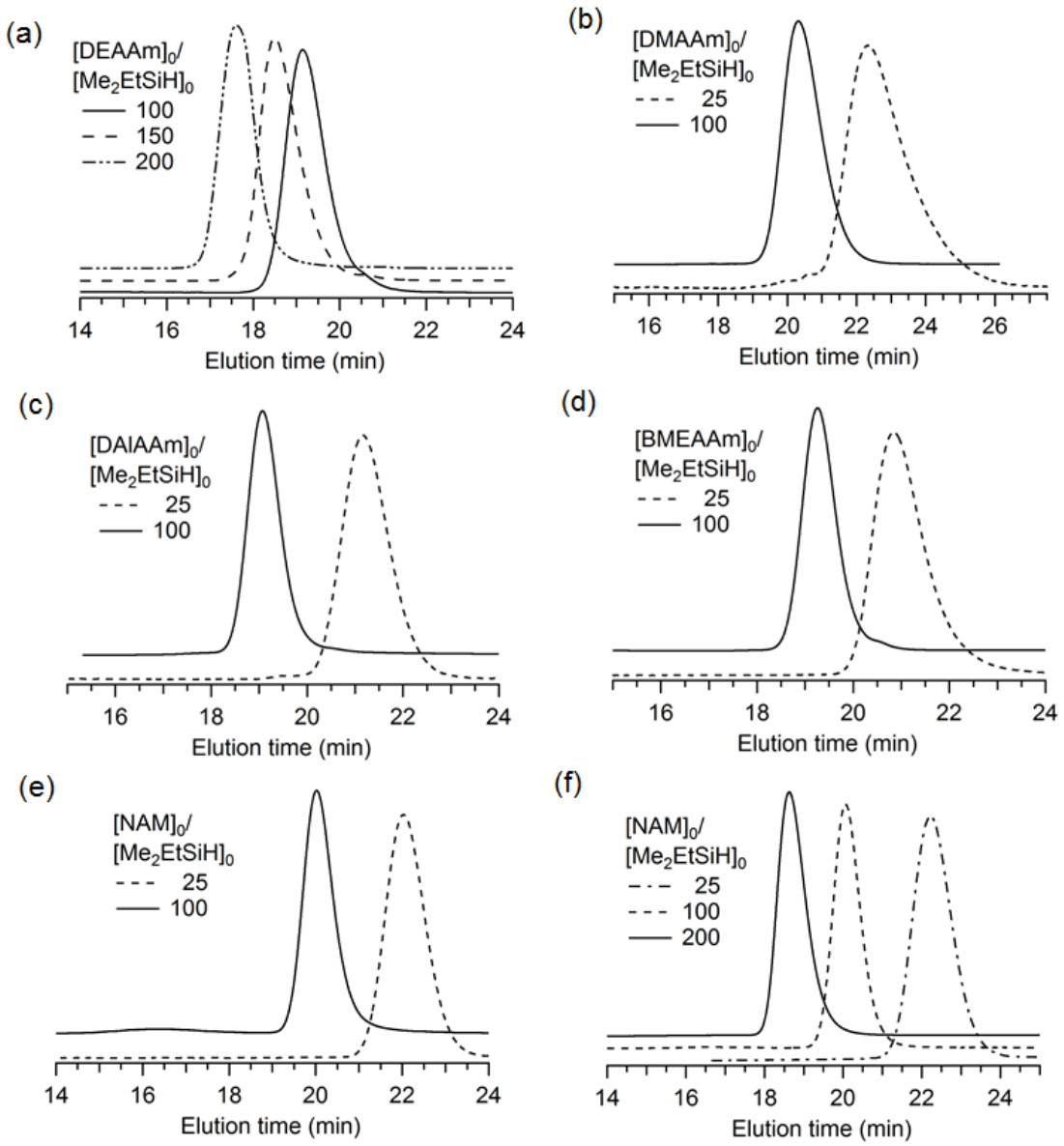

Figure 4-4. SEC traces of (a) PDEAAms obtained by the $B(C_6F_5)_3$-catalyzed GTP of DEAAm using Me_2EtSiH with $[DEAAm]_0/[Me_2EtSiH]_0$ ratios of 100 (run 4-9), 150 (run 4-10), and 200 (run 4-11), (b) PDMAAms (runs 4-12 and 4-13), (c) PDAlAAms (runs 4-14 and 4-15), (d) PBMEAAms (runs 4-16 and 4-17), and (e) PNAMs (runs 4-18 and 4-19) obtained by the $B(C_6F_5)_3$-catalyzed GTP of DAAms using Me_2EtSiH with $[DAAm]_0/[Me_2EtSiH]_0$ ratios of 25 (dashed line) and 100 (solid line), and (f) PNAMs obtained by the $B(C_6F_5)_3/Me_3SiNTf_2$-catalyzed GTP of NAM using Me_2EtSiH with $[NAM]_0/[Me_2EtSiH]_0$ ratios of 100 (run 4-20, dashed line), and 200 (run 4-21, solid line).

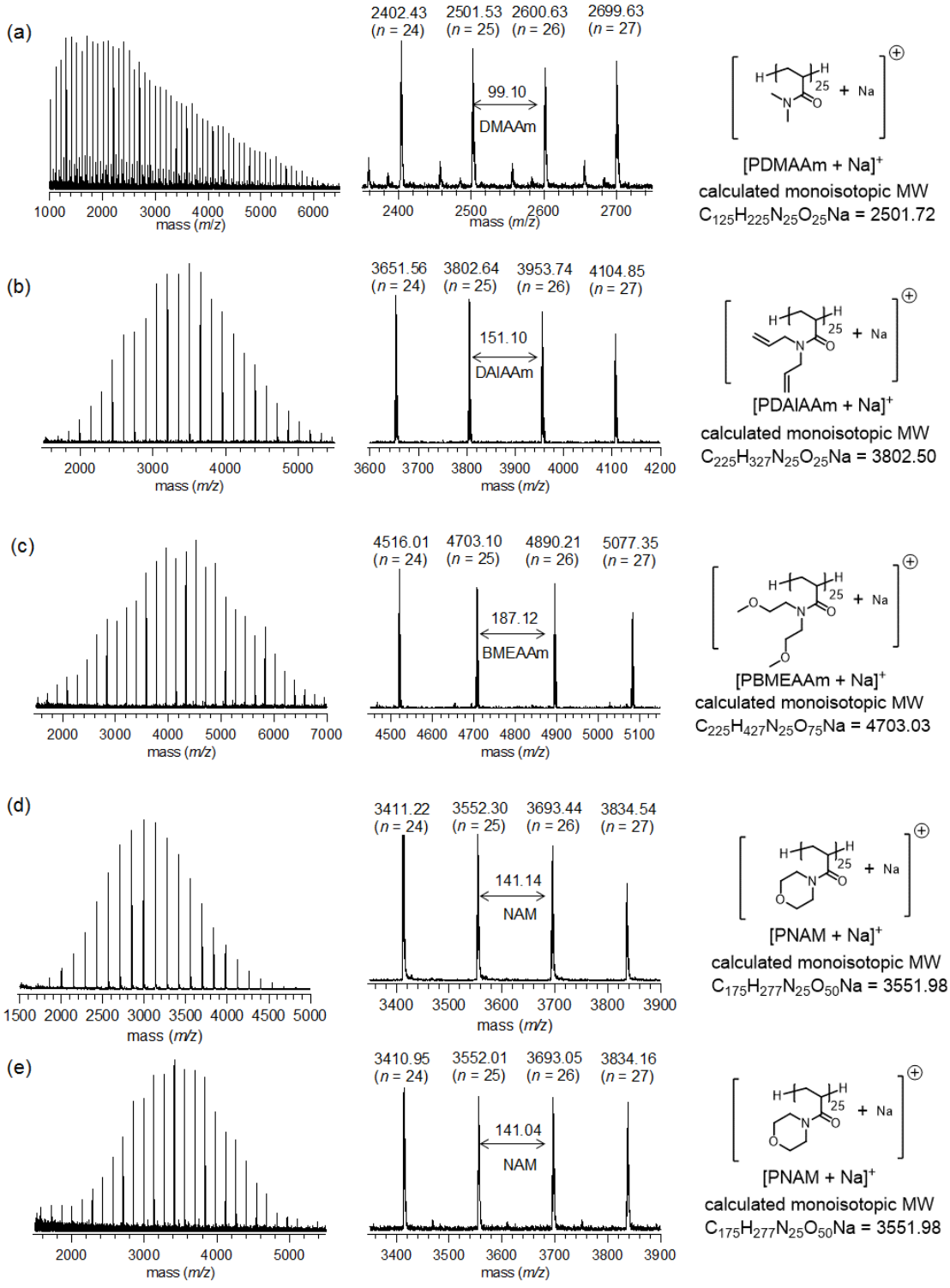

Figure 4-5. MALDI-TOF MS spectra of the obtained polymer by $B(C_6F_5)_3$-catalyzed GTP of DAAm using Me_2EtSiH, (a) PDMAAm (run 4-12), (b) PDAlAAm (run 4-14), (c) PBMEAAm (run 4-16), (d) PNAM (run 4-18) and (e) the obtained polymer by $B(C_6F_5)_3/Me_3SiNTf_2$-catalyzed GTP of NAM using Me_2EtSiH.

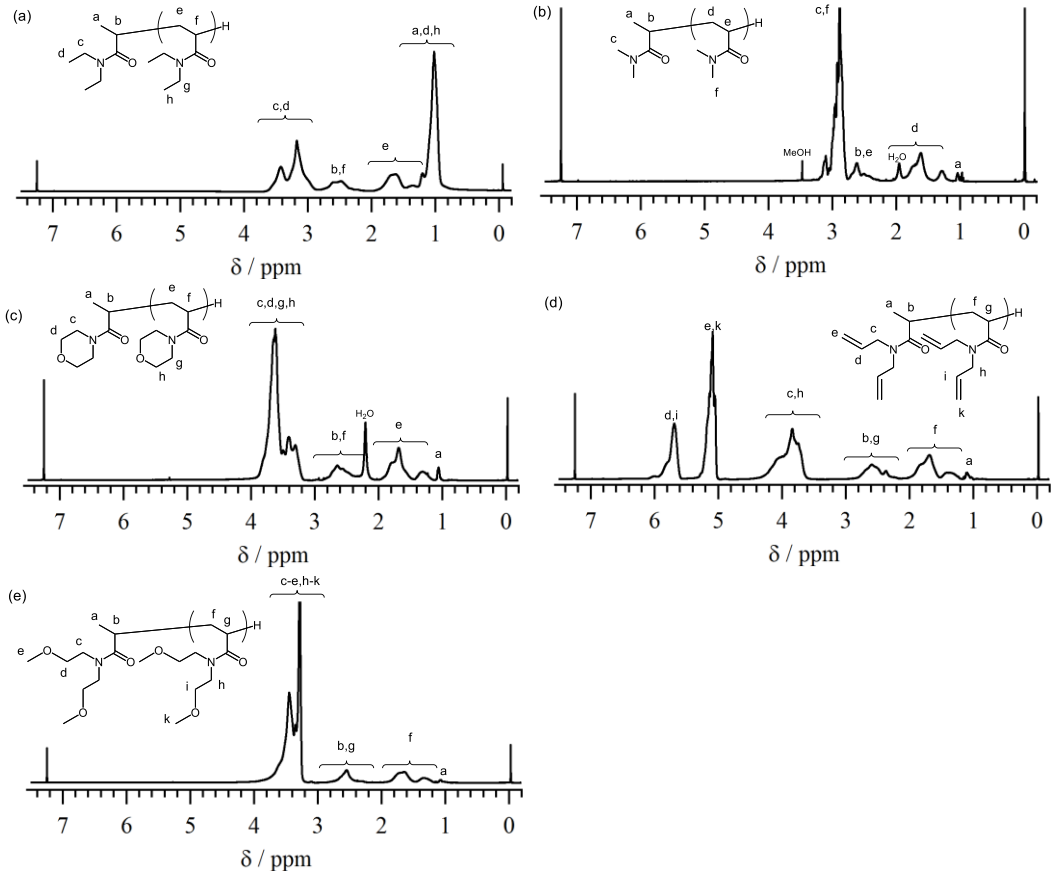

Figure 4-6. ^{1}H NMR spectra of the obtained polymer by $B(C_6F_5)_3$-catalyzed GTP of DAAm using Me_2EtSiH, (a) PDEAAm (run 8), (b) PDMAAm, (run 12) (c) PNAM (run 18), (d) PDAlAAm (run 14), and (e) PBMEAAm (run 16) in $CDCl_3$ (400 MHz).

4.3.3. Polymerization mechanism for the $B(C_6F_5)_3$-catalyzed GTP of DAAm using hydrosilane. We now propose a polymerization mechanism to provide a perspicuous and systematic understanding of the involved elementary reactions. The entire polymerization process involves five elementary reactions, including *i*) activation of monomer, *ii*) abstraction of hydride from H*Si*, *iii*) 1,4-hydrosilylation, *iv*) initiation reaction, and *v*) propagation reaction (Scheme 4-3). We have focused on the elementary reactions of the *i*, *ii*, and *v* steps because these steps significantly affect the polymerization behavior depending on the monomer structure.

For the *i* step, it has been confirmed by comparing the ^{1}H NMR spectra of DAAm and a

mixture of DAAm with $B(C_6F_5)_3$ ($[DAAm]_0$ = $[B(C_6F_5)_3]_0$ = 0.167 mol L^{-1}) in $CDCl_3$, as described in a previous report for DEAAm and the section for MorAAm below.[37] For step *ii*, it has been reported in many other organic reactions and straightforwardly proven by Piers et al. in a recent article,[47] though we did not obtained any direct evidence in this study. For step *v*, it has been confirmed by kinetic studies that the propagation reaction proceeded as a zero-order reaction with a living nature. Among all the polymerization steps, the rate-determining step depended on the monomer structure. For the polymerization of DEAAm, step *ii* turned out to be the rate-determining step. The abstraction of the hydride from H*Si* becomes difficult due to the very strong coordination interaction between $B(C_6F_5)_3$ and DEAAm that does not release enough free $B(C_6F_5)_3$ for step *ii*, for which the hydride abstraction of the H*Si* step (k_a) must be taken into consideration because the propagation rate (k_p) should be greater than k_a at this time. Additionally, for the same reason, the polymerization of DEAAm seemed to be worse controlled in comparison with those of other DAAm monomers though PDEAAm without structural defect could be obtained.

On the other hand, the situation is significantly different when the used acrylamide monomer weakly coordinates with $B(C_6F_5)_3$, *e.g.*, NAM. In this case, all the elementary reactions are still the same as those of the polymerization of DEAAm. The only difference is that the rate-determining step changes to step *v* if NAM is the monomer. The 1,4-hydrosilylation of NAM with Me_2EtSiH proceeded very fast, as confirmed by comparing the kinetic plots for the polymerization of NAM using Me_2EtSiH in Figure 4-7 due to the weak coordination interaction between $B(C_6F_5)_3$ and NAM ($K_{eq.}$ = ca. 5) accelerating the 1,4-hydrosilylation (Figure 4-7), leading to almost no induction period, which occurred during the polymerization of NAM. In this case, both k_a and k_h should be much greater than k_p and their effects on the polymerization can be ignored. This suggestion was also supported by the control experiment involving the polymerization of NAM

using the normally synthesized SKAm initiator of 1-(4-morpholinyl)-1-dimethylethylsiloxy-1-propene (Mor-SKAm^{Me_2Et}), which had the same chemical structure with the propagating end as well as the true initiator produced by the $B(C_6F_5)_3$-catalyzed 1,4-hydrosilylation of MorAAm with Me_2EtSiH. The kinetic plots of MorAAm using Mor-SKAm^{Me_2Et} (Δ) also showed zero-order propagation characteristics, almost the same as that using Me_2EtSiH (□) during the initial several hours (Figure 4-8). This result strongly indicated once again that the 1,4-hydrosilylation process was negligible compared to the initiation as well as the propagation when NAM was used as the monomer. The polymerization plot of NAM using Mor-SKAm^{Me_2Et} showed deviation from the profile of using Me_2EtSiH in the late 300 mins, much likely due to the operative declination.

The mechanism of the polymerization of NAM using $B(C_6F_5)_3$ and Me_3SiNTf_2 as a double catalyst system is also discussed. During the polymerization system, it is rather clear now that $B(C_6F_5)_3$ is the only catalyst for the *ii* and *iii* steps, while Me_3SiNTf_2 serves as the main catalyst during the initiation and propagation processes. In the presence of both $B(C_6F_5)_3$ and Me_3SiNTf_2, NAM coordinates to both of them because the amount of NAM, prior to the late stage of the polymerization, is significantly greater than either of the two catalysts. The 1,4-hydrosilylation is very much likely to occur between the adduct of $B(C_6F_5)_3$ with Me_2EtSiH and the free NAM, rather than the coordinated NAM, since Me_2EtSi^+ from Me_2EtSiH needs to bond to the carbonyl oxygen of NAM. During the *iv* and *v* steps, the initiation (or propagation) reaction should then take place between the true initiator (or the propagating end) and the $B(C_6F_5)_3$-activated MorAAm and the Me_3SiNTf_2-activated one. However, initiation (or propagation) occurring between the true initiator (or the propagating end) and the Me_3SiNTf_2-activated MorAAm definitely dominates and that with the $B(C_6F_5)_3$-activated NAM is negligible based on the kinetic plot shown in Figure 7. This is precisely why the polymerization of NAM is greatly accelerated after the addition of a small amount of Me_3SiNTf_2. In spite of the accelerated propagation, the relationship of k_a, $k_h > k_p$

is still suitable in this case. As a result, the polymerization retains its livingness, while significantly accelerated.

Scheme 4-3. A predicted mechanism for the $B(C_6F_5)_3$-catalyzed GTP of DAAm using Me_2EtSiH.

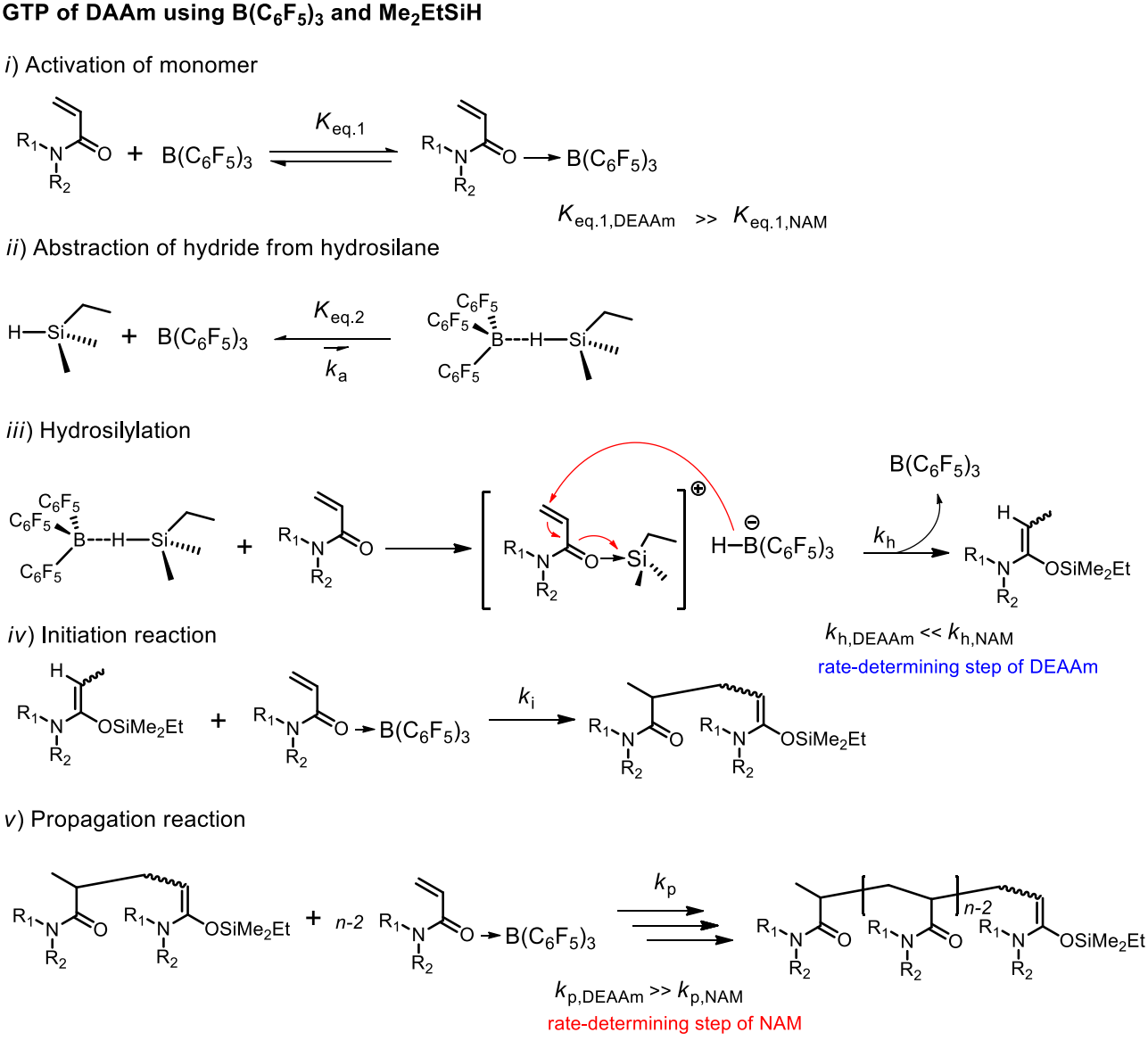

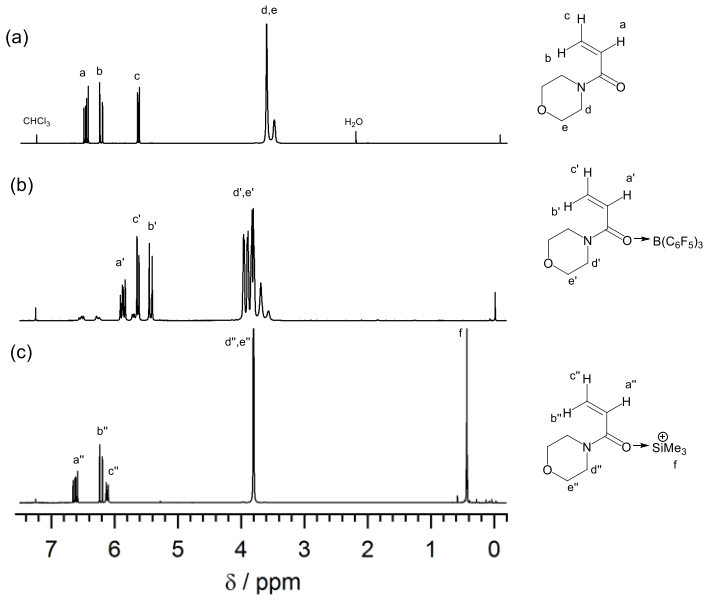

Figure 4-7. ^{1}H NMR spectra of (a) NAM, (b) an equimolar mixture of NAM and $B(C_6F_5)_3$ ($[NAM]_0 = [B(C_6F_5)_3]_0 = 0.167$ mol L^{-1}), and (c) an equimolar mixture of NAM and Me_3SiNTf_2 ($[NAM]_0 = [Me_3SiNTf_2]_0 = 0.167$ mol L^{-1}) in $CDCl_3$ (400 MHz).

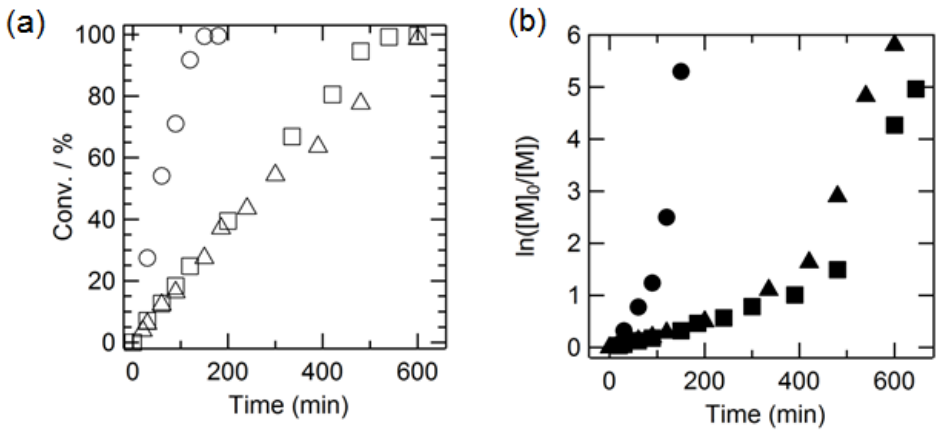

Figure 4-8. (a) Zero- and (b) first-order kinetic plots of the $B(C_6F_5)_3$-catalyzed GTP of NAM using Me_2EtSiH (□,■), the $B(C_6F_5)_3$-catalyzed GTP of NAM using Mor-SKAm^{Me_2Et} (△,▲, $[NAM]_0/[Mor\text{-}SKAm^{Me_2Et}]_0/[B(C_6F_5)_3]_0 = 25/1/0.5$), and the $B(C_6F_5)_3/Me_3SiNTf_2$-catalyzed GTP of NAM using Me_2EtSiH (○, ●, $[NAM]_0/[Me_2EtSiH]_0/[B(C_6F_5)_3]_0/[Me_3SiNTf_2]_0 = 25/1/0.5/0.01$).

4.3.4. Synthesis of α-end-functionalized PDEAAm using functional methacrylamide. Finally, the author attempted to apply the new GTP method to the end-functionalization of PDAAms. The *in situ* preparation of the functional SKA and SKAm initiators prior to the polymerization through the 1,4-hydrosilylation of a functional (meth)acrylic monomer with H*Si* is difficult to achieve because a high monomer reactivity does not allow the quantitative true-initiator formation prior to the polymerization to occur, resulting in the structural defect at the α-chain end. For the α-end-functionalization of PDAAm, we focused on the *N*,*N*-disubstituted methacrylamide (DMAm) because DMAm is well-known to possess an extremely low polymerization reactivity except for a few specific DMAms.[49] Thus, we newly designed a synthetic method for the α-end-functionalized PDAAm using functional DMAms (Fn-MAms), *i.e.*, the $B(C_6F_5)_3$-catalyzed GTP of DAAm with Me_2EtSiH using F-MAms as the key initiator component and Me_3SiNTf_2 as the additional organocatalyst, as shown in Scheme 1b. In order to optimize the polymerization condition, we used *N*,*N*-dimethylmethacrylamide (DMeMAm) instead of the Fn-MAms. The solvent for the 1,4-hydrosilylation and the following polymerization involved toluene and CH_2Cl_2, respectively, because the hydrosilylation of DMeMAm in CH_2Cl_2 occurred some undesirable reactions, such as a second hydrosilylation and silyl rearrangement due to the relatively high polarity. The polymerization results are summarized in Table 4-4 (runs 4-22~4-24). Initially, the hydrosilylation of DMeMAm using Me_2EtSiH was carried out under the condition of $[DMeMAm]_0/[Me_2EtSiH]_0/[B(C_6F_5)_3]_0$ = 1/1/0.1 in toluene. The conversion of DMeMAm ($I_{H,MAm}$) and the efficiency of the initiator formation ($I_{ini.}$) was 97% and 93% after the hydrosilylation time (T_h) of 6 h, and the polymerization of DEAAm following the hydrosilylation was completed in a specific polymerization time regardless of the additional catalyst of Me_3SiNTf_2, to produce narrow-dispersed PDEAAms with the M_w/M_n of 1.07 (runs 4-22 and 4-23). The MALDI-TOF MS spectrum of the product from run 4-22 in Figure 4-9 almost showed

the ion peaks of the targeted polymer products (DMeMAm-$(DEAAm)_n$-H), though a small amount of H-$(DEAAm)_n$-H caused by the 1,4-hydrosilylation of DEAAm was also observed. Meanwhile, the undesirable peaks in the MALDI-TOF MS spectrum of the product from run 4-23 were significantly depressed due to the additional catalyst which enhances the propagation rate (Figure 4-9b). Considering all the factors of the hydrosilylation reaction, such as side reactions and the efficiency of the initiator formation, we carried out the 1,4-hydrosilylation reaction using 10 mol% excess Me_2EtSiH (run 4-24, $[DMeMAm]_0/[Me_2EtSiH]_0/[B(C_6F_5)_3]_0$ = 1/1.1/0.1) and the polymerization using a small portion of Me_3SiNTf_2 as an additional catalyst ($[DEAAm]_0/[DMeMAm]_0/[Me_3SiNTf_2]_0$ = 25/1/0.02). As expected, the polymerization afforded precise control over the molecular weight, molecular weight distribution, and polymer structure because the MALDI-TOF MS spectrum in this case (run 4-24, Figure 4-9c) only showed one symmetric population of ion peaks, and each of them was consistent with the targeted polymer structure of DMeMAm-$(DEAAm)_n$-H. In addition, the top peak showed a molecular weight around 4 kDa, which was close to the theoretical molecular weight of 3.3 kDa. The $I_{H,MAm}$ and $I_{ini.}$ were estimated to be >99% and 97% in this case. This result indicated that the tuning of the amounts of DMeMAm, Me_2EtSiH, and $B(C_6F_5)_3$ significantly affected both the 1,4-hydrosilylation and polymerization, and a small excess amount of Me_2EtSiH relative to DMeMAm was preferred for the control of the polymerization though an excess of Me_2EtSiH would cause a minor unnecessary second 1,2-hydrosilylation of the ene group of the *in situ* produced SKAm, which could slightly decrease the initiation efficiency of the polymerization. Overall, the 1,4-hydrosilylation and polymerization under an optimized condition of $[DMAm]_0/[Me_2EtSiH]_0/[B(C_6F_5)_3]_0$ = 1/1.1/0.1 eventually led to the precise control of polymerization.

The α-end-functionalization of PDEAAm was carried out using Fn-MAms. Table 4 summarizes the synthetic results. The 1,4-hydrosilylation of an Fn-MAm with Me_2EtSiH showed a sufficient $I_{H,MAm}$ and the $I_{ini.}$ was as high as ≥91%. The following polymerization underwent a quantitative DEAAm conversion and each polymerization was well-controlled, though the product by the polymerization using Fn_4-MAm seemed to have a slightly broader distribution. The silyl protecting group of the hydroxyl group in runs 4-25, 4-26, and 4-28 was removed after the polymerization using TBAF. As expected, each polymer showed a satisfactory MALDI-TOF MS assignment with the designed α-end-functionalized polymer structure, as shown in Figure 4-10. For example, the MALDI-TOF MS spectrum of the α-one hydroxyl functionalized PDEAAm (run 4-25, Figure 4-10a) showed one population peaks with the *m*/*z* value of every ion peak (*e.g.*, an observed 4234.69 Da for the sodium-cationized 32-mer polymer) assignable to the targeted sodium-cationized polymer structure of [Fn_1-MAm-$DEAAm_n$-H + Na^+] (the theoretical 32-mer monoisotopic value of 4235.29), strongly suggesting that F_1-MAm was quantitatively introduced without any side reactions. This meant that we succeeded in the syntheses of the α-end-functionalized PDEAAms, which bare one hydroxyl (run 4-25), two hydroxyls (run 4-26), acetal-protected two hydroxyls (run 4-27), and one hydroxyl and one ethynyl groups (run 4-28), respectively.

Table 4-4. Synthesis of α-end-functionalized PDEAAms (Fn-PDEAAms) by the $B(C_6F_5)_3$-catalyzed 1,4-hydrosilylation of *N*,*N*-dimethylmethacrylamide (DMeMAm) and functional methacrylamides (Fn-MAms) with Me_2EtSiH,[a] followed by the Me_3SiNTf_2-catalyzed GTP of DEAAm [b]

run	[DMAm]/[Me_2EtSiH]/[$B(C_6F_5)_3$]	DMAm	$I_{H,MA}$ ($I_{ini.}$) (%) [c]	$M_{n,calcd.}$ (kg mol^{-1}) [d]	$M_{n,SEC}$ (kg mol^{-1}) [e]	$M_{n,NMR}$ (kg mol^{-1}) [c]	M_w/M_n [e]
4-22	1/1/0.1	DMeMAm	97 (93)	3.29	2.95	n.d. [f]	1.07
4-23	1/1/0.1	DMeMAm	97 (93)	3.29	2.89	n.d. [f]	1.07
4-24	1/1.1/0.1	DMeMAm	>99 (97)	3.29	2.72	n.d. [f]	1.06
4-25	1/1.1/0.1	Fn_1-MAm	>99 (93)	3.44	2.73	3.89	1.06
4-26	1/1.1/0.1	Fn_2-MAm	>99 (91)	3.58	2.75	4.89	1.10
4-27	1/1.1/0.1	Fn_3-MAm	>99 (97)	3.47	2.78	3.73	1.08
4-28	1/1.1/0.1	Fn_4-MAm	>99 (92)	3.46	4.61	n.d. [f]	1.16

[a] Ar atmosphere; room temperature; solvent, toluene; 1,4-hydrosilylation condition, $[DMAm]_0/[Me_2EtSiH]_0/[B(C_6F_5)_3]_0$ = 1/1.1/0.1; reaction time, 6 h. [b] In CH_2Cl_2 for 15 min; $[DEAAm]_0$ = 1.0 mol L^{-1}; $[DEAAm]_0/[DMAm]_0/[Me_3SiNTf_2]_0$, 25/1/0.02; monomer conversion, >99%. [c] Determined by ^{1}H NMR in $CDCl_3$. [d] $M_{n,calcd.} = [DEAAm]_0/[DMAm]_0 \times$ (Conv.) $\times$ (M.W. of DEAAm = 127.19) + (M.W. of DMAm). [e] Determined by SEC in DMF containing 0.01 mol L^{-1} of LiCl using PMMA standard. [f] Not determined.

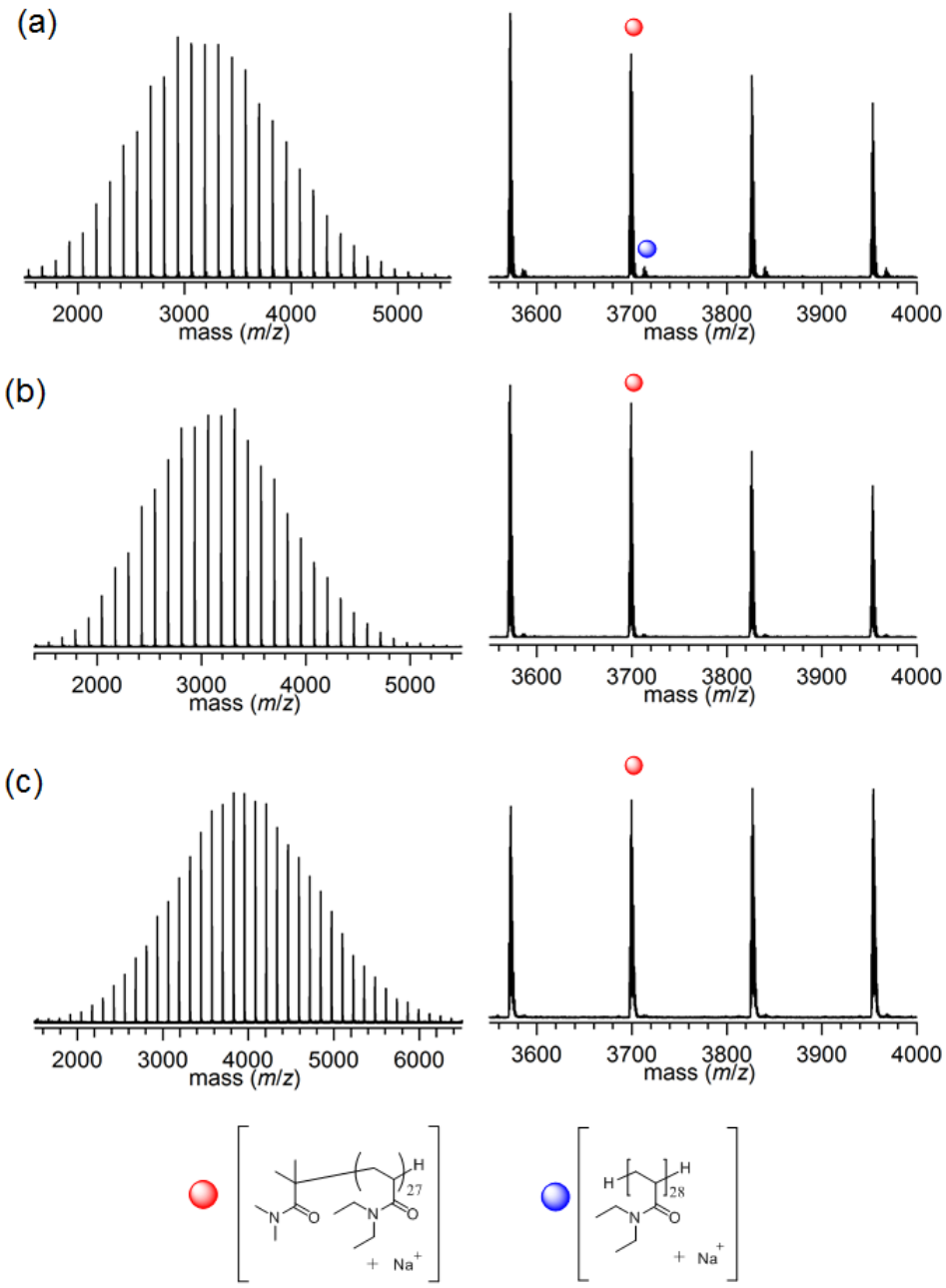

Figure 4-9. MALDI-TOF MS spectra of the products from (a) run 4-22, (b) run 4-23, and (c) run 4-24, obtained by the $B(C_6F_5)_3$-catalyzed GTPs of DEAAm using Me_2EtSiH and DMeMAm under various $[DMeMAm]_0/[Me_2EtSiH]_0/[B(C_6F_5)_3]_0$ ratios.

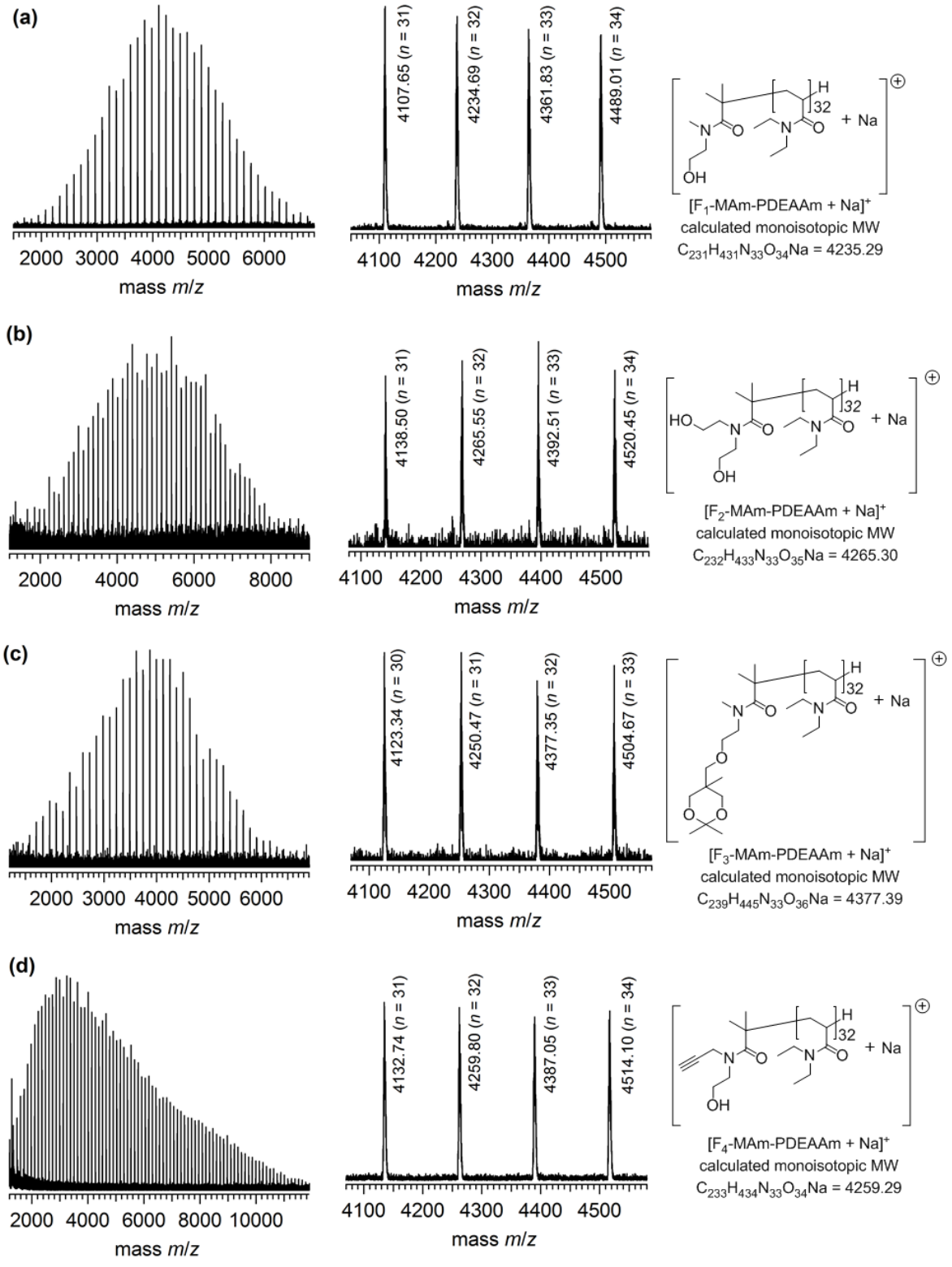

Figure 4-10. MALDI-TOF MS spectra of (a) run 4-25, (b) run 4-26, (c) run 4-27, and (d) run 4-28 obtained by the $B(C_6F_5)_3$-catalyzed GTPs of DEAAm using Me_2EtSiH and Fn-MAms.

4.4. Conclusions

The author demonstrated a convenient $B(C_6F_5)_3$-catalyzed GTP of DAAm using the moisture-tolerant H*Si* through the *in situ* formation of SKAm as a true GTP initiator *via* the 1,4-hydrosilylation of DAAm with H*Si*. The screening experiments using the H*Si*s and DAAm monomers indicated that both the chemical structures of H*Si* and DAAm had significantly affected control of the polymerization. The use of an H*Si* with small steric bulkiness and a DAAm showing a weak coordination interaction with $B(C_6F_5)_3$ was more favorable for the polymerization control. For instance, Me_2EtSiH with the least steric bulkiness was the most suitable H*Si*; the polymerization of DEAAm and DMAAm, which shows a strong coordination with $B(C_6F_5)_3$, only had better control over the molecular weight and polydispersity, while those of NAM, DAlAAm, and BMEAAm, which showed a relatively weaker coordination with $B(C_6F_5)_3$, afforded well-defined polymer products. The kinetic and mechanistic studies suggested that either the abstraction of the hydride from H*Si* by $B(C_6F_5)_3$ or the propagation would be the rate-determining reaction during the entire polymerization reaction, which depends on the structure of the DAAm monomer. In addition, the extra addition of Me_3SiNTf_2 to the polymerization system significantly accelerated the polymerization, which helped to avoid any unnecessary thermo-induced self-polymerization. Finally, we, for the first time, achieved the α-end-functionalization of PDEAAm by the current GTP method using various functional methacrylamides that possessed an extremely low monomer reactivity in the Lewis acid catalyzed GTP. For instance, defect-free PDEAAm with an α-end of one hydroxyl, two hydroxyls, or one hydroxyl and one ethynyl group was obtained by the molecular design of the methacrylamide with functional groups. In summary, this study provided a rather deep insight into the $B(C_6F_5)_3$-catalyzed GTP of DAAms using H*Si*, which, in turn, helps polymer chemists in designing as well as preparing metal-free polyacrylamides for various applications.

4.5. References and Notes

(1) Nederberg, F.; Connor, E. F.; Möller, M.; Glauser, T.; Hedrick, J. L. *Angew. Chem. Int. Ed.* **2000**, *40*, 2712-2715.

(2) Esswein, B.; Möller, M. *Angew. Chem. Int. Ed.* **1996**, *35*, 623-625.

(3) Misaka, H.; Sakai, R.; Satoh, T.; Kakuchi, T. *Macromolecules* **2011**, *44*, 9099-9107.

(4) Nyce, G. W.; Glauser, T.; Connor, E. F.; Möck, A.; Waymouth, R. M.; Hedrick, J. L. *J. Am. Chem. Soc.* **2003**, *125*, 3046-3056.

(5) Makiguchi K.; Satoh T.; Kakuchi T. *Macromolecules* **2011**, *44*, 1999-2005.

(6) Memenger, Jr. W.; Campbell, G. C.; Davidson, F. *Macromolecules* **1996**, *29*, 6475-6480.

(7) Nederberg, F.; Lohmeujer, B. G. G.; Leibfarth, F.; Pratt, R. C.; Choi, J.; Dove, A. P.; Waymouth, R. M.; Hedrick, J. L. *Biomacromolecules* **2007**, *8*, 153-160.

(8) Makiguchi, K.; Ogasawara, Y.; Kikuchi, S.; Satoh, T.; Kakuchi, T. *Macromolecules* **2013**, *46*, 1772-1782.

(9) Kamber, N. E.; Jeong, W.; Waymouth, R. M.; Pratt, R. C.; Lohmeijer, B. G. G.; Hedrick, J. L. *Chem. Rev.* **2007**, *107*, 5813-5840.

(10) Jeong, W.; Shin, E. J.; Culkin, D. A.; Hedrick, J. L.; Waymouth, R. M. *J. Am. Chem. Soc.* **2009**, *131*, 4884-4891.

(11) Pratt, R. C.; Lohmeijer, B. G. G.; Long, D. A.; Lundberg, P. N. P.; Dove, A. P.; Li, H. B.; Wade, C. G.; Waymouth, R. M.; Hedrick, J. L. *Macromolecules* **2006**, *39*, 7863-7871.

(12) Sen, T. K.; Sau, S. C.; Mukherjee, A.; Modak, A.; Mandal, S. K.; Koley, D. *Chem. Commun.* **2011**, *47*, 11972-11974.

(13) Misaka H.; Kakuchi R.; Zhang C.; Sakai R.; Satoh T.; Kakuchi T. *Macromolecules* **2009**, *42*, 5091-5096.

(14) Sanda, F.; Sanada, H.; Shibasaki, Y.; Endo, T. *Macromolecules* **2002**, *35*, 680-683.

(15) Ke, X.; Coady, D. J.; Yang, C.; Engler, A. C.; Hedrick, J. L.; Yang, Y. Y. *Polym. Chem.* **2014**, *5*, 2621-2628.

(16) Webster, O. W.; Hertler, W. R.; Sogah, D. Y.; Farnham W. B.; RajanBabu, T. V. *J. Am. Chem. Soc.* **1983**, *105*, 5706-5708.

(17) Sogah, D. Y.; Hertler, W. R.; Webster, O. W.; Cohen, G. M. *Macromolecules* **1987**, *20*, 1473-1488.

(18) Hertler, W. R.; Sogah, D. Y.; Webster, O. W.; Trost, B. M. *Macromolecules* **1984**, *17*, 1415-1419.

(19) Zhuang, R.; Müller, A. H. E. *Macromolecules* **1995**, *28*, 8035-8042.

(20) Zhuang, R.; Müller, A. H. E. *Macromolecules* **1995**, *28*, 8043-8050.

(21) Fuchise, K.; Chen, Y.; Satoh, T.; Kakuchi, T. *Polym. Chem.* **2013**, *4*, 4278-4291.

(22) Raynaud, J.; Ciolino, A.; Beceiredo, A.; Destarac, M.; Bonnette, F.; Kato, T.; Gnanou, Y.; Taton, D. *Angew. Chem. Int. Ed.* **2008**, *47*, 5390-5393.

(23) Scholten, M. D.; Hedrick, J. L.; Waymouth, R. M. *Macromolecules* **2008**, *41*, 7399-7404.

(24) Raynaud, J.; Liu, N.; Gnanou, Y.; Taton, D. *Macromolecules* **2009**, *42*, 5996-6005.

(25) Raynaud, J.; Liu, N.; Fèvre, M.; Gnanou, Y.; Taton, D. *Polym. Chem.* **2011**, *2*, 1706-1712.

(26) Fèvre, M.; Vignolle, J.; Heroguez, V.; Taton, D. *Macromolecules* **2012**, *45*, 7711-7718.

(27) Zhang, Y.; Chen, E. Y.-X. *Macromolecules* **2008**, *41*, 36-42.

(28) Zhang, Y.; Chen, E. Y.-X. *Macromolecules* **2008**, *41*, 6353-6360.

(29) Zhang, Y.; Lay, F.; García, P. G.; List, B.; Chen, E. Y.-X. *Chem. Eur. J.* **2010**, *16*, 10462-10473.

(30) Kakuchi, T.; Chen, Y.; Kitakado, J.; Mori, K.; Fuchise, K.; Satoh, T. *Macromolecules*, **2011**, *44*, 4641-4647.

(31) Chen, Y.; Fuchise, K.; Narumi, A.; Kawaguchi, S.; Satoh, T.; Kakuchi, T. *Macromolecules*,

2011, *44*, 9091-9098.

(32) Kakuchi, R.; Chiba, K.; Fuchise K.; Sakai, R.; Satoh, T.; Kakuchi, T. *Macromolecules* **2009**, *42*, 8747-8750.

(33) Fuchise, K.; Sakai, R.; Satoh, T.; Sato, S.; Narumi, A.; Kawaguchi, S.; Kakuchi, T. *Macromolecules* **2010**, *43*, 5589-5594.

(34) Takada, K.; Fuchise, K.; Chen, Y.; Satoh, T.; Kakuchi, T. *J. Polym. Sci. Part A: Polym. Chem.* **2012,** *50*, 3560-3566.

(35) Fuchise, K.; Chen, Y.; Takada, K.; Satoh, T.; Kakuchi, T. *Macromol. Chem. Phys.* **2012**, *213*, 1604-1611.

(36) Chen, Y.; Takada, K.; Fuchise, K.; Satoh, T.; Kakuchi, T. *J. Polym. Sci. Part A: Polym. Chem.* **2012**, *50*, 3277-3285.

(37) Takada, K.; Fuchise, K.; Kubota, N.; Ito, T.; Chen, Y.; Satoh, T.; Kakuchi, T. *Macromolecules* **2014**, *47*, 5514-5525.

(38) Takada, K.; Ito, T.; Kitano, K.; Tsuchida, S.; Takagi, Y.; Chen, Y.; Satoh, T.; Kakuchi, T. *Macromolecules* **2015**, *48*, 511-519.

(39) Kikuchi, S.; Chen, Y.; Kitano, K.; Takada, K.; Satoh, T.; Kakuchi, T. *Polym. Chem.* **2015**, *6*, 6845-6856.

(40) Fuchise, K.; Tsuchida, S.; Takada, K.; Chen, Y.; Satoh, T.; Kakuchi, T. *ACS Macro Lett.* **2014**, *3*, 1015-1019.

(41) Chen, Y.; Kitano, K.; Tsuchida, S.; Kikuchi, S.; Takada, K.; Satoh, T.; Kakuchi, T. *Polym. Chem.* **2015**, *6*, 3502-3511.

(42) Xu, T.; Chen, E. Y.-X. *J. Polym. Sci. Part A: Polym. Chem.* **2015**, *53*, 1895-1903.

(43) Liu, S.-T.; Wang, H.-E.; Cheng, M.-C.; Peng, S.-M. *J. Organomet. Chem.* **1989**, *376*, 333-342.

(44) Efthymiou, T. C.; Huynh, V.; Oentoro, Peel, B.; Desaulniers, J. P. *Bioorg. Med. Chem. Lett.* **2012**, *22*, 1722-1726.

(45) Parks, D. J.; Piers, W. E. *J. Am. Chem. Soc.* **1996**, *118*, 9440-9441.

(46) Parks, D. J.; Blackwell, J. M.; Piers, W. E. *J. Org. Chem.* **2000**, *65*, 3090-3098.

(47) Houghton, A. Y.; Hurmalainen, J.; Mansikkamaki, A.; Piers, W. E.; Tuononen, H. M. *Nat. Chem.*, **2014**, *6*, 983-988.

(48) For the detailed analyses in regard to the propagation behavior, see Ref. 39.

(49) Suzuki, T.; Kusakabe, J.; Kitazawa, K.; Nakagawa, T.; Kawauchi, S.; Ishizone, T. *Macromolecules* **2010**, *43*, 107-116.

Chapter 5

Conclusions

In this thesis, the author described the development of the organocatalyzed group transfer polymerization (GTP) for acrylamide monomers, involving an initiating system, applicable monomer, and design of the macromolecular architecture. The combination of an organic acid as the catalyst and silyl ketene acetal (SKA) as the initiator was efficient for the synthesis of various acrylamide polymers. This initiating system for the first time achieved the sequential synthesis of a block copolymer with poly(methyl methacrylate) and poly(*N*-acryloylmorpholine) (PNAM) segments by the organic acid-promoted GTP. The α,ω-end-functionalized poly(*N*,*N*-diethylacrylamide) (PDEAAm) was successfully synthesized by the tris(pentafluorophenyl)borane ($B(C_6F_5)_3$)-catalyzed GTP using the designed silyl ketene aminal with hydroxyl-, ethynyl-, and vinyl-groups (F-SKAms) as the initiators and 2-phenyl acrylate derivatives with hydroxyl-, ethyl-, and bromo-groups (PhA-Fs) as the terminal reagents. In addition, these end-functionalized PDEAAms precisely lead to the complex macromolecular architectures, such as cyclic and star-shaped by the intra- or inter-molecular click reaction, and the topological effect on the thermoresponsive properties among the synthesized PDEAAms with linear, cyclic, and star-shaped architectures was comprehensively elucidated through both experimental and computational approaches. The author described the new type of GTP of acrylamide using $B(C_6F_5)_3$ and moisture-tolerant tri-substituted hydrosilane (H*Si*), which the SKAm as the true initiator was *in situ* formed by the hydrosilylation of a monomer with H*Si* before the polymerization reaction proceeds. Therefore, the author believes that the achievement of this study should provide a diversity to the GTP field and the deep insight for the synthesis and design of macromolecules for smart materials.

A summary of this thesis is as follows:

In Chapter 2, the author described that the GTPs of DAAm using the combinations of acidic

organocatalysts (Me_3SiNTf_2, $C_6F_5CHTf_2$, and $B(C_6F_5)_3$) and SKAs (SKA^{Me}, SKA^{Et}, SKA^{iPr}, and SKA^{Ph}) was significantly efficient to produce well-defined PDAAms, among which the polymerization using $B(C_6F_5)_3$ and SKA^{Et} showed a better control over the molecular weight distribution. The $B(C_6F_5)_3$-catalyzed GTP using SKA^{Et} was applicable to various *N*,*N*-disubstituted acrylamides (DAAms) including the water-soluble, thermoresponsive, and reactive ones. All the $B(C_6F_5)_3$-catalyzed polymerizations showed an obvious induction period of tens of minutes, after which it proceeded as a zero-order reaction in a living fashion. The occurrence of the induction period was clearly attributed to the structural mismatch between the SKA and DAAm. In addition, the initiation and propagation rates of a DAAm were significantly dependent on its *N*-disubstituents and the balance between them was the key factor for well controlling the polymerization. The livingness of the polymerization system was suitable for synthesizing homo block copolymers composed of different acrylamide blocks and hetero block copolymers of PMMA-*b*-PNAM by the sequential GTP method.

In Chapter 3, the author demonstrated a facile end-functionalization method of PDEAAm at both the α- and ω-chain ends demonstrated by the $B(C_6F_5)_3$-catalyzed GTP of DEAAm using functional silyl ketene aminals (SKAms) as the initiator and functional 2-phenyl acrylates (PhA-Fs) as the terminator. The SKAm designed with hydroxyl, ethynyl, and vinyl groups was quantitatively introduced at the α-chain end of PDEAAm with well-controlled molecular weights, narrow polydispersities, and structural fidelity. As well as the initiation approaches, PhAs functionalized with hydroxyl, ethynyl, and bromo groups were quantitatively introduced at the ω-chain end of PDEAAm, whose structural fidelity was definitely confirmed by ^1H NMR and MALDI-TOF MS measurements. In addition, the intra- or inter-molecular azide-alkyne cycloaddition of the end-functionalization of PDEAAm successfully produced the PDEAAms

with nonlinear topological architectures, *i.e.*, macrocyclic and star-shaped. Both the cyclic-PDEAAm and 3-armed star-shaped PDEAAm were successfully prepared with three different DPs of 26 - 29, 50 - 52, and 78 - 80. The topological effect of the polymer architectures, such as linear, cyclic, and star-shaped PDEAAms on the thermoresponsive property was intensively evaluated in terms of the molecular weight dependence and responsivity for the phase transition, among which the cyclic and star architectures led to a lower phase transition temperature compared to its linear counterpart. Furthermore, the molecular dynamics (MD) simulation significantly helped in realizing the influence of topology on an atomic scale.

In Chapter 4, the author demonstrated a convenient $B(C_6F_5)_3$-catalyzed GTP of DAAm using the moisture-tolerant H*Si* through the *in situ* formation of SKAm as a true GTP initiator *via* the 1,4-hydrosilylation of DAAm with H*Si*. The screening experiments using the H*Si*s and DAAm monomers indicated that both chemical structures of H*Si* and DAAm had significantly affected control of the polymerization. The use of an H*Si* with a small steric bulkiness and a DAAm showing a weak coordination interaction with $B(C_6F_5)_3$ was more favorable for the polymerization control. For instance, Me_2EtSiH with the least steric bulkiness was the most suitable H*Si*; the polymerization of DEAAm and DMAAm, which shows a strong coordination with $B(C_6F_5)_3$, only had a better moderate control over the molecular weight and polydispersity, while those of NAM, DAlAAm, and BMEAAm, which showed a relatively weaker coordination with $B(C_6F_5)_3$, afforded well-defined polymer products. The kinetic and mechanistic studies suggested that either the abstraction of the hydride from H*Si* by $B(C_6F_5)_3$ or the propagation would be the rate-determining reaction during the entire polymerization reaction, which depends on the structure of the DAAm monomer. In addition, the extra addition of Me_3SiNTf_2 to the polymerization system significantly accelerated the polymerization, which helped to avoid any unnecessary thermo-

induced self-polymerization. Finally, the author, for the first time, achieved the α-end-functionalization of PDEAAm by the current GTP method using various functional methacrylamides that possessed an extremely low monomer reactivity in the Lewis acid catalyzed GTP. For instance, defect-free PDEAAms with an α-end of one hydroxyl, two hydroxyls, or one hydroxyl and one ethynyl group were obtained by the molecular design of the methacrylamide with functional groups.